WATER FLOW AT THE BASE OF A SURGING GLACIER

Thesis by

Melinda Mary Brugman

In Partial Fulfillment of the Requirement

for the Degree of

Doctor of Philosophy

California Institute of Technology

Pasadena, California

1987

(Submitted July 7, 1986)

ACKNOWLEDGEMENTS

This study could not have been completed without the encouragement, and assistance of a great many wonderful individuals. First I wish to acknowledge my advisor, Barclay Kamb, for his careful evaluation, unfailing support, and boundless scientific insight into each aspect of this thesis.

To Herman Engelhardt it is difficult to completely express my gratitude for his thoughtful determination to ensure that all field aspects of this research were sucessfully completed as originally planned. In addition, I wish to thank Herman for being the very special and delightful person he is, and being such a joy to work with in the field. I am also very grateful to Mark Meier who provided a great amount of encouragement, and critical guidance on various aspects of this thesis, and my separate research on Shoestring Glacier, Mount St. Helens. Also, I am grateful to Almut Iken for her patient support.

Bob Krimmel, of the U.S. Geological Survey Glaciology Project Office in Tacoma, Washington, gave initial instruction on dye-tracing techniques, and generously provided a Turner Filter Fluorometer for use during the course of this research. In addition to people already mentioned, invaluable assistance in field aspects of this study was generously given by Neil Humphrey, Lili Mezger, Peter Mullen, Charlie Raymond, Will Harrison, Linda Kamb, Magnus Magnussen, Tad Pfeffer and others from the Caltech, University of Washington and University of Alaska glacier research crews.

When at the glacier terminus, perpetual amusement was provided by the Neil and Tad "Laurel-and-Hardy" comedy team, who gave special performances during rainy days (when any sane person would be safe and warm in their tent). Also, the "three-blind-mice" bird at the glacier terminus can not be forgotten, or thanked enough for its endless music. I just hope the repetitive tweety will someday learn the rest of the song.

Several different members of the U.S.G.S. Glacier Project Office including Carolyn Driedger, Suzanne Brown, Stan, Bob, Ginger and Austin gave useful advice, encouragement, and assistance in several different aspects of my graduate research. Don Mullineaux, Sue Kieffer, John Power, Bruce Furakowa, Harry Glicken and several others at the U.S.G.S. Cascade Volcano Center in Vancover also helped and were good company. At Caltech, critical scientific advice and support was given by Robert Sharp, Sam Epstein, Brad Hager, Ray Weldon, Sally Newman and many others who can not all be mentioned here.

Preparation of the manuscript was done with the help of two angels, named Patty Batten and Marta Nyiri, who dropped in from heaven and saved me in times of need. Other angels who dropped in and helped prepare the final thesis version(s) and save lost computer files include the Sally Newman (and her side-kick "keel"), Astrid Howard, Elise McConnell, Shebear, Lucianna Astiz (alias "The Commandeer General"), Patty Brugman, Bob Svendson and Mark Fahnestock (yes, guys can be wonderful angels too). Apologies to Patty Batten's sweety who tolerated, and aided our final efforts to complete the thesis. The drafting miracles were performed by Jan Mayne. Her continual advice and warm friendship smoothed many a rough road. Patient answering of computer questions was done by Edith Huang, and I wish her only the best. I am grateful to Robert Clayton and others at Caltech Seismo Lab, who graciously tolerated the invasion of Kermit into their VAX, and allowed the final copies of my thesis to be printed.

For the fine support by personnel in the Caltech Geology Division, Geology Library and Seismo Lab, I am grateful. Dorothy Coy, Fran Barnard, Anne Freeman, Linda Carson, Barbara Niles, Cheryl Contopulous, Jean Grinols, Sue Yamada, Dee Page, Daphne Plane and the others are a true Godsend when it comes to needing assistance on a moments notice. Thanks for your tireless efforts to make our lives just a bit easier.

Support from friends is a necessary ingredient for the completion of any major piece of work, and I am grateful to all of my friends. Particularly I must mention,

Lucianna Astiz, Dana and Bill Truslow, Ray Weldon, Anita and John Granchich family, Elaine and How-Man Wong family, John Robert Brugman, Loraine Hwang and, of course, Oliver, because each of them took darn good care of me, and they all are special. Thanks also to Marcus Bursik; your verbal abuse, crazy skiing and extended discussions were all quite helpful. The fresh, and enduring support of Lili Mezger deserves more than just a special note of gratitude, you are a jewel.

I would like to acknowledge Keith Echelemeyer, a close friend, who gave me encouragement, advice, assistance, shared enjoyable adventures with me, and enforced in me the value of being self-reliant.

Last, but certainly not least, I acknowledge my brothers, John and Bill, and sisters, Pat and Barbara, for their encouragement, and I especially thank my parents, Margaret and Barry, for their unfailing support, love, and belief in me as I am. Their patient optimism is best expressed by by Dad's "life is a bowl of cherries " attitude, and their determination to cheerfully solve each difficulty encountered is a trait I strive to match.

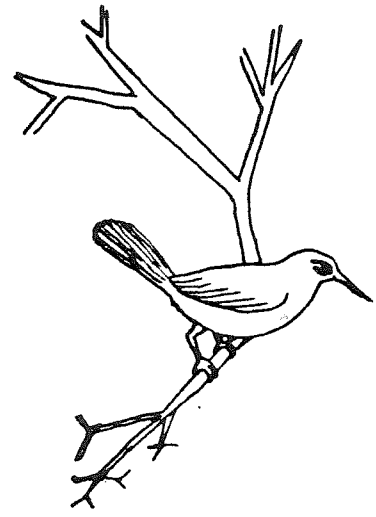

ABSTRACT

Water tracing experiments were successfully conducted over a distance of ten kilometers along the base of Variegated Glacier for the purpose of characterizing the water drainage system of the glacier in the surging as compared to the non-surging state. Three tracing experiments were conducted, and fluorescent dyes, Rhodamine WT and Tinopal AMS, were injected into boreholes at separate locations. The two Rhodamine WT experiments were conducted over a 10 km distance, both during the most rapid surging motion of the glacier, and after its cessation.

In each experiment, the terminus streams were monitored for stream discharge, sediment content and tracer concentration. Rhodamine WT tracer was significantly adsorbed on the suspended sediment, particularly during the surge. The adsorption behavior followed the Langmuir model, and calculated distribution coefficients of K_d = 100 to 1000 ml/g were measured for during the glacier surge. The K_d values measured after the surge were lower than during the surge by a factor of 10 to 1000. The much higher K_d values in the surging as compared to non-surging glacier states can be best explained by a factor of 10 to 1000 decrease in the modal and/or mean grain-size of the suspended sediment. The abundance of fine-grained sediment during the surge is probably due to increased grinding of rock material at the glacier bed.

Theoretical models of tracer dispersion in a single tunnel, were compared to models of dispersion in linked-cavity systems to infer the details of water flow at the glacier bed. The broad, roughly symmetrical, dye-return curve measured during the glacier surge conforms to diffusive dispersion theory, and differs sharply from the highly asymmetrical dispersion curve measured after the surge. Results indicate the dispersion behavior, and calculated Manning roughness, of the post-surge Variegated

Glacier is similar to those of glaciers that do not surge. The drainage system of the Variegated Glacier in the surging state is consistent with a model of tracer dispersion in an interconnecting network of conduits and cavities, and is strikingly different from the tunnel system indicated for the non-surging state.

TABLE OF CONTENTS

Chapter I:
INTRODUCTION

The flow of water in the basal drainage system of a temperate glacier in the surging state is studied and compared to the flow during normal, non-surge conditions. The movement of water is followed by dye-tracing techniques, using fluorescent dyes injected into glacier boreholes.

A dye-tracer experiment, as performed for this thesis, involves the injection of an easily detected, soluble dye into a water drainage system, and the monitoring of dye concentrations at one or more locations down stream. The spreading of the dye pulse in time and space and the mean dye transport velocity give a measure of the mechanics of water flow within the drainage system, and of the size and distribution of water conduits at the glacier bed. Tracer experiments provide information about glacier hydrology that is impossible to determine by other methods.

The dye-tracer experiments discussed in this thesis were conducted in 1983. These are the first dye-tracer experiments ever carried out on a glacier in surge. The conclusions bear on the processes responsible for glacier surges.

The glacier studied is Variegated Glacier, in southeastern Alaska. A location map for the glacier is given in Fig. 1.1. Photographs of the Variegated Glacier before and during the 1983 surge are shown in Kamb et al. (1985, Fig. 8).

Up to the present, the glacier surge has been a largely unstudied phenomenon, and there is a paucity of information on the mechanics of surging. This discussion is confined to temperate glaciers whose flow instability is not due to periodic unfreezing at the glacier bed as advocated by Clarke (1976) for polar glaciers. The most detailed information on a glacier surge, to date, has been obtained from the Variegated

Glacier, Alaska, by groups from Caltech and the Universities of Washington and Alaska (Kamb et al., 1985). The research presented here is one aspect of that study.

A surge-type glacier, such as Variegated Glacier, flows at normal ice velocities for many years, speeds up as much as a hundredfold during the surge which lasts a few months to a few years, and then returns to normal flow velocities. Post (1969) showed that Variegated Glacier surges with a period of about 20 years. The glacier began to develop a pattern of unstable flow behavior in 1979-81, which culminated in a major surge during 1982-83 (Kamb et al., 1985). The highest velocity was reached early in the summer of 1983. Five kilometers from the glacier terminus the velocity reached 65 meters per day, more than one hundred times the pre-surge glacier speed. The end of the surge occurred suddenly, in early July, soon after the surface melt had peaked. A large flood of water was discharged from the glacier as the ice halted its rapid motion, suggesting that a close relationship exists between the surge instability and the hydraulic properties of the glacier's basal water system. The high flow velocities of the surge were correlated with high water pressures and increased turbidity of the outflow streams. Results suggest that the high flow velocities are caused by increased basal sliding at the ice-rock interface.

C. F. Raymond, W. D. Harrison and coworkers Bindschadler and others began the first detailed monitoring and surveying of Variegated Glacier ten years prior to the 1982-3 surge. During the buildup phase of the surge cycle there was a gradual increase in thickness and velocity in the upper reaches of the glacier accumulation area. As the glacier approached surge, this increased thickness and flow in the upper reaches began to propagate down towards the glacier terminus in a series of mini-surge pulses (Kamb and Engelhardt, 1986, in press). In minisurges the glacier flow

velocity reaches a peak value at the same time as a maximum in basal water pressure. The basal water pressure at times rises high enough to locally float the glacier.

Large ice streams and major ice sheets may also undergo surging behavior similar to Variegated Glacier, but perhaps with much longer recurrence intervals. These large ice masses have the potential for discharging enormous volumes of icebergs into nearby oceans, thereby dramatically increasing the mean albedo at polar latitudes. The mean temperature of the earth is expected to decrease and the global sea level suddenly increase if a major surge of a polar ice sheet were to occur. There is evidence to suggest that the West Antarctic, or temperate portions of the Greenland and Laurentide ice sheets, may undergo periodic surges (Hughes, 1973; Denton et al., 1975).

Other possible effects of a surge or rapid glacier advance include destruction of manmade structures such as highways, oil pipelines and water intake systems (for example, Black Rapids and Muldrow glaciers, Alaska; Findelen Glacier, Switzerland), ice avalanches from unstable hanging glaciers, cyclical excessive sediment discharge from terminus streams and extremely rapid silting of hydroelectric reservoirs (for example, several surge-type glaciers in upper Susitna Valley, Alaska), and periodic damming of valleys and related flooding (i.e., the Tulsequah and Taku glaciers, Juneau Icefield, Alaska; the surge-type glaciers that periodically block the Alsek River, St. Elias Range, Alaska; the Hubbard and tributary glaciers that recently caused the blockage of Russell Fiord - allowing the reformation of "Lake Russell" - near Yakutat, Alaska, shown on Figure 1.1).

In the course of the dye-tracer experiments on Variegated Glacier, it was discovered that the amount of dye adsorbed on sediment composes a significant

fraction of the total amount of dye delivered in the outflow stream during the surge, and that it was therefore important to measure the adsorbed dye, contrary to the experience of earlier experiments on (non-surging) glaciers. The measurement techniques for adsorbed dye, presented here, should be useful in future dye-tracing experiments on glaciers with large suspended-sediment concentrations in outflow streams.

It is shown in this thesis (Section 6.2) that if the stream discharge is known then the roughness parameterization of glacier water conduits can be determined from standard dye-tracing experiments (Chapter 4 and Section 6.4). An application of this work includes the measurement of glacial runoff using dye, by application of the theory of turbulent diffusion in a single conduit (Section 6.2.2) to dye-tracing results. If the average conduit roughness, tracer retardation, dispersivity and mean transport velocity are known, then the water discharge in the conduit is theoretically determined.

Results of the dye tracer experiments indicate that a great difference exists in the hydrology of glacier in surge and not in surge. The glacier after surge termination looks hydrologically like a normal, non-surging glacier. There is strong indication that the glacier in surge tends to retain water, which helps explain why high basal water pressures can be maintained during the surge and thus can sustain the high sliding velocities. These interpretations are supported by consideration of theoretical models for explaining the detailed shape of dye-return curves for dye transport through a variety of types of conduit systems and hydraulically permeable porous media.

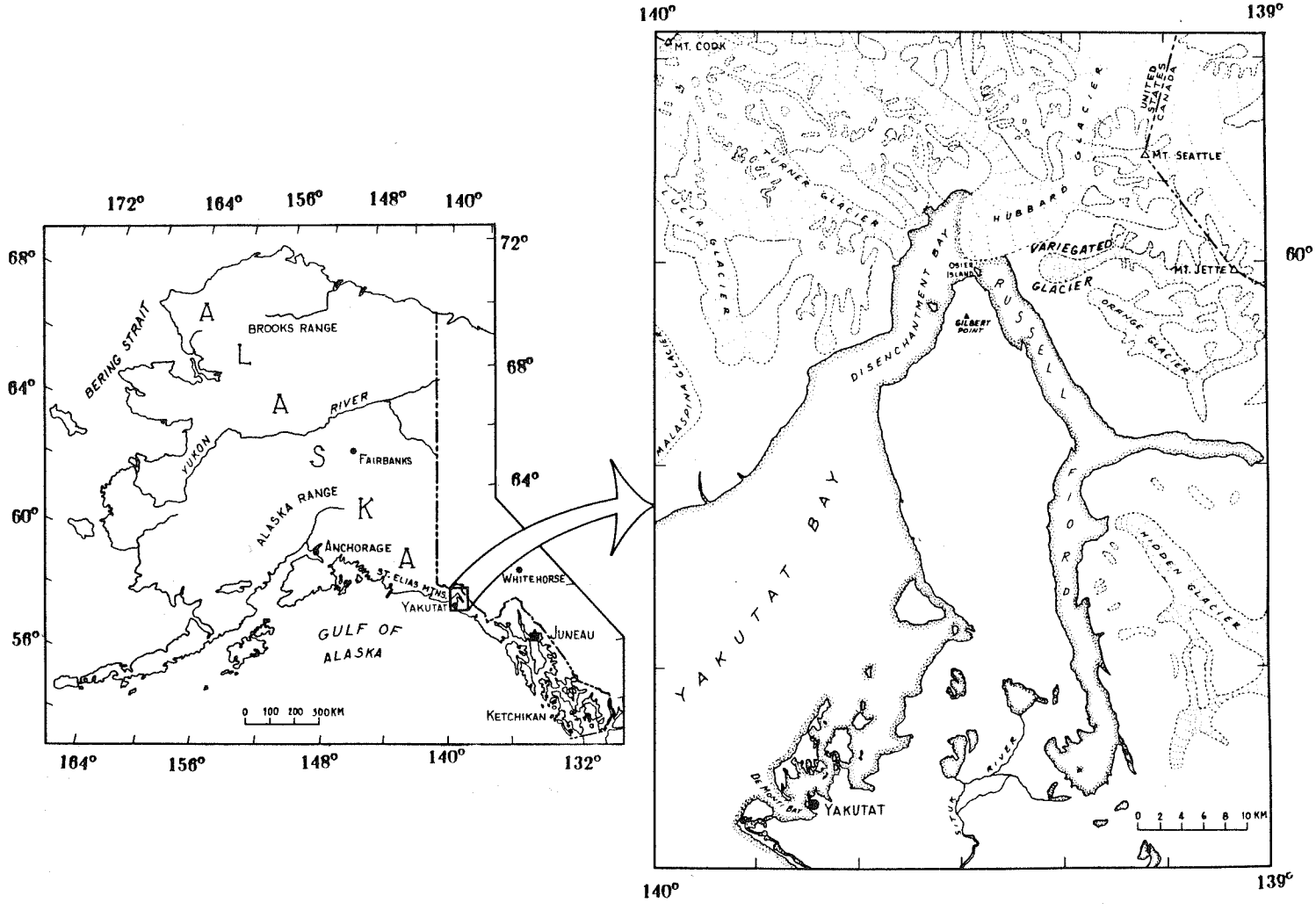

Figure 1.1 Location map of the study area: Variegated Glacier Alaska.

Chapter II:
TRACER TECHNIQUE

2.1. Fluorescent Tracers

2.1.1. Introduction

The dye tracing technique used in this work involves injection of a highly fluorescent dye into the basal water system of the glacier at one location, via a borehole, and detection of the dye at one or more points down glacier where basal water emerges from the glacier in outflow streams. Dye detection is by fluorometry on water samples collected at the downstream locations. The strength of measured fluorescence of each water sample is related to dye concentration in the water through comparison to the fluorescence of calibration standards. Descriptions of fluorometric techniques are given by Wilson (1968), Turner (1977), and Smart and Laidlaw (1976).

In order to trace water through a glacier over horizontal distances of several kilometers, a very sensitive tracer is required. A number of requirements were considered in order to choose dye tracers for the Variegated Glacier experiments. The dyes were chosen to optimize a combination of the several desirable traits, namely, low minimum detectibility (or high sensitivity), low adsorptivity on sediment, spectral distinction from other dyes and from naturally occurring fluorescent substances, stability, high solubility in water, minimal temperature dependence of fluorescence, nontoxicity, cost effectiveness, and availability. The dyes had to be measurable at very low concentrations in water with high suspended sediment levels. For this study, two fluorescent dyes were sought, with non-overlapping absorption and emission spectra,

such that the two dyes could be detected independently and thus used concurrently in tracer experiments. The two dyes chosen for this study were Rhodamine WT and Tinopal AMS.

2.1.2. Rhodamine WT

Rhodamine WT is an orange-fluorescent dye especially designed for water tracing purposes (the designation "WT" stands for "water tracer"). The dye has a long record of reliability in this type of use. Thorough discussions of standard techniques in the use of Rhodamine WT are given by Smart and Laidlaw (1976). Rhodamine WT is an organic molecule related to Rhodamine B (Basic Violet 10, $C_{28}H_{31}N_2O_2Cl$), which is a water tracer widely used since about the 1960. Rhodamine WT is adsorbed less strongly on sediment and has a lower toxicity than Rhodamine B. It is very soluble in water, more soluble than most other common dyes (Turner Designs, 1981; Smart and Laidlaw, 1976). Rhodamine WT is more than adequately stable under normal temperature, light and water conditions. This dye, as supplied in 20 percent aqueous solution, is very dark red in color, somewhat viscous, and has a specific gravity of 1.19. The Rhodamine WT used in this experiment was manufactured by the Crompton and Knowles corporation (Skokie, Illinois) and purchased from Keystone Ingham Corp. (Santa Fe Springs, California). All of the dye used was purchased at the same time and all calibrations and field experiments were conducted with the same batch of dye.

In this study, the *tracer* Rhodamine WT is defined as the 20% solution. All results are given in terms of *tracer* concentration in parts per billion, which represents the volume of 20% dye solution per unit volume of sample water (including

suspended sediment). This is a normal practice followed in dye tracer studies (Turner, 1977; Krimmel et al., 1973). An alternative, widely used unit is μg/l (Smart and Laidlaw, 1976; Lang et al., 1979; Moeri, 1983); the Rhodamine WT concentration in units of μg/l is equal to the *tracer* concentration in units of ppb divided by 1.19.

2.1.3. Tinopal AMS

The second dye chosen for this study was Tinopal AMS, a colorless, blue-fluorescent dye which adsorbs strongly on cellulose. This dye is a stilbene-based "optical brightener", one of many available on the market. These brighteners (used for "brightening" fabrics) adsorb strongly in the ultraviolet, at approximately 340-355 nm, and fluoresce at 430-460 nm, in the blue. The evaluation of several optical brighteners (Leucophor C, Photine CSP, Photine CU and Fluolite BW) by Smart and Smith (1976) and Smart (1976) was a valuable asset in choosing the appropriate dye and measurement techniques for the present study. However, the optical brighteners tested by Smart (1976) were not readily available, and it was therefore necessary to test other brighteners that were available locally. The objective was to find a brightener very similar to the stilbene-based brighteners discussed by Smart. This was made difficult by the additives and filler materials present in many of the brighteners sold commercially. In most cases the additives were designed to reduce the solubility of the active fluorescent ingredient so that the brightener would adhere strongly to cloth or paper. This limited the choice of brighteners, since water tracing requires a dye with very high water solubility. Tests were carried out on the solubility and the excitation and emission spectra of Tinopal AMS, Tinopal CBS, Optiblanc, and Tinopal 5BM. Results are summarized in Fig. 2.1. Due to its high water solubility, the

brightener best suited for the present study was Tinopal SFP, which is normally used as a rinse for photographic paper. This dye is similar to Tinopal AMS (Fig. 2.1), but is more concentrated and more expensive. Tinopal SFP was not available in time for the 1983 field season. The tests indicated that Tinopal AMS would be a satisfactory alternative, and it was chosen. The excitation and emission spectra of Tinopal AMS indicate that it may be chemically very similar to the Fluolite BW brightener tested by Smart (1976, Figure 2, p. 64). The Tinopal dye used in this study was manufactured by Ciba-Geigy Corporation (Greensboro, North Carolina) and purchased from Keystone Ingham Corporation. Tinopal concentrations are given on the basis of ppb by weight.

Prior to the initiation of this study there were no published results on the use of Tinopal brighteners in glacier water. Moeri (1983) has since reported moderate success using a Tinopal dye in Findelen Glacier, Switzerland. The Tinopal AMS used in a tracer experiment on Variegated Glacier in 1983 proved to give considerable difficulty in the field. The difficulties stemmed from the fact that the dye was in powdered form. Although the dye seemed sufficiently water soluble in laboratory tests, in the field it proved difficult to dissolve the large quantity (130 kg) that had to be used. Also, the powdered dye was readily picked up and blown about by the wind; this dispersed dye, which is not visible in small quantities or when dissolved, was a possible source of contamination in the handling of water samples in the field.

2.1.4. Comparison Between Tracers

Excitation and emission spectra of Rhodamine WT and Tinopal AMS were measured by means of a spectral fluorometer in the Division of Chemisty and Chemical Engineering, made available through the courtesy of Janet Marshal. The spectra are compared in Figure 2.2 . The excitation spectra of the two dyes overlap hardly at all; likewise, the emission spectra hardly overlap. This is a favorable situation for measuring independently the concentrations of both dyes when both are present in the same solution. The measured fluorescence level at the emission peak for Rhodamine dye was found to be unaffected by the presence of Tinopal dye at concentrations up to about 1000 ppb.

Table 2.1 contains a summary of the principal characteristics of seven dyes tested, including the positions of the spectral peaks, the minimum level of detectability, and the price. This information may be of use in the design of future dye-tracing experiments.

The detection level for Rhodamine WT is a factor of 100 smaller than for Tinopal AMS. A correspondingly larger quantity of Tinopal dye is needed to achieve a comparable detectability in field experiments. Because of its good performance record and high sensitivity (low detection threshold), Rhodamine WT was the dye chosen for use in the tracing experiments carried out over a distance of about ten kilometers in Variegated Glacier. Tinopal AMS was used in a tracer experiment over a short distance near the glacier terminus.

2.2. Fluorometry

To measure the fluorescence of the dyes, a filter fluorometer, Turner 111, was used. The basic instrument is described by Wilson (1968) and major components of the Turner 111 filter fluorometer used in this study are shown in the Turner Manual (1977, pg. 4). The instrument was kindly loaned by the U.S. Geological Survey, Glaciology Project Office, Tacoma, Washington, and initial training in its use was provided by Mr. Robert Krimmel of this organization. Fluorescence measurements made with this instrument were initially checked in relation to detailed absorption and emission spectra made with the spectral fluorometer noted in the previous section. Approximately twenty samples and standards were crosschecked with the two instruments.

Filter and lamp optimization was carried out using standard procedures for both the filter and spectral fluorometers (Smart and Laidlaw, 1976; W. Turner, personal communication, 1983). Different lamps and filter sets were used for Rhodamine WT and Tinopal AMS. A near-UV lamp (Turner standard number #10-049), which excites between 310 and 390 nm, was used for Tinopal AMS, and a F4T5 clear quartz lamp without phosphor (#10-046), with maximum excition at 555 nm, was used for Rhodamine WT. For Rhodamine WT a Turner #10-056 filter (marked #546) was used as the excitation (or primary) filter, and two Kodak filters (#23-A and #3-66) were combined for use as the emission (or secondary) filter.

Measurements of sample fluorescence are given in "fluorometer units" as read from the meter of the Turner 111 instrument. The background fluorometer reading for blank samples (zero concentration of tracer) was set to 0.16 fluorometer units for Rhodamine WT and to 7 fluorometer units for Tinopal AMS. Since the meter of the

instrument does not give readings below zero, these arbitrary blank (background) settings were chosen to insure that all meter fluctuations could be followed. Information provided by Turner Designs (1981) indicates that the concentration of Rhodamine WT tracer dissolved in clean water can be measured down to the 0.001 ppb level with the Turner 111 instrument. In the present work it was found that Rhodamine WT tracer concentration could be reliably measured down to only the 0.01 ppb level. The level of detection for Tinopal AMS was about 1 ppb. In order to obtain the limit of detectibility for each tracer, it was necessary to consistently read the midpoint of fluctuations of the meter needle and maintain standard measurement conditions.

A second instrumental setting is called *span*; it affects the proportionality relation between the fluorometer reading, in "fluorometer units", and the actual intensity of fluorescent radiation from the sample. Its adjustment, which directly affects the fluorometer calibration, is discussed in Section 2.4. Once the optimum choice of filters, lamp and instrument settings was found for each dye, this instrumental configuration was standardized and was held constant throughout the study. The instrument was regularly checked for calibration using standard samples.

2.3. Procedures for Fluorometric Measurement of Water Samples

The accuracy and reproducibility of filter-fluorometer measurement at very low tracer concentrations is crucial to this work because of the very low peak levels (ppb and below) at which the tracers were returned in the outflow water from the glacier in some of the experiments carried out. Special precautions in the fluorometric measurement procedure, as well as in the sampling, were necessary to work successfully at the low detection level needed.

Throughout each set of fluorometric measurements, which involved running a group of samples and a set of standards, the type and orientation of the glass cuvette holding the water sample in the fluorometer had to remain unchanged, because a change from one cuvette to another, or in the orientation of a given cuvette in the sample holder of the instrument, changes the low-level fluorescence reading. Similarly, a change in the light bulb or filters, or in their orientations, affects the detected fluorescence; hence, all of these components had to be marked and held fixed in order to achieve reproducible low-level readings. The fluorometer readings are also affected to some extent by the ambient temperature and by the voltage of the battery powering the instrument. The voltage was maintained by keeping the battery as fully charged as possible, and the laboratory temperature held at $22^{o} \pm 1^{o}$ C. Water or sediment on the outside surface of the sample cuvette affects the readings at the ppb level. Hence, before each cuvette was introduced into the fluorometer, its surface was wiped clean of outside water and sediment. Towels used for this purpose must not contain any material fluorescent in the wavelength range employed. Towels, glassware, rinse water, methanol, sample bottles, and all other materials and implements associated with the experiments (including human bodies) were thoroughly tested and cleansed of fluorescent materials before measurements were undertaken. This was particularly important for measurement of Tinopal AMS, because contamination by optical brighteners is widespread, these substances being extensively used in the detergent, fabric, and paper industries.

Before loading each sample into a cuvette for measurement, the cuvette was first rinsed repeatedly with clean water until the rinse water in the cuvette gave the fluorescence reading for zero concentration. In the measuring a set of samples

containing Rhodamine WT, normally two to five rinses were required to reach the background level. In the measuring of Tinopal AMS, normally more rinses were required (three to ten), suggesting a significant tendency for this dye to be adsorbed on the glass of the cuvette.

Important further experimental procedures were required to deal with the effects of suspended sediment in water samples. These are discussed in Chapter III. With the above procedures, it was possible in this work, as noted above, to make reliable laboratory measurements of Rhodamine WT tracer concentration down to 0.01 ppb, and of Tinopal AMS concentration down to about 1 ppb.

In fluorometric measurements made in the field, which were undertaken in an attempt to follow the results of the tracer experiments in real time and to guide the water-sampling schedule, some of the requirements specified in the foregoing procedures could not be fully met. By far the greatest limitation on useful field measurements was the effect of water turbidity, discussed in Chapter III. In addition, nonconstancy of ambient temperature, fluctuations of battery voltage, difficulty in maintaining a dust-free, condensation-free, and contamination-free environment for the fluorometer under field condition and other such factors interfered with the validity of the field measurements and caused some discrepancies between fluorometric readings made in the field and repeated later in the laboratory. Except for data on clean water standard solutions (prepared with triple-distilled water), all concentration data given in this thesis are based on measurements made in the laboratory on samples brought back from the field.

To minimize the photochemical degradation of the dye, samples were kept out of the sunlight as much as possible. Repeated fluorometric comparisons between freshly

made standards and standards that had been made up initially and retained showed no detectable degradation of the older samples. The spontaneous degradation of the undiluted dye stock cannot have been great, because calibration curves did not change detectably over the course of the work, lasting about eight months.

2.4. Fluorometer Calibration

Fluorometer calibration for measurement of Rhodamine WT and Tinopal AMS was done in the laboratory and also in the field. For Rhodamine WT, four sets of calibration standards (dye diluted with triple-distilled water) were measured in the laboratory. The results are in Figures 2.3, 2.4 and 2.5. For each set of sample measurements the fluorometer units read from the instrument were calibrated in terms of dye concentration units (ppb). The calibration was done by plotting fluorescence readings for different standard samples against the known tracer concentration of each solution. Figure 2.3 is plotted on linear scales for fluorescence reading and actual tracer concentration. Figure 2.4 gives the calibration data for Rhodamine WT at the lower end of the concentration range, in a log-log plot. Figure 2.5 is a log-log plot of the calibration data over the range 1 to 1000 ppb. The calibration measurements were repeated throughout the study to check the reproducibility of the calibration curves.

The calibration curve for Rhodamine WT is linear for concentrations ranging from 0.1 to 1000 ppb. The curve becomes nonlinear below 0.1 ppb (Fig. 2.4). Detection may be made to concentrations as low as 0.01 ppb if the sample is free of suspended sediment, and all measurement precautions are taken (Section 2.3). The feasibility of the detection limit of $\sim$ 0.01 ppb can be judged from the data points in

Figure 2.4.

Three sets of calibration standards were made up in the field, using water samples obtained from Variegated Glacier outflow streams during May, June and July 1983. The calibration data for these standards, which are affected by water turbidity, are discussed in Chapter III. The effect of methanol solvent on dye fluorescence had to be assessed because methanol was used in the measurement of Rhodamine WT adsorbed on suspended sediment, as discussed in Chapter III. Calibration curves for Rhodamine WT dissolved in pure methanol are shown in Figures 2.4 and 2.5. The calibration curve for the dye dissolved in methanol differs significantly from that for the dye dissolved in water. The emission fluorescence spectra for the dye dissolved in methanol and in water are not qualitatively different. The only difference between the spectra is in the height of the emission peak. Rhodamine WT is more fluorescent in pure methanol than in water by a factor of about 1.9 in the range 0.1 to 1000 ppb (Figs. 2.4 and 2.5).

Calibration data for Tinopal AMS solutions are shown in Figures 2.3 and 2.6 . The limit of detectibility for Tinopal AMS indicated by Figure 2.3b is approximately 1 ppb. A change in slope of the calibration curve occurs at approximately 60 ppb (Fig. 2.6). At concentrations below about about 0.5 ppb the fluorescence of Tinopal AMS cannot be detected above the background.

2.5. Tracer Injection Technique

The tracing experiments were carried out by injecting dye at the bottom of the glacier (or as close to it as possible) via boreholes. The borehole drilling for the dye tracer injection was done with a hot-water drill designed mainly by Phil Taylor and

Barclay Kamb. The capability of this drill to reach the glacier bed through the overlying debris-laden ice was enhanced by occasional use of a drill tip with a hot-water jet inclined 45^o away from the downward vertical. The 45^o tip allowed drilling of a a side hole into which rock debris that had accumulated at the bottom of the main hole was diverted. In the process of trying to make sure that the bed was reached, the drill was normally run at full power for several hours after it had come to a complete stop at the maximum depth reached. In this process a cavity of some size must have been melted out at the bottom of the borehole. Boreholes were about 400 m deep in the area of the glacier where the Rhodamine WT dye injection was carried out, which was about 10 km upstream from the glacier terminus.

Dye injection in each experiment was done at a time when borehole conditions for injection were optimal, to the extent that this was possible under prevailing operational constraints. An optimal condition consists in a good connection of the borehole to the basal water system, so that dye pumped to the bottom of the hole will rapidly leave the hole and enter the basal water system. The quality of the connection was judged before dye injection by the height and fluctuations in height of the water level in the hole in comparison to adjacent boreholes, and by any signs of downflow of water in the borehole near the bottom, as discussed in detail later (section 4.2). After dye was injected, the quality of the connection was judged by the rate at which dye disappeared from the bottom of the borehole. This was monitored by obtaining water samples from the bottom of the hole every few hours after injection, with use of a water-sampling device, or, more crudely, by noting any dye visibly adsorbed on the drill stem or hose when they are removed from the hole after injection.

Introduction of dye into the borehole was carried out by pumping the dye to the bottom of the borehole through the drilling hose, at a pumping rate of about 15 l/min, which injected a 23-l slug of tracer in somewhat less than 2 minutes. The dye injection was followed by pumping down clean water, first through the drilling system, until the input tank was clean of dye, and then directly into the top of the borehole, after the rinsed drilling hose had been withdrawn. The dye injection and drilling-hose rinse required about 20 minutes. Subsequent pumping of water into the hole at the top was continued for several hours with the aim of maximizing the throughput of water through the borehole to the basal water system and thus completing the dye injection as quickly as possible. As explained later (Section 4.5), injection of Tinopal AMS was a more cumbersome process and took about two hours.

2.6. Sampling of Glacier Outflow Water

Water samples for dye fluorescence measurement were obtained from the terminus outlet streams on a sampling time schedule to be described later for the individual tracer experiments. The samples were dipped from the stream margins in places of the fastest moving water accessible from the stream bank. Each sample was dipped directly into its sample bottle, after the bottle had first been rinsed once or twice with the stream water, to reduce any chance of contamination from the bottle. The water was drawn into the bottle just below the stream surface. Sample bottles were new, of 250 ml capacity, with tightly sealing screw caps; about half of the bottles used were glass; the rest, Nalgene. Such bottles were also used to store the prepared tracer standards. Calibration tests showed that no detectable contamination is attributable to the bottles as received (new), except for the occasional presence

of brightener-type contamination in the paper gaskets of the caps for the glass bottles; such gaskets were accordingly not used in sampling for detection of Tinopal AMS.

In the sampling we attempted to obtain water from all outlet streams that were delivering a significant part of the total water discharge from the glacier. Limitations on the feasibility of doing this were placed by manpower and by remoteness and inaccessibility of some outlet streams, particularly on the north side of the glacier. The actual location of streams sampled is given in Section 4.1.

Table 2.1
Properties of Fluorescent Dyes Tested

Type of Dye[1]	Spectral Peak		Detection Level	Price[2]
	Excitation (nm)	Emission (nm)	(ppb)	(dollars)
Rhodamine WT	555	580	0.01	8.31
Tinopal AMS	353	443	1.0	3.44
Tinopal 5BMY	352	440	1.0	3.15
Tinopal CBSX	349	431	0.3	11.50
Optiblanc	350	478	0.50	41.00
Fluoresceine[3]	490	520	0.29	
Rhodamine B	555	580	0.01	5.50
Amino G Acid	355	445	0.5	

1. As dissolved in water.
2. Price per pound quoted by Ciba-Geigy Corp., 1983.
3. Smart and Laidlaw (1976, p. 16).

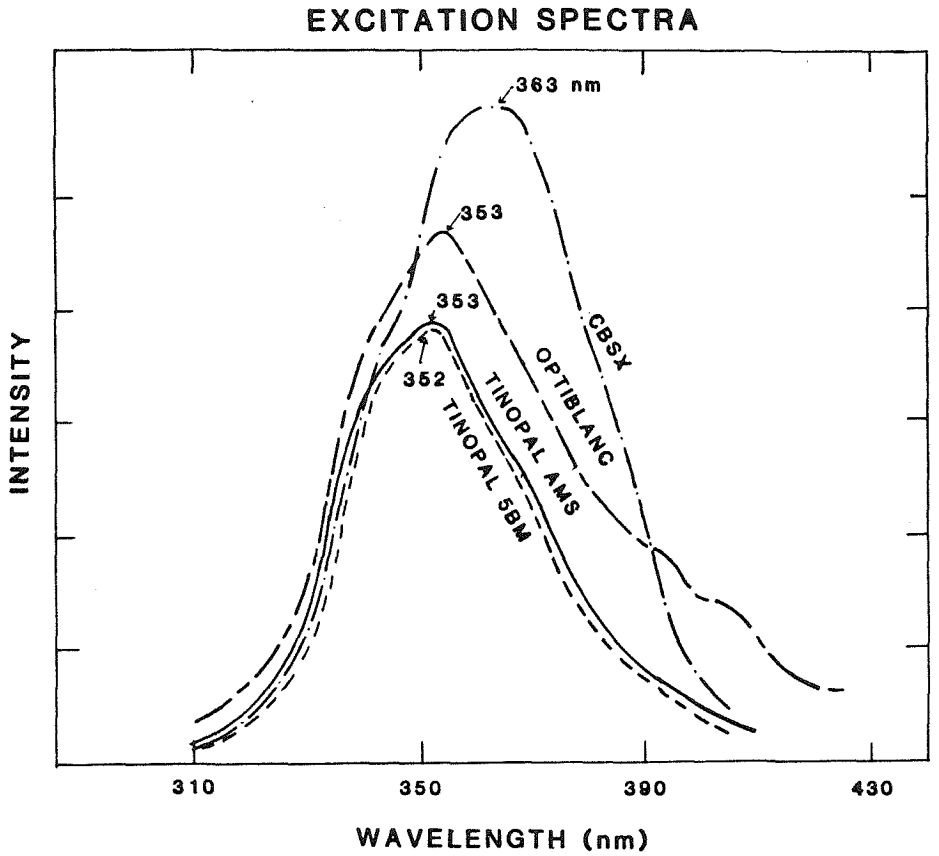

Figure 2.1 Excitation (absorption) spectra of optical brighteners tested in this study.

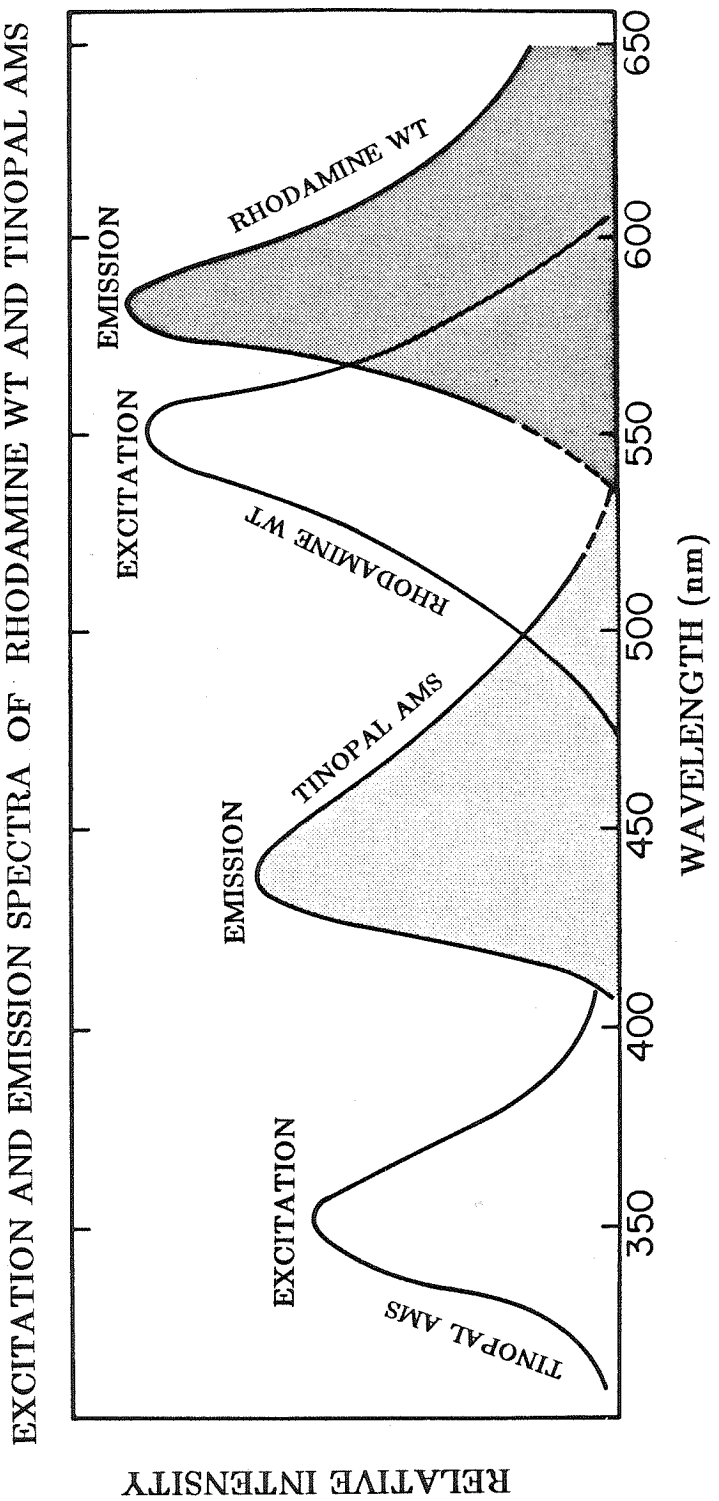

Figure 2.2 Excitation and emission spectra of Rhodamine WT and Tinopal AMS. Unshaded curves are excitation spectra and shaded curves are emission spectra.

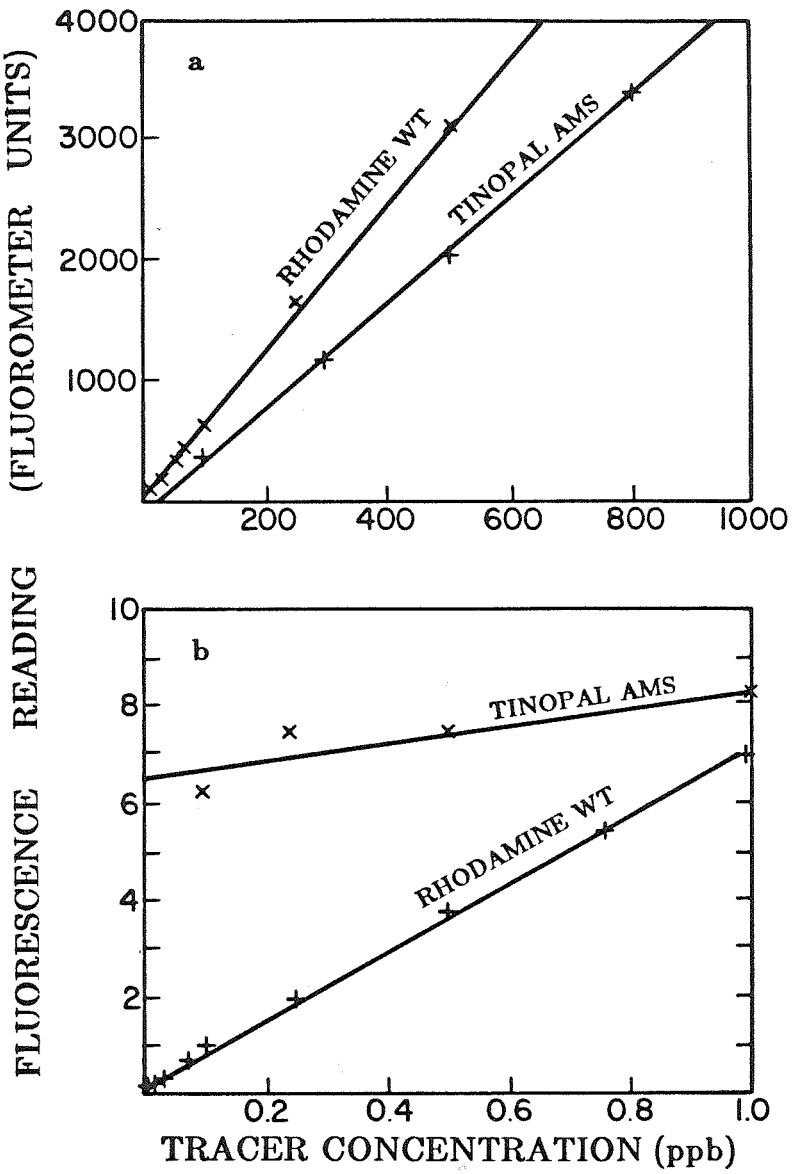

Figure 2.3 Fluorometer calibration curves for Rhodamine WT and Tinopal AMS in water. Fluorescence reading (Turner 111 fluorometer) is plotted versus tracer concentration (a) over the range 0-1000 ppb, and (b) over the range 0-1 ppb.

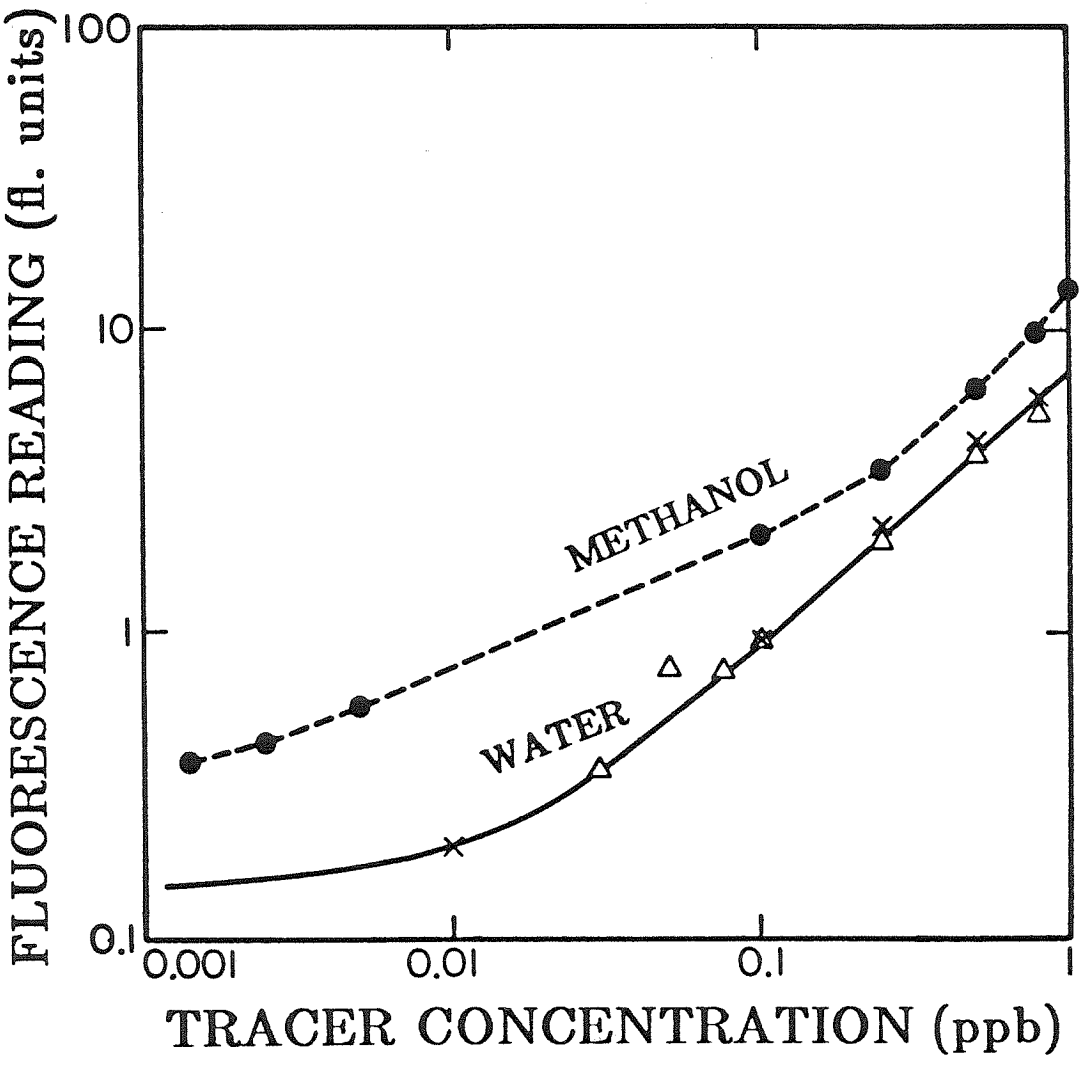

Figure 2.4 Fluorometer calibration curves for Rhodamine WT in water and in methanol. Fluorescence reading is log-log plotted versus tracer concentration from 0.001 to 1 ppb.

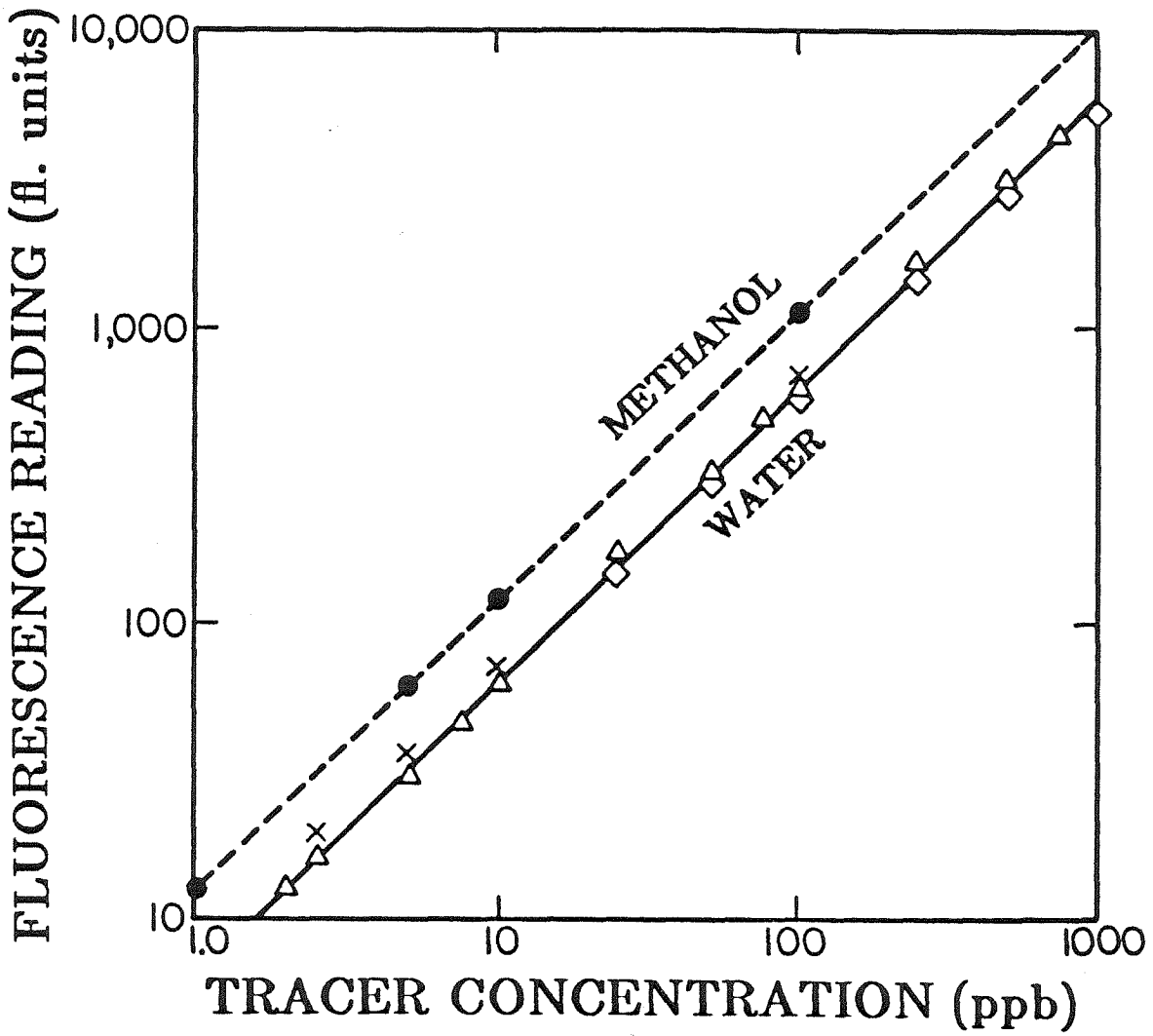

Figure 2.5 Fluorometer calibration curves for Rhodamine WT in water and in methanol. Fluorescence reading is log-log plotted versus tracer concentration from 1 to 1000 ppb.

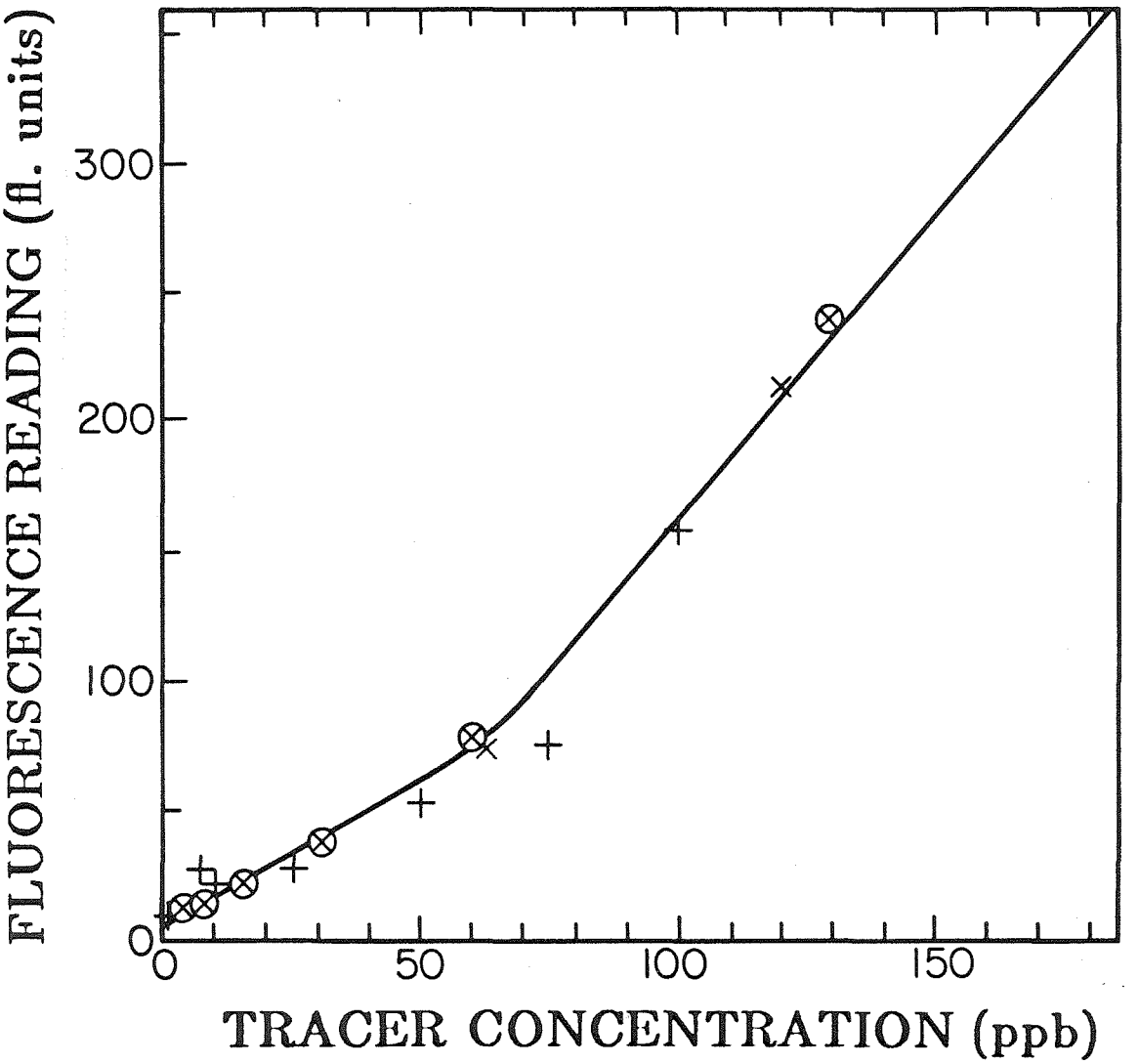

Figure 2.6 Fluorometer calibration for Tinopal AMS in water, range over concentrations 0 to 130 ppb. The different symbols are represented as follows: "+" and "x" represent standard solutions prepared from triple-distilled water at different testing dates, and the "x" represent sample solutions prepared from turbid water, with a suspended sediment content of about 35 g/l, collected on June 21, 1983 from terminus stream TC (Fig. 4.1).

Chapter III:
EFFECTS OF SUSPENDED SEDIMENT IN DYE-TRACER EXPERIMENTS

3.1. Introduction

The water samples obtained from the Variegated-Glacier outflow streams were without exception highly turbid due to fine suspended sediment (glacial flour). The complications that turbidity can cause in dye-tracer experiments have been discussed by Smart and Laidlaw (1976) and by Smart and Smith (1976), but in most published dye-tracer studies of glaciers these complications have not been taken into consideration. Suspended sediment in the outflow water from Variegated Glacier in surge was at a much higher concentration than normally encountered in glacier outflow, so high that its effects on the dye-tracer experiments cannot be ignored. It was necessary to develop new concepts and procedures for dealing with these effects in the present study. The approach developed may also be useful in future water-tracing experiments in glaciers where large amounts of rock flour are present or where there is extensive contact between basal sediments and the water whose movement is being traced.

Suspended sediment has two quite separate effects on the dye-tracer experiments: 1. Turbidity interferes in a somewhat complicated way with the measurement of tracer concentration in the water phase. 2. Adsorption of dye on the sediment particles can withdraw a significant fraction of the dye from solution in the water phase, removing it from detection by standard fluorometry. It was necessary to deal with both of these effects in the present experiments.

3.2. Effect of Turbidity on Fluorometry

Water turbidity causes an increase in the apparent fluorescence background level registered by the filter fluorometer for turbid water samples containing no dye. This effect is shown by the data in Fig. 3.1, in which fluorescence readings from turbid, dye-free samples are plotted as a function of the time that each sample was allowed to stand and settle after being dipped from an outflow stream, before being measured in the fluorometer. To measure such a sample, the less turbid supernatant water in the sample bottle is decanted off the settled sediment at the bottom, directly into the sample cuvette. The fluorescence readings in Fig. 3.1 were obtained with filter and lamp configuration for detection of Rhodamine WT. As the figure shows, there is an initial rapid rise in fluorometer reading, followed by a gradual fall, as settling gradually clarifies the supernatant. The broad spread of the individual data points around the general trend is due to variations from sample to sample in initial turbidity and in particle size distribution as it affects settling rate and light scattering by the sample.

It is not known exactly how the water turbidity causes the fluorescence readings in Fig. 3.1 to be increased over the background value of 0.16 fluorometer units for pure, dye- and turbidity-free water. Three possible explanations may be suggested: 1. The scattered light intensity from the sample may be so great that the long-wavelength tail of the spectrum passed by the excitation-band filters, weak as it is, may contain detectable energy in the band passed by the emission-band filters. 2. The sediment (rock) particles may have a weak but detectable fluorescence with excitation and emission bands in the ranges selected by the filters. 3. A similar fluorescence in the emission-band filters might be excited by scattered light from the sample.

The increase in apparent fluorescence background for turbid samples has been noted by Turner (1977) but has been overlooked in the hydrological and glaciological literature on dye-tracer experiments.

Because of the turbidity-caused increase in background fluorescence reading, tracer concentrations at low levels will be falsified toward higher values. In relation to the calibration curves in Figures 2.3 and 2.4 for turbidity-free water, the background levels in Figure 3.1 cause a serious interference with detection of Rhodamine WT tracer at the 0.2 ppb level, for settling times of less than about 10 days. For settling times of a day or less, there is strong interference with tracer detection at a level of several ppb. Within the first few hours, the turbidity is so high that it blocks light from reaching the photomultiplier. After a settling time of one day, a peak is reached indicating false concentrations of several ppb, and more than a week of settling is required for the background to reach 1 fluorometer unit. The detection limit of 0.01 ppb can be reached only after a settling time much longer than 20 days.

The effect of turbidity on the fluorometry of calibration samples containing known amounts of dye is shown in Fig. 3.2, in which, again, fluorescence readings are plotted versus settling time. Samples T1, T2, and T3 were outflow-stream samples that had clarified by settling for about three months. Fluorometry of the supernatant from each settled sample indicated no Rhodamine WT tracer present. To each supernatant sample a chosen amount of tracer was added; this resulted in the fluorometer readings indicated by the data points shown at abcissa "-1" in Fig. 3.2. Each supernatant was then returned to its original sample bottle and shaken to resuspend the previously settled sediment. Fluorometer readings obtained immediately after shaking are plotted at time 0, and readings after subsequent periods of

settling are plotted at the corresponding times in Fig. 3.2. The initial high turbidity causes an almost complete suppression of the fluorescence readings, presumably because of the opacity of the sample. The first day or so of settling causes partial recovery toward the pre-shaking fluorescence reading. This is followed by a subsequent slow, slight decrease. The initial recovery seems to be an obvious consequence of a substantial decrease in opacity, although after only one day of settling the samples still appear very turbid. With subsequent settling the fluorescence reading decreases an average of three units. The decrease is explainable as a decrease in extra background of the kind seen in Fig. 3.1. Perhaps it is caused by a progressive increase in the amount of dye that becomes adsorbed onto the sediment as time progresses. Adsorption is probably responsible for the fact that the recovery after shaking is to only about 1/3 to 2/3 of the initial fluorometer reading.

Although data to document sufficiently an interference of turbidity with fluorescence measurements for Tinopal AMS were not obtained, effects such as high adsorption on organic material, described in literature for brighteners (Smart, 1976), presumably occur. The instrumental background level for Tinopal AMS in pure water is already high, as indicated by Fig. 2.6. Laboratory tests similar to those shown on Fig 3.2 were conducted for Tinopal dye, and indicate interference from sample turbidity is probably less of a factor in the use of this material than for Rhodamine WT.

To minimize the interference of sample turbidity with the fluorometer measurements in the field, samples were allowed to stand and settle for as long as possible, generally at least several days, before being measured. This procedure was, of course, in conflict with the need for the tracer data in real time, to guide the conduct of the

experiment in terms of sampling locations and schedules. In two of the three experiments carried out, the highest tracer levels in the samples were too low to be detected in the presence of the turbidity that remained after even several days' settling, and at the time, in the field, it was thought that these experiments were failures.

All samples were returned to Pasadena and remeasured in the laboratory after a settling time of two to four months. During this time, and with the possible assistance of natural flocculation, the supernatant clarified completely in all samples. The laboratory fluorometer measurements could therefore be carried out without interference from turbidity. All fluorometrically determined tracer concentrations reported in this thesis are based on the fluorometer measurements carried out in the laboratory on clarified samples.

3.3. Dye Adsorption on Sediment

The suspended sediment in Variegated Glacier outflow water absorbs an appreciable fraction of any Rhodamine WT present, so that the tracer concentration in the water phase, which is what is detected fluorometrically, is appreciably less than the total content of tracer in turbid samples. This effect was noted already in the data of Figure 3.2.

More extensive examples of the effect of dye absorption are given in Figures 3.3 to 3.6, which show data from three sets of calibration samples prepared with turbid water from the glacier. Measured amounts of rhodamine dye were added to the turbid water samples, the turbidity was allowed to clarify by settling, and the fluorescence was measured. In Figures 3.3 through 3.6, the fluorescence readings are plotted against total sample content of tracer based on the amount of tracer stock added to

each sample in preparing the standard. The extent to which the data points in Figure 3.3 fall below the calibration line for standards made up from turbidity-free water is an indication of the extent to which dye has been withdrawn from solution in the water phase by adsorption on sediment.

The samples in sets A and B have a much larger sediment content than the samples in set C. Correspondingly, the data points for sets A and B in Fig. 3.3 fall much farther below the calibration line than do the points of set C, as is reasonable if the decrement is due to dye adsorption on the sediment. Sets A and B consist of water samples taken when the glacier was in surge and the outflow water was extremely turbid, whereas the samples of set C were taken after termination of the surge, when the turbidity had decreased. Sediment-content values for the various sample sets are given in Figure 3.4b and summarized in Table 3.1. Set-A samples have sediment concentrations in the range 50 to 100 g/l, and set-B samples have 10 to 20 g/l. The irregularities in the pattern of data points for set A in Fig. 3.3 and 3.4a are to a considerable extent explainable by the variations in sediment content from sample to sample (Fig. 3.4b). The samples of set B were all collected at the same time (12:00 on June 18, 1983), whereas those of set A were collected at various times during May and June; hence, set A has a greater variation in sediment character and content, and consequently a greater irregularity of data points in Fig. 3.3 and 3.4, than does set B.

The data for sets A and B in Fig. 3.3 suggest that as much as half to two thirds of the dye volume in these samples is carried in adsorption on the suspended sediment. Such a large fraction, if generally applicable to the water samples of the dye tracer experiments on Variegated Glacier, definitely needs to be taken into account in any quantitative interpretation of the experiments, and particularly in the

quantitative assessment of the total dye return in each experiment. For these purposes it is important to be able to determine the amount of dye actually carried in adsorption on the sediment in each sample. A method for doing this was therefore developed, as described in the next section.

Tests with Tinopal AMS indicated no detectable adsorption of this dye on the suspended sediment, in agreement with the lack of adsorption of similar brighteners tested by Smart and Laidlaw (1976).

3.4. Measurement of Adsorbed Rhodamine WT

To measure the amount of Rhodamine WT carried in adsorption on suspended sediment in a turbid water sample, the method that I have developed consists of extraction (desorption) of the dye from the rock-particle surface into solution in methanol, followed by fluorometric measurement of the methanol solution with the filter fluorometer. It is a modification of a method suggested by Aley and Fletcher (1976, p. 13).

The desorption procedure is as follows. After the turbidity of the sample has spontaneously cleared by long-term settling in the usual way (Section 3.2), the clear supernatant water (amounting to about 230 ml) is decanted off, leaving in the sample bottle the settled sediment and only a small amount (normally less than 1 ml) of undecanted water. Methanol in an amount equal to the volume of water decanted is then added to the bottle, and the bottle is capped tightly and shaken to resuspend the sediment. After resettling, the clear methanol supernatant is decanted into the sample cuvette and its fluorescence is measured in the filter fluorometer. The solution is then returned to the sample bottle, shaken again, and the procedure repeated until

the fluorescence reading becomes constant, showing that an equilibrium has been reached between dye dissolved in the methanol solution and dye remaining absorbed on the sediment. This normally requires several repetitions and can be accomplished in about 12 hours. A final measurement is made after once more resuspending the sediment and allowing the sample to stand for several days. Tests on some samples after standing an additional several weeks showed no further change in fluorescence reading.

The settling of suspended sediment from the methanol solution proceeds much faster than the initial settling from the water samples. Settling from methanol is for practical purposes complete in 3 hours, whereas the initial settling required many weeks. The increased settling rate is in part due to the lower viscosity of methanol (0.39 cp at 20^{o} C, as compared to 1.01 cp for water), but the increase in settling rate is much greater than expected from the decrease in viscosity. It seems likely that natural flocculation during the initial settling period gathers the very fine (micron-sized) particles into larger aggregates that settle faster. Perhaps flocculation is also promoted by the methanol.

In the desorption procedure, methanol is used rather than water because of a chemical interaction between methanol and Rhodamine WT, which greatly weakens the adsorption of the dye on most solid surfaces. This effect is readily noted when methanol is used, as it is in practice, to clean up spills of Rhodamine WT. In developing the desorption procedure, other solvents were tried, but methanol was the most effective.

The fluorometric measurement of Rhodamine WT in methanol solution requires, of course, calibration. This is dealt with in Section 2.4, where it is shown that the

dye fluoresces more strongly by a factor of about 1.9 in methanol solution than in water. The calibration curve is shown in Figures 2.4 and 2.5 . It applies to the fluorometer configuration (lamp and filters) used for measurement of Rhodamine WT in aqueous solution.

If in the desorption procedure the volume of methanol used is the same as the volume of supernatant water initially decanted, then the concentration of tracer measured in the methanol solution after extraction, based on the calibration curve just discussed, can be equated directly with a bulk concentration in the original sample after correction for the small volume of water and sediment left behind in the original decantation. In those instances where the volume of methanol used was not the same as the volume of decanted water, the measured dye concentration in the methanol solution was first corrected by scaling to correspond to the volume of decanted water. The dye in solution in the small amount of water left behind with the sediment in the original decantation of the supernatant water will appear in the methanol solution and thus be counted as absorbed dye, so that on this account the ratio of adsorbed to dissolved dye should be slightly overestimated by the measurement method.

The effectiveness of the desorption procedure and fluorometry in yielding a quantitative measurement of the dye carried in adsorption on sediment is tested in two ways. First, it is readily shown that the methanol extraction procedure leaves no dye that can be detectably extracted by a repetition of the extraction with a second aliquot of pure methanol. This was tested on several samples. The extraction is therefore complete for all of the adsorption surface to which the methanol has access. There is, however, the possibility that some dye molecules may become trapped inside

aggregates of fine particles during the flocculation process and may thereby become inaccessible to methanol extraction.

The second and more general test is the test of mass balance in recovery of Rhodamine WT from standard calibration samples prepared from turbid water by the addition of known amounts of tracer. Data on the tracer carried in solution in such samples, henceforth called the *dissolved tracer,* are in Fig. 3.3, already discussed. In Fig. 3.4a are shown the fluorescence readings obtained for the methanol extracts from these samples by the extraction and fluorometry procedure described above. From the fluorescence readings the detected amount of *adsorbed tracer,* the amount of tracer carried in adsorption on suspended sediment in a turbid water sample, is obtained from the calibration curve for methanol in Figure 2.5, with volumetric correction (if needed) as discussed above. The contents of adsorbed (as well as dissolved) tracer are expressed as concentration in ppb, tracer volume per bulk volume of water sample including suspended sediment.

On the abscissa in Figure 3.4a is the total bulk concentration of tracer based on the known amount of tracer initially added to each sample in preparing the standard. Figure 3.4a shows that within each sample set the concentration of adsorbed tracer generally increases with the total tracer concentration, as would be expected for adsorption equilibrium in samples having a fixed sediment component. There are, however, two marked deviations from this monotonic relation; in the case of the set-A sample at total concentration 50 ppb, the deviation to a high absorbed-tracer level may be due to the particularly high sediment content of this sample (see Figs. 3.4b). The lower concentration of adsorbed tracer measured in the set-C samples, at any given level of total tracer reflects the lower sediment content of these samples (Fig.

3.4).

The mass-balance test is obtained by combining the measurements of dissolved tracer from Figure 3.3 with those of absorbed tracer from Figure 3.4 . This is done in Figures 3.5 and 3.6. The dissolved plus adsorbed tracer concentration is plotted on the ordinate in terms of the "equivalent fluorescence," the fluorometer reading for the same concentration of tracer in aqueous solution. Mass balance is therefore satisfied if this procedure regenerates the calibration line for Rhodamine WT in pure water, which is plotted in these figures, from Figure 2.5. The set-C data (Fig. 3.6) satisfy mass balance best, with few complications. The sediment content of these samples being relatively low (0.2-18 g/l), there is relatively little absorbed tracer and it constitutes only a small addition to the dissolved tracer, which brings the total measured tracer close to the known amount. For some samples there is a slight deficit, up to about 10% of the total tracer amount. For the set-A samples, with high sediment loads (50-100 g/l), mass balance is more poorly satisfied (Fig. 3.5). The discrepancy is particularly glaring for the set-A sample at total tracer concentration 70 ppb. The discrepancies are probably not due to a trapping of dye molecules in flocculating particles, because this would probably give a more systematic deficit from mass balance than is seen in Figures 3.5. The discrepancies in mass balance could be caused in part by manipulation errors in carrying the samples through the desorption and fluorometry procedure, but their cause is not known, and they indicate that there are unresolved problems in the procedure. (There were not enough samples to permit these tests to be repeated.) Nevertheless, the improvement in mass balance obtained by including measurement of the absorbed tracer is substantial and indicates that a considerably improved picture of the dye return in tracer experiments, under

conditions of high sediment load, is obtained by measuring the dye content by the method described. It is later shown (Section 4.3) that during the surge, more than half of the return of dye in a tracer experiment was often carried in adsorption on suspended sediment, and at times more than 90% was so carried.

3.5. Characteristics of Dye Adsorption on Sediment

If the effects considered in the last section are correctly attributed to adsorption of dye on suspended sediment, then they should conform to known physical principles governing the adsorption phenomenon. When the dye has reached adsorptive equilibrium with the sediment at a given temperature, there should be a definite relation, known as the adsorption isotherm, among the concentration C of dissolved tracer (dye per unit volume of turbid water), the concentration m of sediment (grams of sediment per liter of turbid water) and the amount of adsorbed tracer S (expressed as bulk concentration, tracer per unit volume of turbid water). The Langmuir adsorption isotherm, given in standard treatments of the subject (e.g. Fried et al., 1977, p. 712-23), has the form

$$\frac{S}{m} = \frac{k_1 C}{1 + k_2 C} \tag{3.1}$$

where k_1, and k_2 are constants. Also often used is the Freundlich isotherm

$$\frac{S}{m} = k_3 \, C^n \tag{3.2}$$

where k_3 and n are constants. The exponent n has values in the range 0.2 to 0.5 for adsorption relationships to which (3.2) is typically applied. From the thermodynamic point of view, the Freundlich isotherm is usually regarded merely as an

empirical approximation to (3.1), representing, over limited ranges of concentration C, the effect of the nonlinearity contained in the denominator on the right in (3.1).

In order to test the conformity of adsorption data given in Figures 3.4 to 3.6 to the description of adsorption behavior given by (3.1) or (3.2), dissolved tracer concentrations (C), adsorbed tracer concentrations (S), and sediment concentrations (m) are plotted in terms of S/m versus C in Figures 3.7 and 3.8. Figure 3.7 is based on adsorption values S calculated by difference, subtracting the measured concentration of dissolved tracer from the total bulk concentration that was established by the amount of tracer initially added to each standard sample. Figure 3.8 is based on S measured by the desorption and fluorometry technique described in Section 3.4. The two plots are roughly consistent; they differ in a way indicating that the absorbed tracer levels as directly measured are slightly lower than as determined by difference, which reflects in a general way the shortfall of the measured values in satisfying mass balance, discussed in the previous section. Figure 3.9 is a similar plot of S/m versus C for regular samples collected from the glacier outflow streams during June and July, 1983, and not used for preparation of standards.

The general trend of the data points in the log-log plots in Figures 3.7 to 3.9 follows a line of slope 1, indicating a linear relation between S/m and C. This conforms to the Langmuir adsorption isotherm (3.1) at low dye concentrations C such that $k_2C << 1$. Since the concentrations are very low ($C < 10^{-6}$), the condition $k_2C << 1$ is entirely reasonable in relation to typical values of k_2 for other adsorption systems (Fried, Hameka and Blukis, 1977, p. 615). There is no indication, within the scatter of the data points in these figures, of a log-log slope differing from 1, and a slope in the range 0.2 to 0.5 is certainly precluded; hence, the Freundlich isotherm

(Eqn. 3.2) can be dropped from consideration, and the Langmuir isotherm can be simplified (with neglect of k_2C) to

$$\frac{S}{m} = k_1 C = K_d C \ . \tag{3.3}$$

The Langmuir constant k_1 is called the absorption constant and designated K_d when m in (3.3) is taken in units of g/ml, so that K_d has dimensions ml/g. In plots of the type given in Figures 3.7-3.9, the indicated K_d value can be read off as the numerical value of S/m at $C = 1$ ppb.

The rather large scatter of the data points about the regression lines in Figures 3.8 and 3.9, particularly for the set-C data, reflects either rather large errors (as much as a factor of 10) in the measurements and procedures on which the data are based, or else rather large variations in the adsorptive properties of the suspended sediment in the different samples on which the calibration and desorption measurements were made. Large variations in the effective adsorption constant K_d from sample to sample could result from large variations in sediment particle mineralogy as it affects the surface-specific adsorptive property of the sediment, or from large variations in sediment particle size distribution as it affects the relative proportions of very fine and coarser particles and therefore the particle surface area per unit mass of sediment. Available information is insufficient to examine completely the possible variations that could contribute to variations in K_d from sample to sample in the data of Figures 3.7 to 3.9.

Closed (solid) symbols in Figures 3.7 and 3.8 are data points for calibration standards prepared from highly turbid water (sediment content 50-100 g/l, sample sets A, B and T), and open symbols are for standards prepared from moderately turbid water

(sediment content 10-20 g/l, set C). In spite of the large scatter of the data points from set C, there is a definite indication in Figures 3.7 and 3.8 that K_d for the set-C samples is as a whole larger by a factor of about 3 than K_d for sample set A. This possibly suggests a change in the sediment particle size distribution toward a higher proportion of finer particles in the set C samples, which could be due to a change in the geometry of the basal water-conduit system and the water flow through it, from surge conditions (sets A and B) to non-surge (set C).

Figure 3.9 is a plot of S/m against C for water samples containing Rhodamine WT coming from the glacier, that is, from dye injected into the glacier in dye-tracer experiments. The different symbols used for data points on Figure 3.9 are grouped in terms of the sampling time intervals as indicated in the key, and separated as follows: open circles for June 10-12; solid triangles for June 13-15; "+" for June 15-23, "x" for June 24-26, and solid squares for July 16-18. A line of slope 1 fitted to the strong cluster of points at concentrations C around 1 ppb (10^{-9}) passes through the upper part of the widening fan of points at lower concentrations, where there are a few points that fall at S/m values as much as an order of magnitude below the line. There is no motivation to consider fitting a line of steeper slope to the data, because Equation (3.2), the possible alternative to adsorption isotherm (3.3), always has in practice a log-log slope n less than 1, and also because the data points that suggest a steeper slope are at extremely low tracer concentrations (< 0.1 ppb), where the errors of measurement are unavoidably larger than at ~ 1 ppb. The best-fit line in Figure 3.9 corresponds to a K_d value of about 30 ml/g, approximately the same as for set A in Fig. 3.8. Curiously, the post-surge data from all streams in Figure 3.9 (July 16-18) correspond to a lower K_d (ca. 10 ml/g), in contrast to the post-surge

data from only the Lower Stream in Figure 3.8 (Set C), which, as noted above, corresponds to a higher value.

In Figure 3.10 the data points in Figure 3.9 are replotted with symbols indicating the outflow stream from which each sample was taken. The symbol format for each stream is standard and is used consistently throughout the thesis for the Rhodamine WT tracing experiments. The stream locations are shown mapped in Figure 4.1, and are discussed in Chapter 4. Streams symbolized as VR, LS and TC carried water throughout most of the study period from May through July 1983, while the stream locations TCC and TCS each contained water only over a limited time interval. The adsorption data plotted in terms of S/m versus C cluster in terms of the sampling date as shown on Figure 3.9, and do not indicate that adsorption behavior is related to the sampling location as shown on Figure 3.10. The only exception is suggested for data from TCC stream and perhaps TCS, and the apparent cluster of data points on Figure 3.10 can be explained by the fact each stream (TCC and TCS) carried water for only a limited period of time, while the other streams (VR, LS and TC) carried water throughout most of the study period.

To check on whether the measured amounts of absorbed tracer respond to the amounts of suspended sediment in the direct proportionality that (3.3) requires, values of S/C can be plotted against m. This is done in Figure 3.11 for the turbid water calibration standards, from the data on which Figure 3.8 is based. For a constant K_d value, the data points should lie on a line through the origin, whose slope is the K_d value. The dashed line in Figure 3.10 has a slope $K_d = 15$ ml/g. The scatter of the points in the figure is so large that the expected proportionality between S/C and m is only vaguely recognizable. This result suggests that either

the measurement error is very large, or that there is large variability in adsorption constant among the samples tested.

A spurious possible dependence of K_d on m could arise because of the systematic overestimation of S caused by dissolved dye retained in the settled-sediment sample (see Section 3.4), which will cause the measured value of S/m to increase at low sediment loads m. An apparent dependence of K_d on m, but in the opposite direction (K_d increasing with increasing m), was reported by Smart and Laidlaw (1976).

If a variation of K_d with sediment concentration occurs, it would be in contradiction to the Langmuir adsorption isotherm, and would make invalid Eqn. (3.3 in interpretating the dye tracing results. In Figure 3.12, values of K_d, calculated from Eqn. (3.3) for each standard sample in sets A, B and C, from the data on which Figure 3.8 is based, are plotted versus the sediment load m of each sample. Although there is a considerable scatter in the K_d values in Figure 3.12, there is no clear trend of variation in K_d with m, except for samples with the lowest sediment concentrations ($\leq$ 2 g/l), for which the K_d values are on average somewhat high, as expected from the systematic experimental error noted above. The mean value of K_d is about 15 ml/g for sample set A, about 7 ml/g for set B, and about 55 ml/g for the post-surge samples (set C). Distribution coefficients K_d for regular stream samples, from the data on which Figure 3.9 is based, are plotted against the sediment concentration m in Figure 3.13. There is a large variation in K_d values for samples collected at different times, but again, there does not appear to be any well-defined variation in K_d with sediment concentration. This is in disagreement with the results of Smart and Laidlaw (1976), which correspond to an increase of K_d with m in the range 0-100 g/l, for Rhodamine WT and other tracers.

The highest K_d values (up to 1,700 ml/gm) as well as the highest sediment concentrations were measured for samples collected in the time period between June 13 to 15. The suspended sediment in these samples has K_d values that are about a factor of 10 higher than those for the suspended sediment in the other samples taken during June 1983, and is about a factor of 100 times greater than for samples taken after the surge had ended in July. The significance of the samples from 13-15 June will be considered later (Section 4.4). The measured tracer concentrations from June 25-26 were at the limit of detectibility (0.001 ppb) as discussed by Turner (1981), and below the limit of reliable detectibility (0.01 ppb) as discussed in this thesis (Chapter 2). The values of S and C may be in error by perhaps a factor of 10 or more for samples taken on June 25-26. The adsorption data fro June 25-26 is plotted as a separate symbol on Figures 3.9 and 3.13, because the significance of these unusually adsorbing samples is questionable - due to the very low tracer concentrations involved for both S and C.

K_d values in the lowest part of the observed range in Figures 3.12 and 3.13, $\sim$10 ml/g, are comparable to the values 6-10 ml/g reported by Smart and Laidlaw (1976) for quartz sand (of unspecified grain size). The range of values reported (op. cit.) for clays (kaolinite and bentonite), 13-62 ml/g, includes many of the observed values in Figures 3.12 and 3.13, which is consistent with the fine particle size of the suspended sediment in the outflow stream water, with median particle size about 4 μm (R. Krimmel, personal communication). However, the K_d values observed here, particularly those in Figure 3.13, extend to much higher values (up to $\sim$2000 ml/g) than have been reported for sedimentary materials in previous field or laboratory studies. Because it seems unlikely that the mineral components in the suspended

sediment of Variegated-Glacier outflow-stream water have inherent adsorptive capabilities much more powerful than those of bentonite or kaolinite, the reason for the outstandingly high K_d values in Figure 3.13 must lie in an unusually high content of ultrafine particles in the sediment.

The role of particle size in the aggregate adsorption constant K_d of a particulate material is based on the fact that the fundamental adsorptive property is specific to the particle surface; thus, a fundamental surface-specific adsorptive constant K_a can be defined, such that K_d is given by:

$$K_d = K_a A_m = K_a \frac{6\gamma}{\rho\delta} \tag{3.4}$$

where A_m is the surface area of the particles per unit mass of particulate material. If the particles were spheres of a given size (diameter) δ, A_m would be $\frac{6}{\rho\delta}$, where ρ is the density of the substance of which the particles are composed. For actual particles of a shape that differs from spherical, we can take $A_m = \frac{6\gamma}{\rho\delta}$, where γ is a dimensionless shape factor somewhat greater than 1; this form of A_m is used in the second equality in (3.4). For a given particle substance, the adsorption constant K_a is independent of particle size, and if the particle shape is also independent of particle size, K_d will increase as the particle size gets smaller. This effect will be reinforced by the likely increase of γ with decreasing particle size (smaller particles less nearly spherical). Equation (3.4) can be generalized to a particle size distribution $f(\delta)$, where $f(\delta)d\delta$ is the mass fraction of particulate material in the size range between δ and $\delta + d\delta$, as follows:

$$K_d = \int \frac{6K_a\gamma}{\rho\delta} f(\delta)d\delta \ . \tag{3.5}$$

Equation (3.4) or (3.5) provides a specific basis for considering what changes in suspended-sediment characteristics may be responsible for the very large range of K_d values, from $\sim$10 to $\sim 10^3$ ml/g, found for samples of Variegated-Glacier outflow-stream water during surge and post-surge (Figures 3.12 and 3.13). Some of this variation may be due to measurement error – perhaps as much as a factor of ten in unfavorable cases, based on the scatter of K_d values within individual groups of samples in Figures 3.12 and 3.13. Variation in adsorption constant K_a among the minerals composing the sedimentary particle is probably less than an order of magnitude (Smart and Laidlaw, 1976). Hence, at least an order of magnitude variation in the predominating particle size is required to account for the observed variations in K_d.

In some cases, special explanations may be given for apparent variations in K_d due to systematic errors arising in the experimental procedures. The high K_d values for the set C samples with sediment concentrations $\leq$ 2 g/ml may be so explained, as noted earlier.

The particle frequency distribution $f(\delta)$ of stream sediment from Variegated Glacier terminus streams during 1983 was analyzed and is shown in Figure 3.14. Three examples of the size distribution of suspended sediment are shown. All three samples were dipped from the major stream outlet on the south margin of the glacier, referred to in this thesis as Variegated River (symbol VR in Fig. 4.1). The size distribution measurements (Fig. 3.14) were made using standard pipette techniques. The grain-size-distribution data for May 31 and June 1 were obtained from Robert Krimmel (unpublished, 1984), and measured by U.S. Geological Survey scientists at Cascade Volcano Observatory sediment laboratory. The size analysis in Fig. 3.14 is

graphed in the standard format: weight percent of sediment finer than each sediment size δ is plotted versus the sediment grain-size δ in millimeters. The results shown in Fig. 3.14 for June 1 roughly follow a log-normal distribution (Aitchison and Brown, 1957, p. 8-9).

The log-normal mean μ_δ for the particle size distribution is defined as

$$\mu_\delta = \overline{\ln\left(\frac{\delta}{\delta_0}\right)} = \int \ln\left(\frac{\delta}{\delta_0}\right) f\,(\delta) d\,\delta$$

where δ_0 is a reference particle dimension, which is chosen here to be 1 mm. The mode of the frequency distribution $f\,(\delta)$ is defined as the particle size of the peak in $f\,(\delta)$. The log-normal variance in grain-size distribution is designated ν^2 in this thesis, and discussed, for example, by Burington and May (1970, p. 124). For a large ν^2 value the modal particle size will be much smaller than the mean $\overline{\delta}$, and the frequency distribution will be greatly skewed towards small particle sizes. The log-normal size distribution is given by

$$f\,(\delta) = \frac{1}{\delta\sqrt{2\pi\nu^2}}\, e^{-\left(\frac{(\ln\left(\frac{\delta}{\delta_0}\right) - \mu_\delta)^2}{2\nu^2}\right)} . \qquad (3.6)$$

Substituting $f\,(\delta)$ for the lognormal distribution into Equation (3.5) and solving for K_a the following expression is obtained:

$$K_a = \frac{K_d\,\rho\delta_0}{\gamma}\, e^{\mu_\delta - \frac{1}{2}\nu^2} . \qquad (3.7)$$

The mean of the lognormal distribution is $\mu_\delta = -4.8$, (for δ_0=1 mm). The variance of the grain size-distribution (Fig. 3.14) is estimated from the population "quantiles" ξ of order 16, 50 and 84 % as described by Aitchison and Brown (1957, p. 32), where

$\xi_{16\%} = \exp(\mu_d - \nu)$, $\xi_{50\%} = \exp(\mu_d)$ and $\xi_{64\%} = \exp(\mu_d + \nu)$. The lognormal variance can be only estimated for June 1, 1983 if the nearly straight line plot on Figure 3.14 in the the size range from 0.002 mm to 0.032 mm extends to both smaller and larger grain sizes, so that ξ of 16 and 84% can be immediately estimated from the available data. The variance of size distribution of suspended sediment for June 1, 1983 (Fig. 3.14) is $\nu^2 \approx 2.5$.

The suspended sediment sampled on May 31 contains a greater cumulative weight percent of rock particles smaller than 0.002 mm in size than does sediment taken on June 1, 1983 (Fig. 3.14). Assuming the grain-size distribution for May 31, 1983 continues as a dashed curve (Fig. 3.14) governed by measured data points indicated on Fig. 3.14, data plotted on Fig. 3.14 suggests that $\xi_{16\%}$ for May 1 is perhaps a factor of ten or more smaller than $\xi_{16\%}$ obtained for June 1. By the method outlined above for June 1, the calculated value of ν^2 for May 31 is several times greater than for June 1. The particle-size distribution for suspended sediment obtained on May 31, 1983 is highly skewed towards fractions smaller than 0.002 mm, and the actually the size distribution deviates significantly from lognormality at these smallest size fractions. Because of the extremely fine size of this sediment, the detailed grain-size distribution for sizes smaller than 0.002 mm cannot be separately measured by standard pipette methods. Consequently, only approximate values of μ_δ, ν^2 and the corresponding K_a can be determined from the grain-size information given on Figure 3.14. Assuming the particles are roughly spherical ($\gamma = 1$), and the sediment density is $\rho = 2$ g/ml, then for June 1 the calculated areal distribution coefficient is $K_a \approx 10^{-6} K_d$ to about $10^{-7} K_d$.

The average value of K_d for the time period of late May to early June is on the order of 100 ml/g, with a range on the order of 10 to 1000 ml/g (Table 3.2 and Figures 3.12 and 3.13). Therefore, the average value of K_a for Rhodamine WT adsorption on suspended sediment from Variegated Glacier during the 1983 surge is estimated to be on the order of 10^{-4} m. This value of K_a for Rhodamine WT is about a factor of 10 less than the K_a calculated by Nerentieks et al. (1982) for surface sorption of radionuclides $^{85}Sr^{2+}$ and $^{134}Cs^{+}$ on crushed granite of mixed grain-size. Detailed information on the grain-size distribution of the crushed granite is not discussed by Neretnieks et al. (1982), except the particles were greater than 0.45 μm in size and small enough in size to form a particle suspension in water. The areal distribution coefficient measured for Variegated Glacier sediment during the surge is in close agreement with the value of $K_a \sim 10^{-4}$m calculated for Rhodamine WT adsorption on mixed-lithology gravels (0.1 to 6.3 mm in size) from K_d and grain-size data published by Benecala et al. (1983) and cited on Table 3.3.

About 30 to 40% of each sediment-size distribution for May 31 and June 1 (Fig. 3.14) was not measured, because of the exceedingly small, clay-sized particles involved. Since these very fine particles have the highest surface area for adsorption per mass of sediment, they greatly influence the value of K_d. For a measured volume (or mass) distribution coefficient K_d and a measured size-distribution, the areal distribution coefficient, K_a, may be overestimated if the surface area of finest grained sediment is underestimated. Because of the possible measurement error in K_a due to incomplete measurement of the smallest size fraction of sediment, it is reasonable to assume that the areal adsorptivity is nearly constant at a value of $K_a \sim 10^{-4}$m, and that large variability of K_d (1 to 1,000 ml/g) is primarily due to changes in grain-size

distribution, within the smallest size fraction of < 0.002 mm.

The high values of K_d observed for the glacier surge is best explained by the great amount of surface available for tracer adsorption on the extremely fine, clay-sized sediment. In the future, it is possible to obtain additional information on grain-size distributions for the Vareigated Glacier sediment, since samples are carefully stored. The adsorptivity of rock material within the glacier and the retardation of the tracer due to this adsorption behavior is discussed in Sections 6.3.2.

Evidence from the grain size distributions (Figure 3.14) strongly suggests that the observed variation among different K_d values (Table 3.2) measured for stream samples obtained during 1983 at Variegated Glacier can be explained even though there is a constant value of K_a on the order of 10^{-5}m, and a constant value of the log-normal mean μ_δ. If the variance of the lognormal distribution ν^2 increases by an amount $\Delta\nu^2$, then the K_d value increases by a factor of $e^{\frac{1}{2}\Delta\nu^2}$. An increase in K_d value from 10 to 100 ml/g was measured for the change from non-surge to surge states (Table 3.2), and suggests that the effective mean grain size $\overline{\delta}$ decreased by a factor of 10 during the surge, and that by Eqn (3.7) the log-normal variance ν^2 increased by about 4.6. The variation in K_d values measured during the surge, from 100 to 1000 ml/g, can be explained by a further increase of 4.6 in the value of ν^2, and thus a major shift of the mode of $f(\delta)$ towards smaller grain sizes.

The nearly identical size-distribution curves obtained for water samples taken at 9:30 and 10:30 on June 1 (Fig. 3.14) shows that the measurement error in $f(\delta)$ is probably less than 2% . The much higher abundance of very fine sediment on May 31 as compared to June 1 cannot be attributed to measurement error. The mode of the best-fit log-normal distribution for the data obtained on June 1 is shifted by

about an order of magnitude towards smaller radii, as discussed earlier. The observed change in the abundance of particles with radii smaller than 0.002 mm between samples taken on May 31 and June 1, was about ten percent. The size distribution for May 31 sediment suggests particles in the size range between 0.008 and 0.002 mm (or perhaps even smaller sizes) had been ground to finer particles.

The distribution coefficients for regular samples – containing tracer – taken after the surge are 7 ml/g $\pm$ 3.7 ml/g as shown in Table 3.2, and are the lowest K_d values obtained for Variegated Glacier sediment. The scatter in K_d values of unmodified stream samples for July 16 to 20 (Table 3.2) is approximately 1/20 of the error for modified stream samples taken after the surge (set C on Table 3.1). The modified samples consist of regular stream water and suspended sediment that were altered by adding prescribed amounts of additional tracer, in order to make standard solutions used in fluorometer calibration and measurement of adsorption properties of the sediment, as discusssed earlier in this chapter. Distribution coefficients for unmodified regular samples that contained detectible tracer after the surge are less variable than K_d values obtained from regular samples that contained tracer taken during the surge. The average distribution coefficient measured for sediment taken during the surge for standard samples (averaging 20 ml/g for set-A) is only slightly less than K_d values for regular samples (averaging 35 ml/g for June 10 to 12 and 60 ml/g for June 15 to 21). The mean distribution coefficient (Table 3.2) for suspended sediment for the morning of June 13 (800 ml/g) is a factor of 40 times larger than the mean K_d value for the standard solutions made from stream water taken between May 31 and July 1 (20 ml/g for set A), and approximately a factor of 100 times larger than mean K_d value for standard solutions decanted from stream water taken at

12:00 on June 18 (10 ml/g for set B). The lower K_d value for set B is probably due to the fact that some of the finest grained suspended sediment, with the highest available surface area for adsorption per weight of sediment, had been inadvertently removed during the decantation procedure involved in making the standard solutions from a single stream sample taken in a large pail. The variability of K_d values for set B (standard deviation 5 ml/g) gives a rough estimate of the measurement error which cannot be attributed to a significant change in grain size distribution of the sample. Also, the difference of 10 ml/g in K_d values between set A and set B strongly suggests that removal of even a small amount of the finest-grained suspended sediment causes a major decrease in mean sample adsorptivity and verifies the importance of grain-size distribution in the observed pattern of sediment adsorptivity.

The low standard deviation of K_d values for samples taken after the surge differs from the the earlier observation of a large scatter in K_d values for standard stream samples taken after the surge had ended (Table 3.2). The apparent discrepancy in the variability in K_d observed for post-surge samples may, perhaps, be explained by a biased measurement error caused by unavoidable contamination from the the small amount ($\sim$ 1 ml) of water remaining after decantation and the low sediment contents (less than 2 g/l, such as for set C). Such a measurement error could be the cause for both the higher average K_d values and larger scatter in K_d values for standard samples of set C (Fig. 3.8).

Distribution coefficients for different sediment types from published literature (Smart and Laidlaw, 1976; Bencala et al., 1983) are summarized in Table 3.3. The distribution coefficients for any water collected during the glacier surge (excluding the

time period June 13-15) are very similar to coefficients measured for kaolinite or bentonite (Smart and Laidlaw, 1976, p. 28). The values of K_d for post-surge samples (Table 3.2) are quite similar to published adsorption data, shown on Table 3.3, for orthoquartize sand (Smart and Laidlaw, 1976, p. 28) and gravel (Benecala, 1983, p. 949). Data provided on Table 3.3 indicate that quartzite or mixed-igneous compositions (K_d values of 13 to 62 ml/g) adsorb Rhodamine WT dye the least of all the relevant non-organic subtances, while kaolinite or bentonite compositions (K_d values of 13 to 62 ml/g) adsorb the greatest amount of Rhodamine WT per weight of sediment. Kaolinite appears to be the strongest inorganic adsorbing substance for Rhodamine WT (Table 3.2). For comparison, humus (a typical organic substance suspended in – or lining the walls of – non-glacial streams) adsorbs Rhodamine WT the strongest of naturally encountered substances, with K_d values approximately 2 to 10 times higher than even kaolinite (Smart and Laidlaw, 1976, p. 28). Only sediment types composed of inorganic material, such as those summarized on Table 3.2, would be expected to be found in the field samples taken from a glacier outlet stream, particularly the Variegated Glacier, considering the known local geology and mineralogic composition of rock-material discharged at the glacier terminus. Even if the suspended sediment were composed of material of K_d value equivalent to the most adsorbing substance described in the literature, the material would not adsorb dye strongly enough to account for the extremely high K_d values (500 to 1700 ml/g) observed for Variegated Glacier outlet streams between 7:30 and 14:00 on June 13, 1983 (Table 3.1 and Fig. 3.13). Therefore, although the range in published data on distribution coefficients (Table 3.3) is consistent with the range in K_d values at other times (both during and after the glacier surge), the distribution coefficients observed

for the time period from June 13 to 15 and particularly on the morning of June 13, cannot be explained on the basis of any known mineralogical differences in sediment composition.

There is a suggested inverse relationship between distribution coefficient, K_d, and sediment concentration m in Table 3.3, summarized from studies for sediment concentrations in the range 2 to 20 g/l. Smart and Laidlaw (1976, p.28, p. 11) have stated that such a relationship exists, but adequate information was not provided in the publication to check the validity of this statement. The apparent inverse relationship between sediment content and adsorptivity in published data might be attributable to a systematic measurement error from contamination, agitation or non-uniformity in experimental procedures used, or systematic sampling error for each sample group cited on Table 3.3.

The preceding tests indicate that the adsorption of Rhodamine WT on suspended glacial flours in Variegated glacier outflow-stream water conforms generally, though roughly, to expectation based on the standard concepts and principles of absorption on solid surfaces in contact with a liquid phase. The roughness of the observed absorption relationships probably reflects considerable variability from sample to sample in the particle size distribution and/or mineralogical composition of the suspended glacial flour, as well as errors in the measurements of dissolved and adsorbed dye and of sediment content.

Table 3.1
Suspended Sediment Content of Variegated Terminus Streams

Sample Group	Time Period	No. of Data Points	Sediment Content Mean (g/l)	Sediment Content Range (g/l)	Sediment Content Standard Deviation (g/l)
Standard:	During Surge				
A	May-June	15	53	15-103	30
B	June 18	7	12	11-13	1
Regular:	During Surge				
I	June 10-12	24	42	17-62	10
II	June 13	5	52	37-75	18
III	June 13-15	14	51	28-92	19
IV	June 15-24	17	29	10-36	9
Standard:	After Surge				
C	July 6-24	15	6	0.4-17	4
Regular:	After Surge				
V	July 16-20	9	17	13-22	4

Table 3.2
Adsorption of Rhodamine WT Sediment:
Distribution Coefficients K_d

Sample Type	Time Period	No. of Data Points	K_d (ml/g)	Range (ml/g)	Standard Deviation (ml/g)
Standards	During Surge				
A	May-June	15	20	1-88	20
A[a]	May-June	13	20	5-33	10
B	June 19	7	10	2-17	5
T	May 28, 30	2			
Regular	During Surge				
I	June 10-12	24	35	20-60	15
II	June 13[b]	5	800	450-1690	440
III	June 13–15[c]	14	330	35-1050	300
IV	June 15–24[d]	19	60	1-120	20
V	June 25-26	4	800	100-2000	100
Standards	After Surge				
C	July 6-24	15	60	5-280	70
C[e]	July 6-24	9	20	5-33	10
Regular	After Surge				
VI	July 16-20	9	7	2-30	3

(a). Subset does not include high and low values.

(b). Period II begins at 7:30 AM on June 13 and extends to 14:00 on June 13.

(c). Period III begins at 14:00 on June 13 and extends until 11:15 on June 15.

(d). Period IV begins at 17:30 on June 15 and ends on June 21.

(e). Subset C excludes samples with sediment contents below 2.59 g/l.

Table 3.3
Sediment Composition and Rhodamine WT Adsorption Properties

Adsorbing Material[1]	Distribution Coeff.[2] K_d (ml/g)	Sediment Content (ml/g)	Reference
Mixed Lithology Gravel[3]	5	100	Bencala et al. (1983)
"	8	200	"
Quartzite Sand	10	2	Smart & Laidlaw (1976, p. 28)
"	6	20	"
Limestone	38	2	"
"	26	20	"
Bentonite	44	2	"
"	13	20	"
Kaolinite	62	2	"
"	25	20	"
Humus	110	2	"
"	405	20	"

1. All data quoted apply to only one measurement each; i.e., the number of data points for each K_d value is equal to one.

2. Distribution coefficients were measured for mean temperature of 22°C.

3. Mixed lithology gravel refers to sediment with a size between 1 mm and 6.3 mm size.

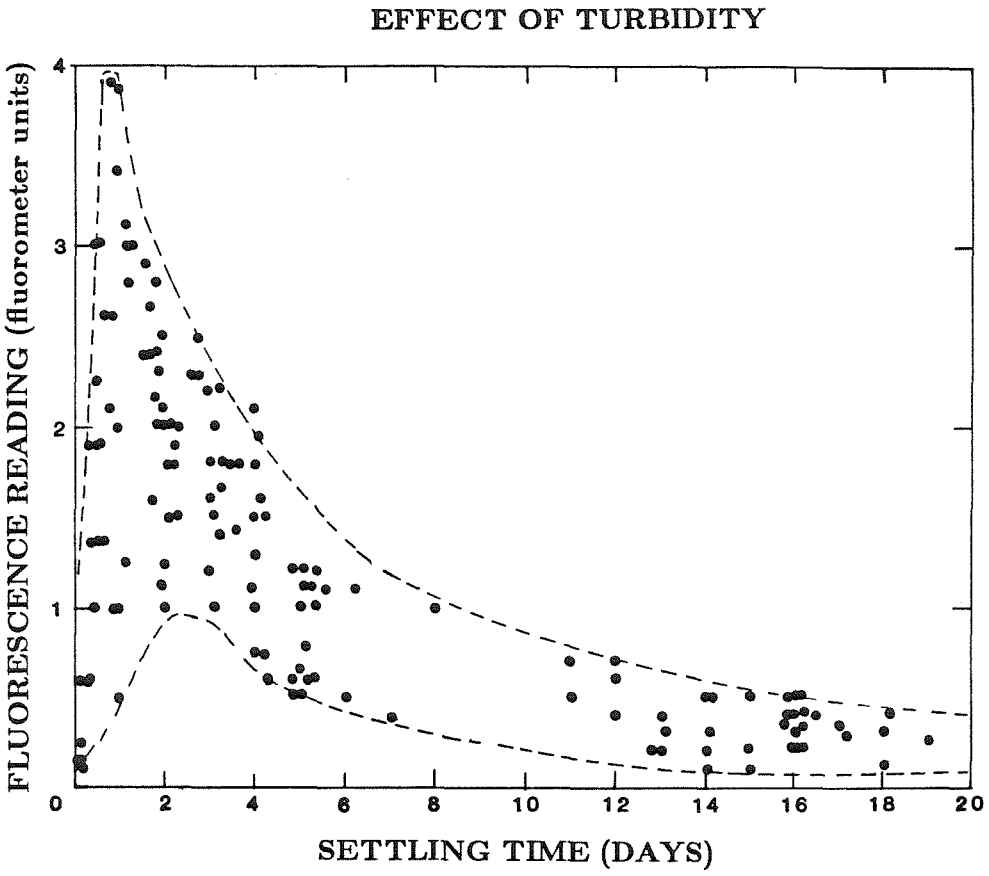

Figure 3.1 Effect of turbidity on fluorescence reading from dye-free samples. Fluorescence reading for Rhodamine detection is plotted as a function of settling time for a group of randomly chosen water samples collected from the outflow streams in May and early June, prior to the first introduction of Rhodamine WT into the glacier in 1983. Settling time is the time that each sample stood undisturbed after collection (or after a subsequent shaking disturbance that roiled up the contained sediment).

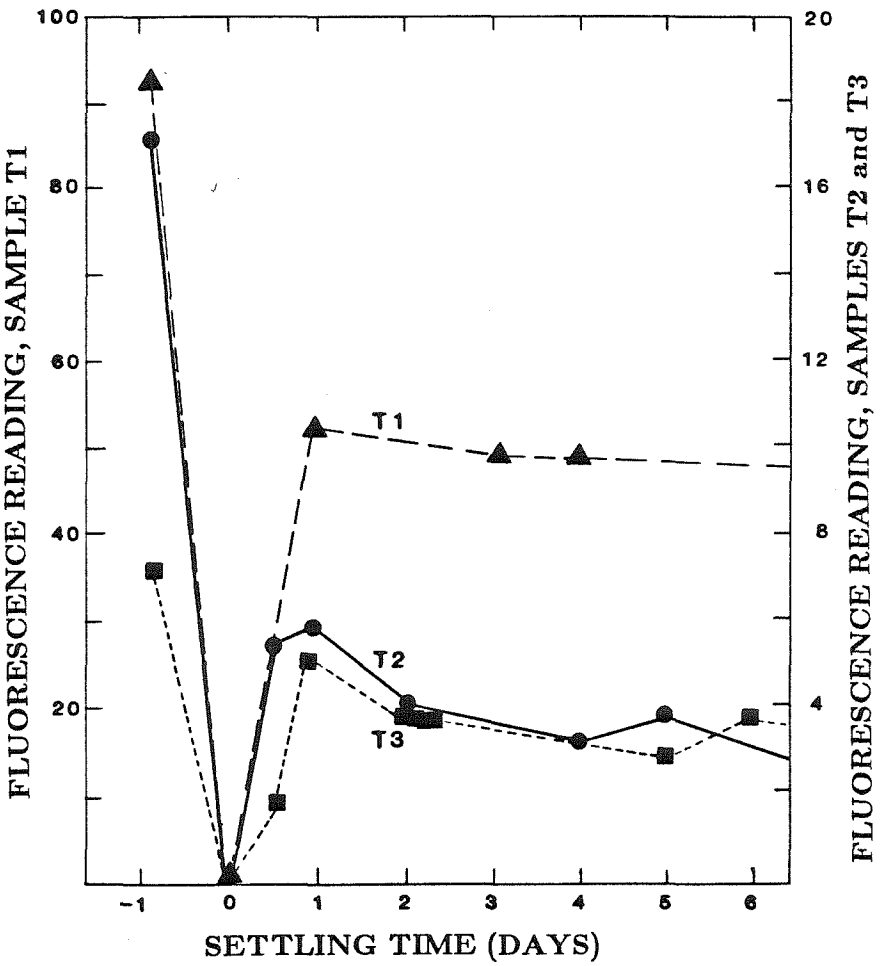

Figure 3.2 Fluorescence reading in fluorometer units versus settling time for three fluorometry standards made from turbid outflow stream water shortly after sampling. Settling time is the time each sample was allowed to stand undisturbed after being shaken to suspend the contained sediment. The fluorescence reading after an initial settling period of about 3 months, and prior to resuspension of the contained sediment, is plotted at abscissa -1 (which does not, of course, represent the settling time in this case). The ordinate scale for standard sample T1 is on the left, and for samples T2 and T3 on the right.

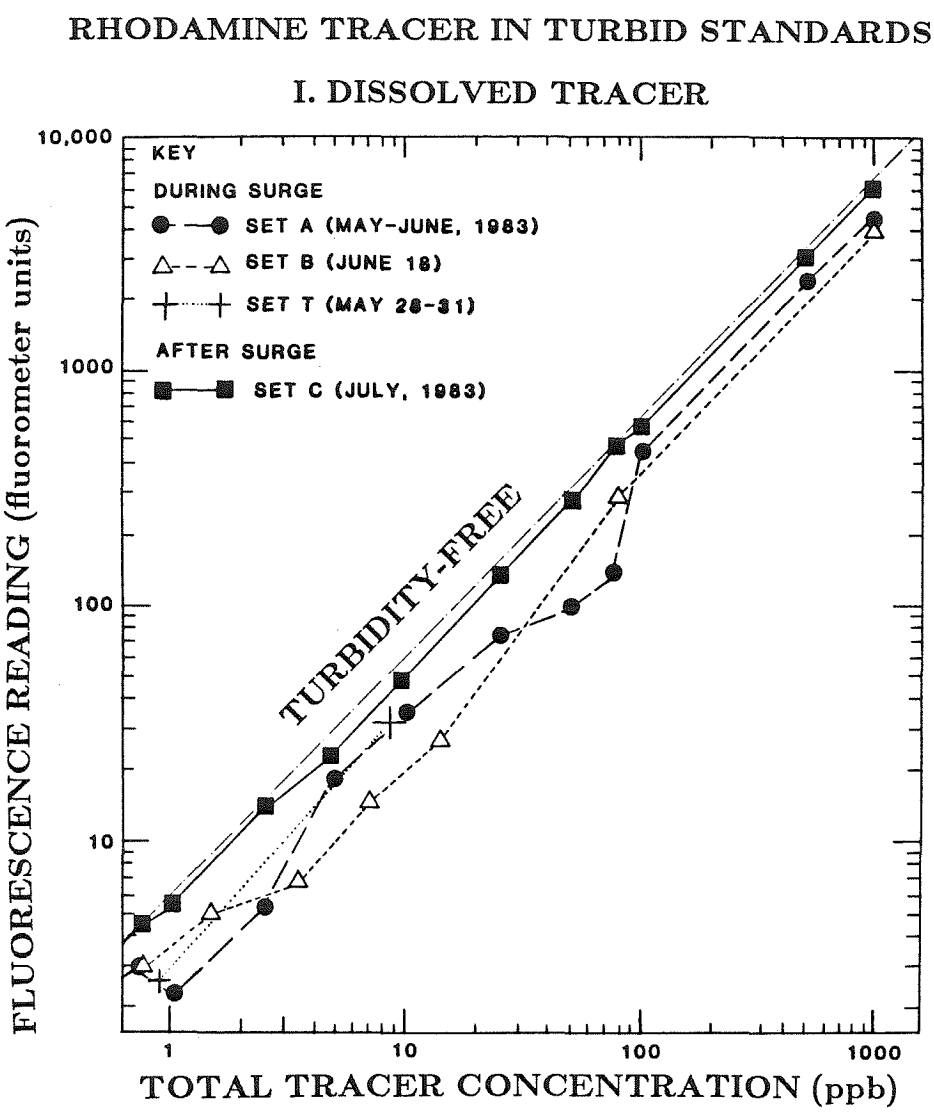

Figure 3.3 Fluorescence reading versus total Rhodamine tracer concentration for standard samples prepared from turbid glacial outflow-stream water and then clarified by settling. Samples of sets A, B, and T consist of highly turbid water issuing from the glacier in surge, while samples of set C, collected after surge termination, have lower turbidity. See text for details of sampling. "Total tracer concentration" is based on the amount of tracer added to each sample in preparing the resulting standard. The dashed line labelled "turbidity-free" is the calibration line for tracer in pure water, from Fig. 2.5. The distance that each point falls below this line is a measure of the fraction of the total tracer that has been removed from water solution by adsorption.

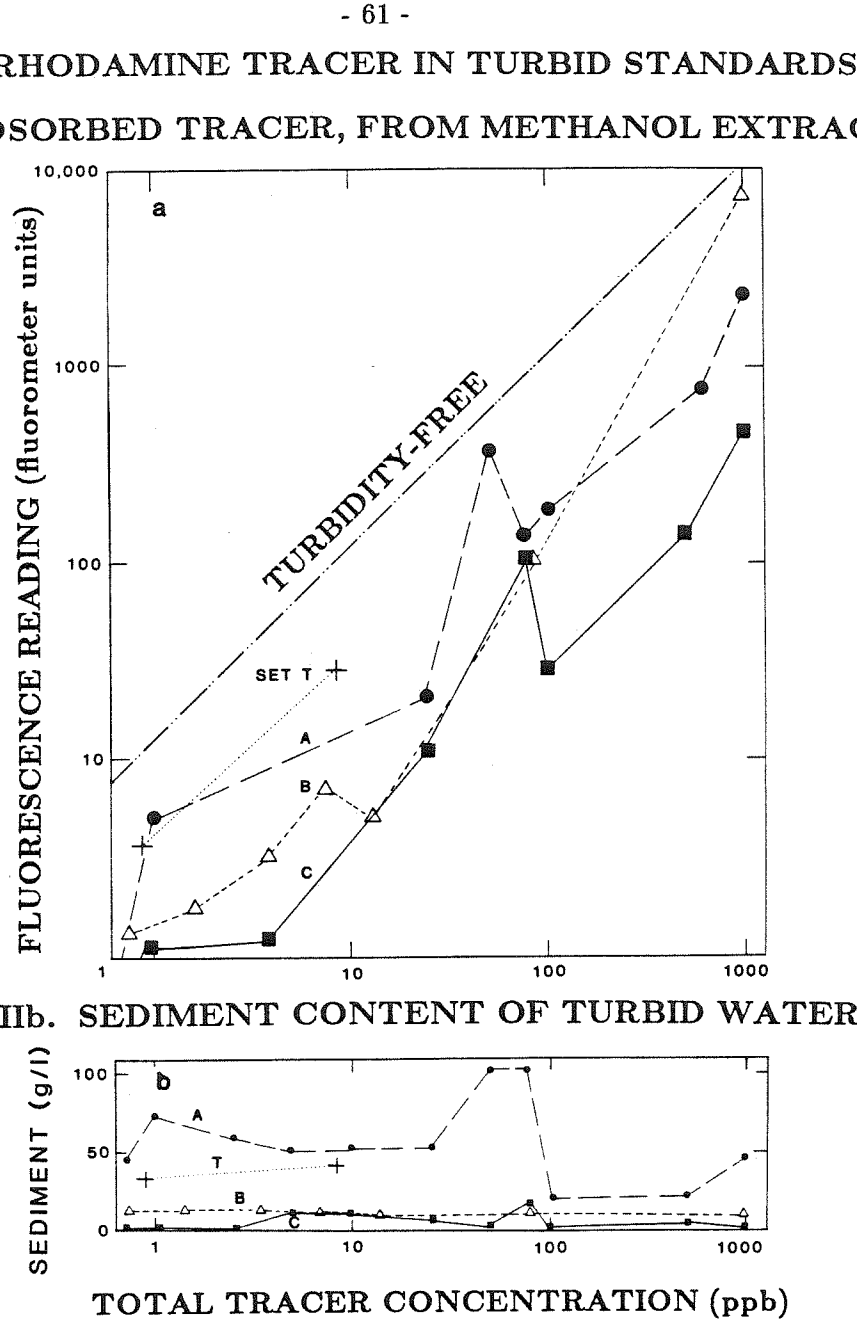

Figure 3.4 (a) Rhodamine WT desorbed from sediment in standard samples of sets A, B, C, and T. Desorbed tracer is reported in terms of the measured fluorescence reading obtained from the methanol extraction aliquot. The line labelled "turbidity-free" is the calibration line for tracer in methanol solution, from Fig. 2.5. The closeness of approach of the data points to this line is a measure of the fraction of the total tracer that was carried in adsorption on sediment in each sample and released by the methanol extraction procedure.

(b) Sediment content of samples of sets A, B, C, and T, in grams of sediment per liter of turbid water, plotted as a function of the total tracer concentration introduced in preparation of standards. Details of sampling are in the Fig. 3.3 caption and text.

RHODAMINE TRACER IN TURBID STANDARDS
III. DISSOLVED PLUS ADSORBED TRACER

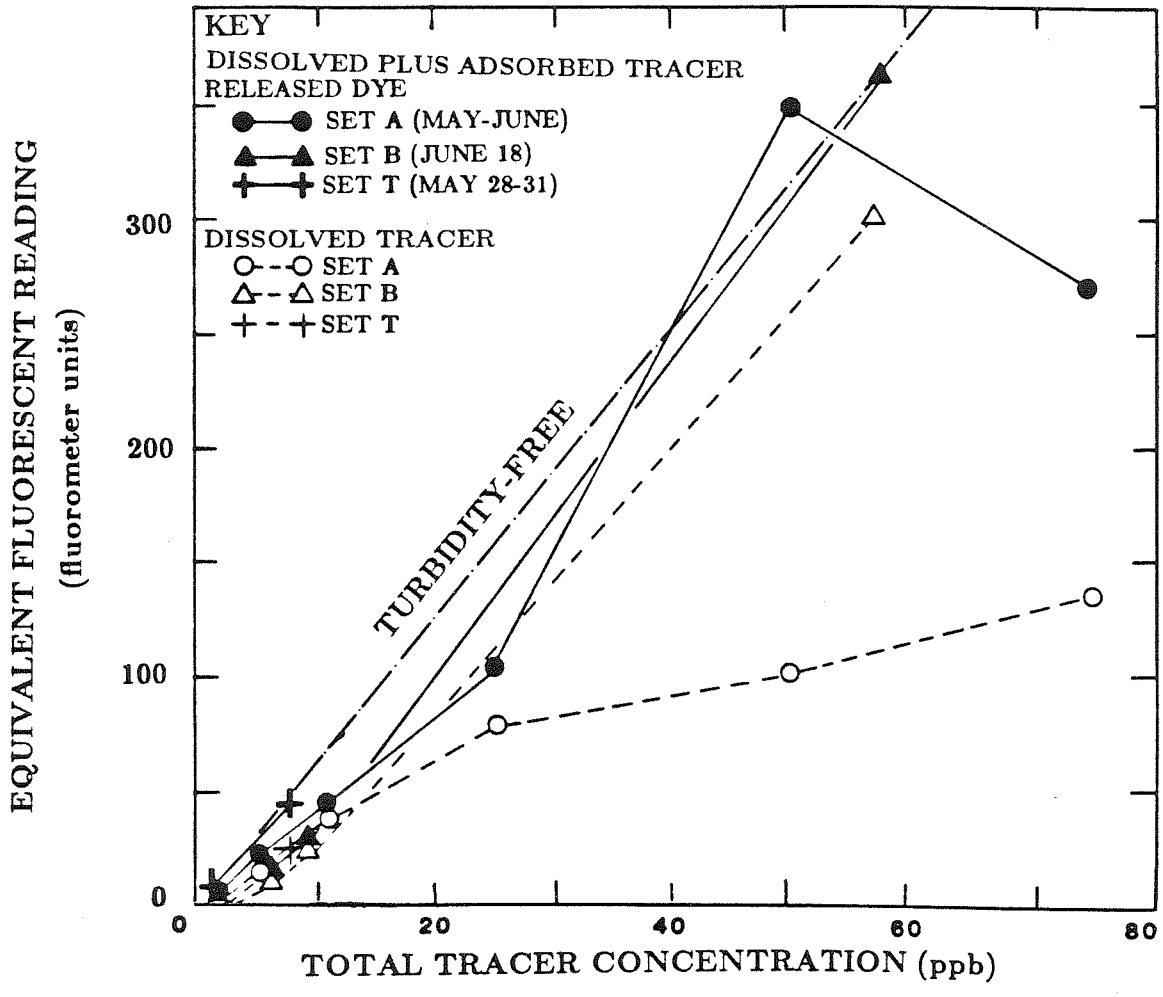

Figure 3.5 Sum of dissolved tracer and adsorbed tracer measured in standard samples of sets A, B, and T, plotted against total tracer concentration introduced in preparation of standards. Sum is expressed in terms of "equivalent fluorescence reading" as explained in text, and is plotted with solid symbols as indicated in the key. Line labelled "turbidity-free" is the calibration line for tracer in pure water, from Fig. 2.5. If a data point falls below this line, the sum of the measured amounts of dissolved and adsorbed tracer falls short of the total amount introduced in standard preparation. Also shown (with open symbols) is the amount of dissolved tracer measured for each sample (expressed as equivalent fluorescence), so that the size of the addition from the measurement of adsorbed tracer can be seen.

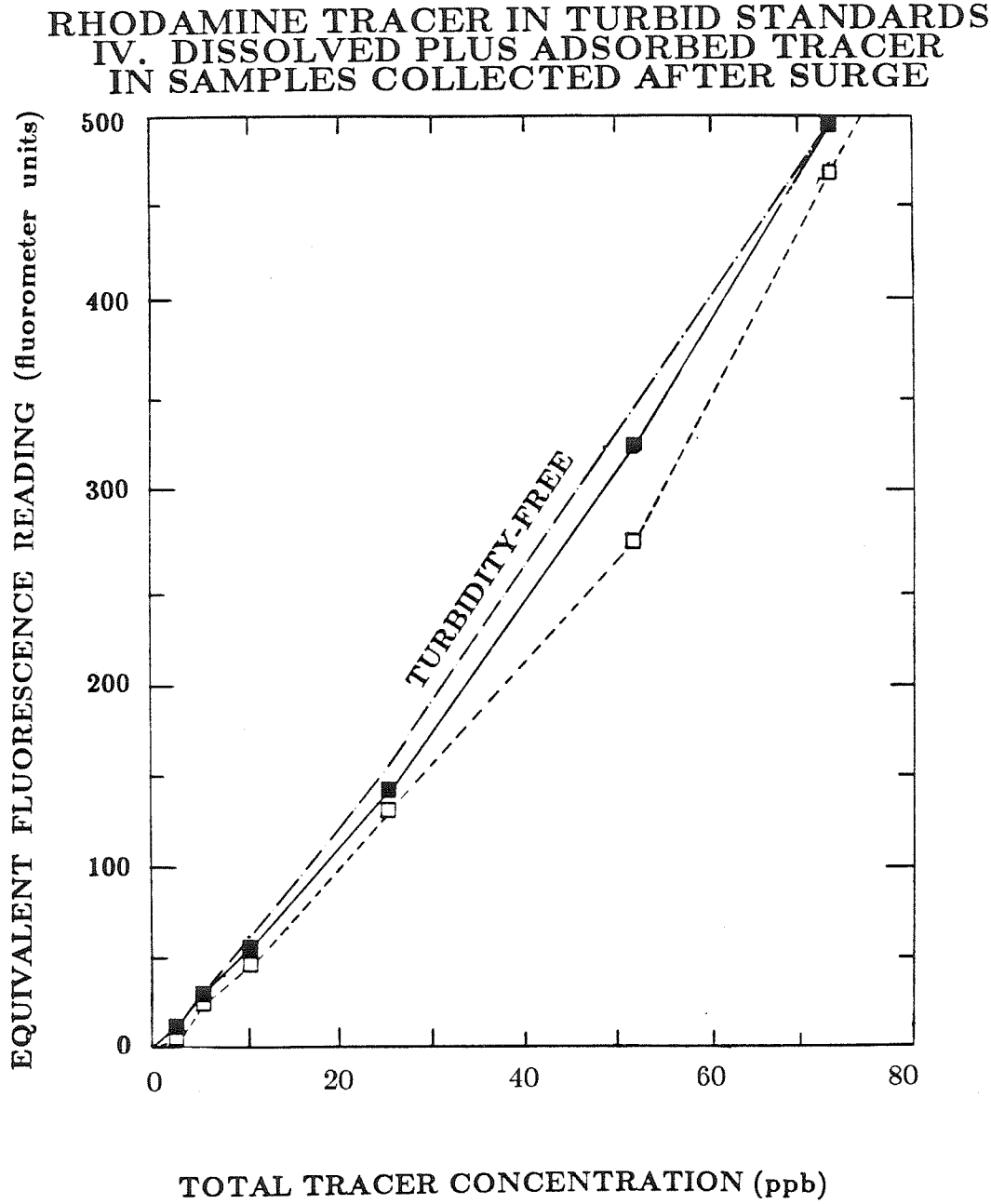

Figure 3.6 Sum of dissolved and adsorbed tracer for samples of set C, collected from glacier outflow streams after surge termination. Explanation as for Fig. 3.5.

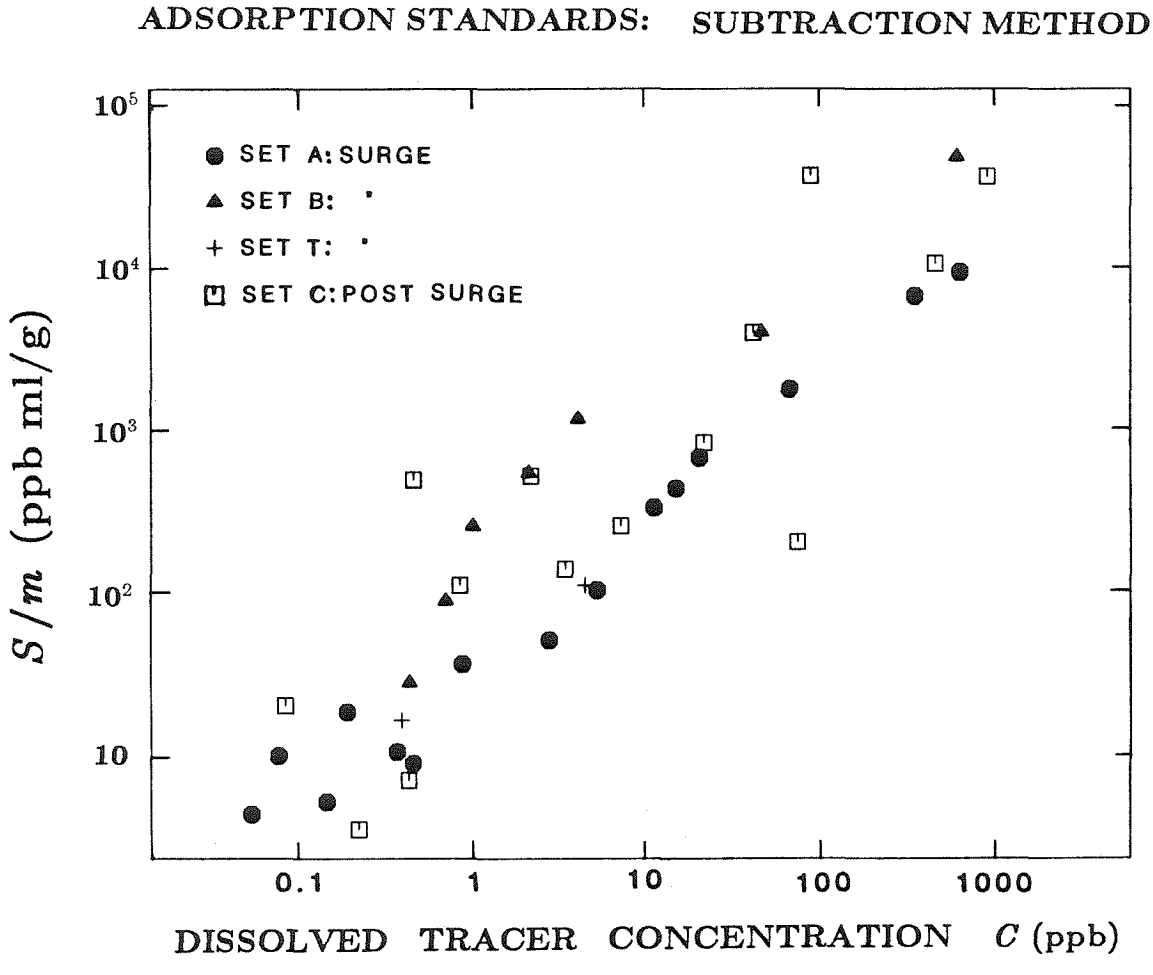

Figure 3.7 The quantity S/m plotted against dissolved tracer concentration C in standard samples of sets A, B, C, and T, made from turbid glacier-outflow-stream water (adsorbed Rhodamine tracer concentration divided by suspended sediment concentration). Values of S/m are based on S values obtained as the difference between the total tracer concentrations and the dissolved tracer concentration measured by fluorometry on the turbidity-clarified water fraction. m is taken in units of g/ml.

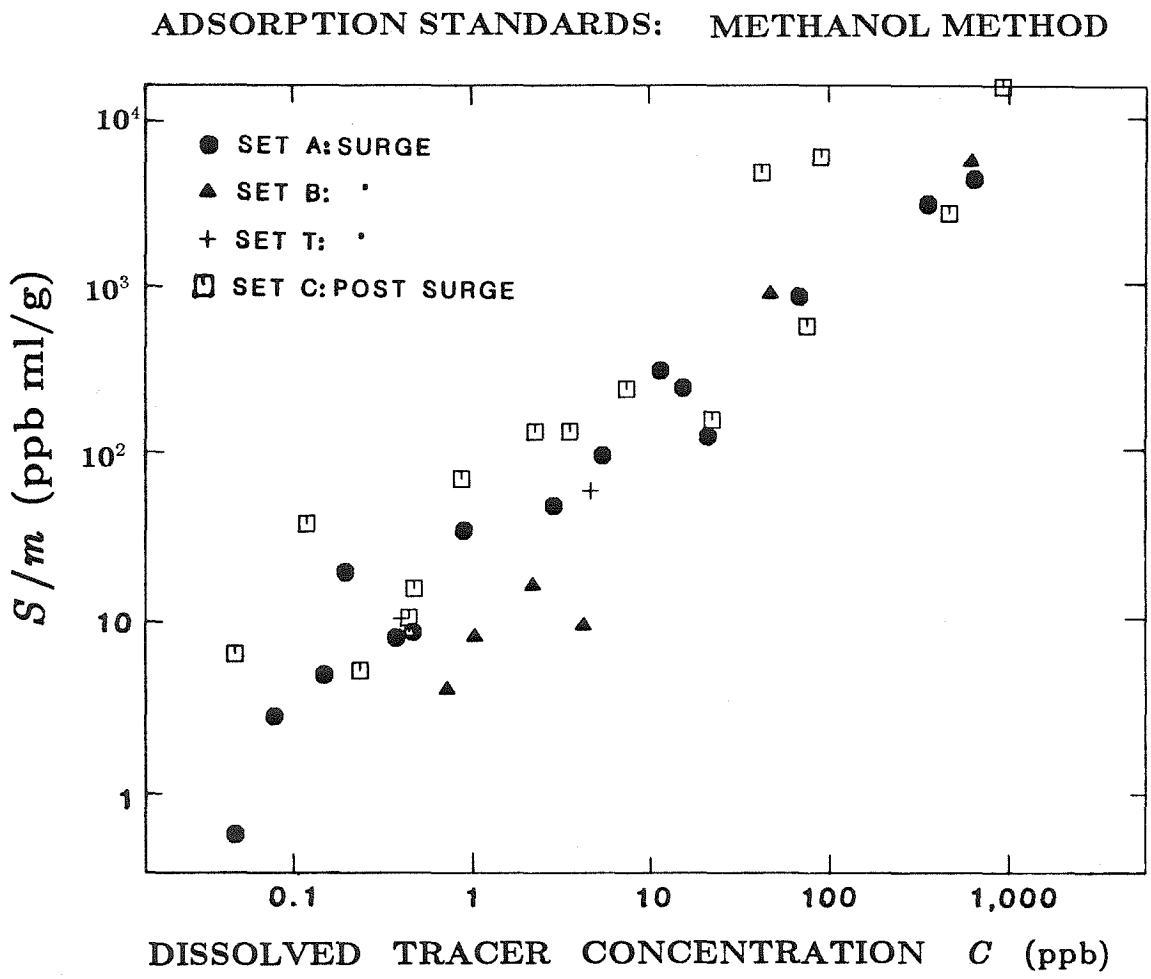

Figure 3.8 Plot of S/m versus C as in Fig. 3.7, based on S values measured by the method of methanol extraction and fluorometry.

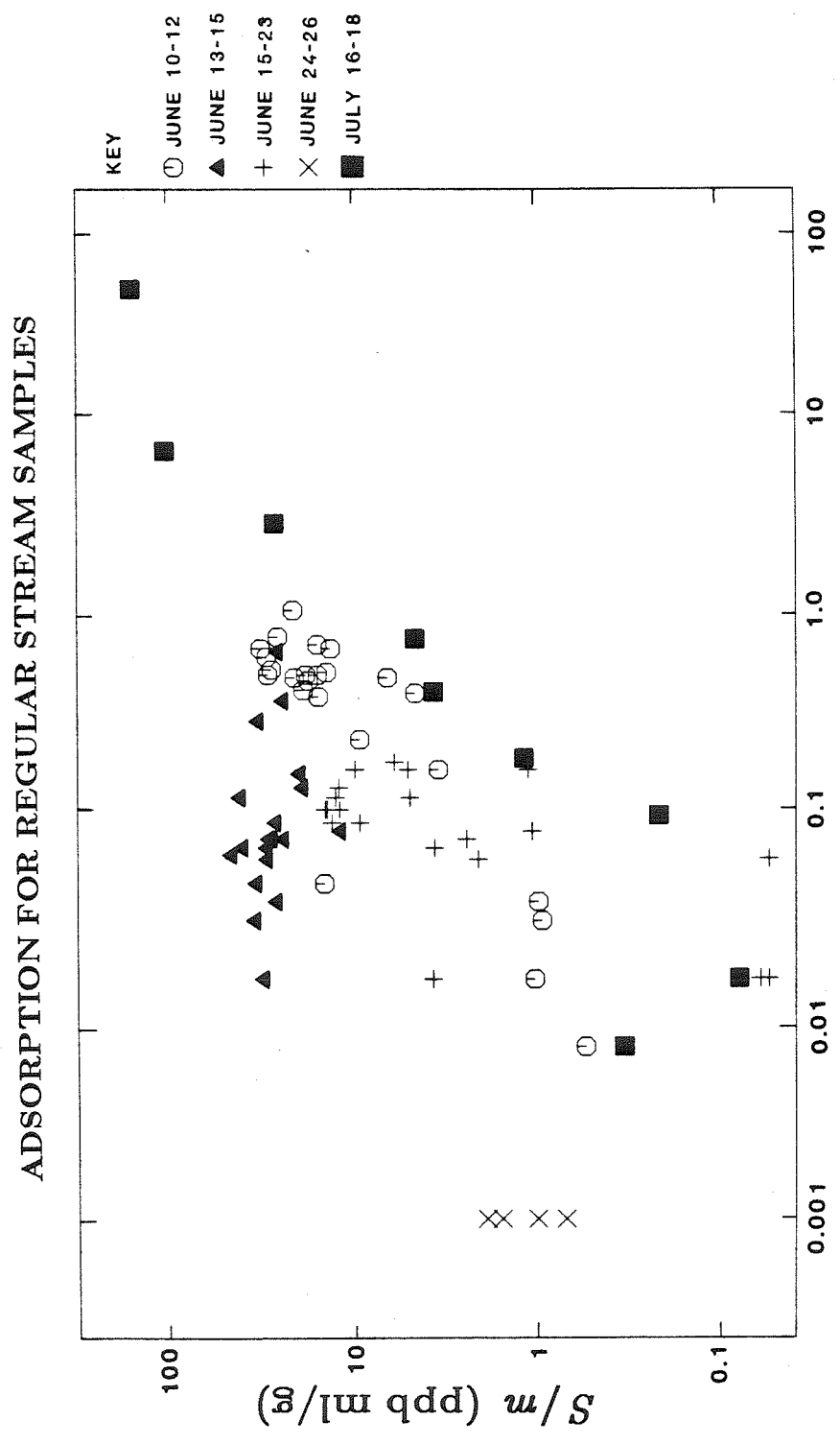

Figure 3.9 The quantity S/m for routine samples of glacier outflow stream water collected in June and July, 1983, plotted against the dissolved tracer concentration C in these samples. ("REGULAR" samples are samples other than those used to prepare special standards.) The individual data points are tagged in accordance with the date of sampling, as indicated in key.

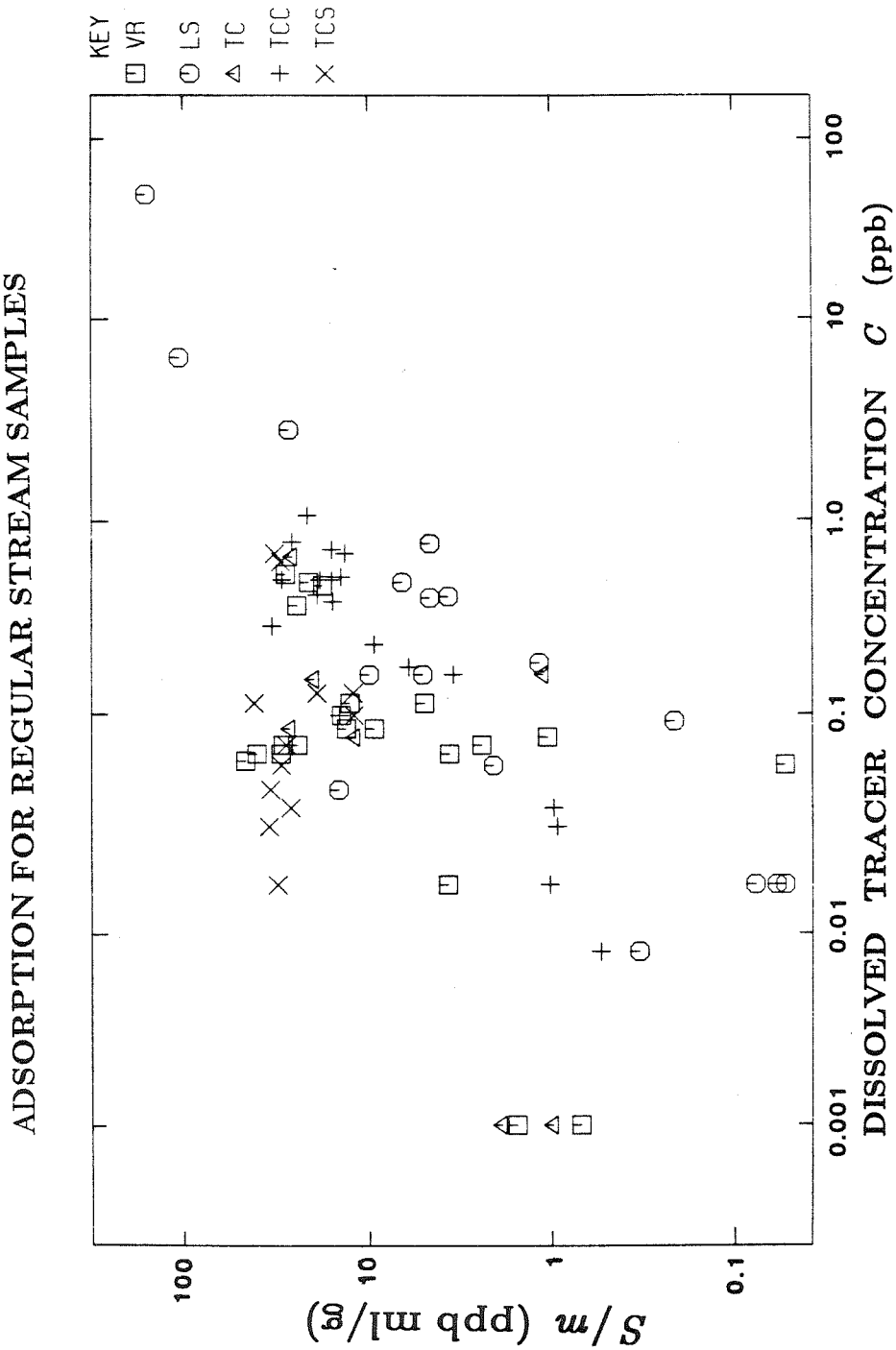

Figure 3.10 Same data points as in Fig. 3.9, tagged in accordance with the sampling location, as indicated in the key. Letter designations of sampling locations are explained in Section 4.1 and shown on the map in Figure 4.1.

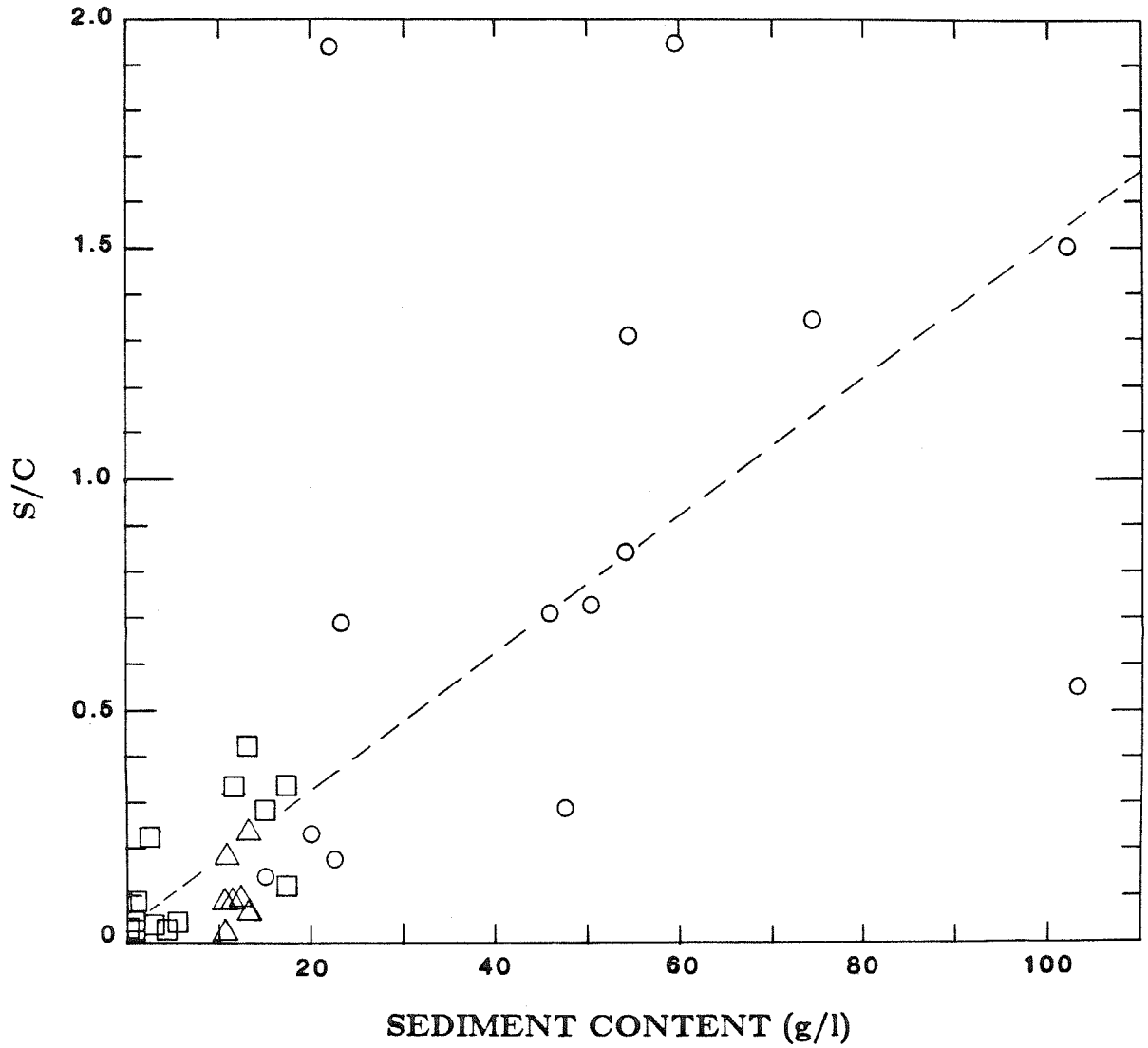

Figure 3.11 Ratio of adsorbed to dissolved tracer (S/C) as a function of sediment content m, for standard samples: Set A, circles; set B, triangles; Set C, squares.

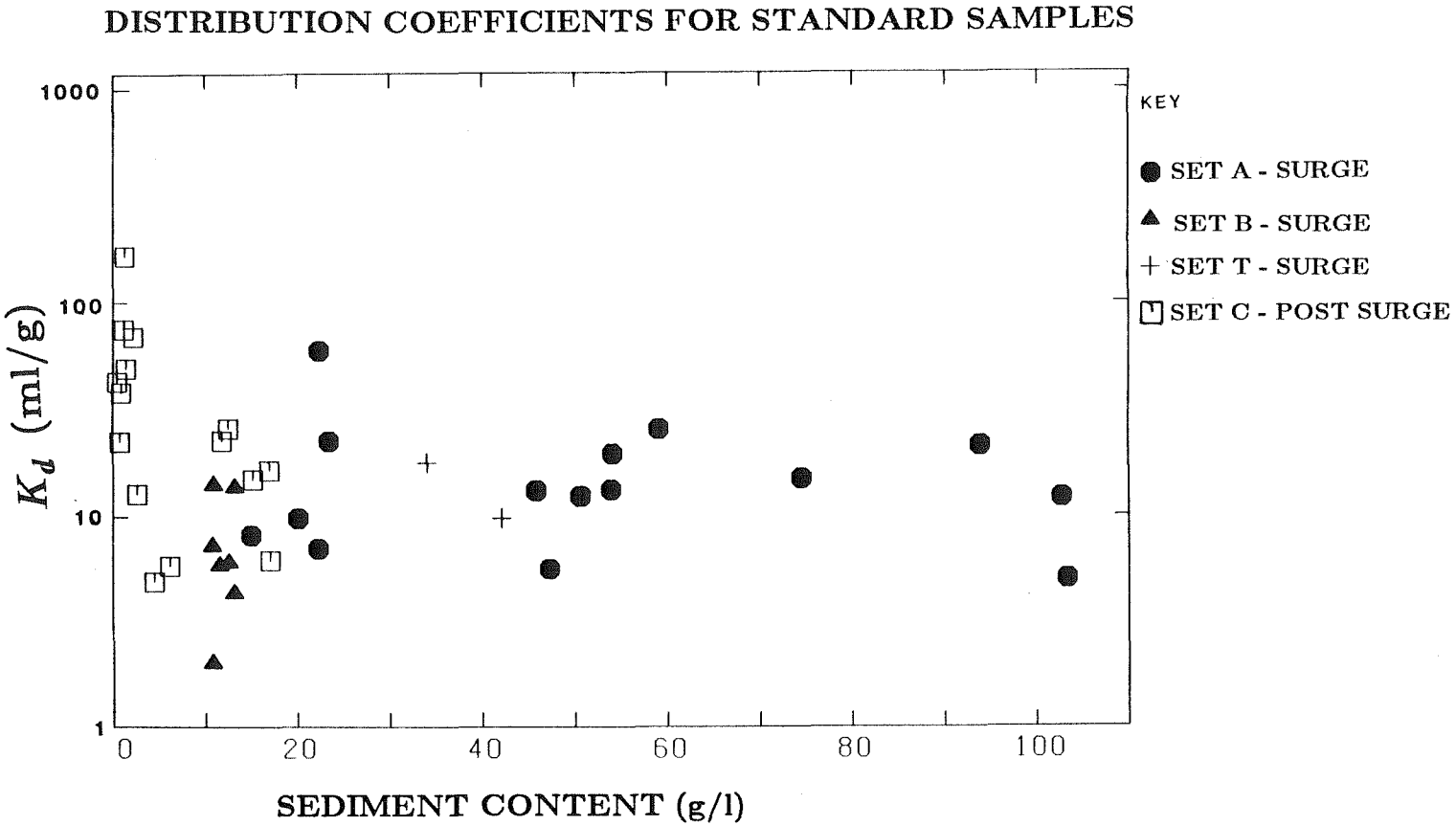

Figure 3.12 Distribution coefficient versus sediment content for standard samples. Sample sets A, B, C, and T are as explained in Section 3.5.

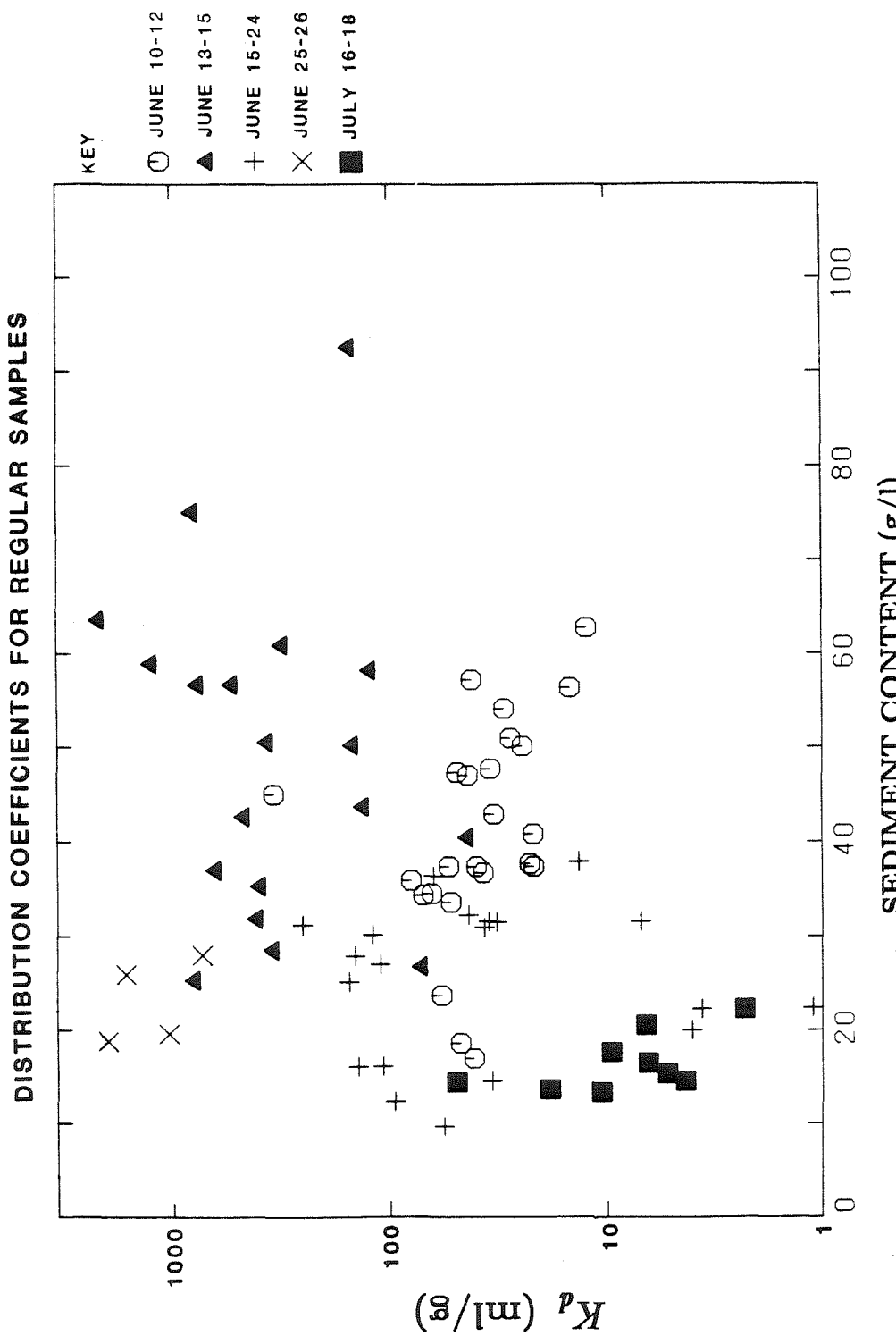

Figure 3.13 Distribution coefficient versus sediment content for samples taken in June and July 1983. The data points are coded in accordance with the data of sample collection.

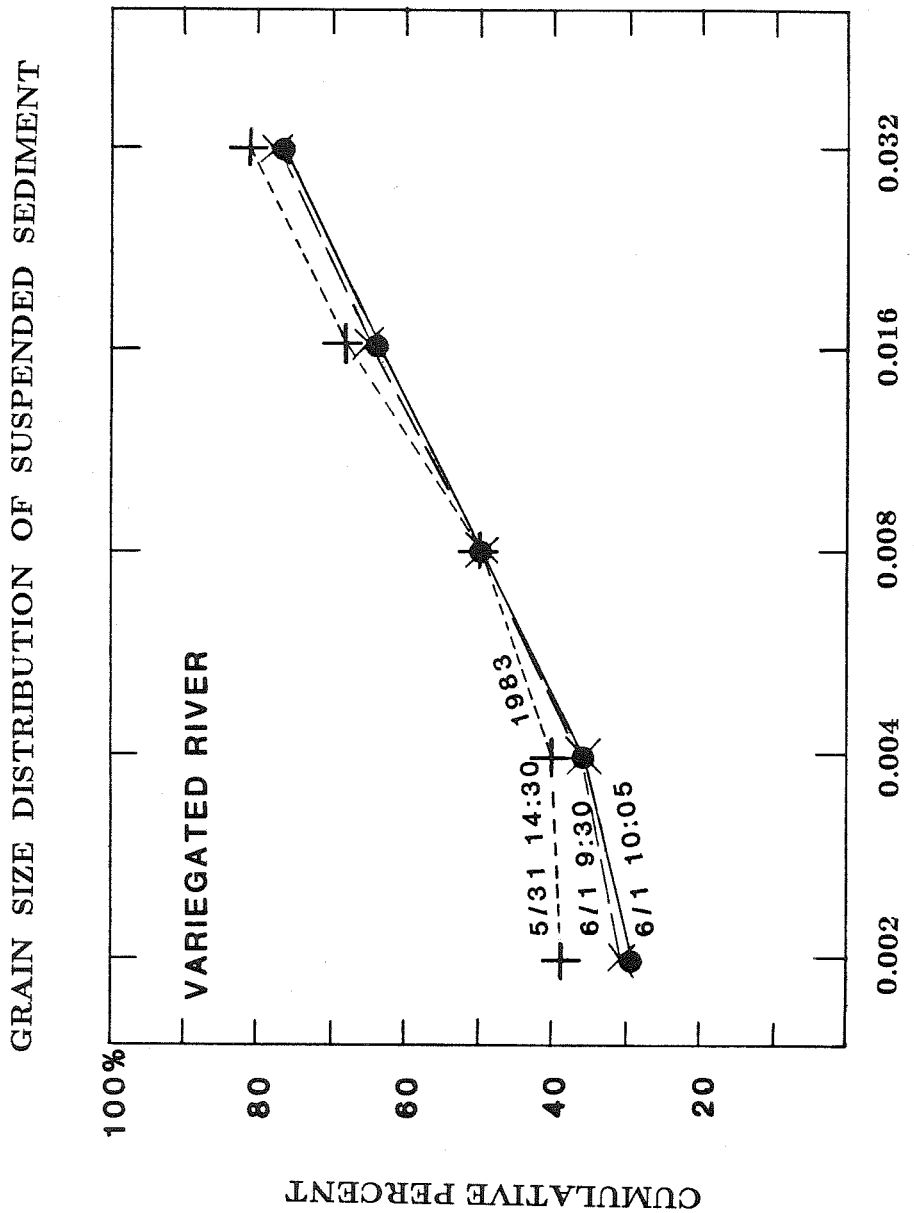

Figure 3.14 Grain size distribution of sediments suspended in Variegated River May 31 and June 1, 1983.

Chapter IV:
Dye Tracing Results

4.1. Introduction

During the summer of 1983, three dye tracing experiments were conducted on Variegated Glacier. This chapter discusses the three experiments and presents the results. A map showing the glacier borehole injection sites, the terminus streams used for water sampling, and the Variegated Glacier longitudinal coordinate system is given in Figure 4.1 . The longitudinal coordinate (stated in "Km") follows the centerline of the glacier, with origin at the head of the glacier; it is the same coordinate system used in previous publications (Bindschadler et al., 1977; Kamb et al., 1985).

The first dye-tracing experiment was carried out while the glacier was in surge, by injection of dye in a borehole at Km 9.5, about 8 km above the nearest terminus outflow stream (VR) (Fig. 4.1). The third experiment was carried out by injecting dye at approximately the same place, after the surge had terminated. Rhodamine WT tracer was used in the first and third experiments, whereas Tinopal AMS was used in the second experiment, in which injection was at Km 17.2 (Fig. 4.1), much closer to the terminus than in experiments 1 and 3. The dye-tracing results obtained in experiments 1 and 3 proved to be much more informative than those from experiment 2; hence, most of the presentation and interpretation in this thesis concerns the results of experiments 1 and 3, which form a contrasting pair of great usefulness.

Before June 1983, most of the glacier outflow stream discharge was carried in the terminus stream called "Variegated River." Its location is indicated in Figure 4.1 and labelled "VR." After June 1983, most of the discharge emanated from the outlet

called "Lower Stream," labelled "LS" in Figure 4.1. During June, the discharge was divided in a variable way among streams, including, in addition to VR and LS, also "Thief Creek" (TC), "Thief Creek Cauldron" (TCC), "Thief Creek Shear" (TCS), "North Terminus Stream" (NTS), and "Burglar Creek" (BC). These are indicated in Figure 4.1. In the three dye-tracing experiments, outflow stream water was collected repeatedly from among the foregoing streams in accordance with which ones were contributing significantly to the total discharge from the glacier at the time.

4.2. First Dye-Tracing Experiment: June 9-26, 1983

4.2.1. Preliminaries

The first objective of our dye tracing program was to inject Rhodamine WT into the basal water system of the actively surging region of Variegated Glacier. At the outset of the study it was not known how the surge would proceed, nor how long it would last. There was only a small area within the actively surging glacier, near Km 9.5, where the glacier surface remained sufficiently unfractured that it was feasible to drill boreholes for tracer injection. Taking a chance on the longevity of the drill camp and the people working there, Barclay Kamb, Hermann Engelhardt, Keith Echelmeyer and three assistants established a borehole drilling camp at Km 9.5. The drill camp was at a longitudinal position between two major zones of extensional crevassing, and at a transverse position near the center of the glacier, well away from marginal zones of brecciated ice. The drill site was just a few hundred meters upglacier from a steeper portion of the glacier where the surging mass of ice broke into an impassable jumble of towering ice blocks and deep fractures.

Survey observations used to obtain ice velocities during the 1983 field season were taken by several different members of the Variegated research team from six separate locations. The velocities at Km 9.5 showed more than a tenfold increase from before the surge began in 1982 to the time of the first tracer experiment, when the drill site was being carried toward the glacier terminus at a speed of 15 m/day. The fastest ice velocities measured during the surge were near Km 14.5. Velocities at about Km 14.5, near the middle of the reach through which the tracer travelled in the experiment, are shown in Figure 4.2a.

In order to provide a basis for computing the total amount of tracer returned in the experiment, the terminus outflow streams were monitored for total discharge. Data on stream discharge during the course of the first experiment are shown in Figure 4.2b. The data from TCC and LS were obtained by Neil Humphrey and colleagues from the University of Washington, with remaining data by the author. During the first tracing experiment, the surge front had just begun to push into the nearly stagnant ice of the terminal lobe (Fig. 4.1), crushing the terminus stream tunnels and disrupting the streams. Data plotted in Fig. 4.2b give approximately the total discharge from the entire glacier cross section, and represent data from the single main terminus stream (TCC) for the time period June 5 to 9, from all streams (TCC, VR, TCS, TC, NTS,LS) between June 11 to 17, and for the lower main stream (LS) for June 15 to 27.

Mean stream velocity was estimated from timing the speed of small floats tossed into the middle of the stream. To check on accuracy, estimates of discharge based on surface level and width variations of each stream were compared several times to complete measurements of stream cross section. Visual estimates of discharge agreed

well with detailed measurements and allowed us to estimate discharge at as many outlet locations as necessary during stream sampling. Visual estimates were continued even when the main discharge was emanating from a well-gaged location. Where direct observations were not made, peak discharges at remote locations or during the night were estimated from the height of new stream terraces, distribution of stranded ice chunks, and behavior of other streams.

The surging action of the glacier caused repeated destruction of stream outlet locations, even after they had just been reestablished. Sometimes a major discharge river would be reduced to a mere trickle, while a nearby outlet suddenly developed. For the first week of the tracing experiment, the main outlet stream changed its location frequently. Several times during this tracing experiment, major water floods gushed out of different places along the surge front, including recently abandoned stream channels, cauldron-like springs, and active englacial thrust surfaces.

Total stream discharge from all streams during experiment 1 is given in the middle section of Fig. 4.2b. The stream discharge may be underestimated by as much as 5 m^3/sec throughout the entire period of measurement, because of the continually changing location and pulsating discharge of glacier outlet streams. The total peak discharge during flood events could be underestimated by perhaps 10 m^3/sec because of the difficulty in monitoring discharge in the numerous locations where water emanated during these events. During the first week of the experiment, VR was just pinched off by the advancing surge front, yet the closure was not complete, and at each major flood the stream was rejuvenated for a short time. On June 5 to 9 most of the stream discharge emerged primarily from TCC (Fig. 4.1). The water and sediment coming out of Variegated Glacier between June 9 and 15 was discharged

through almost every possible outlet location including TCC, TCS, TC, LS, NTS1, NTS2, VR. During this time interval each stream characteristically fluctuated in relative discharge. At times during June 1983, the water from TCC and TCS probably joined the discharge at LS; whenever field observations suggested this was occurring, the effect was accounted for in stream discharge calculations.

The repeated occurrence of outburst floods, as well as the continually changing location of terminus streams, wreaked havoc on our sampling plans. An attempt was made to employ an automatic water sampling device at the lower stream site, but this proved to be impossible. The automatic sampler was either nearly destroyed by floods, left stranded in abandoned stream channels, or clogged by sediment at each water intake. In order to sample water and sediment from terminus streams, samples had to be taken manually.

Preparation for the first tracer experiment included the drilling of several test boreholes. The first boreholes reached to various levels within the glacier and were used to study the variation of basal water pressure in the area. The choice of injection borehole was based on the requirement that the hole must be directly connect to the subglacial water drainage system.

To find out if the borehole chosen for dye injection was directly connected to the basal water system, it was necessary first to monitor regional water level changes. The variation in borehole water levels from June 5 to June 24 at Km 9.5 is shown in Figure 4.3. These data were obtained primarily by H. Engelhardt. On June 5 borehole E was drilled to a depth of 200 m, and late on June 8 the borehole drilling was completed to a depth of 386 m by the author, H. Engelhardt, and two assistants. Prior to June 9 glacier water levels were monitored several times a day using a float

lowered from the surface into boreholes C, D and E. After June 9, continuous measurement of borehole water level was obtained for borehole E using a pressure transducer and Rustrak recorder. Boreholes C and D were abandoned after June 9. Although C and D had been drilled to a depth of 380 m or greater, the water levels in these holes were at the same position as levels in nearby shallow boreholes.

On June 5, boreholes at Km 9.5 (Fig. 4.3) had water levels at a depth of 44 to 45 m below the glacier surface. At this same time borehole E showed a water level of 42 m. From June 5 to 8 the water level in borehole C rose 5.2 m and the water level in the uncompleted borehole E rose 3.4 m. Prior to completion of borehole E on June 8, water levels in all boreholes monitored at Km 9.5 (Fig. 4.3) were at essentially the same level and all rising. This suggests that a basal water system that was isolated from the near-surface water table did not exist at Km 9.5, or that boreholes C and D did not connect with the active basal water system.

As a depth of 386 m in borehole E was approached for the first time, the progress of the drill slowed down and advanced irregularly for approximately 20 minutes before coming to a halt at 18:10 on June 8. Simultaneously with the halt, a forceful downward pull on the drill stem and hose occurred and the borehole water level began to drop. Within minutes the heater supplying hot water to the drill stem suddenly blew off steam at its relief valve, and the heater had to be turned off. The overheating of the heater was caused by an insufficient flow of water through the drilling system, and suggests that an obstruction had formed in the hose or the drill stem. The obstruction apparently formed within seconds after the downward pull had begun. As the drill hose was suddenly dragged downwards it must have collapsed in the borehole, forming a kink in the hose and temporarily obstructing the

flow of water. Immediately upon our noticing the overheating problem, our attempts to drill deeper were discontinued and attention was focussed on trying to pull the drill stem from the borehole. Luckily the equipment had not become stuck at the base of the borehole and it was possible to pull up the drill hose, but not without great effort. The strong downward pull on the drilling hose continued to hamper retrieval efforts until a depth of approximately 200 m below the glacier surface was reached. At shallower depths there was a marked decrease in tension on the drilling hose. When the drill stem was finally brought to the glacier surface, the metal was distinctly scratched and abraded, probably from rocks at or near the glacier bed.

Proof that borehole E actually did reach the glacier bed comes from data on the decrease in borehole water level (Fig. 4.3) after the drilling progress stopped, and from independent confirmation of glacier depth 386 m by radio-echo sounding (unpublished Caltech data, 1983). Radio-echo sounding depths were measured at the borehole E site just after drilling was completed on June 8. Additional glacier depths have been measured by Bindschadler et al. (1977) and during earlier Caltech drilling studies (unpublished, 1980-83). Centerline depth measurements from all sources taken at Km 9.5 are in general agreement when the large uplift of the local glacier surface during the surge ($\sim$ 100 m) is taken into account.

The downward pull on the drill stem was undoubtedly due to a large volume of water flowing into borehole E at a depth of near 200 m and discharging at the base of the glacier at a depth of 386 m. This observation is important by itself and indicates that the basal water system of the glacier during the surge, at Km 9.5, was well sealed off from the bulk of the glacier water in the immediately overlying ice. This separate water system was apparently perforated at the bottom of borehole E.

To insure that borehole E did not close and lose its connection to the basal water system during the tracer injection, on the morning of June 9 the hole was widened over the depth range 380 m to 386 m with the hot water reamer. Before widening of the borehole was initiated, it was found that the the drill hose became slack at a depth of 386 m. Along the length of the borehole the downward pull on the drill hose and stem was barely noticeable at the time of reaming. This indicates that the flow of water down the borehole had decreased from the previous day. The base of the borehole almost certainly consisted of rock debris or solid bedrock at a depth of 386 m. These results suggest that the borehole might have been partially obstructed by the morning of June 9, or that the basal water pressure had increased from June 8 to early on June 9. The downward pull on the drill stem experienced on June 8 resumed, at least in part, after being reamed on the morning of June 9. By repeated lowering and raising of the drill hose it was possible to isolate a location at 200 m below which the tension on the drill hose suddenly increased by 20 to 50 percent below this level. This indicates that a large englacial conduit was intersected and discharged water into the borehole at 200 m depth. The water then flowed down the borehole and exited at the glacier bed. The downward flow of water in the borehole between depths of 200 m and the glacier bed at 386 m varied in strength, but continued from early evening on June 8 through the entire day of June 9.

Further indication that borehole E remained open up to the time of tracer injection on the morning of June 9 is obtained from the variation of borehole water levels. The water level in borehole E (Fig. 4.3) was 46 m below the surface just before the base of the glacier was reached at 18:10 on June 8.. The water level progressively decreased for the following 24 hours. Over the first sixteen hours the borehole water

level dropped to 78 m. The water level lowered to a depth of 81 m by 10:00 on the morning of June 9 and reached a low point of 106 m (319 ft) by 15:11 the same day. Apparently, the borehole continued to drain water out the bottom throughout this time interval.

The forceful downward flow of water and the extended time duration of the draining indicated that a good connection with the basal water system existed at borehole E. Consequently, the borehole was chosen for dye injection in the first tracer experiment. Without further delay, final preparations were immediately made at both the glacier terminus and the injection site.

4.2.2. Injection of Rhodamine WT into Borehole E

At 11:20 on June 9, the injection of 50 lbs of Rhodamine WT tracer into borehole E was initiated. The injection was done at a depth of 386 m through the drilling apparatus, including the full length of hose and the reamer stem lowered in the borehole. The volume of dye tracer injected was 0.0286 m^3, and the basin holding the tracer was emptied in three minutes. This implies that the tracer entered the base of the borehole as a slug of highly concentrated dye solution.

Immediately following the injection, at 11:23, rinsing of dye from the input basin and drilling equipment was initiated. After 15 minutes of rinsing with clean water through the drilling apparatus into the borehole, tracer concentrations in the basin had dropped to 1000 ppb. By 12:12 on June 9 very little rhodamine was left in the drilling equipment. At 12:39, after more than an hour of rinsing the injection apparatus into the borehole, the reamer was pulled from the borehole. The rinsing of the borehole was continued throughout the rest of the day, by introducing water at

the surface, in order to keep a continued strong flow of water down the borehole and out at the glacier bed, into the basal water system.

At 13:20 and 15:10 on June 9, an inclinometer was lowered into borehole E to measure the hole orientation. When the inclinometer was lowered to depths below 200 m, instrument readings fluctuated wildly, but above this level stable readings were obtained. The unsteady inclinometer readings suggest there was a highly turbulent flow of water moving down the borehole. The pressure seal of the inclinometer case was broken at a depth of 386 m despite careful efforts to lower the instrument gently, suggesting that the turbulent flow extended to the glacier bed. At 13:30 the inclinometer was pulled to the surface and opened; the inside of the instrument was found filled with pink turbid water with a rhodamine tracer of concentration 1000 ppb. Before inclinometry was started the inside of the instrument had been clean and dry. The water, sediment and Rhodamine WT probably entered the instrument at the moment the instrument suddenly stopped working at a depth of 386 m. The tracer concentration of 1000 ppb shows that most of the tracer had left the base of the borehole within two hours after injection. In addition, the impossibility of obtaining inclinometer readings through the afternoon of June 9 suggests that the strong flow of water down the borehole continued for at least four hours after tracer injection.

It was not until the morning of June 10 that borehole inclinometer readings finally steadied and inclinometry could be completed. The steady inclinometer readings suggest that the rate of water flow down borehole E had decreased.

Despite the unusually strong flow of water down the borehole, the maximum water level drop was only fifty-seven meters. The water level in borehole E (Fig. 4.3)

reached a low point of 97 m below the glacier surface at 15:11 on June 9, as the strong flow of water down the borehole was disturbing inclinometer readings. Late in the day on June 9, the water level started to increase (Fig. 4.3). Borehole water levels rose about ten meters during June 10, as the flow of water down the borehole decreased below detectable levels.

At 0:10 on June 10, the glacier water level at E had risen 5 m, reaching 92 m below the surface (Fig. 4.3), and 11 hours later was at 87 m depth. Repeated fluctuations in borehole water level of 10 to 20 meters about an average level of about 75 m suggests that borehole E remained connected to the basal water system during the following two weeks.

The minimum in borehole water level on June 9 just discussed occurred at about the same time as a marked minimum in glacier flow velocity (Fig. 4.2a). Similarly, the rise in mean borehole water level from June 9 to 12 was accompanied by an acceleration in glacier flow. Short term changes in borehole water level (Fig. 4.3) and glacier flow velocities (Fig. 4.2a) were roughly correlated during the height of the surge.

The borehole observations discussed above show that most of the rhodamine tracer quickly left the base of the borehole and immediately entered the basal water system, and that connection to the basal water system lasted for several weeks after tracer injection.

4.2.3. Borehole Tracer Concentrations Following Injection

To test how rapidly the tracer left the base of borehole E after injection, water samples were taken using a sampling device lowered into the borehole.

Before this samping device was used, a basal water sample was inadvertantly taken at 13:30 on June 9 during an unsuccessful attempt to do inclinometry in the borehole, as described in Section 4.3.1. This water had a tracer concentration of 1000 ppb, as already noted.

Tracer concentrations in samples obtained with the borehole sampling device are shown in Fig. 4.4 . The concentration decreased with time in roughly a linear trend at a rate of 10 ppb/hr from late afternoon on June 9 to early June 11. Tracer concentrations had dropped to about 1 ppb by June 11, 48 hours after tracer injection. The change of borehole tracer concentrations with time confirms that most of the tracer left the base of the borehole within the first two hours, and essentially no tracer remained in the borehole 48 hours after tracer injection. Thus, most of the tracer entered the basal water system of the glacier almost immediately after injection.

4.2.4. Return Pattern for Dissolved Tracer

For the first three days after tracer injection, water samples were taken by Neil Humphrey of the University of Washington. On June 11, helicopter transportation was available from the drill site, isolated by crevassing, and I was able to take over sampling the terminus streams. From June 9 to late on June 11, sampling was done only from outflow stream TCC. This is not a major problem because on June 9, 10 and 11 most of the glacier water discharge was emanating in TCC. It was not until June 12 that TCC no longer carried most of the terminus discharge but by then I had begun sampling all significant terminus outflow streams shown in Fig. 4.1 . Only streams with a discharge of at least 1 m^3/sec were sampled, except that, for

continuity of record, stream samples were taken from each of of the main outlet streams (VR and LS) as often as possible, even when their discharge was very low. In several instances between June 11 and June 15, samples could not be obtained at a normally significant outlet stream, because the outlet had been pinched off by the advancing front of the glacier surge.

A plot of the concentration of dissolved tracer for the time period from June 9 to 26 is given in Figure 4.5 . Dye was found in all terminus streams monitored. The streams where water was found between between June 9 and 12 included TCC, TCS, LS and VR.

At 7:10 on June 10th, the first detectable rhodamine tracer reached the glacier terminus at TCC. Later in the morning of June 10th, approximately twenty-six hours after the dye was injected, tracer concentrations had slowly risen to 0.03 ppb, just three times the limit of detectability. The time of appearance of dissolved tracer concentration at the terminus provides us with a maximum velocity of tracer movement through the glacier. The fastest tracer traveled the 8 kilometer distance to the main outflow at TCC in about 20 hours; the maximum velocity was 0.1 m/sec.

The concentration of dissolved tracer (Fig. 4.5) continued to rise smoothly for 26-31 hours, following its initial appearance until a peak of 0.96 ppb was reached at 14:00 on June 11. On June 12 the concentration slowly decreased. A progressive, but irregular, decline in tracer concentrations continued until early morning on June 13, when there was an abrupt decrease. Between 7:30 and 13:30 on June 12, dissolved tracer concentrations at main outlets TCS, VR, ranged between 0.01 to 0.7 ppb. Concentrations began to increase sporadically throughout the afternoon of the 13th, and settled to a level of 0.1 to 0.2 ppb between June 15 to 18. Afterwards, the

dissolved dye concentrations steadily decreased. No dissolved tracer could be detected in water samples taken after 21:30 on June 24.

The scatter in data is much larger than can be explained by experimental error. The possible source for the scatter is an interesting problem by itself and will be be the subject of further discussion later in this chapter.

Early on June 12, LS experienced several small floods, while simultaneously TCC was boiling wildly with a discharge of about 10 m^3/sec. At TCC early on June 12 large rocks were carried out with the flow, and a rim of "ejecta" formed around the spring. This rim of silt and rock debris was partially washed away on June 13 by a vigorous new outlet called TCS, emanating from an active thrust surface just up glacier from TCC. It was on the morning of June 13th that the largest flood occurred since June 9. Apparently, just as the flood emanated from the glacier, the concentration of dissolved tracer (Fig. 4.5) suddenly decreased. Why the dissolved tracer concentration decreased at the time of the flood is unclear without a discussion of adsorbed dye.

4.2.5. Return Pattern for Tracer Adsorbed on Suspended Sediment

The measured concentration of adsorbed tracer returned in the outflow streams in the course of the first tracer experiment is shown in Figure 4.6.

The return pattern for adsorbed tracer closely resembles that for dissolved tracer until 7:30 on the morning of June 13. At this time, when the concentration of dissolved tracer dropped to low values, adsorbed tracer concentrations reached their highest recorded values of 1.0 to 2.0 ppb. They remained at high levels until 20:45 on June 14 and thereafter decreased steadily. By the early morning of June 16, adsorbed

and dissolved tracer concentrations were once again approximately equal, at a level of 0.1 to 0.2 ppb. The pattern of adsorbed tracer concentrations from TC, TCC, VR, LS and TCS during this time period are in general agreement.

The tracer return for adsorbed plus dissolved rhodamine tracer, here called "total tracer," is shown in Fig. 4.7 . The total tracer concentration showed a broad maximum centered at about 7:30 on June 13. Superimposed on this maximum are sharp peaks. The first peak in total tracer occurs early on the second day following dye injection, at 14:00 on June 11. This sharp peak coincides with the maximum in dissolved dye concentration (Fig. 4.5). There are two other sharp peaks in total dye, one on day four of the experiment and another on day five to six (Fig. 4.7). The timing of these later peaks in total dye is determined by the pattern for adsorbed dye shown in Fig. 4.6. The second peak shown in both the adsorbed and total dye plots reached the highest concentration value between 7:30 to 13:30 on June 13. A third maximum in total dye occurred at 12:45 on June 14. Concentrations remained above 1 ppb from 9:45 in the morning to 13:25 throughout the afternoon of June 14. After 13:25 on June 14 the scatter in total dye concentration was substantially reduced, from $\pm$ 0.5 to $\pm$ 0.1 ppb. The general trend of total dye concentrations shows a gradual decline after mid-day on June 14, reaching the limit of detectibility on June 26. Dye adsorbed on sediment emanated from the glacier at barely detectible levels for two days following the last detected appearance of dissolved dye.

In summary, dye first reached the glacier terminus 20 hours after injection. Dye was released for 17 days following the injection. The maximum in total dye concentration occurred 92 hours after injection. This corresponds to a transport velocity of 0.024 m/sec for the total dye.

4.2.6. Integration of Tracer Return

The cumulative output of dye tracer in the terminus streams during the first tracer experiment is shown in Figure 4.8. It is obtained by integrating over time the product of tracer concentration and water discharge in the streams. The total discharge was assumed constant at 15 m^3/s, approximately the average indicated by the data in Figure 4.2b. The integration was done as a sum over the successively measured tracer concentration values in all streams, the quantity summed being

$$\sum_i \frac{1}{2}(C_{i+1} + C_i)(t_{i+1} - t_i)$$

where C_i is the i^{th} concentration value, measured at time t_i. The total integrated tracer return shown in Figure 4.8 is 0.012 m^3. This is about half of the volume of tracer injected, 0.022 m^3 (Section 4.2.5). Of the detected dye return, about 80% was carried in adsorption sediment (tracer volume 0.009 m^3) and about 20% came out in solution in the water (0.0025 m^3). The total amount of dye returned is at a level normally considered acceptable for water tracing experiments in glaciers (Moeri, 1983; Krimmel et al.,1978).

Four floods exceeded the mean discharge of 15 m^3/sec. A small flood occurred at 15:30 on June 12; a larger flood happened during early morning on June 13; a very large flood occurred late on June 17, extending to June 18, and then again on June 21. These floods may be responsible for small irregularities in the cumulative tracer return curve, but cannot account for the total amount of missing dye, amounting to 50% of the amount initially injected.

4.2.7. Suspended-Sediment and Tracer Concentrations

A rapid drop in dissolved tracer concentration from 0.7 ppb to 0.4 ppb early on June 13 (Fig. 4.5) was synchronous with a rapid rise in stream sediment load in all major outlet streams. Sediment content in each water sample for the time period of experiment 1 is shown Figure 4.9. The highest observed sediment concentrations, more than 100 g/l, were in TCC on June 9, before any dye return was detected. At this time a large flood was discharged (Fig. 4.3b) and TCC outlet was first getting established. Sediment loads increased from about 40 gm/l on June 12 to values in the range 50 to 100 gm/l on June 13. The increase in sediment discharge from June 12 to 13 happened during the stablization of TCS. The discharge at TCS rose from less than 1 m^3 /sec in the morning to 4 m^3/s by the afternoon of June 13th at the same time as the amount of dye in the water was decreasing. Some streams showed lower sediment concentration than others, but all of the streams with water discharge above 1 m^3/s generally had about the same total dye concentration. The streams which had been pinched off by the rapidly advancing glacier ice were probably strongly diluted by local surface melt at this time. Sediment loads and adsorption of tracer on sediment were highest for a set of streams emanating from the englacial thrust surface at TCS.

4.2.8. K_d Values for Adsorbed Tracer

Adsorbed tracer concentration (Fig. 4.6) tends to reach a maximum value at the time of maxima in suspended sediment load (Fig. 4.9) but high values occurred at other times as well. In order to understand the dye return curve further, we must discuss the time variation of adsorption distribution coefficient values K_d for

adsorption of dye on sediment during the course of experiment 1. Distribution coefficients, calculated as described in Section 3.5, are shown in Figure 4.10 . The grouping of different distribution coefficients has been pointed out in Section 3.5. Abnormally high distribution coefficients were found for the time period between June 13 to 18. Distribution coefficients were particularly high on June 13 to 15; at this time K_d values (Fig. 4.10) were 10 to 100 times larger than at any other time, except June 21.

The highest ice flow velocities observed in the surge occurred during the first tracing experiment. The dye injection on the morning of June 9 was made at the time of the highest measured ice flow velocity. Ice velocities remained at high levels and fluctuated wildly during the tracing experiment. The glacier velocity plot for Km 14.5 (Fig. 4.2a) and velocity data for other locations on the glacier (Kamb et al., 1985) show that a major velocity event occurred on June 13, just as the distribution coefficient for sediment in terminus stream water suddenly increased (Fig. 4.10). The velocity maximum measured in this motion event was 63 m/day at Km 14.5 (Fig. 4.2a); since this velocity represents an average over ten hours between sucessive surveys (from 20:00 on June 12 to 6:00 in the morning of June 13), the actual peak in motion was probably significantly higher than 63 m/day and therefore probably larger than the peak measured velocity of 65 m/day on June 9.

The sudden rise in distribution coefficient on the morning of June 13 (Fig. 4.10) happened at about the same time as the ice velocity peak and a corresponding stream-discharge peak (Fig. 4.3) and during a major increase in the concentration of suspended sediment, which peaked a few hours later (Fig. 4.9).

In Section 3.5 it was shown changes in the adsorptivity of Variegated Glacier sediment are inversely related to a change in mean and variance of the particle grain-size distribution. The K_d data shown on Figure 4.10 suggests that either the mean, the mode, or both the mean and the mode of the grain-size distribution must have significantly varied during the experiment. A large change in ν_d or μ_d must have occurred on the morning of June 13, and perhaps again on June 21. The suggested decrease in average size of suspended sediment appears to be correlated with, and immediately follow times of highly accelerated glacier flow velocity (i.e., June 13 shown on Fig. 4.2). When a high glacier flow velocities are followed by a sudden flow decrease - such as on the morning of June 13 and June 21 (Fig. 4.2) - the peak in flow velocities are closely followed by a sudden change in the grain-size distribution of suspended sediment, as described in Section 3.5.

The suggested changes in average size distirbution of suspended sediment might be closely correlated to changes in glacier flow velocity for several reasons. One possibility is that the accentuated grinding action during a speed-up in sliding that occurred between June 13 to 15 may have pulverized rock material to a much finer grain size than at other times when the glacier was moving more slowly. A second possibility is that, perhaps during the peak of the glacier surge, basal water moving under the glacier was exposed to an additional reservoir of fine sediment normally separated from the main drainage system. This might have happened if widespread cavitation opened up new reservoirs of basal sediment during major velocity events. Both increased pulverization and release of stored clay-sized sediment could occur simultaneously.

4.3. Post-Surge Dye Tracing Experiment: July 16-20, 1983

4.3.1. Preliminaries

The third tracing experiment was initiated on July 16, 1983, after the surge of Variegated Glacier had ended. It will here be called the "post-surge dye tracing experiment." As in the first experiment, Rhodamine WT tracer was injected into the base of the glacier through a borehole at Km 9.5 (Fig. 4.1). The borehole (called "G") was enlarged at the bottom with additional hot water reaming in an effort to achieve a good hydraulic connection to the basal water system. The borehole drilling and dye injection were done by Hermann Engelhardt and Paul Titus. The sampling of terminus stream discharge was done by Barclay Kamb, Linda Kamb, and Thomas Johannsen.

Outflow stream discharge was monitored during the post-surge tracing experiment by Charles Raymond and Thomas Johannsen. Most of the outflow was in LS (Fig. 4.1). Its discharge is shown as a function of time in Figure 4.11b.

The motion of the glacier at a location approximately halfway between the borehole drill site and the glacier terminus, at Km 14.5, is shown in Figure 4.11a for the time interval 13-22 July that includes the dye-tracing experiment. Ice flow velocity ranged between 0.4 to 0.65 m/day; it averaged .55 m/day on July 16, and .6 m/day on July 17. A low, broad peak in flow velocity centered at July 17 to 18 is superimposed upon the longterm trend of slow deceleration that followed termination of the surge on July 4-5 (Kamb et al., 1985). A major maximum in discharge (flood) on July 17-18 correlates with the weak maximum in glacier flow velocity on July 17-18. Between July 16 and 22, glacier flow speeds at the Km 9.5 site were 0.4 to 0.5

m/day, only slightly higher than pre-surge velocities.

Water levels in deep boreholes at Km 9.5 provide information on basal water pressures at this location during the post-surge tracer experiment. For the week prior to tracer injection, water levels in the deepest borehole at Km 9.5 fluctuated around a depth of 100 m, ranging from 60 m to 195 m below the glacier surface (Fig. 9 in Kamb et al., 1985). On the morning of July 16, at the time of tracer injection, water levels were gradually rising; in the late afternoon, they reached a depth of 40 m and then rapidly dropped to 100 m depth. Further drop occurred on July 17. The water level went down to 170 m depth on July 18 before beginning to rise again. The drop in water level correlates with the terminus outflow flood on July 17-18, noted above.

On each day from July 16 to July 20, the glacier discharged a significant flood of water during the late evening hours (Fig. 4.11b). The highest stream discharge occurred in the late-evening or early-morning hours (20:00 to 02:00) and the lowest discharge occurred during mid- to late-morning hours (6:00 to 12:00). The peak in the diurnal cycle occurred six to ten hours after the maximum mid-day surface melt (about 14:00). The daily floods during this time were much larger than the normal diurnal discharge fluctuation, but the timing was normal. On the day of tracer injection, stream discharge was relatively constant by comparison with its behavior during the following three days. Stream discharge on July 16 varied between 35 to 45 m^3/sec and averaged 40 m^3/sec (Fig. 4.11b).

4.3.2. Return Pattern for Dissolved Tracer

At 10:05 hours on July 16, a volume of 0.022 m^3 of Rhodamine WT tracer was injected at the borehole G. The injection took ten minutes. After the drill hose was lifted part way up the borehole, the remaining tracer was flushed out of the drilling equipment, with clean water. Clean water was introduced into the top of the borehole for several more hours thereafter.

Sampling of water from near the bottom of the borehole on July 17, 24 hours after injection, showed a tracer concentrations somewhat higher than 1000 ppb (Engelhardt, personal communication, 1983). This indicates, by comparison with the data in Fig. 4.4, that the tracer exited more slowly from the base of borehole G in the post-surge experiment than from the base of borehole E in experiment 1. The amount of tracer remaining after a few hours in either case was negligible as compared to the amount in the initial injection pulse. It can be reasonably assumed that in both experiments most of the tracer left the borehole and entered the basal water system soon after injection.

In order to measure the dye return at the glacier terminus in the post-surge experiment, water samples were taken from streams LS, BC, TC, and VR (Fig. 4.1) on July 16 to 22. Initially, stream samples were taken at 40 minute time intervals. After eight hours the interval between sampling was lengthened.

The measured values of dissolved tracer concentration for the samples from LS are shown in Figures 4.12 and 4.13, plotted versus time. They show a high, sharp peak in tracer return, arriving at the terminus about 4 hours after the injection. Within the constraints provided by the sampling, an initial peak in dye concentration could have arrived between 13:40 hours (tracer concentration 0.01 ppb, barely

detectable) and 14:20 hours (dissolved tracer concentration at 37 ppb). The time for the peak concentration to travel the 10 kilometers from borehole G (Km 9.5) to outflow stream LS (Km 19.6) thus lies between 3 hours 35 minutes and 4 hours 15 minutes. This means that after the surge the tracer was carried from Km 9.5 to the terminus at a speed of 0.7 - 0.8 m/s, 20 to 25 times faster than during the surge. The dye not only traveled rapidly to the glacier terminus, but arrived with little spreading in time, the width of the main tracer pulse being only about 3 hours above a concentration of 1 ppb. The observed spreading of tracer concentration with time is distinctly asymmetrical, with a sharp onset and a tail extending over several hours. This asymetrical shape of the dye-return curve is markedly different from the shape of the curves obtained in the first rhodamine experiment.

Rhodamine WT tracer in detectable amounts was found only in terminus stream LS. No tracer was detected in the water from outflow streams VR, BC, and TC, which, while small compared to LS, nevertheless carried an appreciable discharge. There is a marked contrast here with the first tracer experiment, in which dye was returned in all of the terminus outflow streams sampled.

On the day following tracer injection, a weak but distinctive secondary peak in tracer return was observed (Fig. 4.13). Starting from a low concentration of 0.095 ppb at 08:00 in the morning of July 17, it rose to a maximum of 0.7 ppb at 14:00 in the afternoon. The peak was reached as stream discharge was sharply rising. The discharge increased from 25 m^3/s in the early morning of July 17 to a high of 70 m^3/s in the late evening, constituting a major outflow flood, as noted earlier. The shape of the secondary dye pulse must have been affected by this flood, which apparently purged the glacier of dye, so that no further peaks in the dye return were detected

(Fig. 4.12). The shape and timing of the dye-return secondary peak relative to the diurnal variation in glacier outflow stream discharge are similar to what has been observed in a normal, non-surging temperate glacier (Moeri, 1984).

4.3.3. Return Pattern for Adsorbed and Total Tracer

Adsorbed, dissolved and total tracer return in the post-surge experiment are shown in Fig. 4.14. Most of the tracer was carried in solution. The peak concentration of adsorbed tracer was about 1/20th the peak concentration of dissolved tracer. The arrival time of the two peaks is identical, (Fig. 4.14) and their shapes are nearly the same.

4.3.4. Integration of Tracer Return

The integrated volume of tracer that should have been returned at the glacier terminus, to account for the volume injected, is 0.022 m^3 . In the afternoon of July 16, as the peak tracer concentration reached the glacier terminus, the stream discharge at LS was 37 to 40 m^3/s. In the evening the discharge climbed from 37 to 44 m^3/s (Fig. 4.11b). Cumulative tracer return for an assumed constant discharge of 40 m^3/s is shown in Figure 4.15. The integrated volume of adsorbed tracer is 0.001 m^3, dissolved tracer 0.010 m^3, total tracer 0.011 m^3 (Fig. 4.15). Only eight percent of the total tracer was carried in adsorbtion on suspended sediment. The total amount of detectable tracer returned at the glacier terminus was only half of the amount of tracer initially injected. The missing fifty percent of the tracer either never reached the glacier terminus or was somehow missed in the sampling, as could have happened if, for example, a sharp, high peak of tracer concentration appeared in the outflow

stream between sampling times. A fifty percent tracer return is generally considered to be acceptable tracer return for glacier tracing experiments in glaciers (Moeri, 1984; Krimmel, 1973), and indicates that the tracing experiment was a success.

4.3.5. K_d Values for Adsorbed Tracer

The reason that only a small fraction of the tracer was carried in adsorption on suspended sediment is partly that the sediment concentration was relatively low at the time of the experiment, considerably reduced from what it had been when the glacier was in surge, as shown in Fig. 4.16.

In mid-July, after the surge, outflow stream LS had both the highest sediment load (Fig. 4.16) and the largest stream discharge (Fig. 4.11b) of all the Variegated Glacier outflow streams. LS was evidently the only outlet for most of the drainage coming from the glacier above the immediate terminus area. Such a stream could pick up a high sediment load if its channel were located at the glacier bed. An englacial stream or small stream traveling over a clean rock bed would have a much lower sediment load. Thus, sediment concentration data for mid July suggest that the secondary outflow streams VR and TC traveled over short englacial paths. The high sediment content of LS suggests that this stream traveled mainly along the glacier bed and/or through a zone of basal rock debris.

A second reason for the low content of adsorption-carried tracer in the post-surge experiment is that the distribution coefficient K_d for suspended sediment in the outflow stream LS was considerably lower than it had been in the outflow streams during surge. In Figure 4.17, K_d values over the period from early June through the end of July are plotted for all routine samples in which K_d could be calculated. K_d

values for outflow-stream sediment in the post-surge tracing experiment, July 16-17, average about 5 ml/g. This is less than the K_d values measured for calibration standards (mean value 10 ml/g), It is about an order of magnitude smaller than the general run of lower values ($\sim$70 ml/g) for outflow sediment from the glacier in surge, and approximately two orders of magnitude smaller than the peak K_d values between June 13 and 15. The lower K_d values imply that the areal adsorptivity was lower and/or the grain size distribution had shifted to coarser grain size in the post-surge sediment. If only a change in grain size was involved, the mean grain size of post-surge sediment, based on the measured K_d values, is one to two orders of magnitude larger than during the surge, which corresponds to a mean grain size of 0.015-0.03 mm. The K_d values of about 5 ml/g for the post surge sediment are normal or perhaps even somewhat low in relation to values reported by other authors, as discussed in Section 3.5.

4.4. Comparison of the Surge and Post-Surge Tracing Experiments

In order to compare the tracing experiment conducted after the surge to the experiment during the surge, the concentrations of dissolved and adsorbed Rhodamine WT tracer in the major outflow streams are plotted versus time in Figure 4.18. The dramatic difference between the first and third tracing experiments is shown also in Fig. 4.19, where different time scales are used to accentuate the details of each dye-return curve. The tracer reached the glacier terminus much more slowly and much more spread out in time during the surge than after the surge had ended. Transport velocites were about 0.03 m/sec during the surge and about 1 m/sec after the surge. The shape of the dye-return curve for the glacier surge is very irregular, but with

smoothing it can be seen as a rough bell-shaped curve, roughly symmetrical. The shape of the tracer return curve for the tracing experiment is markedly asymetrical with a precipitous rise to a peak followed by a quasi-exponential tail-off. During the surge, sediment content and distribution coefficient were at elevated levels relative to the post-surge situation (Figs. 4.16, 4.17). Most of the tracer was carried in adsorption on suspended sediment in the surge experiment, whereas in the post-surge experiment most of the tracer was carried in solution. Although frequent large floods emanated from the glacier during the surge, the average daily stream discharge at the glacier terminus reached its highest values after the surge had ended.

The total cumulative tracer return was similar in both experiments, roughly 50%. No rhodamine tracer was detected at the glacier terminus from June 26 until the time of the post-surge tracing experiment on July 16.

During the surge, the sediment content and K_d were high whereas after the surge they were distinctly lower. The variation in sediment loads at Variegated Glacier terminus streams (Fig. 4.16) has a resemblance to the variation of glacier flow velocity (Kamb et al., 1985) and terminus stream discharge (Fig. 4.5). The sediment loads varied between 20 and 110 g/l prior to mid June, 10 to 50 g/l from mid to late June, and 0.01 to 24 g/l after the beginning of July. Even after the glacier surge had ended, sediment concentrations are higher than observed in outlet streams of "normal", non-surging glaciers. The highest sediment concentration observed during the study period occurred from June 9 through 15; after June 15, sediment loads steadily decreased until reaching low relatively constant values by June 30. Once glacier flow velocities dropped down to 5 m/day on upper glacier at Km 9.5 and 5.5 (Fig. 5 in Kamb et al., 1985) or 20 to 30 m/day on lower glacier at Km 14.5 (Fig. 5c in Kamb

et al., 1985) the sediment loads dropped to levels between 0 to 20 (g/l). Before the termination of the glacier surge in early July, ice flow velocities (Fig. 2 and Fig. 5 in Kamb et al., 1985) varied in rough synchroneity with average trend in suspended sediment shown by the shaded portion on Figure 4.16. During the surge, in June, the sediment load in units of g/l was very roughly equal to three times the glacier flow velocity at Km 9.5, expressed in units of m/day, and roughly equal to ice flow velocity (expressed in m/day) at Km 14.5. For short term events, sediment loads normally reached a maximum after glacier velocities reached a maximum and approximatly at the time terminus stream discharge was most rapidly increasing. Examples of synchronous variations in sediment and water discharge during summer of 1983 occurred on the dates June 3, 9, 13, 24, July 4 to 5 and and July 18 (Fig. 4.16).

The measurements of sediment content made on samples taken at the time of surge termination on July 4 and 5, both by filtering and visual estimates, clearly indicate the peak in sediment loads (50 to 60 g/l at 23:30 on July 4) occurred just at the time glacier velocities most rapidly decreased (Kamb et al., 1985). The sediment load on July 4 is approximately equal to the mean observed during the main part of the surge in mid-June, and approximately three times greater than the sediment loads measured during the post-surge tracing experiment.

The distinctive pattern of sediment content in the terminus streams throughout the summer of 1983 independently verifies the unique situation of the glacier drainage system during the first tracing experiment as compared to the more normal situation for the third experiment.

For the third tracing experiment the rapid velocity of the tracer (order of 1 m/sec) through the glacier indicates most of the travel must have taken place in a

large basal conduit. Such a major channel can probably be stable only at the glacier bed, based on studies of water movement within a glacier by Nye (1976), Röthlisberger (1972), Shreve (1972).

4.5. Tracing Experiment Using Tinopal AMS: June 26-July 10, 1983

The second tracing experiment involved injection of the tracer Tinopal AMS, at an injection site located much closer to the terminus than the injection site for the two experiments already discussed. It was carried out shortly before the surge termination. On June 23, borehole J was drilled to a depth of 70 meters, at longitudinal coordinate Km 17.2, just behind the crest of the surge front; the borehole was 2 kilometers upglacier from the outlet of LS, and roughly at the same longitudinal position as the outlet of VR (Fig. 4.1). Radio-echo sounding of ice depth showed that the borehole reached only about halfway to the glacier bed.

The decision to inject tracer into borehole J on June 26 was made because of the great difficulty in keeping the borehole open under conditions of extremely high longitudinal strain and the impossibility of drilling to the bottom of the glacier due to impenetrable debris zones. The behavior of borehole water in borehole J and several nearby boreholes at the site indicated that these holes were connected to an active englacial water system; sounds of gurgling and rushing water in this system could be heard in deep crevasses cutting through the site.

The dye injection was begun at 17:50 hours on June 26 and completed by 19:40, two hours later. The dye pumped down the borehole was not totally dissolved at the time of injection, consisting of a slurry of the powdered dye in water. a large amount (136 kg) of Tinopal AMS was used because of its low detection sensitivity (Section

2.1.3). This amount was less, in terms of equivalent detectability, than the amounts of Rhodamine WT used in experiments 1 and 3, but the deficit should have been compensated, one would think, by the greater proximity of the injection site to the outflow stream portals.

Since adsorption of Tinopal AMS on suspended sediment was found to be negligible, only dissolved tracer in the outflow is reported. Water samples were initially taken from all major terminus streams at time intervals of to 20 to 40 minutes; after 4 days, the sampling interval was lengthened.

Measured dye concentrations in outflow stream water are shown in Figure 4.20. Many data points for samples showing no detectable dye were not plotted due to space constraints on the horizontal axis. The limit of detection for Tinopal AMS is about 1 ppb (Section 2.4).

Most of the stream samples contained no detectable dye. The samples which do show dye are highly scattered in time, but there is a distinct cluster of high dye-return points on July 4-6, essentially coinciding with the time of surge termination. Only twelve samples had dye at concentration above 2 ppb; the maximum concentration was about 250 ppb. One high dye-return value (50 ppb) was found in a sample early on June 28, about 1.5 days after injection; a few low values above the detection limit were found during July 7-10, following the peak on July 4-6. Possibly a high dye return peak was missed between sampling times, but this is quite unlikely, because the time period of two hours needed for tracer injection was considerably longer than the sampling interval. The pattern of data points - mostly undetectable dye concentration, with a scattering of detected concentrations - may be an indication that the non-zero values are simply the result of contamination. However, maximum

contamination would be expected for the samples taken early, contrary to the observed pattern. Also, the occurrence of all but one of the high values during the period of surge termination seems more than a coincidence resulting from random contamination, and suggests a flushing out of the dye from the glacier during this time, as might result from a pressure peak followed by a large flood in the basal water system. At a concentration of 150 ppb and a stream discharge of 40 m^3/s, the injected 136 kg of Tinopal AMS could have been returned in a period of 6.3 hours, hence the scatter of dye return points in Figure 4.20 is compatible with a full return of the injected dye.

Because the results of the second tracer experiment are subject to the question of possible contamination, whereas the results of experiments 1 and 3 are less subject to this question, the emphasis in this thesis is on experiments 1 and 3, and the results of experiment 2 will not be further discussed.

MAP OF VARIEGATED GLACIER

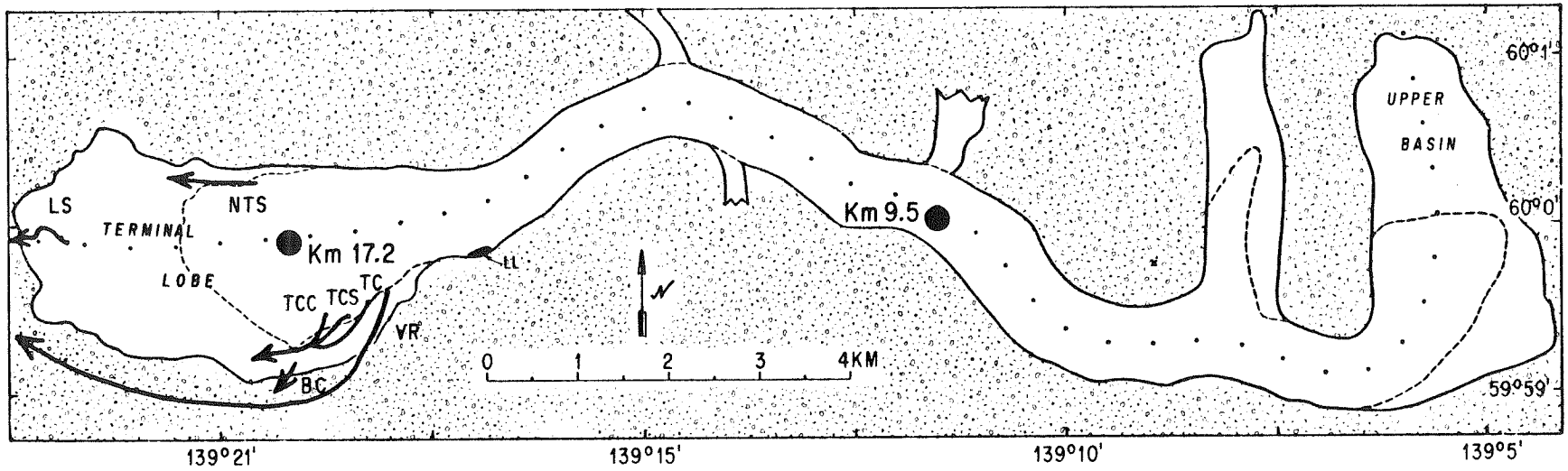

Figure 4.1 Map of Variegated Glacier, Alaska, showing location of tracer injection points (solid circles) and terminus outflow streams sampled in dye tracer experiments. The outflow streams, indicated with heavy sinuous arrows starting at the point of emanation from the glacier, are identified by letters as follows: VR, "Variegated River"; TC, "Thief Creek"; TCC, "Thief Creek Cauldron"; TCS, "Thief Creek Shear"; BC "Burglar Creek"; NTS, "North Terminus Stream"; LS, "Lower Stream". The identifying letters are placed adjacent to each stream, and samples were taken at the glacier terminus. Small numbers at along the glacier centerline give the longitudinal coordinate of the injection points, in Km, measured from the head of the glacier for location of the injection points.

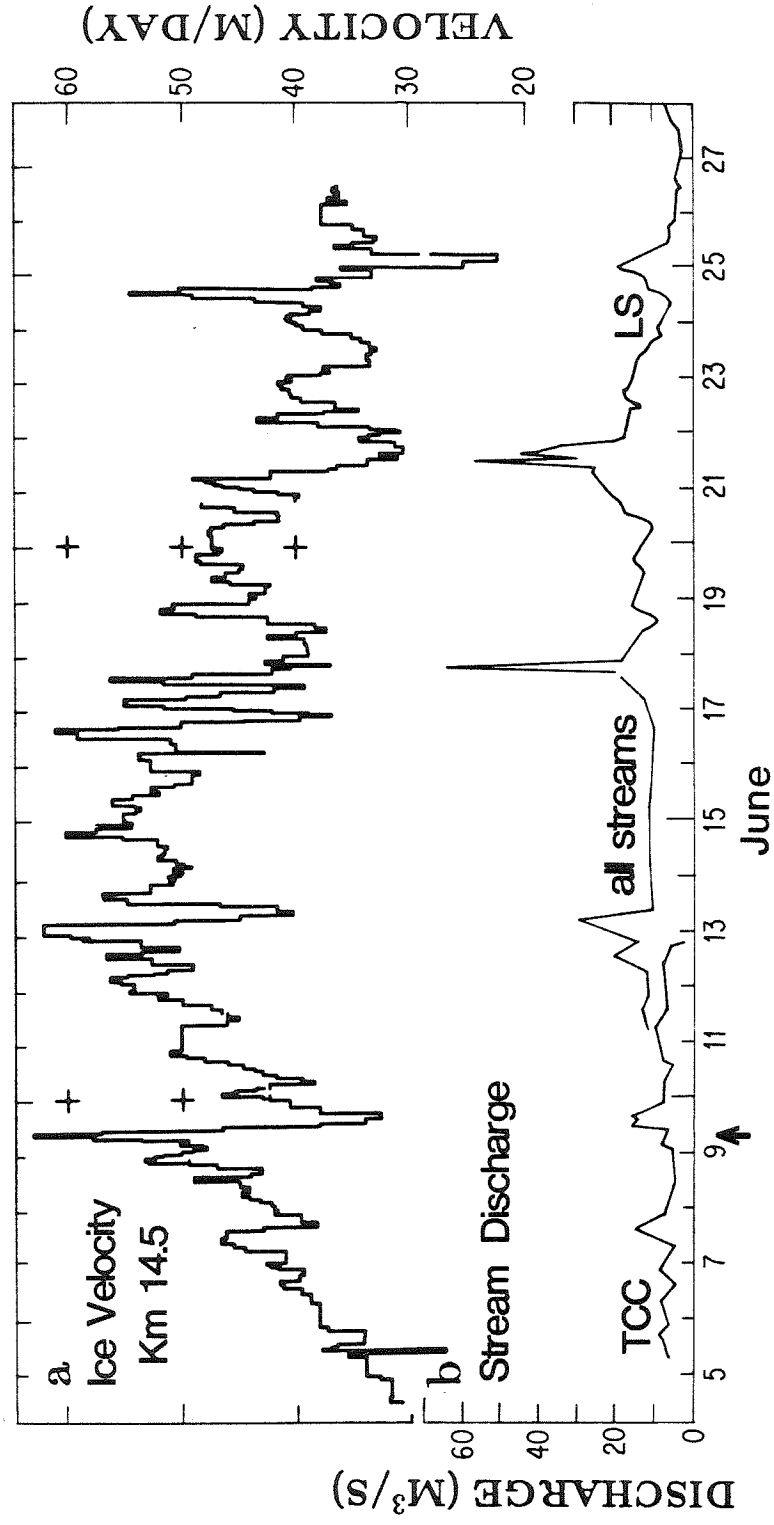

Figure 4.2 Glacier flow velocity and outflow-stream discharge over the period 5-28 June 1983 during which dye tracing experiment 1 was carried out. Flow velocity (a) is for a marker at about 14.5 Km; data are from Kamb et al. (1985). Water discharge (b) in the outflow streams indicated by the letter symbols (see Fig. 4.1) is based on observations by N. Humphrey and the author. Time of tracer injection is marked with arrow.

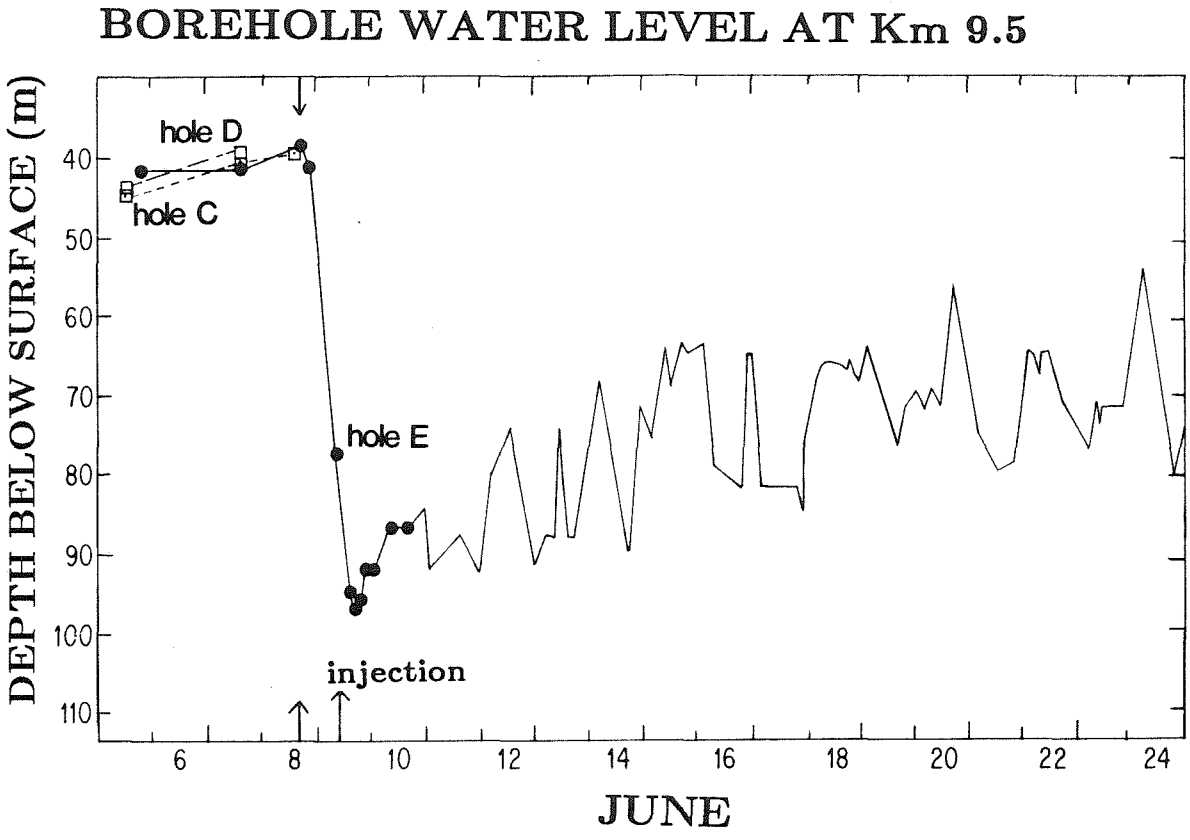

Figure 4.3 The variation in borehole water levels from June 5 to June 24 at Km 9.5. Data points indicate direct measuremnt of water levels using floats lowered in to the borehole. The solid line after June 10 represents data obtained from a pressure transducer lowered into borehole E. Most of the data shown on this figure are from Kamb et al. (1985). The first arrow on the horizontal axis at 18:00, June 8 indicates the moment the hotwater drill first reached the glacier bed at borehole E. The second arrow at 10:05 on June 9 indicates the moment the Rhodamine WT tracer was injected at the base of borehole E. The solid circles plotted prior to June 11 represent spot water level measurements for borehole E, the open square symbol represents nearby borehole D, and an open square with a dot in the center is used to represent nearby borehole C. Further discussion of each borehole is given in the text.

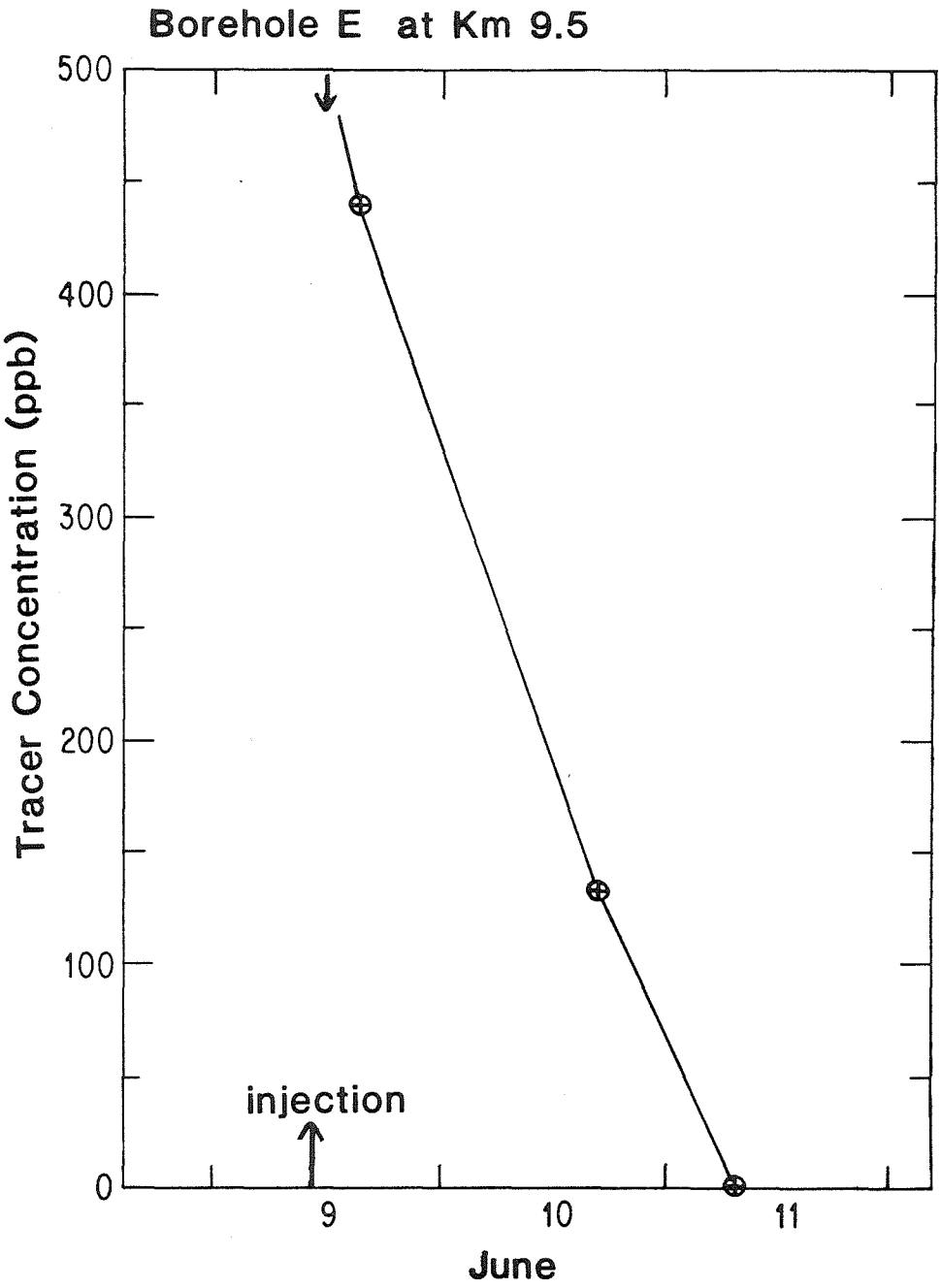

Figure 4.4 Plot of concentration versus time for samples taken from the bottom of Borehole E following the June 9 dye injection.

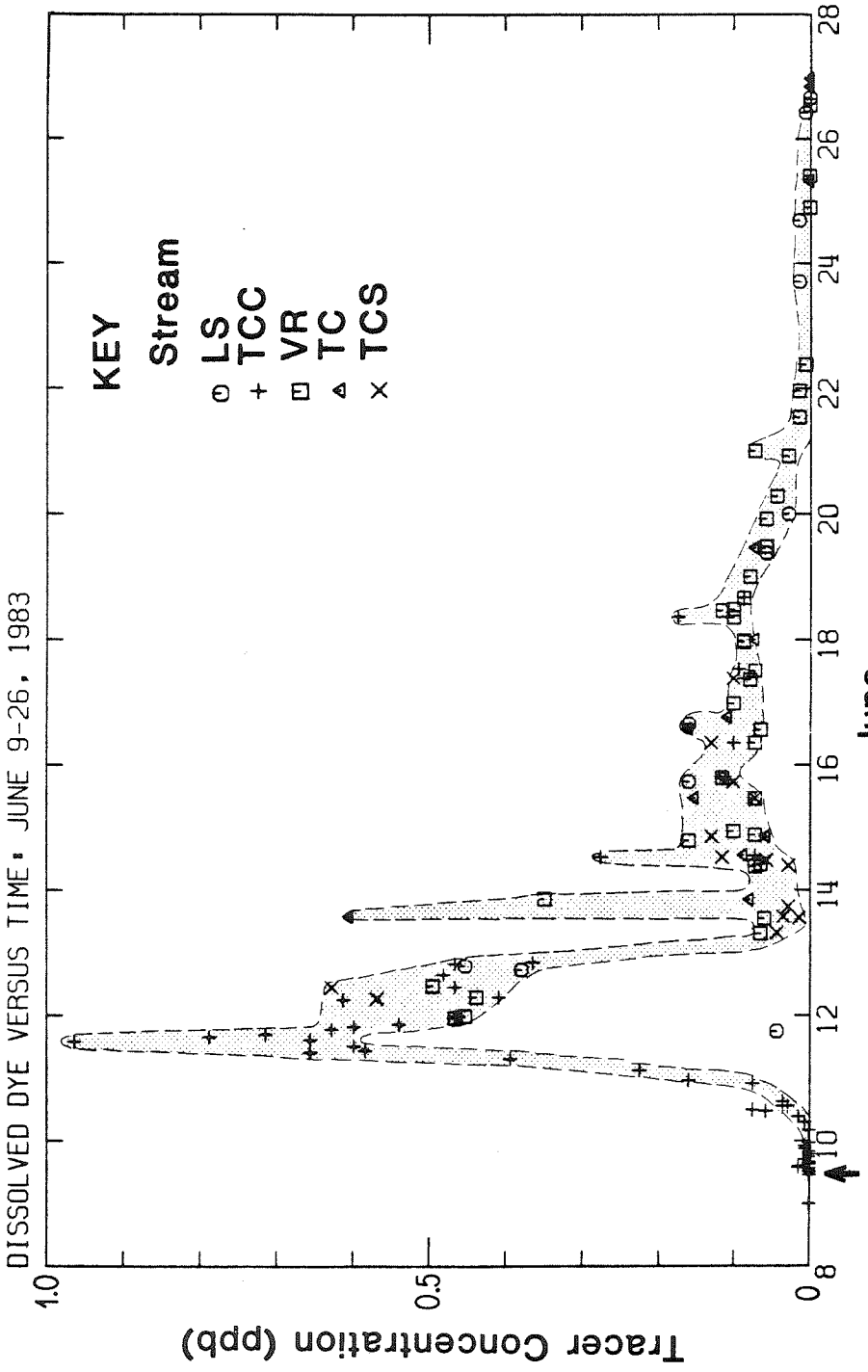

Figure 4.5 Dissolved Rhodamine WT tracer in outflow streams as a function of time following the first tracer injection, over the period June 9-26, 1983. Samples from different outflow streams are identified as indicated in the key.

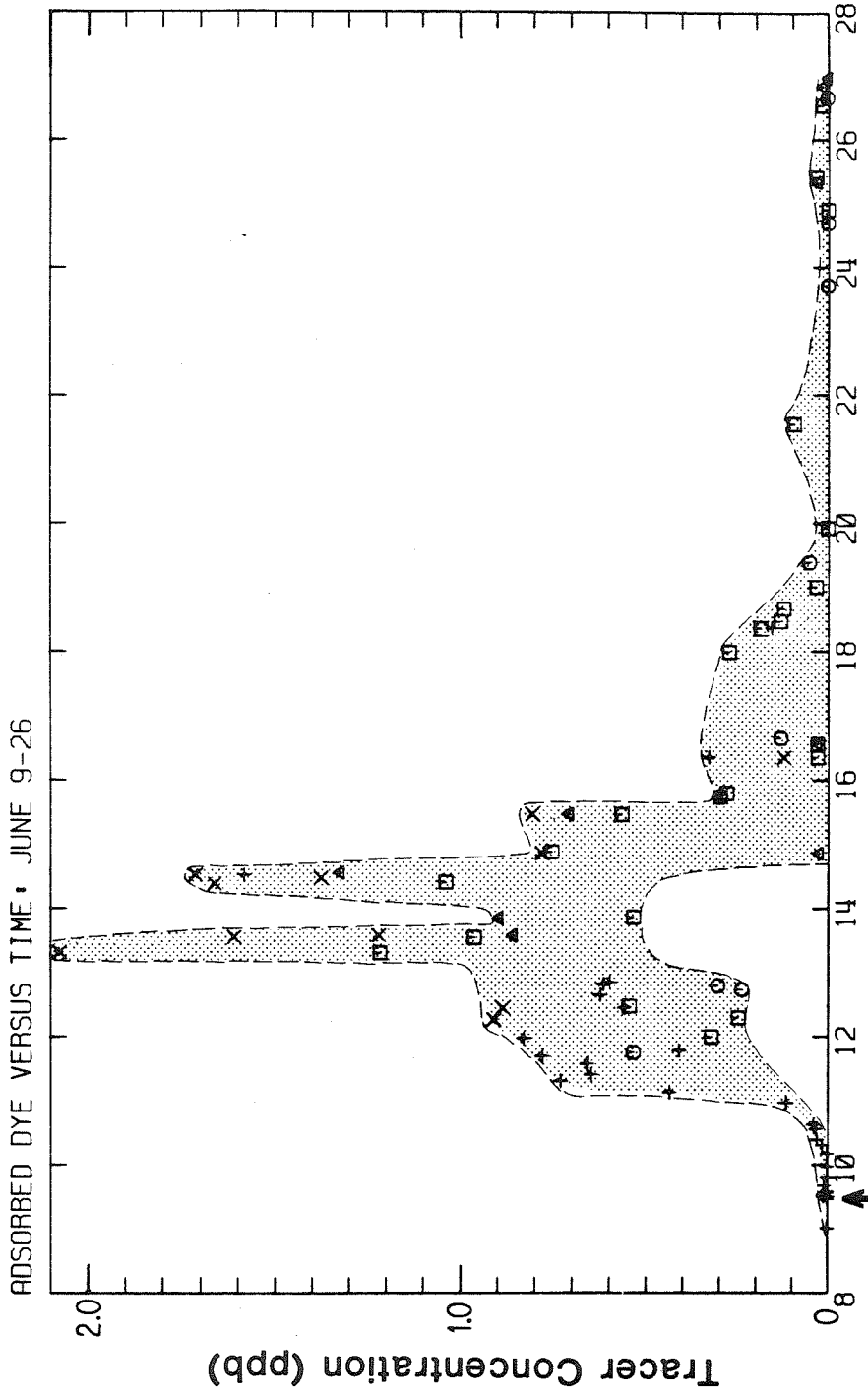

Figure 4.6 Adsorbed Rhodamine WT tracer concentration as a function of time from June 9 to June 28, 1983. Key to identification of data points is in Fig. 4.5.

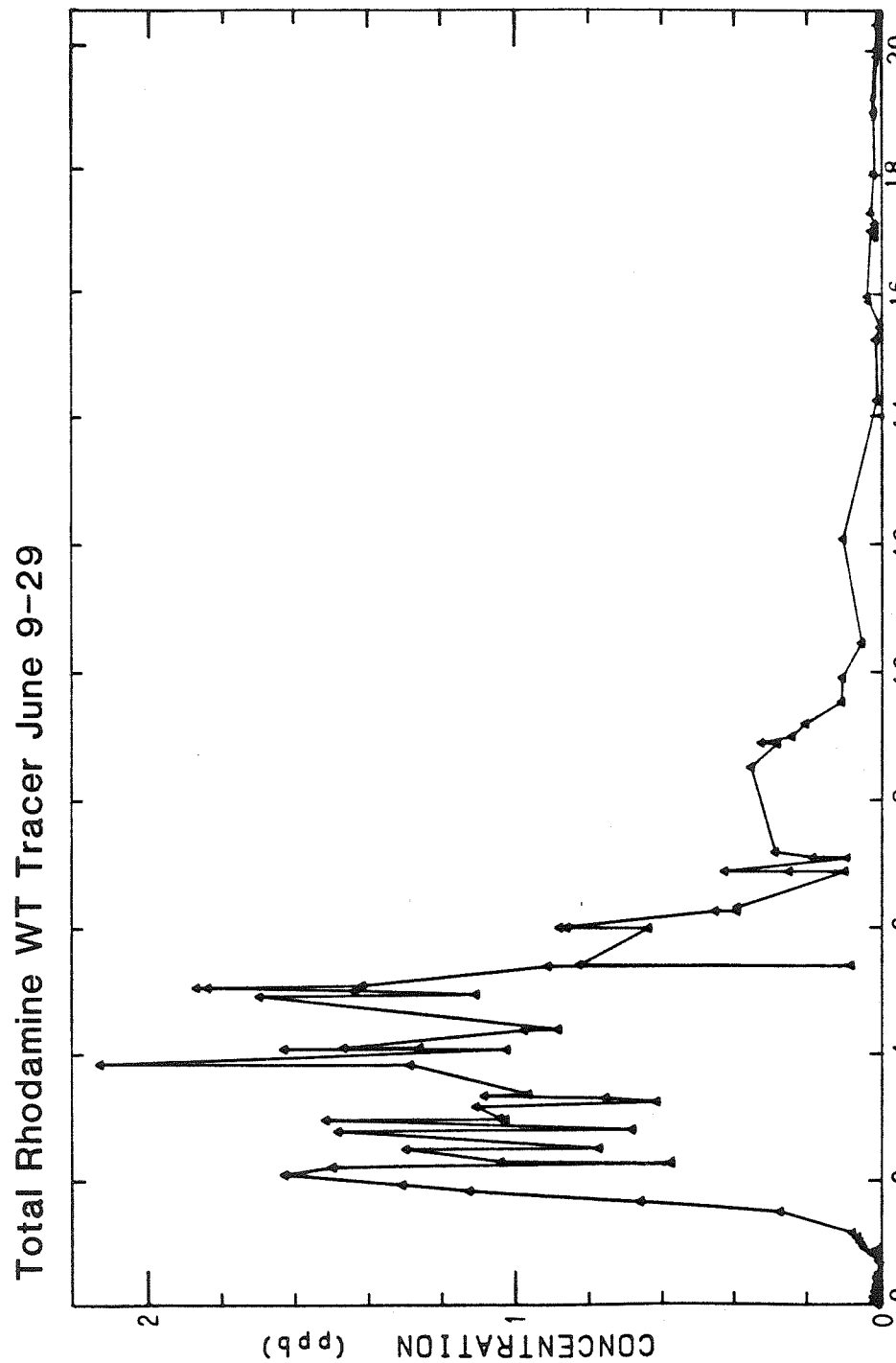

Figure 4.7 Total (dissolved plus adsorbed) tracer concentration versus time for the first trace experiment as measured in samples from all outflow streams monitored.

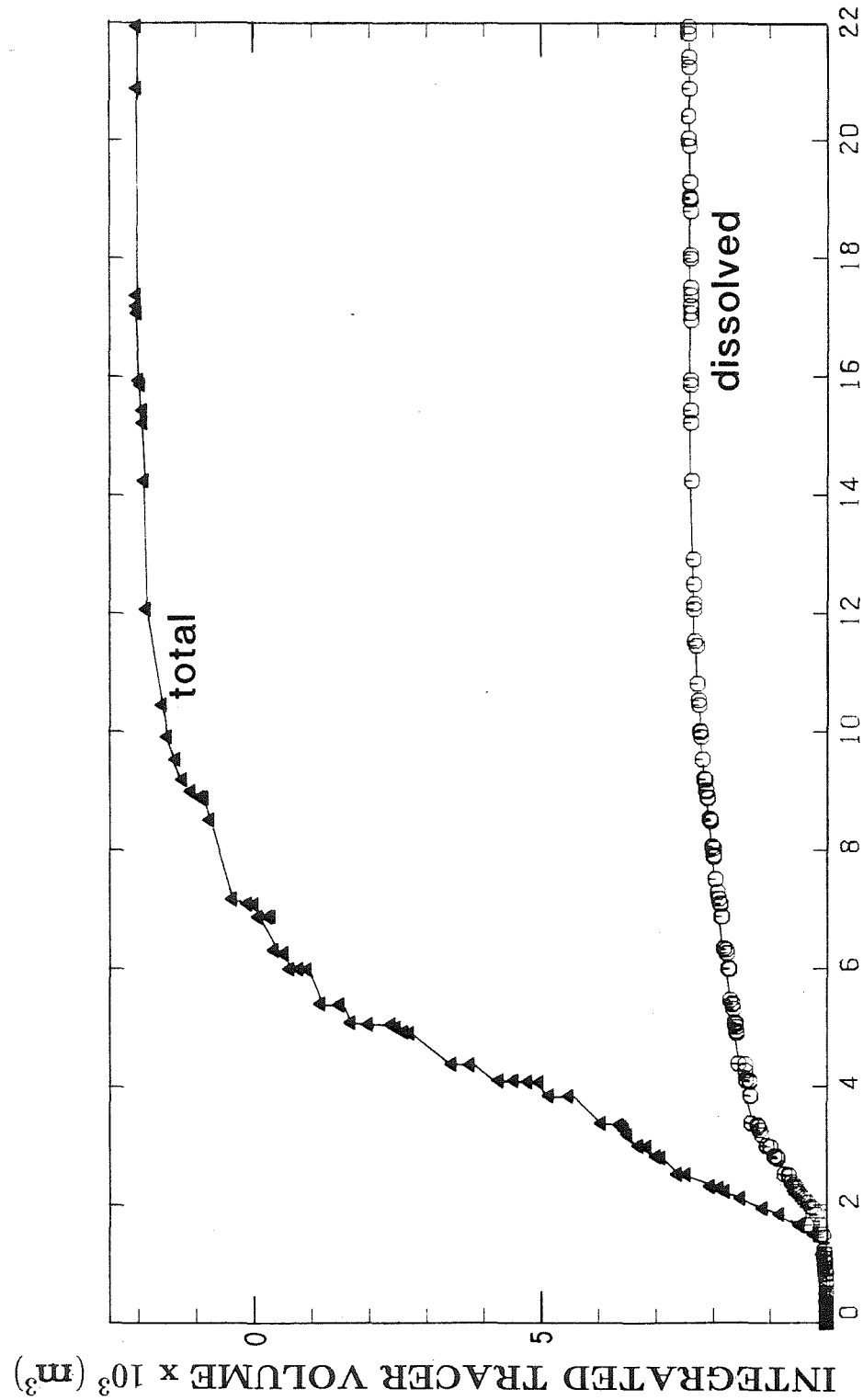

Figure 4.8 Cumulative tracer return for the first tracing experiment (during the surge), showing integrated results for June 9 through July 1, 1983. Return of dissolved tracer is shown separately, as well as the sum of dissolved and adsorbed tracer (i.e., total tracer).

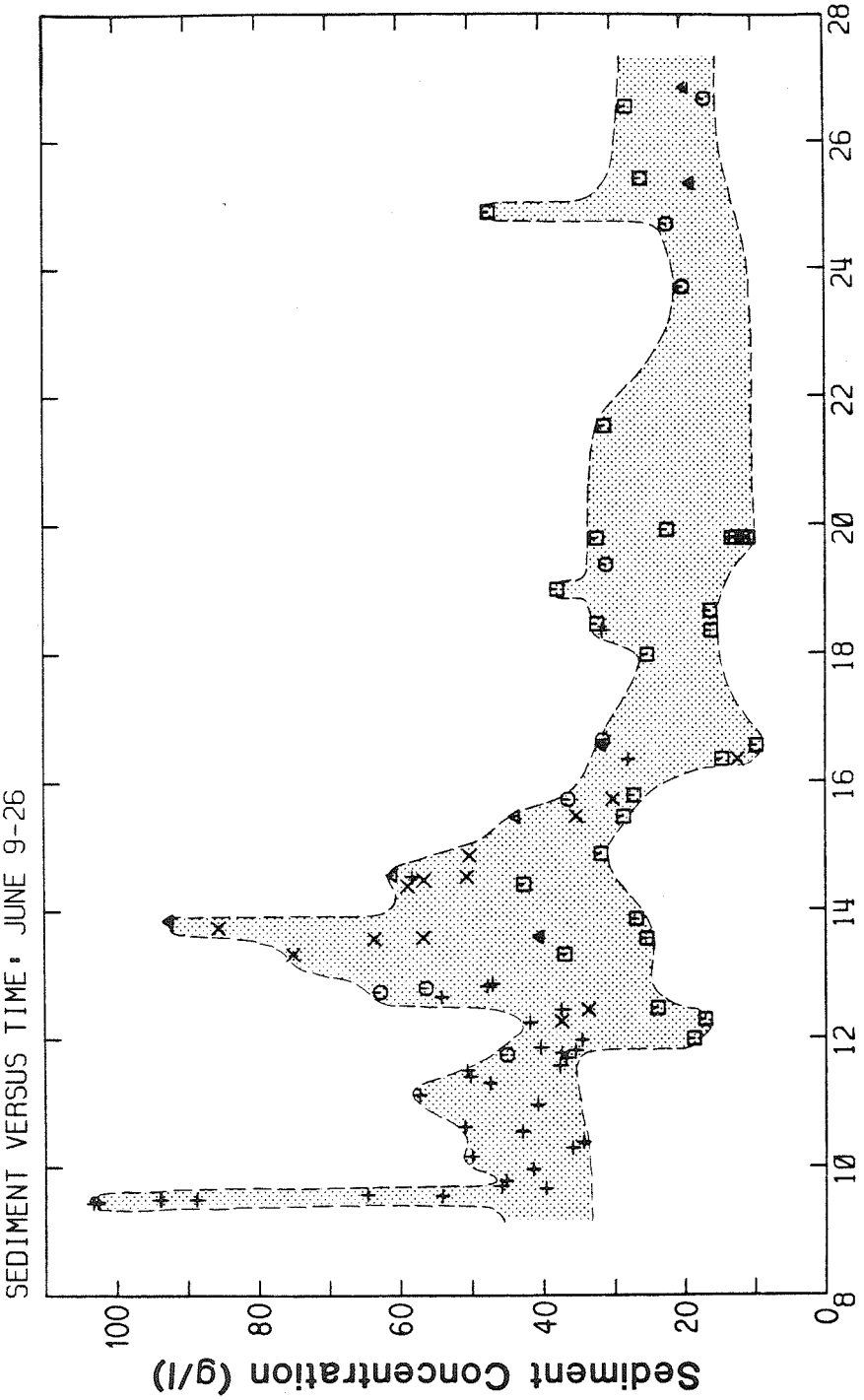

Figure 4.9 Sediment concentration in outflow stream water during the first tracer experiment, as a function of time. Key to identification of data points is in Fig. 4.5.

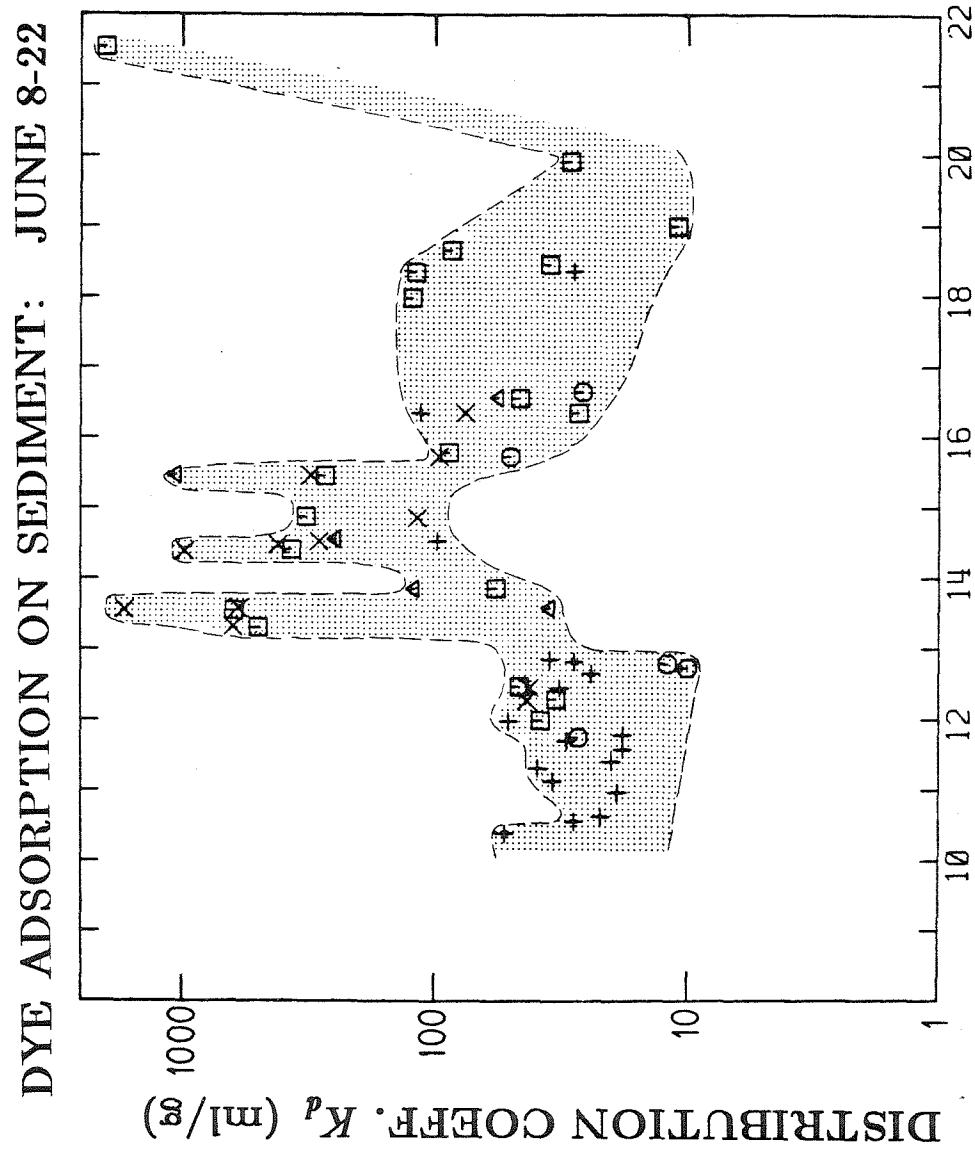

Figure 4.10 Distribution coefficients K_d (ml/g) for Rhodamine WT tracer adsorbed on sediment in water samples taken June 10-22, 1983. Note the increase in K_d values on June 13 and the decrease on June 15.

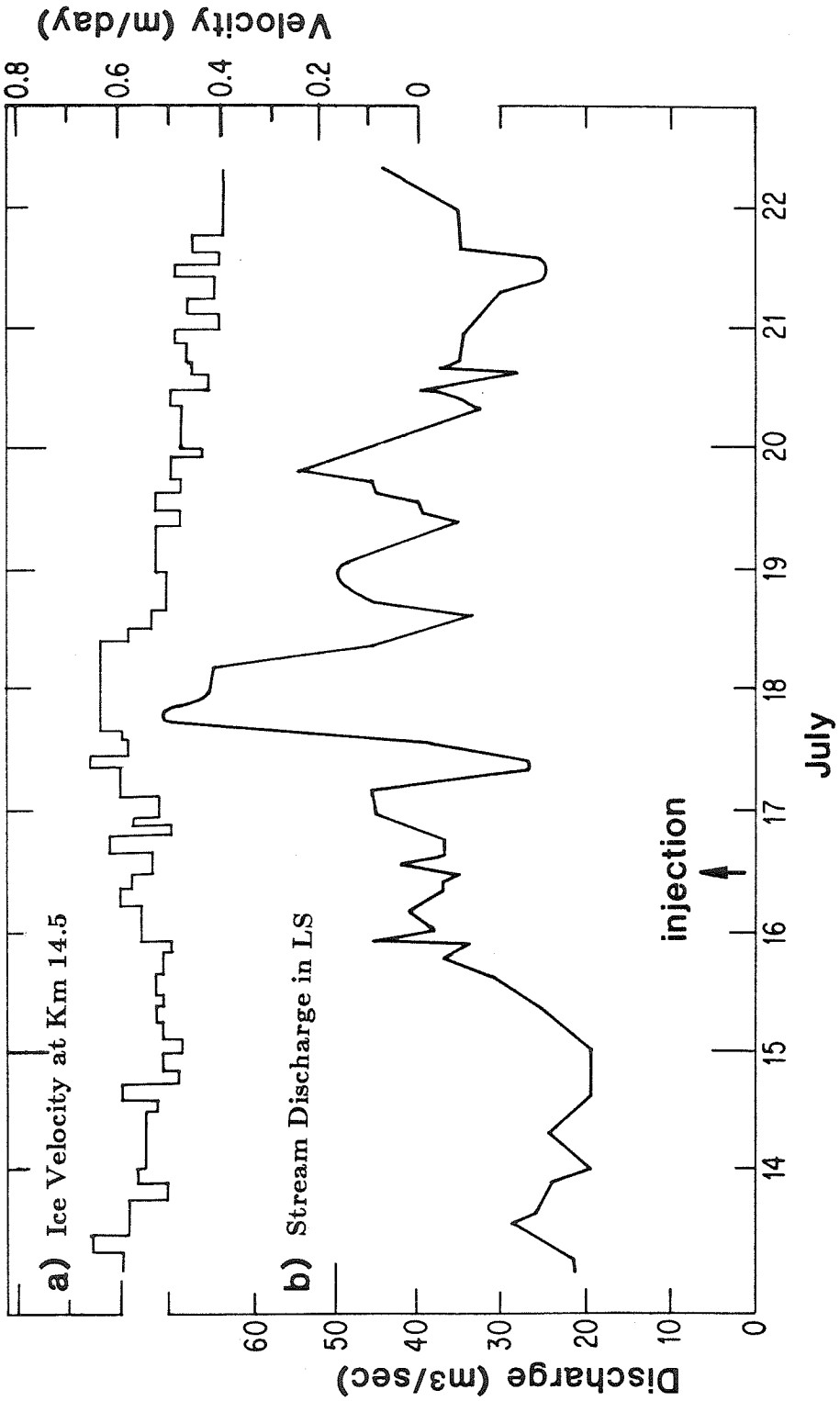

Figure 4.11 (a) Glacier flow velocity at a marker near Km 14.5 during July 15-22. Data are from Kamb et al. (1985). (b) Stream discharge in LS (Fig. 4.1). Data from C. F. Raymond and N. Humphrey.

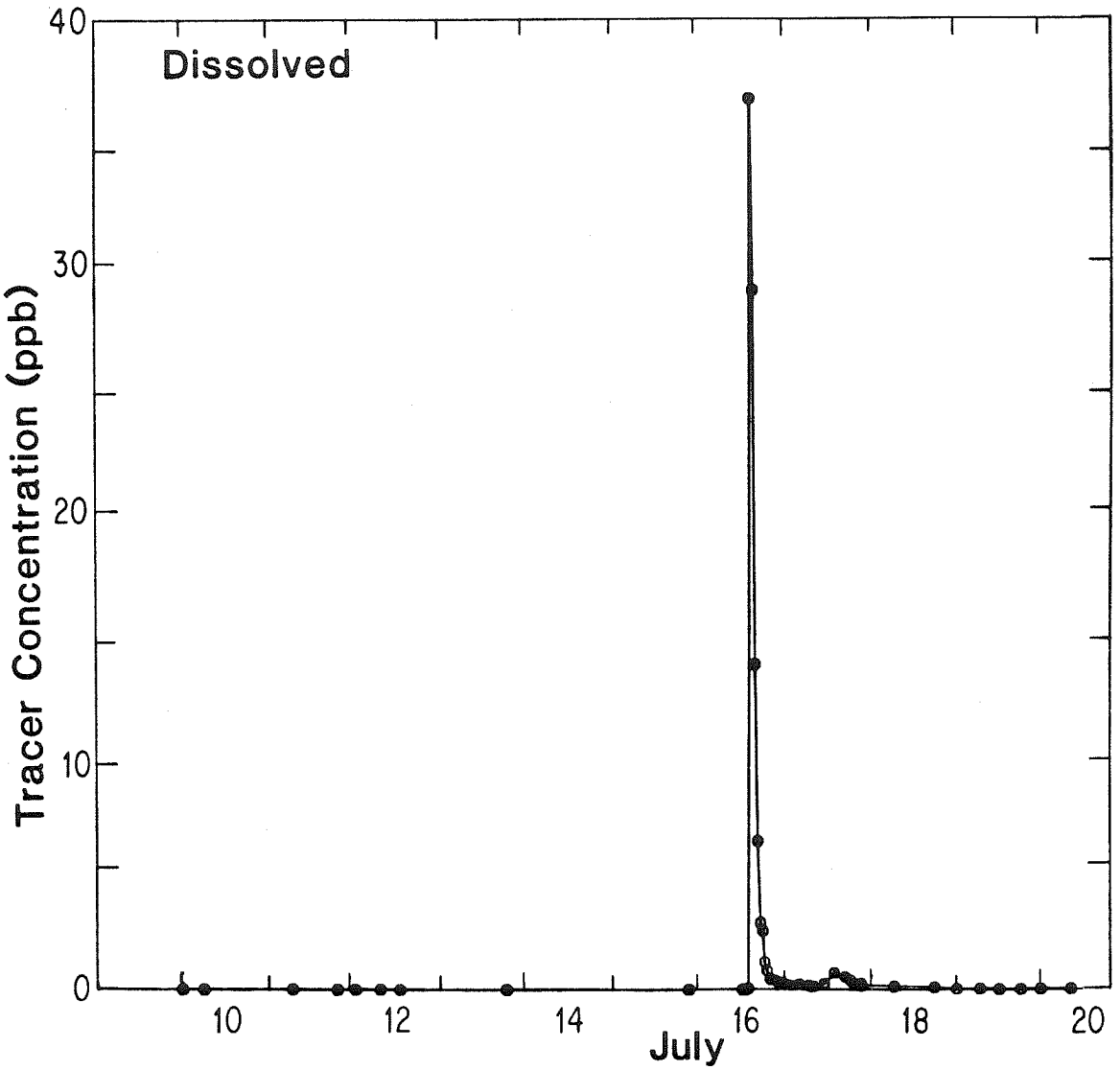

Figure 4.12 Dissolved Rhodamine WT tracer concentration in glacier outlet stream LS versus time, in the post-surge tracer experiment.

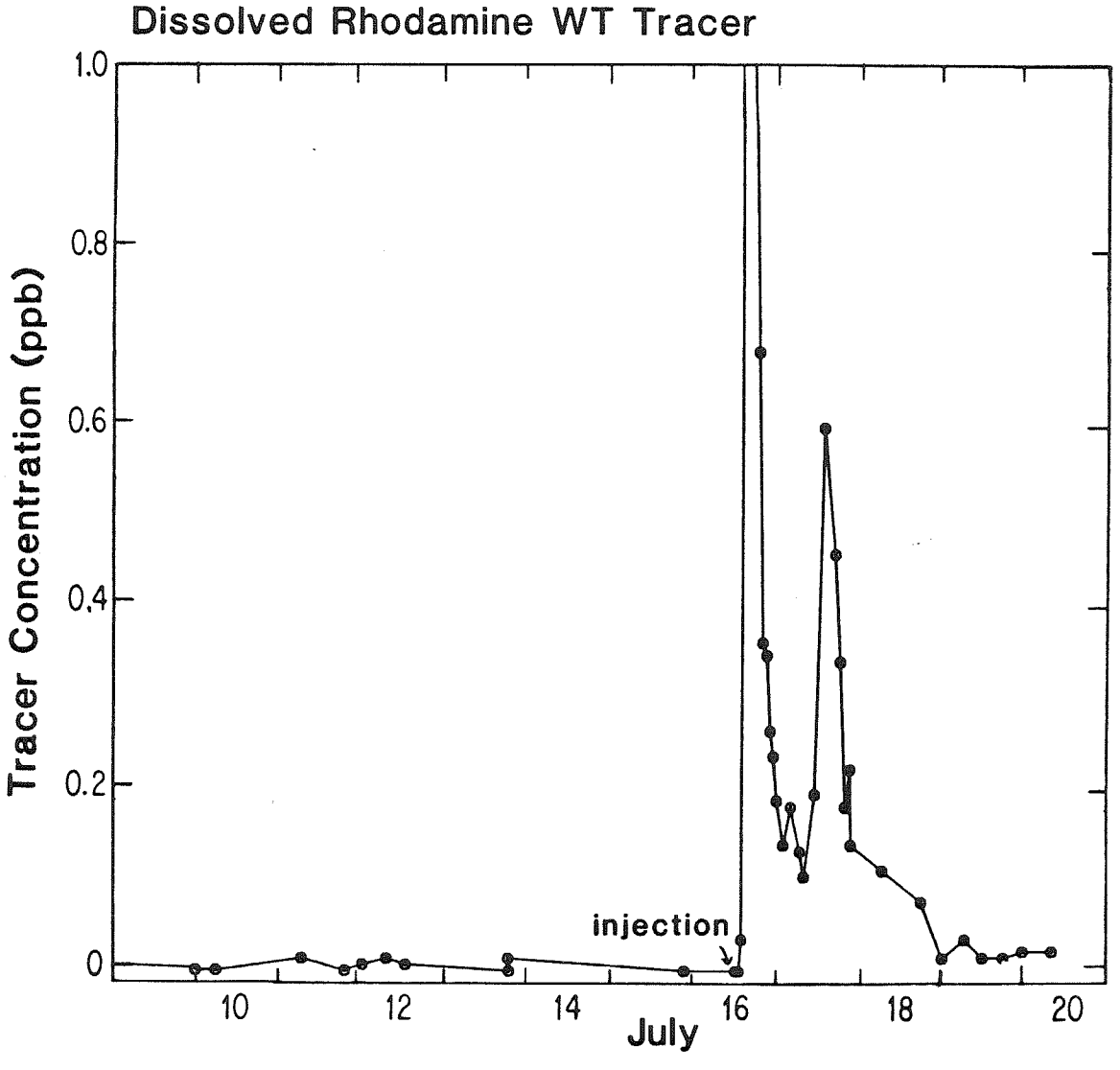

Figure 4.13 Dissolved tracer concentration versus time as in Fig. 4.12, plotted at an enlarged ordinate scale.

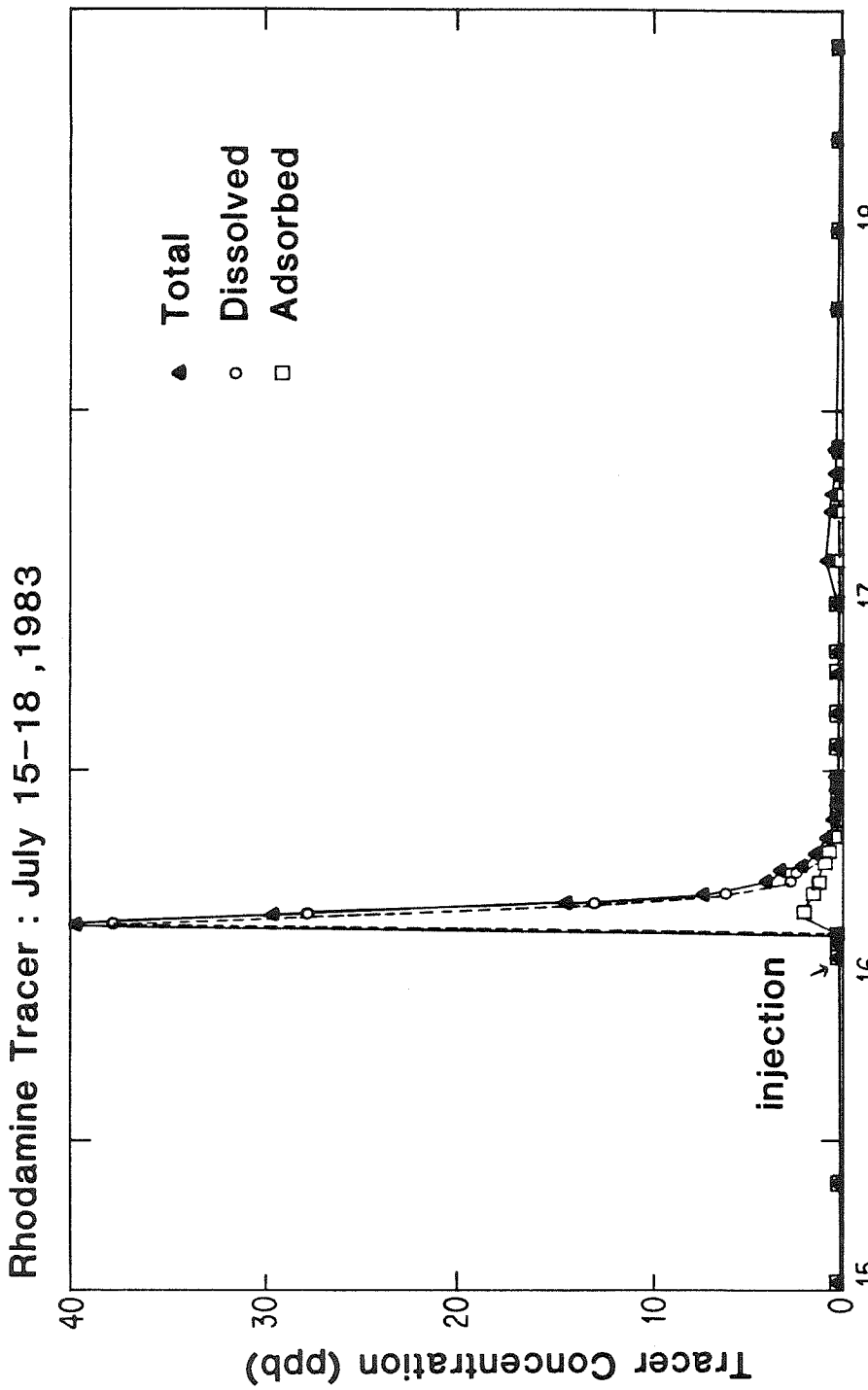

Figure 4.14 Dissolved, adsorbed, and total (dissolved plus adsorbed) Rhodamine WT tracer return in outflow stream LS for the time period July 15 through 18, 1983, in the post-surge tracing experiment. Time of injection at Km 9.5 is marked with an arrow.

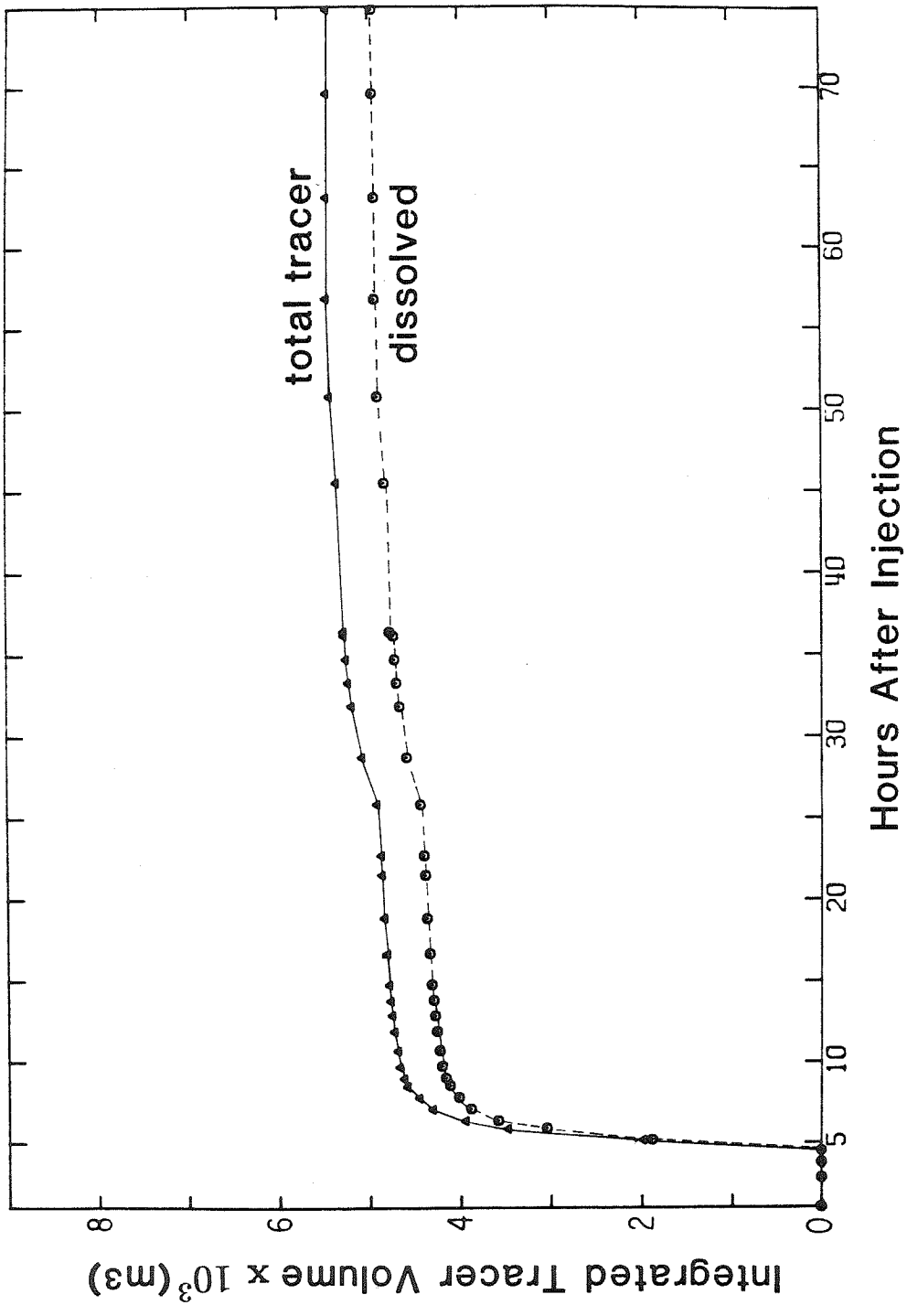

Figure 4.15 Cumulative dissolved and total (adsorbed plus dissolved) Rhodamine WT tracer returned in outflow stream LS in the post-surge tracing experiment.

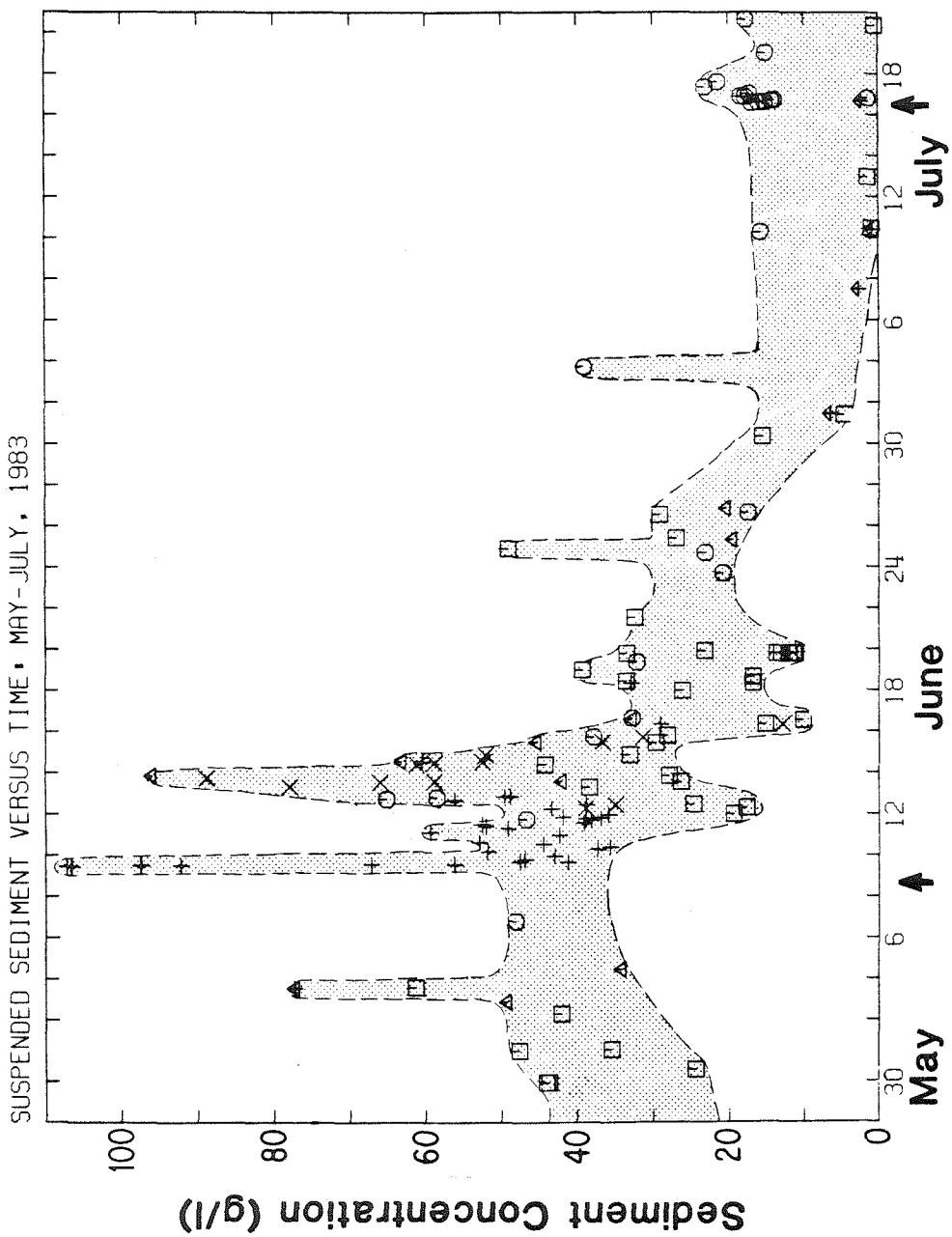

Figure 4.16 Sediment concentration (g/l) of terminus outflow streams from May 28 through July 20. Arrows mark the tracer injection times in experiments 1 and 3. Key to data points is in Fig. 4.5.

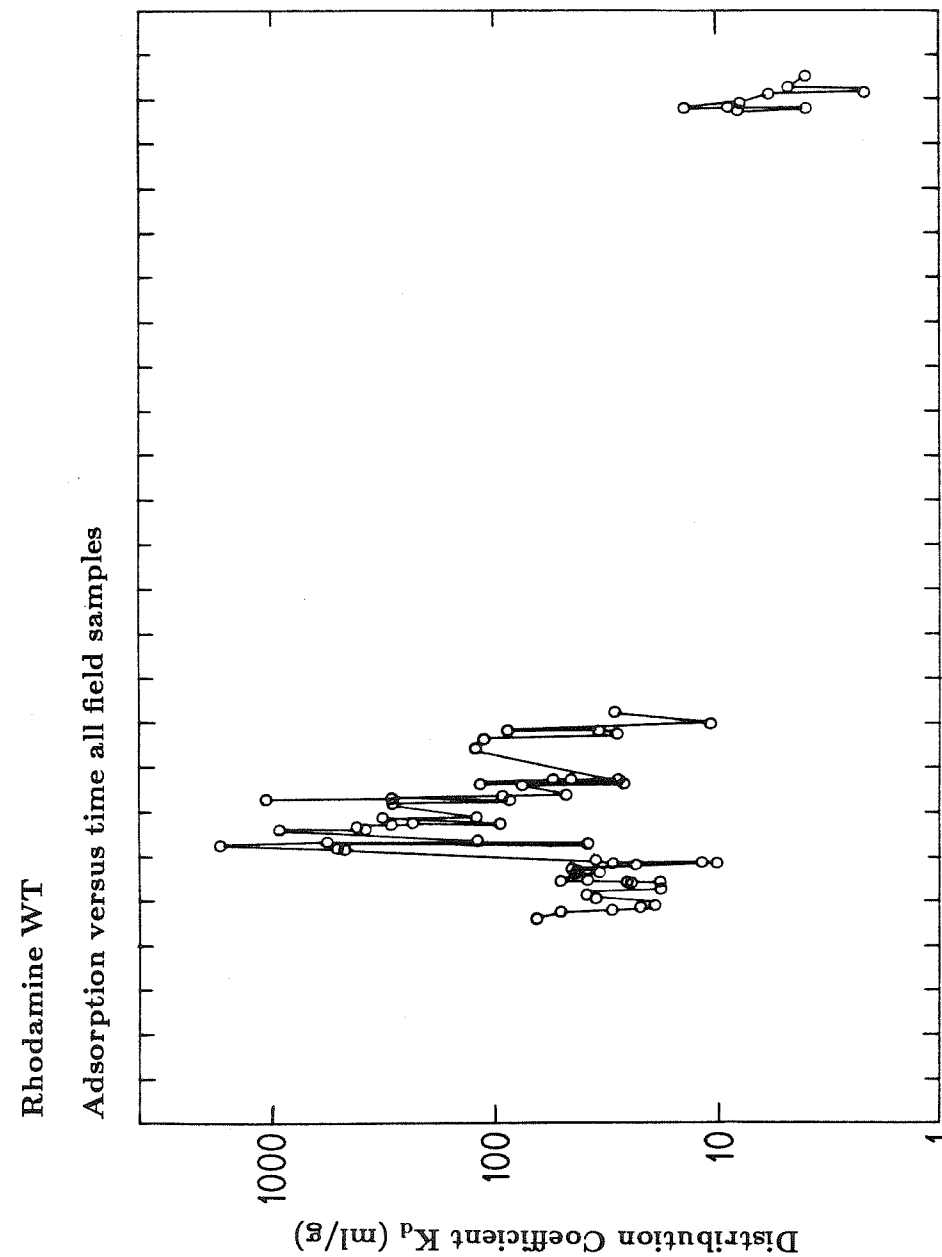

Figure 4.17 Distribution coefficient K_d for Rhodamine WT tracer adsorption in routine outflow-water samples, June-July 1983.

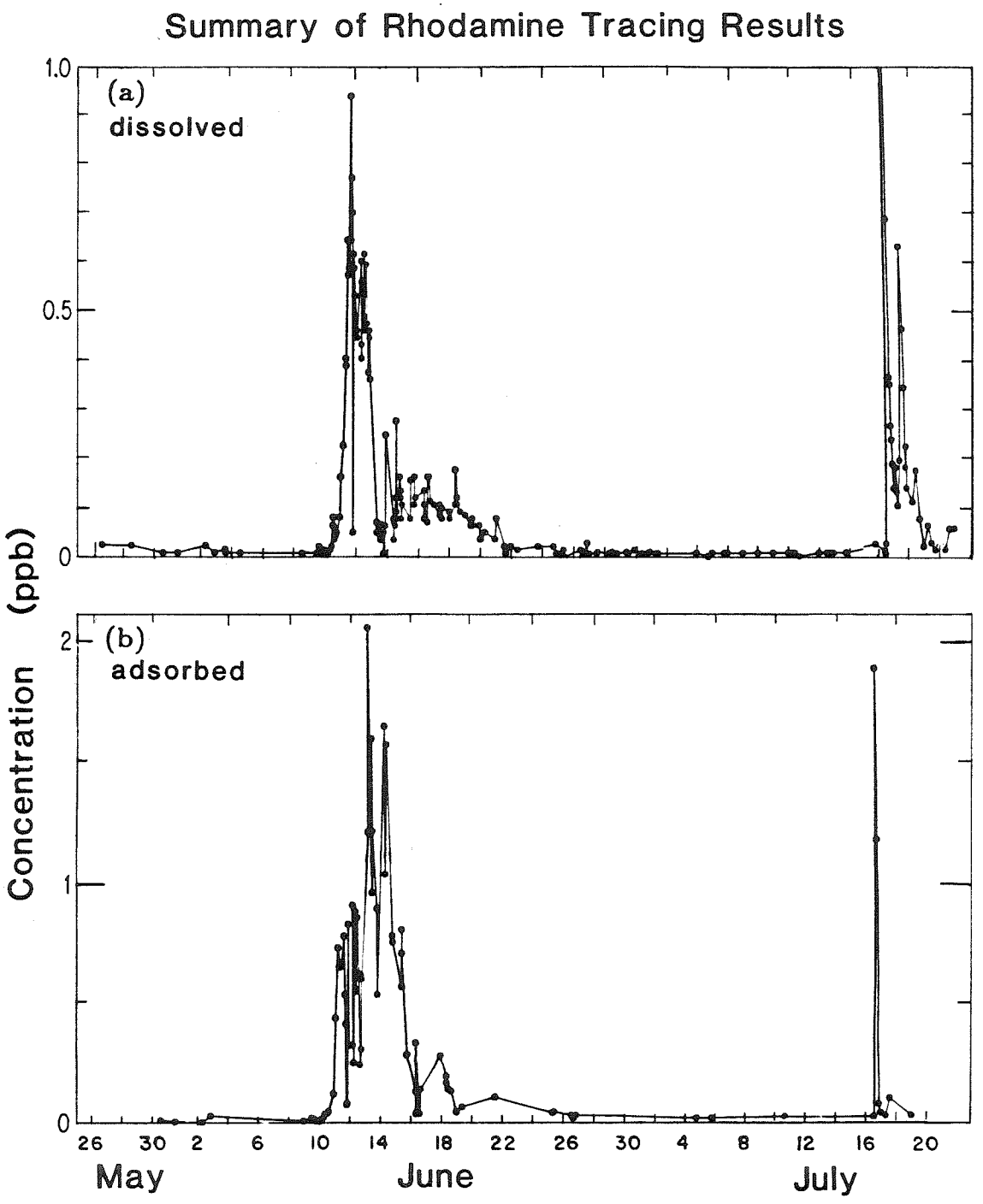

Figure 4.18 (a) Concentration of Rhodamine WT tracer dissolved in stream water for May 26 through July 24, 1983. (b) Same plot but applies to concentration of Rhodamine WT adsorbed on stream sediment.

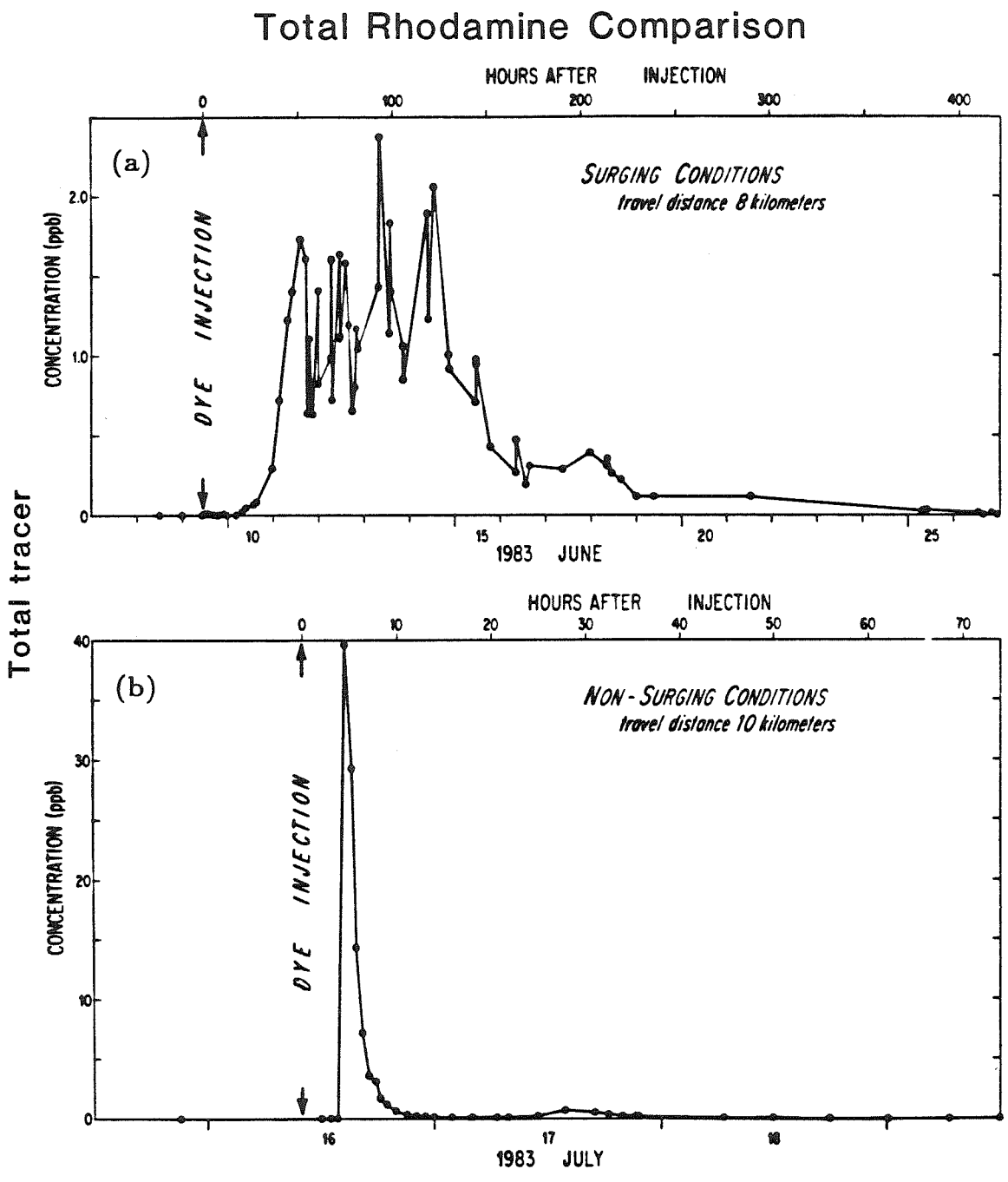

Figure 4.19 (a) Total concentration of Rhodamine WT (adsorbed plus dissolved) for first tracer experiment, conducted during glacier surge. (b) Total tracer concentration for second Rhodamine WT experiment conducted after the glacier surge had ended. Note the different time and concentration scales for each plot.

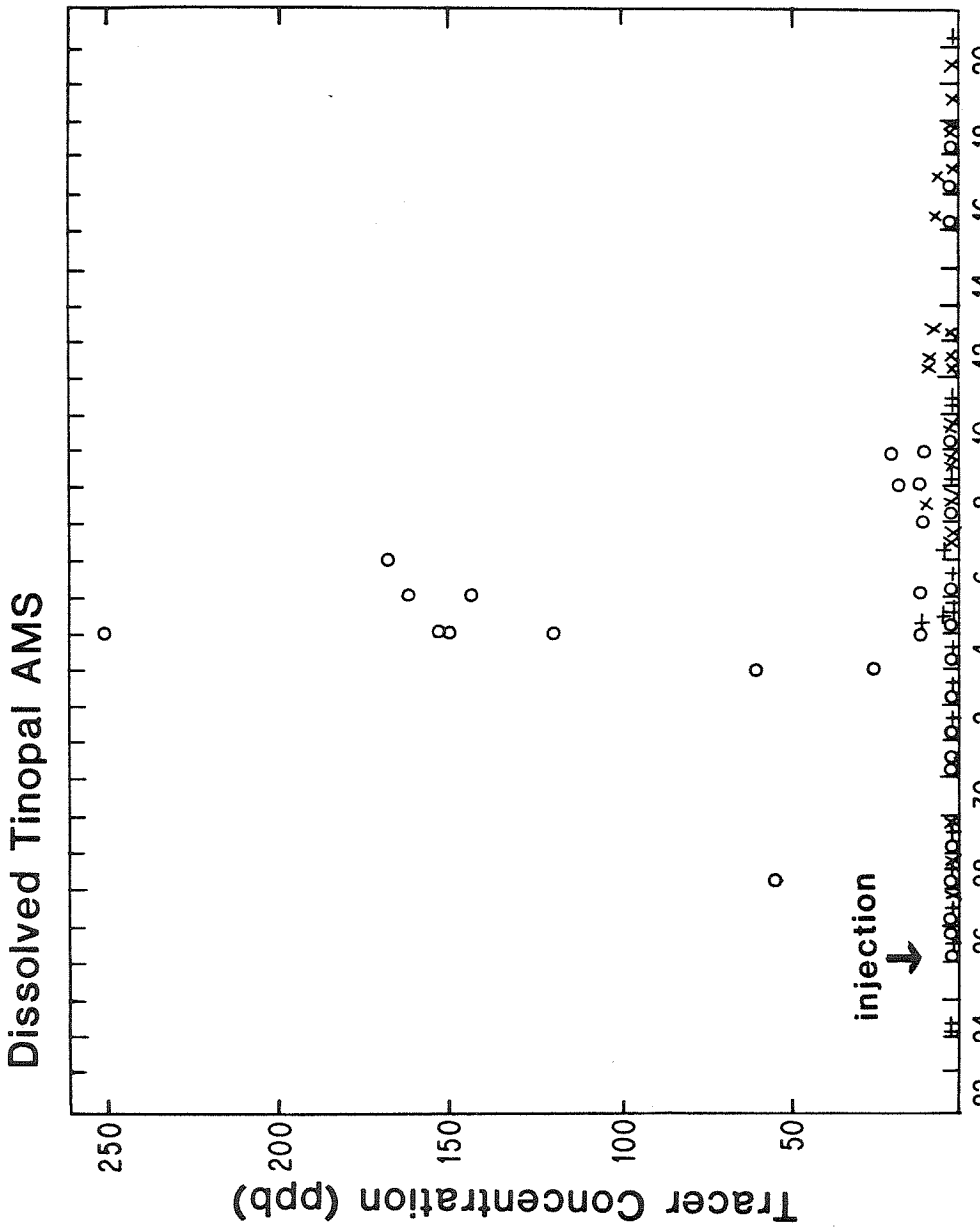

Figure 4.20 Tinopal AMS concentration in outflow stream water (all streams) in the course of the second tracing experiment. Injection time is marked with an arrow. Data points are coded in relation to the sampling locations as follows: open circles represent BC, "+" for VR, "x" for LS.

Chapter V:
THEORETICAL DYE-RETURN CURVES IN RELATION TO DATA FROM VARIEGATED GLACIER

5.1. Introduction

In the interpretation of results of dye-tracer experiments on laboratory materials and on natural water-flow systems, it has become standard practice to evaluate dye-return data in terms of the parameters in theoretical dye-return curves that can be fitted to the data. For experiments carried out by injecting initially a short pulse or "slug" of dye at some point in the flow system, the idealized theoretical curves of dye return at the outlet of the flow system are of two basic, distinct types, illustrated schematically in Figures 5.1a and b. In Fig. 5.1a, the dye pulse broadens as it propagates in such a way that at the outlet it appears as an approximately symmetrical, quasi-Gaussian peak of dye concentration vs. time, $C(t)$. This will be here called a diffusive dye-dispersion curve. In Fig. 5.1b, the onset of dye return is abrupt, and the sharp onset is followed by a quasi-exponential tail of declining $C(t)$. Such a dye-return curve will be here called a dye storage-retardation curve, or simply a retardation curve. As is already evident from the data in Chapter 4, and as will be fully discussed in the present chapter, the dye return in the first tracer experiment on Variegated Glacier conformed approximately to the pattern of a diffusive dispersion curve, whereas in the third experiment the dye return followed more nearly the pattern of a storage-retardation curve.

Theoretical models of dye transport that generate dye-return curves of these two types provide a conceptual basis for reasoning about the nature of the flow systems

that give dye-tracer data approximating the ideal curves. Adjustment of the parameters of the theoretical curves to fit the data allows quantitative conclusions about geometrical and kinematic properties of the flow system. The present chapter concerns itself with the theoretical dye-return curves, their parameterization, and their fitting to the dye-tracer data from Variegated Glacier. In Chapter VI the underlying basis for the theoretical curves is explored, in an effort to reach conclusions about the nature of the water-transport system of Variegated Glacier in its surging and non-surging state on the basis of the quantitative results of the dye-tracer experiments.

In many flow systems, particularly those whose length along the direction of fluid flow is great compared to their width transverse to flow, it is appropriate and useful to analyze the spatial evolution of a dye cloud with time as though the flow were one-dimensional, in the direction of a longitudinal coordinate x along the length of the flow system. In this approach, which is widely used in the literature on dye-tracer experimentation, and which will be followed here, the details of transverse adjustments in dye concentration are temporarily ignored, although they reappear later at the level of a deeper interpretation of the mechanics of the flow system and the underlying causes of dye disperison (Chapter VI).

When the one-dimensional treatment is used, the appropriate measure of dye concentration at coordinate x is the integral of the local volume concentration of dye, $C(x,y,z,t)$, over the transverse plane (y,z plane) at x. We designate this transverse integral by a tilde over, thus $\widetilde{C}(x,t)$. It has the dimensions of dye volume (or mass) per unit length along the flow. In the case of a river or any sort of conduit, natural or artificial, $\widetilde{C}(x,t)$ is the integral of the dye concentration across the channel or conduit cross section at longitudinal coordinate x. For a porous medium or multiple-

conduit system, the integral will include contributions from all of the pores or conduits intersected by the transverse plane at x.

5.2. Dye Dispersion by Generalized Diffusion

As discussed in Chapter VI, it has been found appropriate to assume that in many flow systems, dye (or other tracer) is transported by normal advection in the fluid flow, combined with what will be here called "generalized diffusion," in which dye is transported at a flux rate Q_D proportional to its concentration gradient:

$$Q_D = -D\frac{\partial \widetilde{C}}{\partial x} \tag{5.1}$$

D is called the dispersion coefficient or, more specifically, the longitudinal dispersion coefficient. Equation (5.1) is entirely analogous to dye transport by molecular diffusion (Fick's law), but in fact represents the combined effect of molecular diffusion and other, generally more effective, transport processes such as turbulent or eddy diffusion, as discussed in Chapter VI. D is analogous to the diffusion constant or to the thermal diffusivity in heat flow and has the same units ($m^2 s^{-1}$). The physical basis for the magnitude of D, in terms of the nature of the flow system, is considered in Chapter VI.

The advective contribution to dye transport, which in practice dominates over the effects of generalized diffusion, is given by the advective flux

$$Q_A = U\widetilde{C} \quad . \tag{5.2}$$

Here U is the longitudinal fluid flow velocity, which in the standard one-dimensional treatment is taken to be a constant throughout the system.

The development of a dye cloud in space and time is governed by the continuity equation for the dye, taking into account advective transport of dye from Eqn. (5.2) and generalized diffusion from Eqn. (5.1):

$$\frac{\partial \widetilde{C}}{\partial t} = -\frac{\partial Q_A}{\partial x} - \frac{\partial Q_D}{\partial x} = -U\,\frac{\partial \widetilde{C}}{\partial x} + D\,\frac{\partial^2 \widetilde{C}}{\partial x^2}\,. \tag{5.3}$$

It is entirely analogous to the one-dimensional heat flow equation for a body moving at speed U in the x-axis direction (Carlslaw and Jaeger, 1956).

In the ideally typical dye-tracer experiment, at the start (t=0) a pulse or "slug" of dye is injected instantaneously at some point in the flow system. The dye return curve is the solution of Eqn. (5.3) for this initial condition. The slug injection is idealized as a Dirac delta function $\delta(x)$ at the injection point, taken to be x=0. The initial condition is therefore written

$$\widetilde{C}(x,0) = V_o\,\delta(x) \tag{5.4}$$

where V_o is the volume of dye injected. The solution of Eqn. (5.3) subject to this initial condition and to boundary conditions $\widetilde{C}\to 0$ as $x\to\pm\infty$ (which are somewhat artificial but reasonable), is obtained from the corresponding heat-flow solution for an unmoving body (Carlslaw and Jaeger, 1956) simply by applying a translation velocity equal to the advection velocity U. The resulting solution is

$$\widetilde{C}(x,t) = \frac{V_o}{2\sqrt{\pi D t}}\,e^{-\frac{(x-Ut)^2}{4Dt}}\,. \tag{5.5}$$

This solution has the required property that dye is conserved, so that at any time $t>0$

$$\int_{-\infty}^{+\infty} \widetilde{C}(x,t)\,dx = V_o\,. \tag{5.6}$$

$\widetilde{C}(x,t)$, regarded as a function of x at fixed t in (5.5), is a Gaussian. Thus the spatial distribution of the dye cloud has the form of a Gaussian peak. The peak drifts (advects) forward at velocity U and spreads symmetrically with time. As a measure of the width of the peak it is convenient to take the quantity

$$\sigma_x = \sqrt{2Dt} \tag{5.7}$$

which is analogous to the standard deviation of the Gaussian function as used in statistics. $2\sigma_x$ is the width of the spatially dispersed peak at concentration level $1/e^{1/2}$ times the maximum concentration.

Regarded as a function of t at fixed x, $C(x,t)$ from Eqn. (5.5) describes the dye-return curve expected at any downstream point $x > 0$, x being the longitudinal distance from the injection point to the point where the dye return is observed. Because of the t in the pre-exponential factor and in the denominator of the exponent, the expected dye-return curve is not strictly Gaussian. It is somewhat asymmetric, skewed so that the tail following the peak is somewhat enhanced relative to the onset rise preceding the peak. As shown by practical examples (Figure 5.2), this asymmetry is not a large effect, and the curves can be called "quasi-Gaussian." Because of the asymmetry, the peak of the dye-return curve does not come exactly at the transit time $t = x / U$ of a water parcel moving longitudinally at speed U from the injection point to the dye-sampling point x, the arrival of the peak being shifted to a time slightly earlier; however, the shift is small for typical practical examples.

The dye-return curve given by Eqn. (5.5), with the characteristic features just discussed, is here called a standard diffusive dispersion curve, or, for short, a dispersion curve. It is very widely used in the literature on dye-tracer experiments. For example, Fischer (1968) uses it in analyzing dye transport in surface streams, Bear

(1979) applies it to dye tracer experiments on ground-water flow, and Smart and Smith (1976) interpret subsurface flow in subterranean conduits such as karst systems on the same basis. It has also been widely used in analyzing the results of laboratory dye-tracer experiments on flow in man-made porous media and conduits of various kinds (Taylor (1954), Neretnieks (1982), Ogata and Banks (1961)). The use of dispersion curves in interpreting dye-tracer experiments is reviewed and discussed by Baetsle (1967).

If the delivery of a dye at the outflow point where the dye-return curve is measured were simply the advective flux Eqn. (5.2), the total return of dye in a tracer experiment would be obtained simply by integrating the dye return curve over time:

$$V_R = \int_0^\infty \widetilde{C}(x,t)Udt. \tag{5.8}$$

This is what is done in practice. The procedure omits the contribution of the generalized diffusion flux Eqn. (5.1) to the dye output; however, it can be shown that for the disperison curve Eqn. (5.5) the integral Eqn. (5.8) gives exactly V_o, indicating that the omitted contribution integrates to zero, and justifying the omission.

For calculations of dye return based on actual measurements of volume concentration C of dye in the outflow, the integral equivalent to Eqn. (5.8) is

$$V_R = \int_0^\infty C(x,t)\, Q_w(t)dt \tag{5.9}$$

where Q_w is the discharge of water in the outflow. This assumes that the dye is well mixed in the outflow, so that sample values accurately represent the entire flow.

Consistent with Eqn. (5.8) and Eqn. (5.9), the concentration values C and $\widetilde{C}$ are related by

$$\widetilde{C} = C \frac{Q_w}{U} \quad . \tag{5.10}$$

To illustrate the use of the diffusive dispersion model, two sets of calculated dispersion curves for the volume concentration $C(t)$ are given in Fig. 5.2a,b. The curves in Fig. 5.2b were calculated from Eqn. (5.5) and Eqn. (5.10) by assuming an injected tracer volume V_o of 0.022 m^3, travel distance x =10.5 km, stream discharge 15 m^3/s, flow velocity U = 0.7 m/s, and dispersion coefficient D of 4, 10 and 20 m^2/s. These parameter values are near what is appropriate for the post-surge tracing experiment if dispersion curves are used to try to fit the dye-return data. The calculation gives nearly symmetrical Gaussian-shaped dye return curves. For the curves in Fig. 5.2b, V_o is again taken to be 0.02 m^3 and the stream discharge 15 m^3/sec, while the mean flow velocity is U = 0.003 m/s, the travel distance is x = 8 km, and the dispersion coefficients are D = 20, 40 and 80 m^2/s for the three curves plotted. These curves, which are roughly appropriate to the dye-return data of the first experiment, show a distinct asymmetry, particularly strong for D = 80 m^2/s. The curves become more nearly symmetrical, more nearly Gaussian, as the travel time gets longer, all other things remaining the same. The condition for close approach to a Gaussian shape is $t >> 2D/U^2$, where t is the travel time of the peak. As D increases, the transit time for the peak concentration becomes shorter, as noted earlier.

It was shown by Bear (1972) that if dye travelling in a cylindrical conduit undergoes adsorption on the walls of the conduit with instantaneous adsorptive

equilibration, the dispersion equation (5.3) is modified simply by the appearance of a dimensionless factor R_a on the left had side of Eqn. (5.3). The factor is

$$R_a = 1 + A_v \, K_a$$

where A_v is the specific area of adsorbing surface per volume of fluid in units of m^2/m^3, and K_a is the areal adsorption coefficient of the dye on the conduit wall surface in units of m (see Section 6.3). As the modified dispersion equation indicates, the factor R_a retards the transit velocity of the dye cloud to U/R_a and reduces the effective dispersion coefficient. These effects constitute a form of temporary dye storage in the conduit system, but it is a form quite distinctly different from the "storage" alluded to in Section 5.1 (Fig. 5.1b) and discussed in Section 5.7.

For values of K_a appropriate for Rhodamine WT adsorption on rock surfaces,

$$K_a \sim 10^{-5} \text{ m}$$

(Section 3.5) and for conduits of radius $r \sim 1$ m, R_a differs inappreciably from unity (Section 6.3).

5.3. Methods for Obtaining Dispersion Coefficients from Tracing Data

Several procedures were used to deduce dispersion coefficients from experimental dye-return curves of concentration versus time. First, an estimate of dispersion coefficient was obtained from the standard deviation of the concentration versus time plot, σ_t, and was measured using $t_{1/2}$, defined as the elapsed time from t_1, when the tracer concentration first reached half the peak concentration ($1/2 \, C_{\max}$), to t_m, defined as the time of maximum (or peak) tracer concentration ($C_{\max}$). For this

preliminary estimate of D only the rising portion of the $C(t)$ curve was used. Second, the entire dye-return curve was computed using Equation (5.5), beginning with approximate values of D and U obtained above. Successive iterations were then applied to find the dispersion coefficient and velocity which best fit the observed dye-return curve.

Since for most studies, stream tracing data are taken as concentration versus time from one x coordinate location, preliminary calculations are made on the basis of the half-time $t_{1/2}$, where $2t_{1/2}$ equals the time during which the concentration was greater than half the peak concentration and

$$t_{1/2} \approx t_m - t_1 \ .$$

Similarly, the quantity $X_{1/2}$ is half the distance over which the concentration was greater than half the peak concentration at a particular instant of time. Because the curve $C(x)$ changes shape with time, the relation $X_{1/2} = U\ t_{1/2}$ is not strictly valid but is approximately correct when $X \approx U/t_m$. When the trailing portion of the curve does not fit this simple one-dimensional model without storage, $t_{1/2}$ is estimated along the first portion of the $C(t)$ curve from the initial rise to the peak in dye discharge. Substitution of $X_{1/2} = U\ t_{1/2}$ and $t_m = \frac{X_p}{U}$, where U is the mean velocity, and X_p is the X coordinate distance from the injection point to the sampling position, leads us to the approximate relationship

$$D = \frac{U^3\ t_{1/2}^2}{4\ (ln\ 2)\ X} \tag{5.11}$$

(Taylor, 1954). Using this formula we may estimate the dispersion coefficients from data on $C(t)$ obtained in the field. Dispersion coefficients calculated by this method

agree closely with the final values for D obtained by fitting the entire dispersion curve for $C(t)$ to the observed dye-return curve.

An alternate preliminary estimate of D can be obtained as follows. As in the above discussion, let t_1 be the time when $C(x,t)$ reaches half the peak concentration $C_{\max}$ during the rise to the peak, and let t_2 be the time when $C(x,t)$ reaches $C_{\max}$ during the decline after the peak. Then choose t_m (time of peak maximum) so that D as calculated from t_1 and t_2 is the same.

$$\widetilde{C}_{\max} = \frac{V_o}{2\sqrt{\pi D t_m}} \tag{5.12}$$

From Eqn. (5.5), with the approximately valid substitution $U = X/t_m$, the tracer concentration at t_1 at a distance X from the point of injection is

$$\widetilde{C}(t_1,X) = \frac{1}{2}\widetilde{C}_{\max} = \frac{V_o}{2\sqrt{\pi D t_1}} \exp\left\{ - \frac{X^2(t_m - t_1)^2}{4Dt_1 t_m{}^2} \right\} . \tag{5.13a}$$

Similarly, the relationship for the trailing portion of the C(t) curve is given by

$$\widetilde{C}(t_2,X) = \frac{1}{2}\widetilde{C}_{\max} = \frac{V_o}{2\sqrt{\pi D t_2}} \exp\left\{ - \frac{X^2(t_m - t_2)^2}{4D\ t_2\ t_m{}^2} \right\} . \tag{5.13b}$$

After substitution of $C_{\max}$ from Eqn. (5.12) and taking the logarithm of each equation (5.13a) and (5.13b), the resulting equation for the rising portion of the curve and the trailing portion may be used to obtain two explicit formulations for D. The condition for D calculated from Eqns. (5.13a) and (5.13b) to be the same is

$$D = \frac{X^2(t_m - t_1)^2}{4t_m^2 t_1 \ln\left(2\sqrt{t_m/t_1}\right)} \tag{5.14}$$

$$= \frac{X^2(t_m - t_2)^2}{4t_m^2 t_2 \ln\left(2\sqrt{t_m/t_2}\right)} \quad .$$

Once t_m is chosen so that the equality is satisfied, D is obtained immediately. In theory this fitting procedure is more accurate than the method based on Eqn. (5.11), although in practice both methods produced similar results.

After the dispersion coefficient is estimated using a combination of the three procedures described above, the entire concentration time plot is computed from Eqn. (5.5), with V_o chosen so that the integrated volume of tracer is equal to the amount actually obtained in the dye return. The dispersion curve was calculated by adjusting the integrated volume of tracer at the outflow so that the calculated curve $C(t)$ best conformed to the overall pattern of measured values of tracer concentration for the tracer experiment.

5.4. First Tracer Experiment

5.4.1. General Features

For the first tracing experiment the total dye-return pattern was found to best fit a diffusive model with a dispersion coefficient of 30 m^2/s and an average transport velocity of 0.024 m^2/s. The total dye-return pattern was obtained by adding together the dissolved and the adsorbed tracer concentrations as described in Chapter 4. Calculated dispersion curves for 20, 30, and 40 m^2/s at eight kilometer distance are shown on Fig. 5.3 . The integrated volume of 0.0085 m^3 of Rhodamine WT tracer was used to obtain each of the curves. The dispersion curves (Fig. 5.3) fit the trend of total tracer concentrations.

The closeness of the fit is best for $D = 30$ m^2/s, and can be seen on an integrated tracer plot as shown on Fig. 5.4. Integration of the total dye obtained at all terminus streams is shown on Fig. 5.4 and compared to theoretical curves for dispersion coefficients 20 and 30 m^2/sec, velocity 0.024 m/sec and travel distance of 8 km. The mean stream discharge during this time interval from all outlet locations was 15 m^3/sec (Chap. 4). Integration of the data was performed using all raw data from the many active terminus streams. The total volume of tracer , V_i, integrated from time of injection (t_0) to time t_i, is given by

$$V_i = M_i/\rho = \sum_{j=0}^{i} (\frac{1}{4})[Q(t_j) + Q(t_{j-1})][C(t_j) + C(t_{j-1})](t_j - t_{j-1})]$$

where M_i is the mass of tracer, ρ is the tracer density and Q is the stream discharge. The stream discharge data were discussed in Chapter 4. The integrated tracer volume, V_i, at time t_i in Fig. 5.4 is plotted at time $1/2(t_{i+1} + t_i)$. The integration

was done without applying any prior smoothing to the data, which might bias the results. The integration essentially has the same effect as if a smoothing function had been applied to the data. The curve that best fits the total integrated volume (Fig. 5.4) lies at approximately the average of tracer concentrations from all streams, and results appear as if an averaging window of approximately six hours was applied to the data (Fig. 5.3). The final result is similar to taking the mean of the tracer curve.

In order to compute a dispersion curve that outlines the general shape of the highest concentrations measured, a tracer volume of 0.01 m^3 is necessary. The close resemblance of measured tracer pattern to a theoretical dispersion curve for this parameterization suggests that the diffusive dispersion theory gives a reasonable approximation of tracer dispersion within the surging glacier. Although the asymmetrical shape of the total dye-return pattern is well reproduced by the diffusive-type model , there are several discrepancies which need to be discussed.

Even though the initial rise in tracer concentrations on June 10 (20 to 25 hours after injection) is well modeled by a dispersion coefficient of 30 m^2/sec and velocity of 0.024 m/sec (Fig. 5.3), the fit is not good for the time period from 20 to 48 hours after injection. For parameterized fitting of the rising portion of the dye-return curve from hour 35 to 48, a different curve is required, with a dispersion coefficient of approximately 10 m^2/sec and a mean flow velocity of about 0.04 m/sec. If only several-hour averages of tracer concentration are considered, The dispersion coefficient of 30 m^2/sec fits the total data best for all portions of the curve, even the rising part. The closeness of the fit can be best seen on the integrated plot (Fig. 5.4). There is little justification for adding several dispersion curves in order to fit experimental results, when the fit for the simplest diffusive parameterization is good (Figs. 5.3).

A second feature of the total dye-return plot which is not reproduced by the diffusive model is the multi-peaked maximum from 48 to 124 hours after tracer injection (June 11-15). The peak of the best fit diffusive curve for 30 m^2/sec occurs on June 13, or on the fourth day of the tracing experiment, while the actual data show both a distinctive maximum and minimum in total tracer concentration on the same day (Fig. 5.3). The three main peaks in tracer concentration were observed on the second day (June 11), fourth day (June 13) and the sixth day (June 15) of the tracer experiment. The tracer return data for the entire experiment look suspiciously different than the pattern for most normal tracing experiments cited in the literature, for example Krimmel (1973). On June 13, at the time the maximum total tracer concentration occurred, the terminus stream discharges were changing in relative magnitude as frequently as every few minutes to few hours. It is most likely that on June 13 some of the terminus discharge was not adequately sampled. This could mean that the apparent double maximum centered on June 13 might in part be due to sampling error. The total amount of tracer reaching the terminus at detectable levels may have been as large as 50 percent of the initial injected volume, if the dispersion curve followed a parameterized fitting as shown on Fig. 5.4. There is no reason to suspect that a tracer volume larger than 0.01 m^3 came out of the glacier terminus, because it is unlikely that any consistent sampling bias would have occurred over a time period spanning more than a few hours.

The details of the multi-peaked maximum, from 48 to 124 hours (June 11 to 15), may be due to irregularities of the water drainage system at the peak of a glacier surge. Certainly, a major portion of the scatter in tracer concentrations (discussed in Chap. 4) is probably due to effects of random conduit opening and closure in a glacier

water drainage system at the surge front and within the surging ice mass. Conduit closure and opening of new conduits caused temporary storage of dye. The disturbance was dramatic when the surge front reached the terminal lobe of the glacier. As the surge front progressed through the stagnant ice near the glacier terminus, streams coming from upper glacier were pinched off and apparently diluted by clean local surface melt. The scatter in tracer concentrations is probably in part due to this effect, but since sampling was carried out at many streams simultaneously the effect should average out. Regardless of the reason for the scatter pattern, or multi-peaked maximum, the measured tracer concentration $\widetilde{C}(t)$ for the glacier cross-section is well represented by the parameterized fitting of a diffusive dispersion curve with a dispersion coefficient of 30 m ^{2}/s, a mean flow velocity of 0.024 m/s, and a total returned volume of approximately 0.01 m^3 Rhodamine WT tracer.

5.4.2. Dissolved Tracer

The return pattern of dissolved tracer for the rising portion of the curve between June 10 and 13 is roughly bell shaped. The dissolved tracer data may be approximated by a diffusive-type curve with a dispersion coefficient of 10 m^2/sec, mean flow velocity of 0.042 m/sec and a total returned volume of 0.001 m^3 tracer, as shown in Fig. 5.5. The shape of the rising portion of the curve is particularly well represented by this parameterization, but there are distinct discrepancies in the trailing portion of the curve on June 12 and 13. The spread of the dissolved dye concentrations between June 10 and 13 is approximately three days and is well fit by the curve for a disperison coefficient of 10 m^2/s. The return pattern for total (ie., dissolved plus adsorbed) tracer is primarily determined by the type of glacier drainage

system, while the pattern for dissolved tracer is additionally dependent upon the adsorptivity of suspended sediment. Between June 12 and 13, there was a dramatic change in the adsorptivity of the suspended at the terminus streams, as indicated by the sudden change in K_d -- discussed in Section 3.5. The large increase in K_d values between June 12 and 13 strongly suggests that the dispersion coefficient of 10 m^2/sec and mean flow velocity of 0.042 m/sec are probably not representative of any water transport system for dissolved tracer, separate from adsorbed tracer.

At mid-day on June 12, and for two samples on June 13, the tracer concentrations differed markedly from the theoretical curve shown in Fig. 5.5. As discussed in Chapter 4, on June 13 there was a sudden change in glacier motion and terminus stream discharge, and at the same time there was a dramatic increase in the tendency for sediment to adsorb Rhodamine WT. The transfer of tracer from dissolved to adsorbed phases is shown by the sharp increase increase in distribution coefficients, K_d (Fig. 4.10) on June 13. Between June 13 and 15 the adsorptivity properties of suspended sediment changed enough to affect significantly the shape of the dye-return curves for both dissolved and adsorbed tracer. The broad maximum in dissolved tracer concentration between June 13 and 21, peaking at about 0.1 ppb, was produced as an artifact of changing distribution coefficient of suspended sediment in contact with dye being carried through the glacier.

5.4.3. Adsorbed Tracer

The return pattern for tracer adsorbed on suspended sediment is distinctly asymmetrical. The best fit diffusive parameterization for the general shape of the adsorbed tracer data is shown on Fig. 5.5. The calculated curve (Fig. 5.5) was

obtained using a dispersion coefficient of 5 m^2/s , mean flow velocity of 0.019 m/s, tracer volume of 0.006 m^3, and stream discharge of 15 m^3/sec. As can be seen on Fig. 5.5 the adsorbed tracer data do not lend themselves to fitting with a single diffusive dispersion curve. The fit between diffusive dispersion theory and actual adsorbed tracer data is not very good, for any paramaterization that can be envisioned.

The fact that there is an average peak in adsorbed tracer following dissolved tracer by two to three days is attributable to the changing adsorptivity of the suspended sediment. The rising portion of the adsorbed tracer curve on June 13 is coincident with the sudden decrease in dissolved tracer (Fig. 4.5) and the sudden increase in distribution coefficient K_d (Fig. 4.10). Therefore, it is improper to interpret the dispersion parameterization and mean flow velocity implied by the peak in adsorbed dye separate from the dissolved tracer, as discussed in the previous section.

5.5. Post-Surge Tracing Experiment

For the Rhodamine WT tracer experiment conducted after the glacier surge, the shapes of tracer return curves for dissolved (Fig. 4.12-4.14), adsorbed (Fig. 4.14) and total tracer (Fig. 4.14) are nearly identical. Most of the tracer during this experiment came out dissolved in the stream water, and very little of the dye was found adsorbed on sediment. The adsorptivity of the sediment during this experiment (Fig. 4.17) was small and uniform enough that only the pattern of dissolved tracer need be discussed for dispersion modeling in this section. Only data from Lower Stream (Fig. 4.1) is discussed because all other terminus streams remained free of Rhodamine WT tracer throughout this post-surge tracer experiment.

The best-fit diffusive parameterization for the dissolved tracer is shown on Fig. 5.6, for a dispersion coefficient of 60 m^2/sec, mean flow velocity of 0.65 m/s, tracer volume of 0.008 m^3/sec, mean stream discharge of 40 m^3/s, and travel distance of 10 kilometers. Even though this curve is the "best-fit" diffusive curve for the main peak in tracer concentration measured, the curve rises too early and does not reproduce the distinctive tail in tracer concentrations from four to ten hours after tracer injection. The pattern of tracer concentrations does not conform to a diffusive-type model for the primary peak measured to reach a maximum at 14:20.

It is possible that the main peak in tracer concentration was missed between sampling done at 13:40 and 14:20 on July 16. If this is the case, a hypothetical dispersion curve may be reconstructed and a diffusive parameterization may be used to put constraints on the dispersion coefficient and mean flow velocity for the non-surging Variegated Glacier. A diffusive peak centered between the last clean water sampled at Lower Stream at 13:40 and the first sample showing a significant tracer concentration at 14:20 may be parameterized by a dispersion coefficient of 1 m^2/s, and a mean flow velocity of 0.72 m/s. The total volume of tracer for the parameterized peak shown as a dashed curve in Fig. 5.8 is equal to 75 percent of the amount initially injected into the glacier. This hypothetical diffusive-dispersion curve will be discussed further after the actually measured tracer concentrations are parameterized with a non-diffusive model.

The secondary peak in tracer concentration, seen in Fig. 4.13, may be parameterized by a diffusive curve with a dispersion coefficient of 4 m^2/s, mean flow velocity of 0.1 m/s, tracer volume of 0.0008 m^3, mean stream discharge of 40 m^3/s, and travel distance of 10 kilometers. Even though this diffusive dispersion

parameterization fits the secondary peak quite well, the rapidly changing stream discharge at the time (Fig. 4.11) makes the meaning of such a peak quite doubtful. This secondary peak follows the main dye injection by one day and appears similar to secondary peaks observed at other glaciers, such as Findelen Glacier, Switzerland (Moeri, 1984). The secondary peak for this Variegated Glacier experiment arrives late in the day following the dye injection at a time of rising water pressure within the lower glacier. Information of glacier water pressures is given by Kamb et al. (1985). The calculated dispersion coefficient of 4 m^2/sec and flow velocity of 0.01 m/sec are probably not representative of average conditions within the glacier. The secondary peak is likely due to diurnal variation in dye transport due to daily changes in englacial water discharge, pressure and storage common to all normal non-surging glaciers during the summer melt season.

5.6. Dispersion Due to Storage-Release Mechanisms

The distinctly asymmetrical shape of the dye-return results for the third tracer experiment requires a different type of model that can produce a highly non-Gaussian dispersion curve. This is accomplished by adding a generalized storage term to the differential equation describing dispersion (Eqn. 5.7):

$$\frac{\partial \widetilde{C}}{\partial t} = -U \frac{\partial \widetilde{C}}{\partial x} + D \frac{\partial^2 \widetilde{C}}{\partial x^2} - \frac{\partial \widetilde{S}}{\partial t} \tag{5.16}$$

where $\widetilde{S}$ is the mean concentration of "stored" tracer per unit length, and $\widetilde{C}$ is the mean concentration of "mobile" tracer as described in Section 5.2. The simplest model for the change of stored tracer with time is that tracer exchanges between immobile zones (or storage reservoirs) and mobile zones (the main flow) at a rate that

is linearly dependent upon the concentration of stored tracer in the reservoir, S, and the concentration of tracer in the main flow, C. The time rate of change of tracer concentration stored in the immobile zones is given by

$$\frac{\partial \widetilde{S}}{\partial t} = a\widetilde{C} - b\widetilde{S} \tag{5.17}$$

This formulation has been used in the interpretation of dye return curves for various types of drainage systems (Ogata and Banks, 1961), including glacial water conduits (Ambach and Jochum, 1973). The governing rate constants in the theory are a and b, expressed in units of s^{-1}.

The tracer concentration, $\widetilde{C}$, in the main flow is initially decreased by the storage processes. Later $\widetilde{C}$ decreases to low levels as the main pulse of tracer is advected through water channels within the glacier. As $\widetilde{C}$ decreases below the value of $\widetilde{S}$ in the immobile zone, $\frac{\partial \widetilde{S}}{\partial t}$ becomes negative. Then, immobile zones are no longer net sinks for tracer storage, but rather become net sources. After the main dye peak has passed, more dye is transferred to the main flow from storage reservoirs than is taken from the flow by the storage process.

In order to facilitate obtaining an analytical solution to this problem, the diffusional term $D\frac{\partial^2 \widetilde{C}}{\partial x^2}$ is assumed to be neglible. Equation (5.16) then simplifies to

$$\frac{\partial \widetilde{C}}{\partial t} = -U\,\frac{\partial \widetilde{C}}{\partial x} - \frac{\partial \widetilde{S}}{\partial t}\ . \tag{5.18}$$

The solution to this storage-retardation dispersion problem for an initial slug injection of tracer is available in the literature. Ogata (1964) derived a solution to Eqn. (5.18) for an initial step-function input of dye. From the solution for the step function

input, solution for a δ-function input can be obtained by differentiation. The tracer concentration for the step-function solution is here called C_δ. The step-function solution given by Ogata (1964, p. 118, Eqn. (18)) is

$$\frac{C_\delta}{C_o} = e^{-b\left(t-\frac{X}{U}\right)-a\frac{X}{U}}\, 1\left(t-\frac{X}{U}\right) \tag{5.19}$$

$$\left\{ I_o\left[2\sqrt{\frac{abX}{U}\left(b-\frac{X}{U}\right)}\right] + be^{b\left(t-\frac{X}{U}\right)} \int_o^{t-\frac{X}{U}} e^{-b\tau}\, I_o\left[2\sqrt{\frac{abX}{U}\tau}\right] d\tau \right\}$$

where C_0 is the height of the step in tracer concentration, I_0 is the modified Bessel function of order zero, and $1(t-\frac{X}{U})$ is the unit step-function that rises at time $t = \frac{X}{U}$. Equation (5.19) may be used to obtain the solution $\widetilde{C}_\delta(t)$ for an initial δ-function input by the following differentiation:

$$\widetilde{C}_\delta = \frac{V_o}{U}\frac{\partial}{\partial t}\left(\frac{C_\delta}{C_o}\right) = \frac{V_o}{U}\,\delta\left(t-\frac{X}{U}\right)e^{-a\frac{X}{U}} \tag{5.20}$$

$$+\frac{V_o}{U}\,1\left(t-\frac{X}{U}\right)e^{-a\frac{X}{U}}\, e^{-b\left(t-\frac{X}{U}\right)}\sqrt{\frac{abX}{Ut-X}}\, I_1\left[2\sqrt{\frac{abX}{U}\left(t-\frac{X}{U}\right)}\right]$$

where I_1 is the modified Bessel function of order one, and V_0 is the volume of tracer in the δ-function slug (Kamb, 1986, unpublished). The peak in tracer concentration reaches the sampling point X at time $\frac{X}{U}$.

The Taylor series expansion of the modified Bessel function (CRC Tables, 1974, pg. 448) is

$$I_1(z) = \frac{z}{2} + \frac{z^3}{2^3 1!2!} + \frac{z^5}{2^5 2!3!} + \ldots \quad .$$

For the case of the Variegated Glacier experiments, the argument of the Bessel function in Eqn. (5.20), $z = 2\sqrt{abX(t-\frac{X}{U})/U}$ will be less than one if coefficients a and b are sufficiently small (on the order of $10^{-4}\ s^{-1}$ or less). By assuming z is small, only the first term of the series expansion is significant, and the modified Bessel function may be simplified to

$$I_1\left\{2\sqrt{\frac{abX}{U}(t-\frac{X}{U})}\right\} \approx \sqrt{\frac{abX}{U}(t-\frac{X}{U})} \ . \tag{5.23}$$

This approximation allows the δ-function solution to be simplified as follows:

$$\widetilde{C}_\delta \simeq \frac{V_o}{U}\ e^{-\frac{a}{U}X}\left[\ \delta(t\ -\frac{X}{U}) + 1(t\ -\frac{X}{U})e^{-b\,(t-\frac{X}{U})}\ \frac{abX}{U}\ \right] \tag{5.24}$$

$$= A\ \ \delta(t-\frac{X}{U}) + B\ \ 1(t-\frac{X}{U})\ e^{-b\,(t-\frac{X}{U})}$$

where A and B are constants for a fixed travel distance X (Kamb, 1986, pers. com.). This shows that the dispersion curve for the storage-retardation model discussed here may be approximated by an initial δ-function pulse arriving at time $\frac{X}{U}$, immediately followed by an exponentially decreasing tail of tracer concentration. In this model, prior to the arrival of the peak concentration, no tracer reaches the glacier terminus. The pre-exponential coefficient B for the storage-retardation tail is

$$B = \frac{V_0}{U^2}\ abX\ \ e^{-\frac{a}{U}X} \tag{5.25}$$

From this formulation it can be seen that the tail becomes more pronounced for large values of the initial volume of tracer V_0, large travel distances X, small mean flow velocities U and for large values of a or b. For $a \rightarrow 0$, the tail vanishes. As

mentioned previously, the values of both a and b are required to be sufficiently small for the simplification of the Bessel function to apply.

The simplified storage-retardation solution, Eqn. (5.24), provides a good form for direct comparison between model and experimental results. In the next section this model solution is compared to the post-surge Variegated Glacier dye-return curve.

5.7. Retardation and Dispersion Parameters for the Post-Surge Experiment

If the dye return pattern conforms to the storage-retardation model, then the theory (Eqns. 5.24 and 5.25) predict that following the peak value the tracer concentration should decrease exponentially with time by the formula:

$$\widetilde{C}(t) \approx \frac{V_0 abX}{U^2} \; e^{-\frac{a}{U}X} \quad e^{-b\left(t-\frac{X}{U}\right)}, \quad t > \frac{X}{U} \tag{5.26}$$

where a and b are small positive constants. To test the applicability of the storage-retardation model for the post-surge tracer experiment, the ordinate in Fig. 5.7 and 5.8 is taken as the logarithm of tracer concentration. The dashed line in Fig. 5.8 is the best fit of Eqn. (5.26) to the tracer data. The fit indicates that a decreasing exponential is a good approximation and the storage-retardation model adequately describes the non-Gaussian shape of the dye return curve (Figs. 4.14; 4.19b; 5.8).

The arrival time for the peak concentration along the dashed line in Fig. 5.9 is estimated to occur at the mid-point of a sampling interval, 3 hours 55 minutes after injection (14:00 on July 16). The peak concentration may actually lie anywhere between the last clean sample taken at 13:40 and the first sample showing significant dye at 14:20 on July 16. This gives a range of velocity U from 0.78 to 0.65 m/sec.

The mean velocity of 0.72 m/sec chosen for parameterized fitting (Fig. 5.8) is calculated from the estimated travel time (3 hours 55 minutes), and the measured travel distance, X, of ten kilometers. The value of the peak concentration (C_{max}) read from the dashed line at time 14:00 is 43 ppb.

The linear curve in Fig. 5.8 allows the results for the third tracing experiment to be parameterized in terms of coefficients a and b [Eqn. (5.26)]. The slope [or coefficient b, Eqn. (5.26)] of the best-fit line is 1.97 x 10^{-4} s^{-1}. The value of a is obtained from the estimated peak concentration and from the value of b. To obtain the value of a, the storage-retardation model is expressed as follows:

$$\ln(C_{max}) = \ln\left(\frac{V_0}{Q_w}\frac{abX}{U}\right) - \frac{a}{U}X \qquad (5.27)$$

where Q_w is the terminus stream discharge. For a stream discharge of 39 m^3/s (Fig. 4.11 and 5.10) and a total tracer volume of 0.022 m^3, the value of coefficient a from the above equation is 0.61 x 10^{-4} s^{-1}.

The rate coefficients a and b derived for the Variegated Glacier after the surge are 10 to 100 times smaller than the values obtained by Ambach and Jochum (1973, p. 185) for an open glacier stream in Austria (a = 0.003, 0.001 s^{-1}, b = 0.01, 0.03 s^{-1}). For dispersion data where the exponential tail is highly extended in time, the value of b will be small. Tracer data from Moeri(1984) obtained at Findelen Glacier, Switzerland may be parameterized by a and b coefficients that are approximately equal to the values obtained from the third tracing experiment at Variegated Glacier. This suggests that the storage-retardation processes governing dispersion within the water drainage system of the Findelen Glacier is similar to the Variegated Glacier after the surge had ended.

The general pattern of dye return for Findelen Glacier (Moeri, 1984) is a roughly Gaussian-shaped initial peak followed by an exponential tail. To my knowledge, previous glacier tracing experiments have never exhibited only an exponential tail, without an initial symmetrical peak. If a diffusive-dispersion peak reached the Variegated Glacier terminus between sampling intervals, it most likely arrived just prior to the the peak concentration actually measured (ie., prior to 14:20).

The storage-retardation model (Eqn. 5.24) predicts that a δ-function peak arrives at the terminus at time $t = \frac{X}{U}$. In reality, any sharp pulse of tracer would be spread out by diffusive processes as the dye slug advects through the glacier. For a relatively small diffusive spreading of the δ function, we can assume that the non-diffusive storage-retardation solution is modified by replacing the δ function in Eqn. (5.24) by a Gaussian given by the diffusive dispersion solution Eqn. (5.5).

The dispersion coefficient, D, parameterized for the diffusive peaks (Fig. 5.8) is 1 m^2/sec, and the mean velocity for each is 0.72 m/sec. The value of σ_t (or equivalently t) for the curve in Fig. 5.8 is 3 $\frac{1}{2}$ minutes. As stated earlier (Chap. 4), the initial volume of Rhodamine WT tracer was 0.022 m^3 and the dye was injected at the base of borehole H located at Km 9.5 (map on Fig. 4.1). The dashed curve shown in Fig. 5.8 was computed on the assumption that the actual integrated tracer volume should have been 75 percent of the amount injected if more detailed sampling had been done. A higher curve is expected for a hypothesized 100 percent dye return. The peak concentration for 75 percent total return is 350 ppb and the peak concentration for 100 percent dye return is 650 ppb. Such concentrations are high enough that they could have been visually detected at the glacier terminus. Perhaps the high

turbidity of the stream, averaging 20 g/l suspended sediment on June 16 (Fig. 4.16), precluded the visual detection of the tracer.

The storage-retardation parameterization combined with the diffusive-dispersion model gives a reasonable fit with the data for the third tracer experiment at Variegated Glacier, and can account for the total amount of dye initially injected. The dispersion theory (Eqn. 5.17 and 5.18) suggests the fitting of a narrow diffusive peak between the sampling times immediately prior to the time the peak concentration was detected. The hypothetical dispersion curve (dashed in Fig. 5.8) not only is in close agreement with the dye data obtained at Variegated Glacier for the post-surge experiment, but also is in accordance with previously published tracing data from other non-surging temperate glaciers. The a , b , U and D parameterization of the post-surge tracing experiment at Variegated Glacier is similar to the values obtained for other temperate glaciers, where tracing experiments were conducted using boreholes drilled to the glacier bed. The best documented example is for Findelen Glacier, Switzerland (Moeri, 1984). The significance of the dispersion parameterization in terms of the glacier drainage system is discussed in the following chapter.

Table 5.1
Dispersion Parameters: 1983 Variegated Glacier Water Conduits[1]

Without Retardation

Dye	Peak	Volume (m^3) x 10^3	Transit Time (hr)	$t_{1/2}$ (hr)	U (m/s)	D (m^2/s)	α (m)
Surge[2]:	(June 9-26)						
dissolved	major	2	53	10	0.042	10	240
adsorbed	major	8	92	50	0.026	40	1,300
	minor	1	107	20	0.026	4	150
total	major	10	100	40	0.024	30	1,100
Post-Surge[3]	(July, 16-18)						
water	first	10	4	0.2	0.7	1	6
sediment	second	1	4	0.2	0.7	1	6
total	first	10	4	0.2	0.7	1	6
""	second	0.1	28		0.10	4	40

Notes:

1. The amount of Rhodamine WT initally injected in each experiment is 0.022 m^3. The slope of the glacier, dh/dx, is 0.1 m/m.

2. For the surge experiment on June 9-26, the mean discharge $\overline{Q}$ is 15 m^3/s, longitudinal distance X traveled to outlet TCC and VR is 8 km. Dye emanated from many outlet streams.

3. For the post-surge experiment on July 16-19, the stream discharge $\overline{Q}$ is 30-40 m^3 /s ; longitudinal distance traveled to LS X is 10 km. The sampling interval was 40 min. Dye emanated from only one outlet stream.

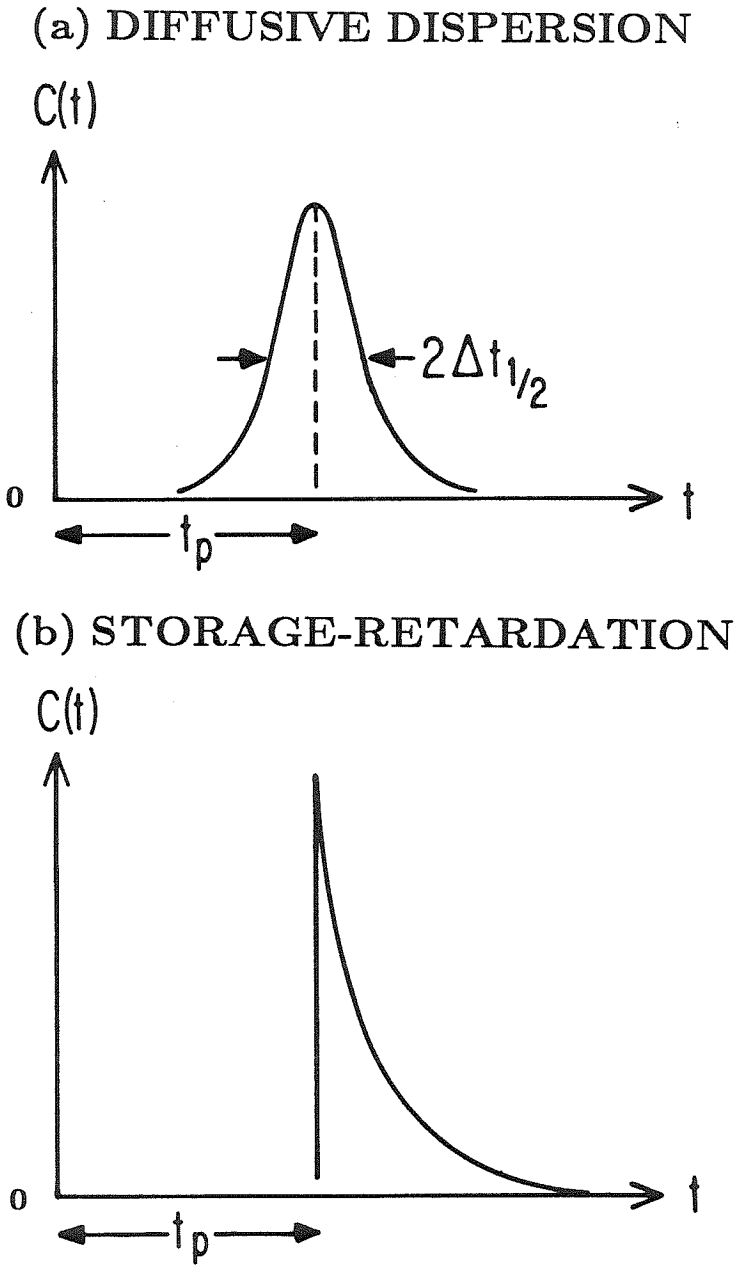

Figure 5.1 Schematic representation of two idealized types of dye-return curves *C(t)* resulting from slug injection of dye at t=0. (a) Diffusive dispersion curve; (b) Storage-retardation curve.

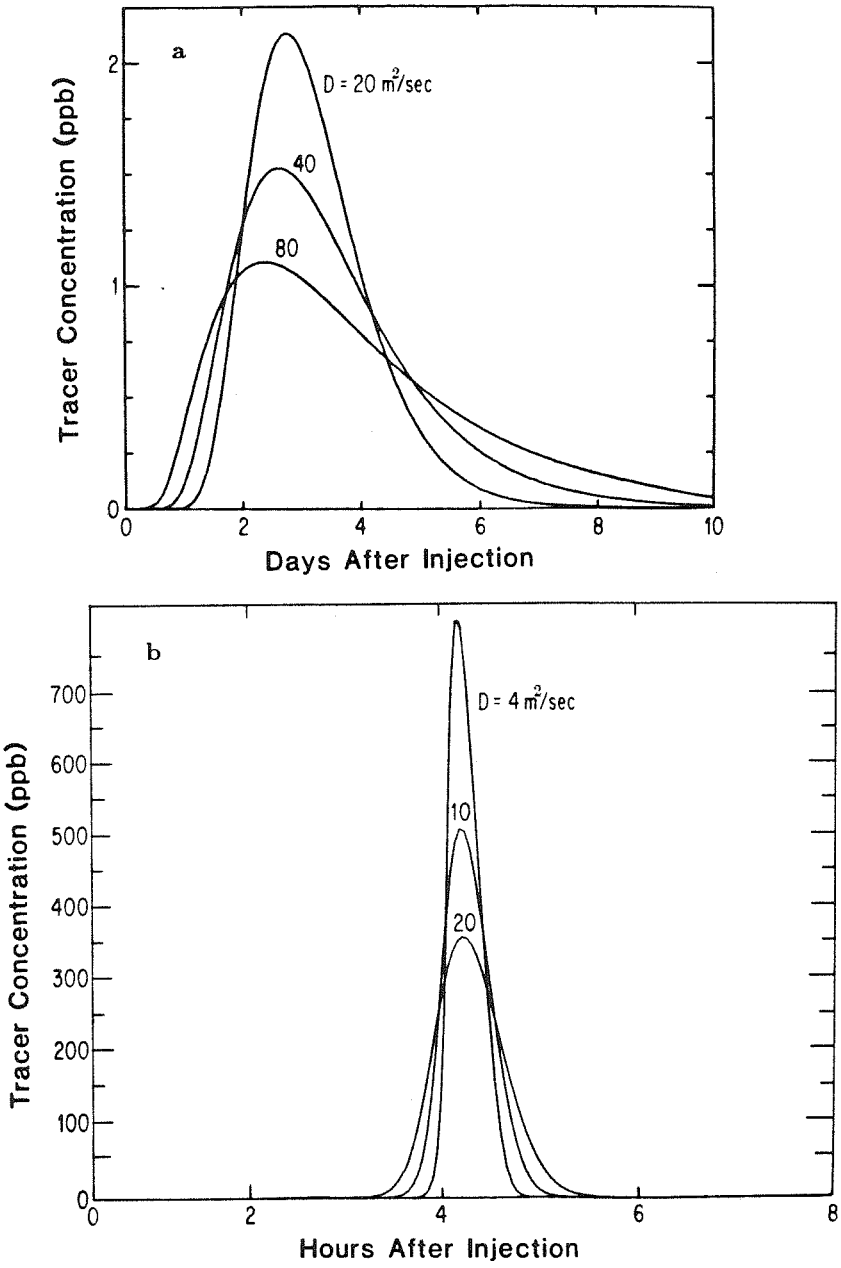

Figure 5.2 Diffusive dye-dispersion curves for parameter values roughly appropriate to the results of tracing experiments 1 and 3. (a) shows curves appropriate to experiment 1, based on $V_o = 0.02$ m^3, $U = 0.034$ m/s, $x = 8.1$ km, and $Q_w = 15$ m^3/s. The curves are calculated from Eqns. (5.5) and (5.10) for the various values of D indicated. (b) shows curves roughly appropriate to experiment 3, and is based on the parameters $V_o = 0.022$ m^3, $U = 0.7$ m/s, $x = 10.5$ km, and $Q_m = 15$ m^3/s.

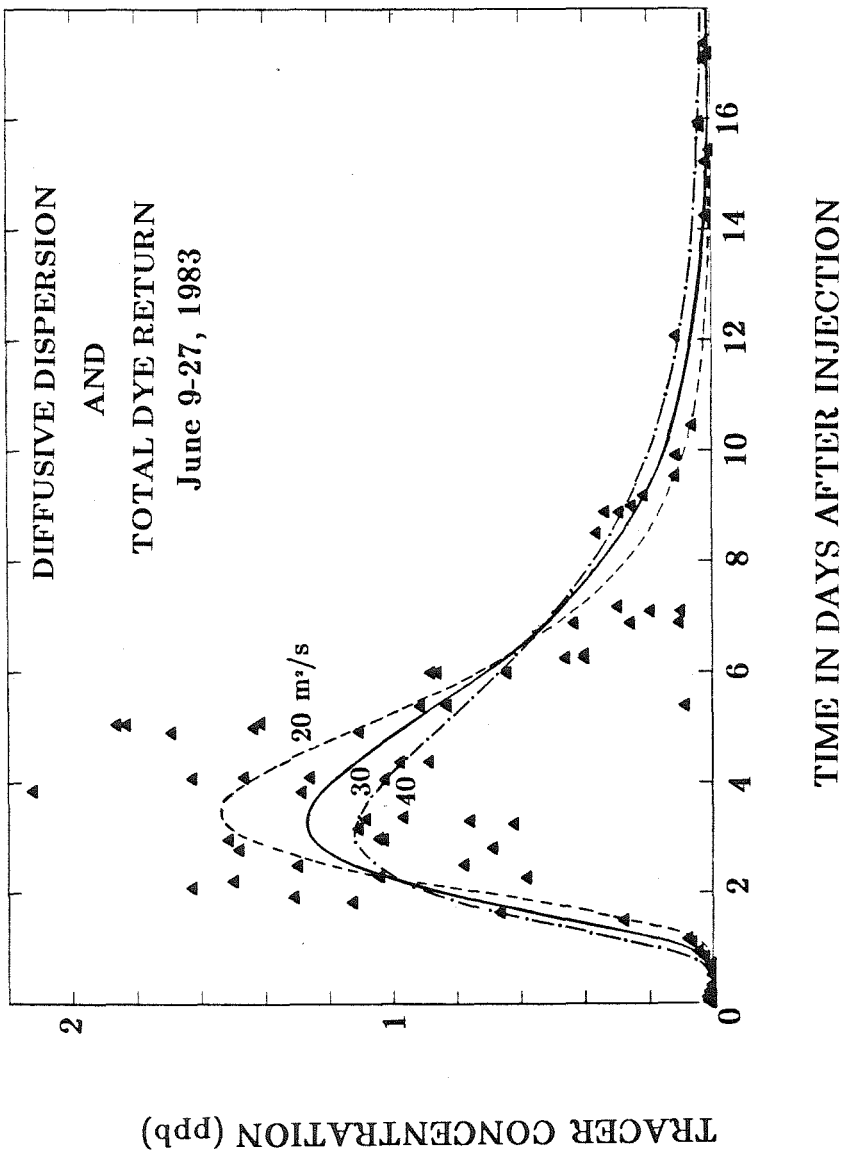

Figure 5.3 Total Rhodamine WT tracer and diffusive-type dispersion curves versus time during glacier surge (in experiment 1) for $D = 20$, 30, 40 m^2/sec, velocity $U = 0.024$ m/sec, total tracer volume $= 0.0085$ m^3. The mean stream discharge was 15 m^3/sec.

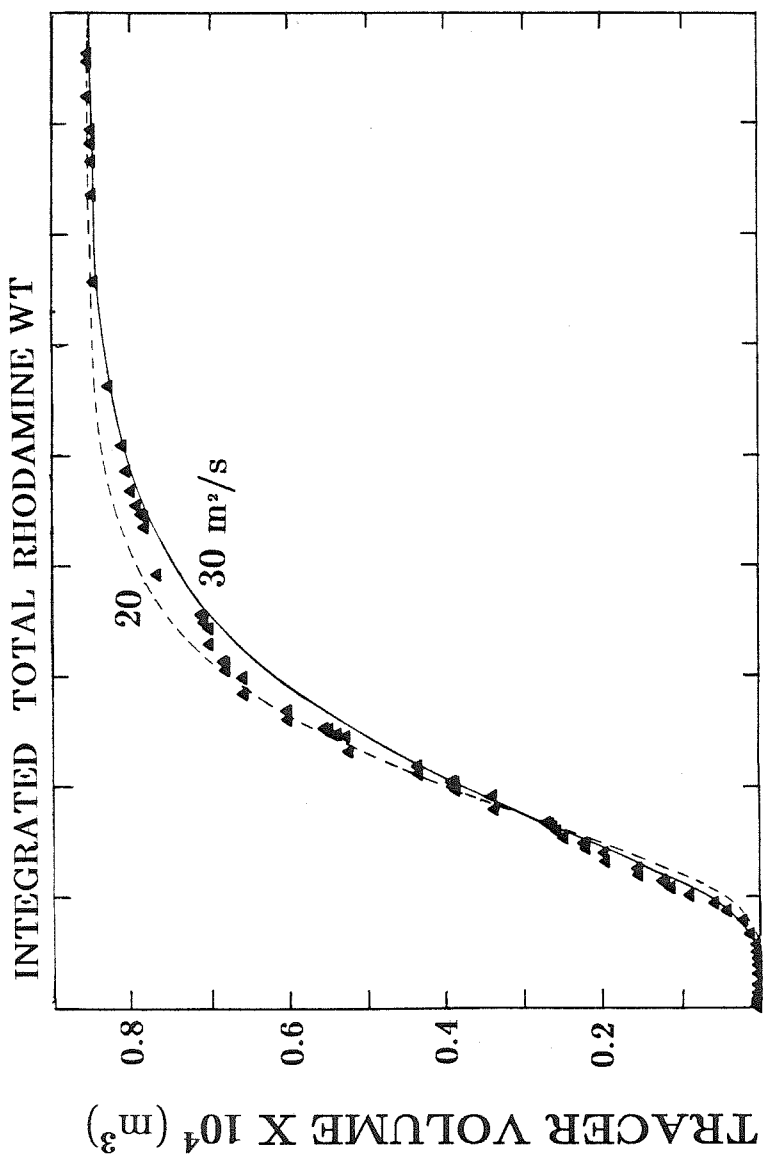

Figure 5.4 Integrated total Rhodamine WT tracer return during the glacier surge (in experiment 1) and integrated diffusive-type disperison curves versus time for $D = 20$, 30 m^2/sec, velocity $U = 0.02$ m/sec, total tracer volume $= 0.0085$ m^3.

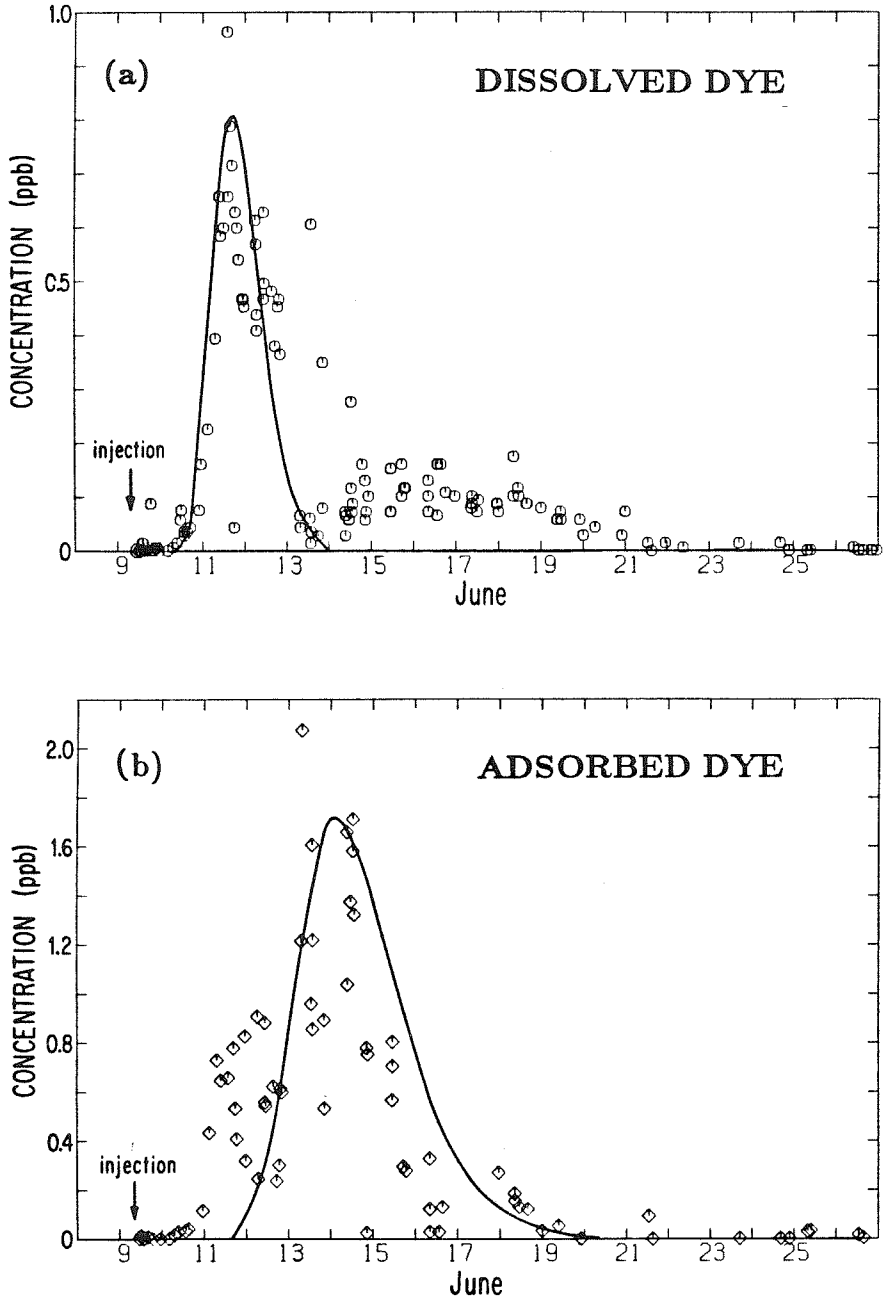

Figure 5.5 (a) Dissolved Rhodamine WT tracer and diffusive-type dispersion curves versus time during glacier surge (in experiment 1) for D =10 m^2/s; velocity U=0.042 m/s and total tracer volume = 0.001 m^3. (b) Adsorbed Rhodamine WT tracer and diffusive-type dispersion curves versus time in experiment 1 for D =5 m^2/s; velocity U =0.010 m/s, tracer volume = 0.005 m^3.

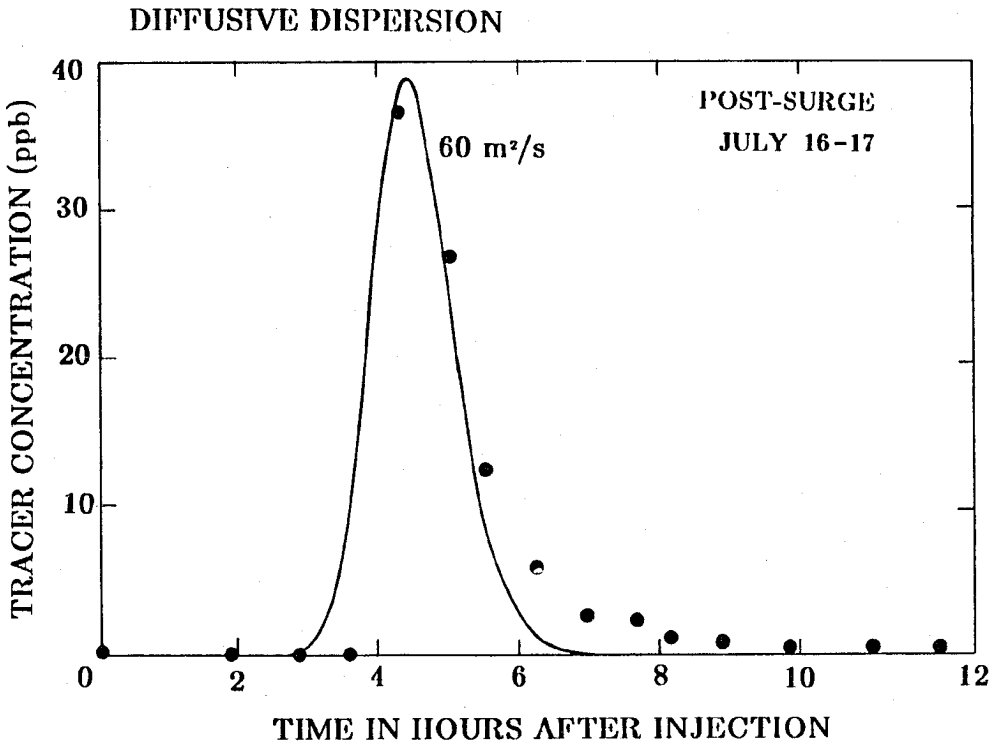

Figure 5.6 Diffusive-dispersion curve for tracer concentration versus time following the July 16 tracer injection in experiment 3, for $D = 58$ m^2/sec, velocity $U = 0.65$ m/sec, total tracer volume $= 0.004$ m^3. Note the poor fit of the theoretical curve to the data for post-surge experiment.

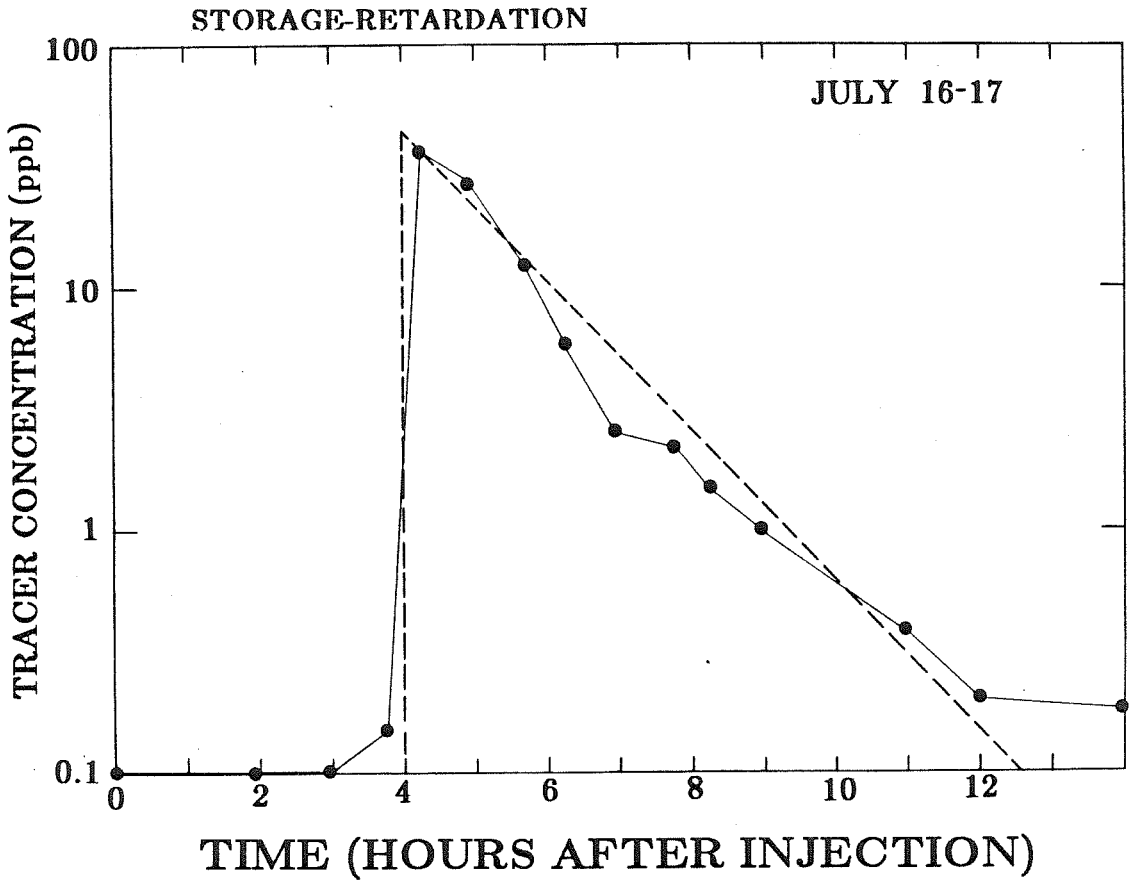

Figure 5.7 Storage-retardation curve and total tracer concentration versus time for experiment 3, following the glacier surge on July 16-17, 1983. The long dashed line is the best fit curve from Eqn. (5.26), and slope $b = 2 \times 10^{-4} s^{-1}$, $C_{max} = 43$ ppb, and $a = 0.6\ s^{-1}$, for stream discharge of 39 m^3/s and injected tracer volume of 0.022 m^3.

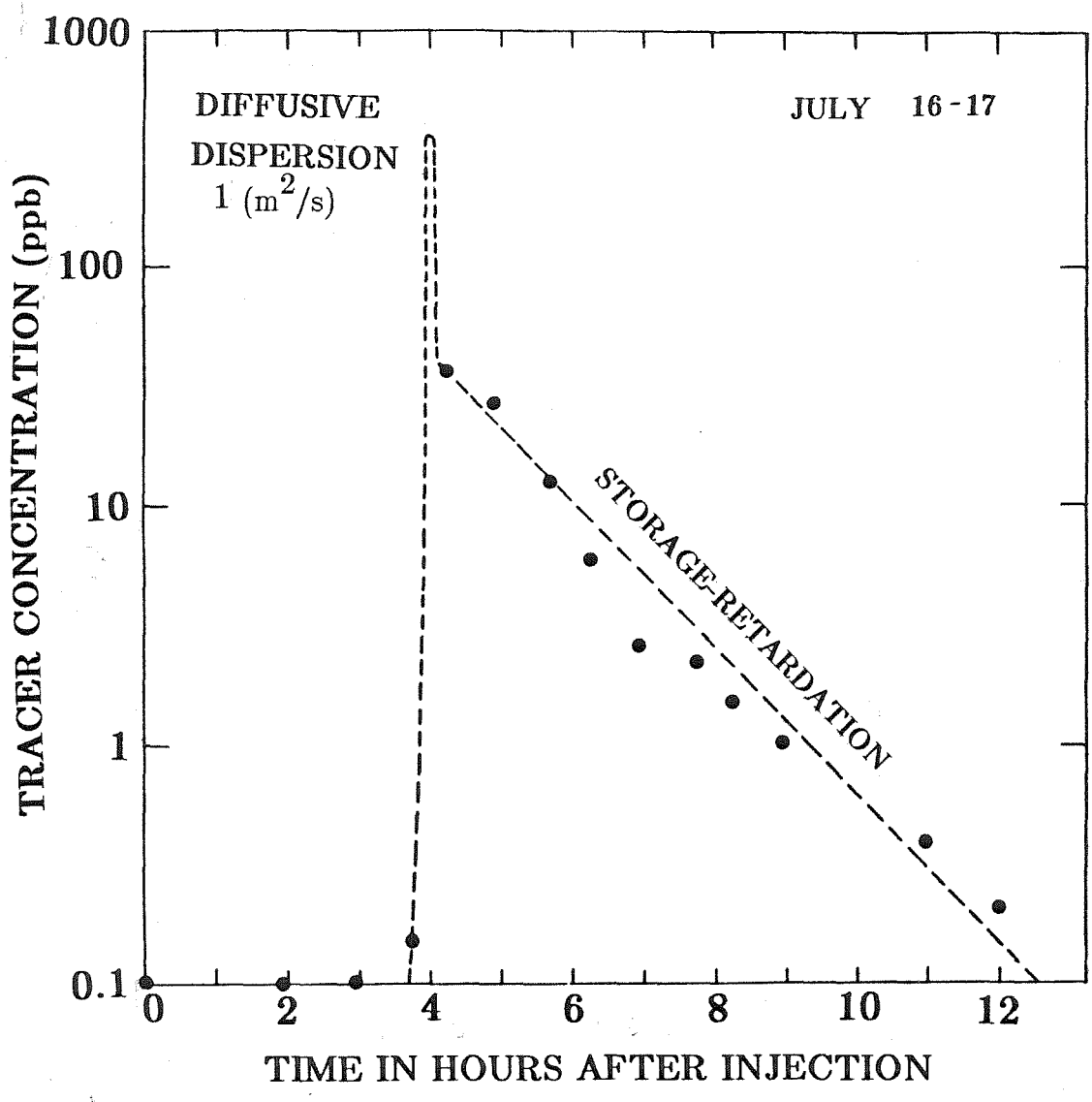

Figure 5.8 Diffusive dispersion curve and storage-retardation curve for $D = 1$ m^2/sec, velocity $U = 0.7$ m/sec, total tracer volume $= 0.017$ m^3. In this plot curves for diffusive dispersion and storage retardation are added together and plotted along with the hypothetical Gaussian curve. The data points are for experiment 3 (conducted after the glacier surge).

Chapter VI:
Interpretation of Dye Tracing Results

6.1. Introduction

In this chapter are examined the possible mechanisms that could cause the observed dispersion of dye tracer during transport through Variegated Glacier. Because of the great difference in dye-transport and dispersion characteristics observed during the surge and after surge termination, it is necessary to consider a variety of different types of flow systems. The goal of this chapter is to infer from the observed dye return curves the nature of the water-conduit system in and at the bed of the glacier.

Dispersion represents variation in the time when different parcels of dye from the original pulse of injected dye arrive at the outflow. The arrival time is determined by the length of the path traveled from the injection point to the outflow, the average transport speed along this path, and the possible effects of a phenomenon of "storage" of dye along the path, followed by subsequent release from storage. The distribution of transport speeds, paths traversed, and storage effects for the different dye parcels retrieved in the outflow stream causes a corresponding distribution of dye concentration with time.

Dispersion may occur due to mixing, transport, and storage processes within a single channel or multichannel network. The size of channels may vary from microscopic in size to several meters in diameter. Cavities may exist along the length of the channel network. As a dye cloud is being advected to the glacier terminus by water flow, many different proceses could affect the spreading of the dye. A wide

variety of analytical and numerical models have been invoked to simulate experimental concentration-time curves obtained from tracer experiments on fluids flowing in surface streams (for example Fischer, 1968), pipes (Taylor,1954), through granular media (Bear, 1972; Ogata, 1964), and through underground fractures or micro- to macroscopic channel networks (Scheidegger, 1961). In this chapter, general observations and concepts of tracer transport, dispersion, and storage in a variety of natural and model flow systems are discussed and compared with the results from the Variegated Glacier dye tracing studies. The objective is to understand how water is transported through the glacier during surge and non-surge conditions. It is thought that the basal-sliding instability that is manifested in fast-moving glaciers is directly linked to the character of the glacier water drainage network and water storage pattern (Meier et al., 1969; Iken et al., 1983). The implications of the results of the dye-tracer experiments for the mechanics of the surge are discussed in Section 6.5 .

6.2. Mechanisms of Diffusive Dispersion of Dye

6.2.1. General Features

For the interpretation of observed dye return in the tracer experiments carried out on Variegated Glacier, we consider here the features of tracer dispersion that are expected for water flow in three distinct, general types of water drainage systems: single-conduit, multiple-interconnecting-conduit, and linked-cavity systems.

The mathematical modeling of tracer dispersion mechanisms leading to generalized diffusion (Eqn. 5.3) is normally based on the "diffusive" or "Fickian" approximation of natural systems (Bear, 1969; Gillham, Sudicky, Cherry and Frind, 1984; Gupta

and Bhattacharya, 1986, p. 161). For each dye-dispersion mechanism that produces diffusive dispersion, i.e., conforms to Eqn. (5.3), a theoretical dispersion coefficient, D, can be derived.

It is generally found, as detailed later, that D as obtained theoretically from models giving diffusive dispersion is proportional to the mean water flow velocity U along the length of the conduit system. For this reason, it is standard practice to introduce a proportionality constant α and to write

$$D = \alpha\, U \quad . \tag{6.1}$$

The proportionality constant α is called the *dispersivity* and is expressed in meters.

It is further found, in the analysis of tracer dispersion in model conduit systems, that α generally turns out to be proportional, or approximately proportional, to a characteristic length scale of the conduit system, which is here designated as L. To express this proportionality a second constant, β, is introduced:

$$\alpha = \beta\, L \quad . \tag{6.2}$$

Equation (6.2) is meaningful and useful when β is scale-independent, as turns out often to be the case, both in the results of theoretical flow models and in empirical data from laboratory experiments.

A compilation plot of D versus U for single and multi-conduit systems is shown in Fig. 6.1. There is a general trend of increasing D with increasing U. The large variance around this trend indicates the that value of α varies significantly within each type of drainage system and between different types of systems.

The objective in examining natural and model flow systems is to obtain relationships between system parameters and the quantities U, D, α, and β, so that the

results of the tracer experiments, which can be cast in terms of these quantities, can be interpreted on the basis of an applicable model.

6.2.2. Single Conduits

6.2.2.1. Water flow in conduits

The mean velocity, U, for turbulent flow[‡] of water in an open channel or conduit is given by Manning's formula:

$$U = \frac{(R_H)^{2/3}}{n^*} \left(\frac{dh}{dx} \right)^{1/2} \tag{6.3}$$

(Manning, 1891, cited by Gardiner and Dackombe, 1983). R_H is the hydraulic radius (see below), n^* is an empirical constant called the Manning roughness, and dh/dx is the gradient of hydraulic head along the length of the conduit. The exponent of R_H in the above equation, 2/3, is an average of a range (0.65 to 0.84) obtained for various channel shapes and roughnesses (Richards, 1982, p. 63).

The hydraulic radius R_H is the channel cross-section area A divided by the wetted perimeter P. For a conduit of circular cross section

$$R_H \equiv \frac{A}{P} = \frac{\pi R^2}{2\pi R} = \frac{R}{2} \tag{6.4}$$

where R is the radius of the conduit.

[‡] Turbulent flow conditions are normally achieved for Reynolds numbers greater than 2,200, where the Reynolds number is defined as $\mathrm{Re} \equiv \rho_w U R_H / \mu$, μ being the viscosity and ρ_w the density of the fluid.

Empirically determined values of n^* for natural streams range between about 0.01 and 0.1 $m^{-1/3}s$ (Gardiner and Dackombe, 1983, pp. 134-45). For ice tunnels in glaciers n^* is 0.05 to 0.15 $m^{-1/3}s$ (Nye, 1976; Röthlisberger, 1972, p. 181; Lliboutry, 1964; Clark, Mathews and Pack, 1984, p. 252). Low values of n^* apply if the conduit is smooth-walled and straight or moderately meandering. High values (greater than 0.1 $m^{-1/3}s$) apply to very rough, tortuous conduits. Such conduits may contain numerous obstructions and have cross-sectional shape and size that vary longitudinally, so that a hydraulic radius R_H cannot really be defined except in some average sense.

In standard engineering practice (Gardiner and Dackombe, 1983), the value of Manning roughness, n^*, is estimated as the summation of the effects of different roughness components. The components primarily affecting the stream flow include the type of bed material, the degree of surface irregularity, the longitudinal variation of channel cross section, and any obstructions (debris, roots or other vegetation, etc.). n^* varies in accordance with the degree of channel meandering by the relation $n^* = n_0\,\omega$, where ω is the coefficient for meandering and the Manning roughness for a straight conduit is n_0. ω ranges from 1 for low sinuosity to 1.3 for high sinuosity (Gardiner and Dackombe, 1983, p. 141).

An alternative relationship used for calculation of mean flow velocity in a single conduit is the Darcy-Weisbach formula:

$$U = \sqrt{\frac{8\,g\,R_H}{f^*}\,\frac{dh}{dx}} \tag{6.5}$$

where f^* is the Darcy-Weisbach friction coefficient and g is the gravitational acceleration (9.8 m^2/s) (Richards, 1982, p. 63-4). Unlike the empirical Manning

formula, the Darcy-Weisbach formula has a theoretical as well as an empirical basis. It is derived by assuming a condition of uniform turbulent flow. For this type of flow no net acceleration occurs. The gain in momentum must be balanced by the loss, and the local energy loss due to boundary resistance must be balanced by the renewal of kinetic energy. A shear stress at the conduit wall is produced by:

$$\tau_{(+)} = \rho_w \; g \; R_H \frac{dh}{dx} \tag{6.6a}$$

where ρ_w is the fluid density. The resisting frictional and turbulent stresses produce an average mean shear stress at the conduit wall, τ^* that is related to a friction coefficient f^*, mean velocity of the fluid U, and the fluid density ρ_w, according to the relationship

$$\tau^* = 1/8 \; f^* \; \rho_w \; U^2 \tag{6.6b}$$

(Leopold et al., 1960, 1966). The condition of uniform flow requires that the driving and resisting stresses be equal, $\tau_{(+)}=\tau^*$, and results in the Darcy-Weisbach formula, Equation (6.5).

The Darcy-Weisbach formula is considered a semi-empirical formula because the value of f^* must be determined empirically. To check the validity of using f^* as a constant for glacier water conduits, the coefficient is compared to information on other the friction parameters that are commonly used in published literature. Friction parameters of importance include the the conduit-wall friction stress τ^* as discussed by Taylor (1954), friction velocity U^* as given by Taylor (1954) and Fischer (1968), and the Manning roughness n^* introduced previously. These friction parameters are related to f^* as follows:

$$(1/8)f^* = \frac{(n^*)^2 \, g}{R_H{}^{1/3}} = \left(\frac{U^*}{U} \right)^2 . \tag{6.7}$$

The Manning roughness and the Darcy-Weisbach friction parameter cannot both be independent of channel size, as indicated by Equation (6.7).

The friction coefficient f^* is determined by the "skin" (grain) resistance, resistance of bedforms, internal distortion resistance caused by channel bends, and spill resistance (Richards, 1982, p. 64). The lowest resistance occurs for a straight, smooth channel. The resistance in a straight channel is normally attributed to a grain effect at the conduit walls. The experimental values of f^* (where $R_H = 1\text{m}$) range from 0.016 a for smooth conduit surfaced with concrete to 0.05 for a rough conduit surfaced with gravel (Bagnold, 1960, p. 142; Richards, 1982, p. 65). The highest flow resistance occurs during spillage of water over the banks and for tumbling streams and streams containing numerous obstructions and localized hydraulic jumps. The value of f^* for a braided channel is several times larger (on average) than f^* for a single channel of the same discharge (Leopold and Wolman, 1957). Most methods available for field estimation of flow resistance are expressed in terms of Manning's roughness (Gardiner and Dackombe, 1983, p. 137), and observations suggest f^* increases with conduit size (Fischer, 1968).

The Darcy-Weisbach formula was derived for straight channels, and a slightly different form is necessary for the balance of forces in a curving channel. The balance of forces in a channel may be generalized if it can be assumed that channel meanders tend to develop similar curvature patterns. It is observed that a stream flowing in a deformable channel tends to develop naturally a meander pattern which can be described by a constant ratio between channel curvature, r_c, and channel hydraulic depth R_H. The resistance coefficient for meandering channels is larger than for a similar straight channel by the relationship

$$f^* = 8\, a_m \frac{R_H}{r_c} + (f^*)_s \tag{6.8a}$$

where R_H is the mean hydraulic radius, and r_c is the mean radius of curvature for the meander bends. r_c, a_m and $(f^*)_s$ are constants (Bagnold, 1969). In open sinuous channels the value given for a_m is 0.05 (Leopold and others, 1960, cited by Bagnold, 1969, p. 142). The curvature ratio, r_c/R_H, is observed to have values between 2 and 3 for natural stream channels with nearly constant cross-section (Leopold et al., 1960). The curvature ratio observed by Ferguson (1973) for supraglacial streams also had a characterisic value of 2 to 3. Because the curvature ratio tends to a constant value ($r_c/R_H \approx 2.5$) the friction coefficient for naturally meandering streams is

$$f^* \approx 0.16 + (f^*)_s \tag{6.8b}$$

(Bagnold, 1960).

In general, turbulent flow in natural and man-made conduits is better described by the empirical Manning formula than the semi-empirical Darcy-Weisbach formula. For glacier conduits it is not known which flow formula is more appropriate, and both are cited in the published literature on glacier water conduits. The empirical Mannings roughness coefficient n^* has more widespread usage than the Darcy-Weisbach friction factor f^*. The parameter n^* is generally considered a better scale-independent indicator of channel roughness than f^* (Richards, 1983), but it is not known whether either parameter can be considered a constant for conduits within a glacier.

6.2.2.2. Tracer dispersion in a turbulent flow

The theory of dispersion of a solute in a turbulent fluid traveling through a single conduit is discussed by Taylor (1954), Elder (1959), and Fischer (1968) for application to flows moving through man-made pipes and natural streams. For natural streams and pipes, observations strongly suggest that α is independent of mean flow velocity as is assumed in writing Equation (6.1) and as theoretically expected (Taylor, 1954; Fischer, 1968). In the case of glacier water conduits, studies of turbulent dispersion of a solute have been carried out by Ambach and Jochum (1972) and Behrens et al. (1975).

The longitudinal dispersion of a solute in a turbulent fluid moving through a single conduit is attributed to the effects of eddy-diffusion acting in a direction transverse to the mean flow (Taylor, 1954; Fischer, 1968). The theoretical coefficient D for longitudinal dispersion of a solute carried by a turbulent fluid is determined by considering tracer mass conservation during advection as described by Taylor (1954) for flow in a pipe, and Fischer (1968) for flow in natural surface streams. The theoretical dispersion coefficient for flow in a single conduit is given by

$$D = \Gamma R_H U^* \tag{6.11}$$

where R_H is the hydraulic radius and U^* is the friction velocity (see Section 6.2.2.1) (Taylor, 1954; Elder, 1959; Fischer, 1968). The coefficient Γ, according to the theory, is independent of the length scale and mean flow velocity. The value of Γ is determined by the normalized cross-sectional flow velocity and depth profiles.

The velocity of a turbulent fluid moving past a fixed boundary surface varies as the logarithm of distance from the surface (Hinze, 1959; Taylor, 1954). Both theory and observations are in agreement on the logarithmic variation of flow speed with

distance from the interface. The steady-state logarithmic velocity profile is used to quantify solute and heat transport in a direction transverse to the mean flow by means of eddy-diffusion (Hinze, 1959).

The theoretical value of Γ for circular straight pipes is 20.2 (Taylor, 1954, p. 463) and is derived from an empirically determined logarithmic velocity profile as described by Taylor (1954). The theoretical Γ for straight pipes is in close agreement with the observed range of 19 to 26 (Taylor, 1954). As expected by Taylor's theory of dispersion, observed Γ values for pipes do not vary with channel roughness f^* or distance traveled X (Table 6.1). Curving pipes (Taylor, 1954) give slightly larger values, $\Gamma = 30$ to 44 for curvature ratio $r_c/R_H = 570$, also included on Tbl. 6.1. The dispersion coefficients for curved pipes appear to increase with channel curvature much more rapidly than can be explained by simply an increase in the flow resistance with channel curvature (Taylor, 1954, p. 463).

If the channel containing the flow is not circular, then a formula for Γ different from that obtained by Taylor (1954) is derived (Fischer, 1968; Elder, 1959; Yotsukura and Cobb, 1972). Fischer (1968) models a turbulent stream as a series of well-mixed parallel tubes that can on average exchange only tracer horizontally, transverse to the mean flow direction. In the case of a wide shallow stream, Fischer (1968) assumes that the depth of a stream channel varies only in the transverse y direction, and no transport is allowed across the sloping lower boundary at the stream bed. The theoretical value of Γ is 5.93 (Elder, 1959) or 5.50 (Fischer, 1968) for an infinitely wide (i.e., two-dimensional) open channel. An "open channel" is defined as a stream conduit that is not completely enclosed by channel walls, and the fluid is at atmospheric pressure. In contrast, a "closed channel" refers to a stream flow that is completely

enclosed by conduit walls, and the fluid may be at a pressure above atmospheric. Three example sketches of simple open and closed conduits are given as item I. on Figure 6.2 .

Fischer (1968) determined an empirical Γ for the Green River, Washington, from the observed dye-return curves, and also a theoretical Γ determined from simultaneously measured cross-sectional depth and velocity profiles. The Green River is a slowly meandering natural stream, with average flow velocity 0.3 m/s , n^* value 0.068 $m^{-1/3}s$, and α value of 10 to 30 m (Fisher, 1968). A theoretical, and empirically verified, value of Γ on the order of 100 is obtained by Fischer for the Green River, as given in Table 6.2.

Similarly, an average Γ of 100 is observed for other natural surface and underground rivers (Table 6.2). This includes the result at One Eye River, Jamaica (Smart and Smith, 1976). The Green and One Eye Rivers have nearly identical mean flow velocities and dispersion coefficients. At One Eye River (Tbl. 6.2) Smart (1976) conducted six tracing experiments over distances of one to six kilometers. They showed flow velocities U of 0.25 m/s, dispersion coefficients D of 2.3 to 2.5 m^2/s, and dispersivities α of 9.2 to 10 m. For an underground stretch of the same stream, through karst terrain, tracing studies (Smart and Smith, 1976) gave an average flow velocity of 0.043 m/s and a dispersivity of 9 m (Table 6.2). The Reynolds number of the flow is well within the regime of turbulent flow for both the underground (Re = 40,000) and surface (Re = 240,000) portions of the One Eye River. The dispersivity values for the underground and nearby surface stretches of the same river are almost identical. These streams traveled over similar terrain, with a low surface gradient, and both had the same hydraulic radius within a factor of two. Consequently, it is not

surprising that their dispersivities are almost identical. The Γ coefficients for turbulent flow in a variety of other natural surface rivers range from 30 to 800 (cited by Fischer, 1968, p. A1).

The agreement between theory and observation is much better for dispersion in pipes than for dispersion in open natural streams. The large range of Γ coefficients (20-800) observed for streams of variable cross-sectional shape may be, in part, due to error in measurement or estimation of the velocity and depth profiles. If U^*, f^*, and/or R_H are underestimated, and U perhaps overestimated, then an erroneously high value of Γ will result. In this study only the average value of 100 for natural streams is considered reliable.

In light of the various unknowns involved in determining the proper form of the dispersion parameterization in terms of Γ and U^*, the combined friction effects for an arbitrary channel are expressed here in terms of the scale- and velocity- independent "constant" β, introduced in (6.2). It is related to Γ by

$$\beta = \Gamma \frac{U^*}{U} \tag{6.12}$$

where $R_H = L$ as justified by Taylor (1954) and Fischer (1968). The longitudinal dispersion coefficient is given as

$$D = \beta R_H U \tag{6.13}$$

which is equivalent to Eqn. (6.1), and the longitudinal dispersivity is

$$\alpha = \beta R_H \quad . \tag{6.14}$$

These formulas for dispersivity α and dispersion coefficient D should allow convenient parameterization of channel dispersion effects for solute tracing experiments

in single conduits.

If a constant friction factor f^* is assumed, as suggested by Spring and Hutter(1982), the longitudinal dispersivity is

$$\alpha = \Gamma \, (\sqrt{1/8 \, f^*}) \, R_H \tag{6.15}$$

where R_H equals half the radius of a conduit of circular cross-section (Taylor, 1954).

Consequently, the Darcy-Weisbach friction coefficient is theoretically determined by the dispersivity and mean conduit size. The value of f^*, constrained by dispersion theory of Taylor (1954) and Fischer (1968), is calculated from stream discharge and standard dye-tracing experimental results (Tables 6.4a and 6.4b, column nine). The f^* and R_H measured during the dye tracing experiments, are used to compute the corresponding value of n^* for each channel (Tables 6.5, 6.1 and 6.2). The n^* obtained from α is compared in the following section (i.e., in Table 6.5) to an independently calculated value of n^* obtained using only the Manning formula and mean values of stream discharge and hydraulic gradient.

In summary, the result of theoretical models of tracer dispersion in pipes and open channels (Taylor, 1954; Fischer, 1968) is that α should be proportional to the hydraulic radius of the conduit. This is expressed in Equation (6.2) in which, for conduits, the scale length L is identified with R_H. The experimental data in Tables 6.1 and 6.2 confirm in a general way this theoretical expectation. The constant of proportionality, $\beta = \Gamma \sqrt{(1/8) f^*}$ in Equation (6.2), is governed by the cross-sectional velocity profile and the channel shape. For a pipe of radius R, $\Gamma = 20$ (Taylor, 1954), and $R_H = R/2$. An open channel that is infinitely wide (depth d) has a theoretical value of Γ of 5.9 (Elder, 1959), and $R_H = d$.

6.2.3. Multiple Interconnecting Conduits and Cavities

In multiple-conduit systems, the tracer can follow several or many different paths in passing from the injection point to the place where tracer return is sampled. A braided stream is such a system, or an undergound karst network of water-conducting passageways fed from a common surface source and discharging downstream to the surface through a common outlet. On a smaller scale, flow through a porous medium, in which there are numerous flow paths through the interconnected pore space, is of the same basic type.

The tracer return in a multiple-conduit system represents the combined time history of tracer outflow from all channels. It is generally thought that the dispersion behavior of a tracer moving through this type of conduit system is primarily due to a distribution of different travel times for flow along different conduits. The local transport speed through each conduit section of the drainage system is controlled by local heterogeneities in conduit roughness, size, tortuosity, and hydraulic gradient.

An important element of a multiple-conduit system is its internal connectivity, the extent of branching and union among the conduits of the system. A porous medium is interconnected on a very local scale, the grain scale, whereas a karst system may have only a few, if any, interconnections among its conduits.

Theoretical models of dispersion in granular porous media (Scheidegger, 1954; Jong, 1958; Saffman, 1959; Ogata, 1964) indicate that the length scale of interconnectivity, the distance between conduit connection points, is the basic length scale pertinent to tracer dispersion and appears as the length scale L in Equation (6.2); Equations (6.1) and (6.2) are applicable to porous media with the length scale being the grain size. The different theoretical models give somewhat different values for the

scale-independent length proportionality factor β in Equation (6.2), in the range 0.1 - 0.8, and they also suggest that there may be a weak (logarithmic) dependence of β on the ratio of travel length X to scale length L, although the form of this dependence is not agreed upon in the different model treatments. For the present purpose, the latter details are not important; what is important is the identification of L in Equation (6.2) with the interconnection scale of the flow paths. These concepts, embodied in Equation (6.2), are verified to a reasonable approximation in laboratory tests on granular porous media of different grain sizes and at a variety of flow-through rates, as shown by Jong [1958, as cited by Ogata (1964, p. G2)]. For porous media of sand-sized grains, the dispersivity α is $\sim 10^{-3}$m or less, much smaller than the dispersivities observed in pipes, and natural streams, discussed in Section 6.2.3; this is as expected from Equation (6.2), with L identified as the grain size in porous media and as the hydraulic radius R_H in single conduits.

A model of dispersion in a multiple-conduit system without internal interconnections (Neretnieks et al., 1982) gives a result of the same type as Equation (6.2), where now the scale length L is the total travel distance X, which here is the interconnection length (since the flow paths must connect at the injection point and sampling point in order that all paths contribute to the tracer return). The model assumes a statistical distribution of conduit characteristics, such that there is a statistical distribution of travel times for dye parcels traversing the various separate conduits. The distribution is characterized by a mean travel time $\overline{t}$ and a variance in travel time ${\sigma_t}^2$. The dimensionless factor β in Equation (6.2) is $\frac{1}{2}(\sigma_t / \overline{t})^2$, half the travel-time variance in units of the mean travel time.

This result for β is readily obtained as follows from the dispersion theory of Section 5.2. The frequency distribution of travel times, when multiplied by the total tracer volume V_0 and divided by the water flux Q_w, is the dye-return curve $C(t)$. Its standard deviation, σ_t, is related to the standard deviation σ_x of the spatial distribution of the dye cloud $\widetilde{C}(x)$ by $\sigma_x \approx U\sigma_t$, which expresses the advection of the cloud at speed U. (The approximation in the equality arises because the spatial dispersion changes as the cloud moves, as discussed in Section 5.2.) The dispersion σ_x at the time $\overline{t}$ of peak tracer return is related to the dispersion coefficient D by ${\sigma_x}^2 = 2D\overline{t}$, as shown in Section 5.2. If the relations just stated are combined with Equation (6.1) and with $X = U\overline{t}$ and solved for α, one obtains

$$\alpha = \frac{1}{2}\left(\frac{\sigma_t}{\overline{t}}\right)^2 X \quad . \tag{6.17}$$

It will now be shown that a relation similar to Equation (6.17) holds for an interconnected multiple-conduit system with arbitrary interconnection length scale $L < X$. The demonstration is based on a stochastic view of the interconnected system. Any parcel of dye traverses a succession of conduit segments from one interconnection or branching point to the next. Its total travel time t is the sum of its travel times t_i over the separate segment intervals (labelled by the interval index i):

$$t = \sum_{i=1}^{N} t_i \quad , \tag{6.18}$$

N being the total number of segment intervals traversed. The stochastic view is that different dye parcels traverse different paths over each segment interval i, so that there is a statistical distribution of travel times t_i for each interval i, just as was assumed in the non-interconnecting multiple-conduit model discussed above. For

simplicity the intervals are taken to be all of the same length L_I, and to have the same statistical distribution of segment travel times, with mean $\overline{t}_I$ and variance ${\sigma_I}^2$ (independent of i). It is also assumed that the variates t_i are mutually independent in the stochastic view of the sytem. As stated above, the dye-return curve is proportional to the statistical frequency distribution of travel times t. Application of the Central-Limit Theorem of statistics (Burlington and May, 1970, p. 195) to the variate t in Equation (6.18) shows that, in the limit of large N, t will be normally distributed with mean $\overline{t} = N\ t_I$ and variance ${\sigma_t}^2 = N\ {\sigma_I}^2$. This indicates that the dye-return curve will be Gaussian, with mean and variance just stated. Thus ${\sigma_t}^2/\overline{t}^2 = {\sigma_I}^2/N{t_I}^2$, and since the number of segments N is $N = X/L_I$, one obtains, upon substituting into Equation (6.17),

$$\alpha = \frac{1}{2}\left(\frac{\sigma_I}{\overline{t}_I}\right)^2 L_I \quad . \tag{6.19}$$

Equation (6.19) has the same form as Equation (6.2). It follows that for tracer dispersion in an interconnected multiple-conduit system, the scale length L in Equation (6.2) is the interconnection distance L_I, and the coefficient β is half the dimensionless interval-travel-time variance in units of the mean interval travel time, $\frac{1}{2}(\sigma_I/\overline{t}_I)^2$.

Models of dispersion in granular porous media, discussed above, are a special case in which the summation in Equation (6.18) has been carried out stochastically for the type of flow-path interconnectivity present in intergranular pore space, with laminar viscous flow in this space. They lead, as already stated, to the result in Equation (6.2), with L equal to the grain size, which is equal (or approximately equal) to the average interconnection distance in such a system. Although the models have not given a specific evaluation of $\sigma_I/\overline{t}_I$ for the flow-path segments in the system, it

seems reasonable intuitively that this travel-time dispersion quantity could have a value $\sim$ 0.4 - 1.3, corresponding via Equation (6.19) to the values of β (0.1-0.8) obtained in the models, as noted above. This means simply that the local dispersion in interval travel times is of the order of the travel times themselves.

In considering the applicability of Equation (6.19) to a natural flow system such as the basal water system of Variegated Glacier in surge, as will be done later (Section 6.4), one has to consider what values of the ratio $\sigma_I / \overline{t}_I$ are physically reasonable or possible. For granular porous media the estimate $\sigma_I \sim \overline{t}_I$ is reasonable, as just discussed. It might seem that for multiple-conduit systems in general, the estimate $\sigma_I / \overline{t}_I \sim 1$ is an upper limit, since frequency-distribution functions of rather broad dispersion, such as a uniform distribution from $t_I = 0$ to a maximum value of t_I, conform to this estimate. If this were the case, then the maximum expectable value of α would be $\alpha \sim L_I$. However, it is in fact possible to obtain much larger values on a physically reasonable basis. This arises because of the likelihood that the interval travel times t_i are log-normally distributed. It is readily shown that if the t_i are log-normally distributed (Aitchison and Brown, 1957, p. 22), with log-normal variance ${\nu_I}^2$, then

$$\left(\frac{\sigma_I}{\overline{t}_I} \right)^2 = e^{{\nu_I}^2} - 1 \quad . \tag{6.20}$$

Since ${\nu_I}^2$ can assume reasonably large values, as explained below, the quantity $(\sigma_I / \overline{t}_I)^2$ can be large, according to Equation (6.20); thus, β in Equation (6.2) can be large.

The likelihood that the interval travel times t_i are log-normally distributed stems from the general tendency for the various factors that determine t_i to be

themselves log-normally distributed. This was recognized by Neretnieks (1982, 1983) in the model earlier discussed, in which water flow occurs in crack-like passageways whose widths are log-normally distributed in accordance with observations of fissure widths in natural rocks (Snow, 1970). The tendency for dimensional entities that occur in geologic systems, such as grain size in sedimentary rocks (Krumbein and Sloss, 1963, p. 96), to be log-normally distributed is rather widely recognized (Aitchison and Brown, 1957, pp. 24-7). It will be assumed here to apply to the factors that control the water flow in the segments of an interconnected multiple-conduit system.

The system is visualized or idealized as consisting of segments of length L_i (the index i again designating the segment interval), each containing a conduit whose cross section has hydraulic radius r_i and whose length is l_i. Each segment may contain one or more relatively large cavities, of dimensions large compared to r_i; when cavities are present along the flow path, $l_i < L_i$. These cavities are inferred to have been formed by a process of cavitation at the base of the glacier, and their present inclusion in the system provides the introduction of the *linked-cavity model* of the basal water system of the glacier, which is discussed later (Section 6.4). The flux of water q_i carried by any segment is controlled by the flow through the conduit part of the segment rather than by the cavities, because of the conduit's small lateral dimensions and large longitudinal dimension.

If the average gradient in hydraulic head over the segment (of length L_i) is γ_i, the hydraulic-head gradient in the conduit part of the segment will be $\gamma_i L_i / l_i$, because negligible drop in head is taken across the large cavities. According to the Manning equation (Eqn. 6.3), the flux q_i will therefore be

$$q_i = \frac{4\,\pi {r_i}^{8/3}}{n_i^*} \left(\gamma_i \frac{L_i}{l_i}\right)^{1/2} \tag{6.21}$$

where n^*_i is the Manning roughness of the conduit. (This assumes that the conduit cross-sectional area is $4\pi {r_i}^2$, as for a circular conduit.) The volume of water in the segment is represented by

$$v_i = {d_i}^3 + 4\,\pi {r_i}^2 l_i \cong {d_i}^3 \tag{6.22}$$

where d_i is the equivalent "cubic" dimension of the cavity in the segment, which is assumed large compared to the conduit, so that the conduit volume can be neglected as indicated on the right in Equation (6.22). (The reasons behind this and the previous assumptions will appear later in the discussion of the linked-cavity model, Section 6.4.) The transit time t_i of a tracer parcel moving through the segment, is v_i / q_i; hence, from Equations (6.21) and (6.22)

$$t_i = \frac{{d_i}^3\, n^*_i\, {l_i}^{1/2}}{4\,\pi\, {r_i}^{8/3}\, {\gamma_i}^{1/2}\, {L_i}^{1/2}} \quad . \tag{6.23}$$

Equation (6.23) provides the means of evaluating the quantity $(\sigma_I / \overline{t_I})$ on the basis of the assumed log-normal distributions of the various factors on the right-hand side. From Equation (6.23),

$$\ln t_i = 3 \ln d_i - \frac{8}{3} \ln r_i + \ln n_i^* - \frac{1}{2} \ln \gamma_i + \frac{1}{2} \ln l_i - \frac{1}{2} \ln L_i - \ln 4\pi \tag{6.24}$$

so that $\ln t_i$ is a linear combination of the normally distributed variates on the right in Equation (6.24). Therefore, as is well known (Aitchison and Brown, 1957), if the variates on the right in Equation (6.24) are distributed independently, then $\ln t_i$ is normally distributed with variance

$$\nu_I{}^2 = 3^2\,\nu_d{}^2 + \left(\frac{8}{3}\right)^2 \nu_r{}^2 + \nu_{n^*}{}^2 + \left(\frac{1}{2}\right)^2 \nu_\gamma{}^2 + \left(\frac{1}{2}\right)^2 \nu_l{}^2 + \left(\frac{1}{2}\right)^2 \nu_L{}^2 \quad (6.25)$$

In Equation (6.25), the quantities $\nu_d{}^2$, $\nu_r{}^2$, etc. are the log-normal variances for the six variates d, r, etc., that is, the quantities $\nu_m{}^2$ that appear in the probability density functions $f\,(ln\ \Psi_m)$ for the logarithms of these variates, the variates being symbolically designated Ψ_m $(m = 1, 2,..., 6)$:

$$f\,(\ln\,\Psi_m) = \frac{1}{\sqrt{2\pi\nu_m{}^2}}\, e^{\frac{-(\ln\,\Psi_m\,-\,\mu_m)^2}{2\nu_m{}^2}} \quad .$$

To get an idea as to what sort of value of $(\sigma_I/\overline{t_I})$ is reasonable or possible on the basis of Equation (6.25), it might be assumed that all of the variates Ψ_m have the same log-normal variances $\nu_m{}^2$. In that case, from Equation (6.25)

$$\nu_I{}^2 = (17.9)\,\nu_m{}^2 \quad . \quad (6.26)$$

If the ratio $\sigma_m/\overline{\Psi}_m$ for each variate Ψ_m is ~ 1, as might be expected from the earlier discussion, then from Equation (6.20), $\nu_m{}^2 \approx \ln 2$, and from Equation (6.26), $\nu_I{}^2 \approx 12.4$, so that, from Equation (6.20) , $[(\sigma_I/\overline{t_I})^2 \sim 10^5]$, an extremely large number. For comparison, if the only variate is the conduit size, then only $\nu_r{}^2$ contributes to $\nu_I{}^2$, and from Equation (6.25) $[(\sigma_I/\overline{t_I})^2 \sim 10^2]$. It is therefore possible, with a relatively modest log-normal scatter of the various variates that control t_i, to obtain a very large value of $(\sigma_I/\overline{t_I})^2$ and hence of the dispersivity α as given by Equation (6.19). There is, of course, no reason to believe that all of the $\nu_m{}^2$ values will be the same, and separate discussions are appropriate for each of the variates in Equation (6.24), particularly for γ_i, n_i^*, and L_i. However, the preceding discussion shows that it is so readily possible to obtain a large value of $(\sigma_I/\overline{t_I})^2$ on the basis of

Equation (6.25) that the uncertainties of detail in the ν_m^2 values do not stand in the way of the basic conclusion that it is possible to obtain rather large values of β, or of dispersivity α, with an internally interconnected, multi-conduit model of the type considered. This contrasts greatly with the situation for single-conduit systems, whose α values are limited by $\beta \sim 1$ and by the length scales $L = R_H \sim$ a few meters, and for porous media, for which again $\beta \sim 1$ and $L \sim 10^{-3}$m (for sand-sized grains).

6.2.4. Linked-Cavity Systems

Distinct from and additional to the tracer dispersion effects in linked-cavity systems considered in the last section, a special feature of linked-cavity dispersion arises in models considered by Bear (1972). If the dye mixes rapidly in the cavities, as it might if the inflow enters in the form of a turbulent water jet at high speed, then even in a single-conduit linked-cavity system (a single chain of cavities linked by conduits) there will be a significant contribution to tracer dispersion due to the mixing in the cavities, in addition to any single-conduit-type dispersion associated with the connecting conduit segments. The dispersion due to the cavities alone conforms to the relationships in Equations (6.1) and (6.2) and, for the simple model of a chain of large equal cavities at longitudinal spacing L_c linked by small connecting orifices, the tracer dispersion can be expressed in terms of dispersivity α by the simple relation

$$\alpha = \frac{1}{2} L_c \tag{6.27}$$

which means that $\beta = 1/2$ in Equation (6.2), with length scale $L = L_c$, the cavity spacing. These results are demonstrated mathematically by Bear (1969).

6.2.5. Composite Drainage Systems

A portion of the variance in β coefficients for natural porous media may be due to the effect of a composite drainage system made up of zones of different hydraulic conductivity or types of drainage conduits. The dispersion of a composite system may be controlled by the section of the water travel path where α is greatest and U is lowest. In such a case, mean flow velocity and tracer dispersion behavior for the total distance traveled X cannot be directly interpreted in terms of system parameters as described in preceding sections.

For example, assume that the observed dispersion behavior for the total distance traveled was controlled by a narrow zone of flow consisting of granular porous material. Over most of the travel path it is also assumed water travels freely in large open channels. Suppose the narrow zone of granular material that the water must traverse is $X' = 100$m long, along the flow path, and suppose the mean grain size of the granular material is about 0.01 m, and the water percolates through this at a velocity of 0.001 m/s. The dispersivity α' corresponding to the slow zone is therefore on the order of 0.01 m, and dispersion coefficient D' is on the order of 10^{-5} m^2/s. By Equations (5.11), (6.1) and (6.17), the dispersivity is

$$\alpha = \frac{X}{2}\left(\frac{\sigma_t}{\overline{t}}\right)^2 .$$

If the standard deviation of the dye-return curve is measured at the outflow at distance X, and the mean travel time is determined by the narrow zone (i.e., $\overline{t} \approx \overline{t}'$), then the ratio between apparent dispersivity α at X = 10 km and actual dispersivity α' of the slow zone of is given by

$$\frac{\alpha}{\alpha'} = \frac{X}{X'} = 1000 .$$

This involves the assumption that $\frac{\sigma_t}{t}$ and $\bar{t}$ are determined only by the flow through the porous medium, as stated above. Thus, for a total travel distance of $X = 10$ km, the apparent dispersivity α at the terminus outflow is 100 m, and the flow velocity U averaged over the entire distance traveled is 0.1 m/s. If the average dye-return curve obtained at the terminus outflow is modeled in terms of a homogeneous, instead of composite, drainage system then obviously the resulting model interpretation will be incorrect.

For any underground water-flow path, the possibility of a composite drainage system should be investigated. If a flow obstruction occurs at a particular location, then the water table should be markedly higher upstream from the the obstruction than downstream from the obstruction. The borehole water level should be nearest the upper surface at the location of the flow obstruction. If the borehole water levels are everywhere parallel to the upper surface then probably a narrow zone of flow obstruction does not exist. Under such circumstances the subsurface water flow pattern should not be modeled as a composite drainage system of the type just discussed.

6.2.6. Summary and Discussion

A roughly linear relationship between dispersion coefficient, D, and mean flow velocity, U, is suggested by the experimental dye-tracing results shown in Fig. 6.1. Thus, the observed dispersivity conforms adequately to the relation $D = \alpha U$ that is expected on the basis of several different conduit-system models. Average values of dispersivity α for different types conduit system are given in Tables 6.1, 6.2 and 6.6.

The value of α is different for different single- or multi-conduit flow systems. This difference is in accord with theoretical expectations, based on dispersion models described. Laboratory studies on dispersion in fluids moving through man-made pipes (Table 6.1 from Taylor [1954]) and granular porous media (De Josselin de Jong, 1958) indicate α values that are 10 to 100,000 times lower than for natural drainage systems (Fischer, 1968; Anderson, 1979) measured in the field. The average dispersivity for rivers (Table 6.2) is much greater than the dispersivities for man-made pipes (Table 6.1). This is explained using the theory of eddy diffusion described by Taylor (1954) and Fischer (1968), and is attibutable to by major differences in conduit size, shape, roughness and tortuosity between the average man-made pipe and natural river.

For each type of conduit system discussed in this section, both theory and observation suggest that the dispersivity α increases linearly with the scale length L, with a constant of proportionality called β. The relevant scale length L may be the mean channel size, length of channel segment or size of sediment grains or distance between cavities as indicated by each model described in the preceding sections. The represented scale length of each type of drainage system is summarized in Table 6.6 and indicated on Figure 6.2.

The model variable of basic importance in natural systems of ground water flow is the relevant scale length L. In the multi-conduit model, L is the distance between conduit intersections (the conduit segment length). For granular media the scale length is normally assumed to be on the order of several times the mean grain size of the sediment. The coefficient relating α and L for all models is defined as $\beta \equiv \alpha/L$. The β coefficient is on the order of 1 for isotropic granular porous media (such as

glass beads or snow), and also for smooth, man-made pipes (Table 6.1). Higher β values, $\sim$ 10, are obtained for rough single conduits. Still larger values of β are obtained for turbulent flow in rough, obstructed and tortuous single conduits. The highest β values of order 10,000 are obtained for natural porous media (for example: Anderson, 1979), and suggested for fractured and heterogeneous multi-conduit systems (Snow, 1970; Neretnieks, 1983; Gillham et al., 1984).

In the experimentally well-studied case of turbulent flow in single conduits, the variable controlling β appears to be the wall roughness or friction coefficient f^*, in agreement with the theory of turbulent eddy diffusion (Fischer, 1968; Taylor, 1954). The β coefficient increases with the wall friction and channel sinuosity approximately as expected.

For surface and underground rivers, and for pipes, D increases approximately linearly with U, with a different slope α for each conduit type as indicated on Figure 6.1, and Tables 6.1 and 6.2. This is in accord with what is expected on the basis of theoretical flow models of such systems (Taylor, 1954; Fischer, 1968) and can be expressed by saying that the dispersivity α in a particular conduit is independent of flow velocity U. The theoretical models also indicate that α should be a direct function of the wall or bed roughness and of conduit sinuosity (i.e., model dispersivity increases as $\sqrt{f^*}$. Artificial conduits are typically straighter and smoother than the beds of natural rivers, and this is doubtless the reason why α is less for pipes than for a natural conduits of similar R_H, as can be seen in Tables 6.1 and 6.2. A similar difference, for similar reasons, is seen in the comparison between the behavior of laboratory pipes and of pipelines in the field.

Field observations on natural porous media strongly suggest that the length of conduit segments is much greater than the mean grain size, and the variance in travel time is larger than can be explained by the simple model of granular porous media. The β coefficient for natural porous media is best described by the the multiple-conduit-cavity model. In this model the spread of the dye-return curve at the outflow is determined by summation of effects from all of the controlling variates, including primarily conduit radius, cavity size, and conduit length, but is also affected by local hydraulic gradient and conduit roughness. The resulting variance for such a multi-conduit system is large and can explain the large values of dispersivity observed in the field (Anderson, 1979) for natural porous media ($\alpha \sim$ 10 to 1000), and the large β values (10^4 to 10^5) (Table 6.1). In contrast, observations of dispersion in natural rivers indicate the average $\Gamma \sim 100$ (Fischer, 1968), and for an average natural river of hydraulic radius 1 m and $f^* = 0.26$, the β coefficient is of order 10 (Table 6.6). If the channel roughness coefficient, the hydraulic radius and the shape of the conduit are known, the dispersivity of a solute in turbulent flow is theoretically determined for flow in pipes and rivers.

6.3. Mechanisms of Dye Storage and Release

6.3.1. General Features

Mechanisms for "storage-release" as normally defined in the hydrology literature (Bear, 1972) result in a long extended tail in the dye-return curve that is not adequately modeled by diffusive processes as described by dispersion Equation (5.3). This storage-release category includes instantaneous and delayed effects of dye adsorption on bedrock or immobile sediment. In addition to storage-release enroute to the outflow, the potentially significant effect of storage and release at the injection site is considered. "Storage-release" mechanisms as defined in this thesis cause modification of a tracer pulse by transfering the tracer between immobile and mobile zones of the drainage system. The immobile zones may consist of zones of slowly moving or stagnant water, or of adsorbing sediment.

6.3.2. Storage and Release at the Point of Injection

Under certain circumstances the injection borehole may also behave as an immobile zone that slowly releases the tracer in a manner similar to storage-release mechanisms that affect the tracer within the main conduit system. If the base of a dye injection borehole is poorly connnected to the main drainage system, and if the dye remaining in the borehole is thoroughly mixed, then the injection borehole may be modeled as a perfect mixer as discussed by Bear (1979). Consider that the dye solution in the borehole to be at concentration is $S(t)$, the volume of dye and water solution in the borehole to be V_b, and the initial volume of dye injected to be V_o. Also assume that the discharge q of clean water entering the borehole is equivalent to

the discharge of dye solution of concentration $C(x,t)$ escaping from the bottom of the borehole, at $x = 0$. The tracer is then tranported at a mean velocity U to the outflow at distance X. According to Bear (1979), the concentration of tracer in the outflow will be

$$C(t) = \frac{V_o}{V_b}\, 1(Ut - X) \cdot \exp\left\{ \frac{q}{V_b} \left[\frac{X}{U} - t \right] \right\} . \qquad (6.28)$$

Thus an exponential dye-return curve results from by this model of a "perfectly mixed" dye solution in the borehole.

A long narrow borehole probably cannot realistically behave as a "perfect mixer" as measured above, because upward mixing of the dye in solution is normally overwhelmed by the continuous downward flow of water. The downward flow of water in boreholes is especially noticeable in boreholes drilled into temperate glaciers. The mixing effects due to molecular diffusion or turbulence in a long narrow borehole are probably negligible over the time scales of a few hours to days, that apply in to this study.

Another possible mechanism for dye storage at the injection site is that dye may be adsorbed on immobile sediment in the vicinity of the borehole outflow, at $x = 0$. If the tracer is adsorbed on granular sediment then the movement of dissolved tracer through the sediment, is described by the theory of mobile-immobile zones, discussed in Section (6.3.5). If the dye were forced to filter slowly through highly adsorbing sediment in order to reach a main transport conduit, the dye-return curve would more closely resemble a nearly symmetrical Gaussian curve (De Smedt and Wierenga, 1984), and the mean transit time to the outflow would be long.

There seems to be no realistic mechanism to generate an exponentially shaped dye-return curve due to storage and release within, or at the base of the injection borehole, particularly if the mean transport velocity is rapid. Regardless, the dye-release curve should be monitored at the base of the injection borehole just to be certain the shape of the dye-return curve at the outflow is indeed attributable to dispersion mechanisms affecting the tracer enroute in the primary conduit system. Only if the tracer concentration within the borehole decreases exponentially in the same manner as observed at the outflow, should dye storage at the base of the borehole be considered significant.

6.3.3. Retardation Due to Adsorption on Sediment

A dissolved dye tracer may react with rock material lining the conduit walls or particles suspended in the moving fluid. For the special case of an instantaneous linear equilibrium reaction, the dye adsorbed on rock surfaces is in local equilibrium with the dye in solution. From Equation (3.3) the stored tracer concentration S (the volume of dye adsorbed per volume of solution) is linearly related to the dissolved tracer concentration C (volume of dissolved dye per volume of solution) by

$$S = K_a \; A_v \; C \tag{6.29}$$

and thus

$$\frac{\partial S}{\partial t} = A_v \; K_a \; \frac{\partial C}{\partial t} \tag{6.30}$$

where K_a and A_v are constants of the system (Bear, 1979; Neretnieks et al., 1982). The coefficient A_v is the specific area available for tracer adsorption per volume of fluid and is directly related to the coefficient A_m discussed earlier in Section 3.5. The

significance of A_v is discussed below. K_a is called the area distribution coefficient and has already been discussed in Chapter 3 (Section 3.5) in relation to Langmuir's equation.

Substituting $\partial S/\partial t$ as given above into the dispersion Equation (5.3), results in

$$\frac{\partial C}{\partial t} R_a = -U \frac{\partial C}{\partial x} + D \frac{\partial^2 C}{\partial x^2} \tag{6.31}$$

where

$$R_a = 1 + A_v K_a \tag{6.32}$$

The coefficient R_a is called the retardation factor. R_a accounts for the slowing down of tracer movement by adsorption on the solid, as described by Neretnienks et al. (1982), and as treated earlier by Bear (1969). It is apparent from Equations (5.3) and (5.31) that the mean velocity U of the dye cloud, under the influence of instantaneous adsorption, is $U_{dye} = U/R_a$ and its dispersion coeffient is $D_{dye} = \frac{D}{R_a}$. By Equation (6.1) $D = \alpha U$ and similarly $D_{dye} = \alpha_{dye} U_{dye}$. The dispersivity of an adsorbing tracer, α_{dye}, can is equated with α of a non-adsorbing tracer through the relationship

$$\alpha = \frac{1}{U} \alpha_{dye} R_a U_{dye} = \alpha_{dye} \quad . \tag{6.33}$$

Consequently, the dispersivity α_{dye} of an adsorbing tracer should be equal to equivalent to the dispersivity α of a non-adsorbing tracer. If adsorption effects are not significant, then the value of R_a is equal to 1, and conversely, if $A_v K_a >> 1$, then $R_a = A_v K_a$.

First, to determine the value of R_a for a particular dye-tracer experiment, the value of K_a is calculated from the volume (or mass) distribution coefficient K_d as described in Section 3.5. For the case of Rhodamine WT adsorption on suspended sediment of mixed lithologies from Variegated Glacier outlet streams the areal adsorptivity is $K_a = 10^{-3}$ to 10^{-4} m. The range of K_a values is consistent with the independent analyses by Benecala et. al (1984) on stream sediment samples (mixed-lithology rock particles); K_d values for sand- to cobble-sized particles studied by Benecala et al. (1984) are included in Table 3.3.

Second, the value of A_v must also be determined for the tracing experiment. The coefficient A_v, or the specific surface area, is defined as the amount of surface area available for adsorption per volume of solution, in units of m^2/m^3. In a cylindrical conduit of radius r and length Δx, the surface area is $2\pi r\,\Delta x$, the volume of the fluid (= volume of solution) is $\pi r^2 \Delta x$, and thus the specific surface area available for adsorption is given by

$$A_v = k_a \frac{2\pi r\,\Delta x}{\pi r^2 \Delta x} = k_a \frac{2}{r} \tag{6.34}$$

where the dimensionless proportionality constant k_a is the surface area available for adsorption per surface area of conduit. In the general case of a conduit of hydraulic radius R_H, the specific surface area is

$$A_v = \frac{k_a}{R_H} \quad . \tag{6.35}$$

The value of k_a depends upon the fraction of the surface area of the conduit walls that is covered with rock, the grain size and roughness of the rock material lining the walls, and the depth of dye penetration for instantaneous adsorption and release of

tracer at conduit walls. The value $k_a = 1$ for a smooth, solid rock conduit. Several times more surface area is available on rough, granular, conduit surfaces than on smooth conduit surfaces, and an additional several-fold increase in rock surface area may result from adsorption below the surface in masses of sediment. At the bed of a glacier a conduit is likely to be only half lined with sediment, and the remainder of the surface area is likely to consist of relatively clean glacier ice. Consequently, for glacier conduits at the base of a glacier, this implies that $k_a \approx 2$. The actual value of k_a may differ by some unknown factor but is unlikely to differ by more than an order of magnitude from a value of 10, and therefore it is assumed that k_a may range from 1 to 100 m^{-1}.

The resulting retardation factor is

$$R_a = 1 + \frac{k_a}{R_H} K_a \tag{6.36}$$

where the value of K_a is on the order of 10^{-4} m for Rhodamine WT dye adsorption on crushed rock particles of mixed lithologies (Section 3.5).

6.3.4. Matrix Diffusion

A model for transport transverse to the flow direction, generating a storage-retardation-type dispersion of dye in the longitudinal direction, is called matrix diffusion (Bear, 1979; Suckindy et al. 1985; Neretnieks et al., 1982, ; Neretnieks, 1983, p.367). It involves diffusion of a tracer into the walls of the conduits. Solution of the transverse diffusion problem by Neretnieks et al. (1982) indicates that the matrix diffusion should generate a retardation tail on the initial dye pulse, the dye concentration in the tail dropping off with time t as $t^{-3/2}$. This tail can be appproximated as a

decaying exponential (Neretnieks, 1983).

6.3.5. Mobile-Immobile Zones

The third category of storage-retardation processes is caused by distributed dye storage, which includes adsorption and later release of dye on sediment, and temporary immobilization of dye in slowly moving or nearly stagnant water pockets, cavities and back eddies.

The time rate of change in dye concentration for a matrix consisting of mobile and immobile flow zones is described by De Smedt and Wierenga (1984, p. 226) in terms of the volume content of mobile water θ_m per unit volume of total water content in the porous medium, and the immobile water content θ_{im} per unit volume total water, and the transfer coefficient between mobile and immobile zones, k_{mim}. The rate of change of dye concentration in the immobilized zone is assumed to be linearly related to the difference between the dye concentration in the mobile zone, C, and the dye concentration in the immobile zone, S. The rate of dye transfer between an immobile zone and the main flow appears to be described by a linear rate law,

$$\frac{\partial S}{\partial t} = aC - bS \tag{6.38}$$

where a and b are rate constants or equivalently

$$\frac{\partial S}{\partial t} = k_{mim} \frac{\theta_m}{\theta_{im}} C - S$$

where k_{mim} is the transfer coefficient (De Smedt and Wierenga, 1984, p. 226; Ambach and Jochum, 1973). The immobile zone may consist of a region of stagnant (or slowly

moving) water connected to the main conduit or perhaps may be an immobile pocket of adsorbing sediment.

This model of mobile-immobile zones can result in a dispersion curve that is not exponential in shape if the transfer coefficient k_{mim} is linearly related to the mean flow velocity. Observations indicate that the transfer coefficient, k_{mim}, for flow through homogeneous porous rock samples is proportional to the mean flow velocity, U (m/sec), through the empirical relationship $k_{mim} = 4.2\ U$ (Krupp and Elrick, 1968; De Smedt and Wierenga, 1984, p. 230). The result of this relationship is that the dye return curve will be approximately Gaussian in shape for long travel times, as discussed by De Smedt and Wierenga (1984). In this thesis the parameters a and b are not dependent upon the mean flow velocity, and, therefore, the dye return curve for this model, will not be Gaussian. If an exponential dye-return curve is obtained, then the water contents θ_m and θ_{im} and the transfer coefficient k_{mim} must not dependent upon the mean flow velocity.

The coefficients a and b are determined by the rates of transfer of tracer between immobile and mobile zones. The predicted values of these rate constants obtained from the parameterization of the dye-return curve may be compared to rate constants determined by the known or hypothetical description of the immobile zones. The parameters a and b are obtained from the dye-tracing data by fitting the dye-return curve to the storage-retardation model of tracer dispersion, given in Chapter 5.

The concept of mobile-immobile zones described by De Smedt and Wierenga can be applied to the storage-release mechanism in sinuous natural streams. The volume θ_{im} of "immobile" water temporarily stored at the inside of meander bends and in

nearly stagnant water pockets associated with river meandering should increase approximately linearly with the channel sinuosity. The more a stream meanders, the larger the number of back-eddies and slow moving zones which can store dye temporarily; hence, the larger the storage-retardation effect. The transfer coefficient, k_{mim}, is proportional to the eddy diffusion coefficient in the direction perpendicular to the mean flow direction (Fischer, 1968). The eddy diffusion coefficient is nearly constant for all well-developed natural meander patterns (Fischer, 1968; Richards, 1982). Therefore, k_{mim} for naturally meandering streams of constant sinuosity is expected to be nearly constant.

6.4. Water Transport Systems of Normal Glaciers

6.4.1. Description of Aquifer Zonation

A temperate glacier (at the melting point throughout) is a spatially zoned aquifer. A sketch of the drainage system zonations for a normal glacier is shown on Fig. 6.3. The five major spatial zones controling the flow of water include the following: I. snow; II. firn; III. glacier ice; IV. basal conduit system; V. sub-basal rock material. The horizontal zonation, from the glacier head to terminus, is a reflection of the spatial extent and thickness distribution of the vertical zones (I-V), and is also affected by the spatial distribution of crevasses and moulins. Crevasses and moulins act as vertical transport conduits for water within the glacier. The zonations vary in extent and relative importance, and each can be affected by the annual pattern of surface melt, snow accumulation, and water discharge. Related seasonal variations in glacier flow, particularly basal sliding, can also affect the aquifers, particularly in the basal zone IV.

The water flow near the upper surface (Regions I and II) in the accumulation area of a glacier is flow in a granular porous medium. Within the snowpack, water drains through the pore space between ice grains and lenses (Colbeck, 1975). The microscopic channels connecting pore spaces gradually feed into ever larger channels within the snow, until water flow either reaches a crevasse, the glacier margin, or still larger conduits within the firn zone (zone II). Water storage can occur within the snow and firn zones in the pore space between ice grains, in small channels, and in crevasses.

In the ablation area of a normal glacier, water flows in open meandering conduits at the glacier surface of zone III, until reaching a crevasse or moulin (deep hole in the glacier). Then the water tumbles down to a lower drainage level, perhaps even reaching the glacier bed through a deep moulin.

The water moving within the central zone of glacier ice (zone III) can travel significant distances without intersecting the glacier bed. A portion of the englacial water travels along the ice crystal grain boundaries (Lliboutry, 1964, p. 112-3; Nye and Frank, 1973). In the central zone, water also travels along thin sediment planes and/or foliation surfaces within the ice mass (Krimmel, personnel communication, 1978). The average upper limit of intergranular water veins observed for Blue Glacier ice is 25 μm and the mean water flux density 3 x 10^{-9} m/sec (Raymond and Harrison, 1975, p. 213-233). A semicircular glacier 1 km in cross-section would transport only 10^{-3} m^3/sec of water by this mechanism. The intergranular water flow through the glacier is much smaller than the meltwater input entering the glacier surface, 1 to 10 m^3/sec in summer. Thus only a minor amount of the total glacier runoff is transported in microscopic conduits. Most of the water discharge traversing the central zone is carried within large ice-walled conduits. The flow of water within englacial conduits may be described by of the theories of Röthlisberger (1972, p. 177-203), Nye (1976) and Shreve (1972).

Surface and englacial water runoff is normally carried downwards, towards the glacier bed, whenever a connection exists with the basal conduit system. Generally the aquifer(s) situated above the glacier bed are only partially connnected to the basal water drainage system (zone IV). Evidence for the poor connnection between different aquifer levels comes from glacier borehole drilling studies by Röthlisberger

(1972), Hodge (1974), and Iken (1982). In cases where a connection suddenly develops, a sudden drop of borehole water level is observed. Some boreholes do not exhibit any significant drop in water level, even though the hole was drilled to the glacier bed. It appears that in many locations of the bed, boreholes never connect directly to the main drainage conduits at the glacier bed, although nearby boreholes drilled to the same depth do connect. The aquifer zones above the bed of a normal glacier (I, II, III) behave as perched aquifers, which are in general only connected vertically by localized conduits, such as moulins, crevasses, and man-made boreholes.

Theoretical consideration and observations strongly suggest that water flow at the ice-bedrock interface of a glacier (zone IV) is particularly important for normal temperate glaciers. Water can flow in this basal zone through several possible paths, including the following:

1. Macroscopic conduits cut into the ice (R-channels) (Röthlisberger, 1972; Nye, 1976; Shreve, 1972)
2. Macroscopic conduits cut into the bed rock material (N-channels) (Nye, 1976)
3. Thin sheet of water of variable thickness (Hallet, 1979; Walder and Hallet, 1972; Weertman, 1972)
4. Linked cavities (Lliboutry, 1968; Walder and Hallet, 1972; Iken et al., 1972; term introduced by Kamb et al., 1985)
5. Permeable subsole drift (Boulton, 1979; discussed by Paterson, 1981, p. 142).

Once the glacier runoff reaches the bottom of the glacier, the water flows either in the bed region IV or descends into the sub-glacial material (in region V). In some cases basal water easily can drain away from the glacier system, through the rock material below the bottom of the ice, if the subglacial rock material is very permeable. Water thus can join the local ground-water flow beneath the glacier. The ground-water flow route beneath glaciers is very likely important if the glacier flows over volcanic or karst terrain. A major loss of basal water may result if the basal water intersects subsurface lava tubes or blocky lava flow deposits (for example, Shoestring Glacier on Mount St. Helens, Washington State), or limestone caves (for example, Columbia Icefield, British Columbia, Canada).

Since Variegated Glacier is underlain by relatively impermeable igneous and metamorphic rock, the ground-water flow is not considered an important drainage path. Most of the water runoff reaching the glacier bed of Variegated Glacier is expected to remain at the ice-rock interface.

6.4.2. Theory and Observation of Basal Tunnels

The water discharge at the glacier terminus normally emanates from a single large basal tunnel that extends for at least some distance upglacier from the terminus (Röthlisberger, 1972). Similar large basal tunnels are found transporting water to the glacier bed from along the lateral margins. Tunnels are also found at the glacier bed carrying water away from the base of deep moulins.

Observed tracer throughflow velocities in normal glaciers are commonly about 1 m/sec for tracer experiments conducted through the basal and central portions of the glacier (regions III and IV) (Röthlisberger). This magnitude of flow velocity can only

be explained by the existence of sizable transport conduits throughout most of the glacier length (Röthlisberger, 1972; Ambach et al., 1972; Behrens et al. 1975; Meier, 1965; Krimmel et al., 1973). Even though water input can reach the glacier bed from a variety of zones within the glacier, field observations suggest that water reaching the glacier bed stays there over most of the remaining distance traveled.

Where observed by the author, conduits that are entirely walled by clean glacier ice, are often approximately circular in cross section. At the glacier bed, the observed conduits are either approximately semicircular or parabolic in shape, and floored with bedrock, rock debris or stagnant ice (Shreve, 1972). Basal conduits are commonly cut upwards into the glacier ice, as R-channels. Less often, major conduits are cut downwards into the underlying bedrock material, as N-channels .

The existence of a basal tunnel system depends upon the local balance between rate of enlargement and rate of closure (Röthlisberger, 1972; Nye, 1976). The model of Röthlisberger is a steady-state model; it assumes that an equilibrium conduit size is achieved. The enlargement of a conduit may occur by melting and by erosion. Ice deformation is unimportant as a channel enlargement process, but channel or cavity capture during basal sliding may enlarge conduits. The major parameters employed in the treatment by Röthlisberger (1972, p. 179) are defined as follows: change of pressure melting point with pressure is k_t (a negative value) with units of $J^{-1}m^3$; the heat capacity of the fluid is k_w with units $Jkg^{-1}deg^{-1}$; the density of water at 0^o C is ρ_w with units kgm^{-3}; the energy of fusion is k_m with units Jkg^{-1}; density of the ice is ρ_i with units kgm^{-3}; channel element length is dx ; volume of ice melted is dV_m with units m^3; stream discharge is Q with units m^3s^{-1}; the energy related to pressure drop dp and elevation change dz is $dE = -Q(dp + \rho_w g dz)$, and the energy needed to

adjust the water temperature to the reduced pressure is dE_t. The volume dV_m of ice melted per unit time in a channel section of length dx is related to the energy available for melting dE_m per unit time and length dx by the relationship

$$dV_m = \frac{dE_m}{k_m \rho_i} \tag{6.41a}$$

and related to the frictional heat available for melting $dE - dE_t$ through

$$dV_m = \frac{1}{k_m \rho_i} (dE - dE_t) = \frac{1}{k_m \rho_i} [-Q (dp + \rho_w g dz) - k_t k_w \rho_w Q dp] \tag{6.41b}$$

and where $dz = 0$

$$dV_m = k_e \; Q \; (-dp) \; . \tag{6.41c}$$

The enlargement constant k_e is

$$k_e = \frac{(1 + k_t k_w \rho_w)}{k_m \rho_i} \tag{6.42}$$

(Röthlisberger, 1972, eqns. 1 to 5, p. 179). In the case of clean water flowing through a clean ice-walled conduit, the enlargement constant is

$$k_e \approx \frac{0.684}{4 \text{ x } 10^8} \sim 10^{-9} \text{ J}^{-1}\text{m}^3 \tag{6.43}$$

(Röthlisberger, 1972, Eqn. 4, p. 179).

The closure of a static conduit is normally thought to occur by ice deformation as described by Nye (1953). The flow law of glacier ice is described in terms of a power-law creep relationship, referred to as "Glen's Law"

$$\dot{\epsilon} = A \; \tau^n \tag{6.44}$$

where the effective strain rate is $\dot{\epsilon}$, the effective stress is τ, and the stress exponent is

n (Paterson, 1981, Eqn. 12, p. 85). The parameter A has units of $s^{-1}Pa^{-n}$ (Paterson, 1981, p. 39). The value of A depends on temperature, crystal size, shape and orientation, and concentration of air bubbles, sediment and other impurities. The flow law exponent n varies with material properties and is approximately three for normal glacier ice (Paterson, 1981, p. 37).

The closure rate, $\dot{r}$, is described by Nye (cited by Röthlisberger, 1972, p. 179) in terms of the ice overburden pressure P_i, the water pressure in the conduit P_w, conduit radius r, and flow law parameters n and A. The change in volume due to channel closure, dV_c, is given by

$$dV_c = 2\,\pi\,r\,(-\dot{r})\,dx \tag{6.45}$$

$$= 2r^2\,\pi\,A\,\left(\frac{P_i - P_w}{n}\right)^n\,dx$$

(Röthlisberger, 1972, Eqn. 7, p. 179).

At equilibrium the volume of ice melted dV_m is equal to dV_c, the volume of ice closing in the hole by creep:

$$dV_m = dV_c \tag{6.46}$$

resulting in the equilibrium relation

$$k_e\;Q\;(-dp) = 2r^2\,\pi\,A\,\left(\frac{P_i - P_w}{n}\right)^n\,dx\quad. \tag{6.47}$$

The radius of a cylindrical conduit can be estimated for the case of turbulent flow using Manning's equation

$$r \equiv 2R_H = 2\left\{U\;n^*(\rho_w\,g)^{1/2}\,\left(-\frac{dp}{dx}\right)^{-1/2}\right\}^{3/2} \tag{6.48}$$

where the hydraulic radius is R_H, mean flow velocity of the fluid is U, and the Manning roughness coefficient is n^*. The resulting pressure gradient along the length of a cylindrical conduit, where $U = Q/\pi r^2$, p is the water pressure, and bed slope is β, is given by

$$\left(\frac{dp}{dx} + \rho_w g \tan\beta\right)^{11/8} - 0.316\left(\frac{dp}{dx} + \rho_w g \tan\beta\right)^{3/8} = \tag{6.49}$$

$$= k_{mc} (n^*)^{\frac{3}{4}} Q^{\frac{-1}{4}} (\cos\beta)^{-11/8}(P_i - P_w)^n \quad .$$

(Röthlisberger, 1972, Eqn. 20). The melting-closure coefficient k_{mc} is defined as

$$k_{mc} \equiv 2^{\frac{3}{4}} \pi^{\frac{1}{4}} (k_e)^{-1} (\rho_w g)^{\frac{3}{8}} (nA)^{-n} \tag{6.50}$$

(Röthlisberger, 1972, Eqn. 20, p. 180).

For both laminar and turbulent flow theories the pressure gradient along the length of the conduit, dp/dx is inversely related to the discharge Q (Röthlisberger, 1972). The pressure gradient is more sensitive to changes in stream discharge if the flow is laminar rather than turbulent. The pressure gradient is also sensititve to the difference between the pressure exerted by the ice at the conduit walls P_i and the fluid water pressure in the conduit P_w.

Large tunnels carrying a large flow of water are predicted by this theory to have lower water pressure than smaller nearby conduits carrying a smaller water discharge (Röthlisberger, 1972; Shreve, 1972). The theory indicates that the water drainage system of a normal glacier is dominated by the flow of water in large basal water tunnels. The contribution to the total water discharge from internal water sources, such as melt produced during ice deformation or basal sliding processes, is normally

insignificant as compared to the total volume of water discharged at the terminus through the large tunnels (Paterson, 1981).

Consequently, in a normal stable drainage system, most of the available glacier water should move into the largest conduits available. A branching drainage system should develop, similar to dendritic drainage pattern of a normal river system. The smallest conduits feed into larger branch conduits, before reaching a main trunk conduit as the glacier terminus is approached (Röthlisberger, 1972; Shreve, 1972).

It is also possible that instead of being comprised of clean ice and water, the base of a glacier is heavily charged with sediment. Röthlisberger (1972) briefly discussed this topic. For conduit walls composed of sediment-rich ice, and highly turbid stream water, the energy of fusion k_m per bulk mass of ice plus rock is lower; the heat capacity k_w, density of dirty ice ρ_i, and density of turbid water ρ_w, are slightly increased. Thus, the predicted value of enlargement coefficient k_e for a sediment-rich basal drainage system is expected to be different than for a similar clean system. The melting closure coefficient k_{mc} is probably higher for a sediment-rich Röthlisberger-Nye system than a sediment-poor ssytem, since it is inversely related to k_e and directly proportional to density of fluid ρ_w. This suggests that the pressure gradient necessary to maintain the same discharge for a sediment-rich system is higher than for an otherwise identical clean system.

A more complicated energy balance than that described by the Röthlisberger-Nye model of clean ice-walled conduits must be considered at the melting ice surface of a sediment-rich conduit wall. The sedimentation and erosion effects will also be different for a sediment-rich drainage system. The melting-refreezing process at the tunnel wall of a sediment-rich system would tend to concentrate melted-out sediment

within the fluid, while refreezing concentrates clean ice at the conduit walls. The flow law parameters A and n of the ice-sediment wall material are undoubtedly different. The sediment-rich ice may deform more easily if the rock material consists of expandable clay with a low internal friction. The ice may deform less easily if the included rock material consists of solid sand and pebbles. The larger solid rock particles would be expected to abrade against each other and thereby inhibit the creeping flow of the ice-sediment material. A dendritic drainage system composed of large macroscopic conduits is still expected to develop in a sediment-rich basal system, but the stability of this type of system to fluctuations in pressure, discharge and deformation is less predictable than the stability of a similar drainage system within clean ice.

Channel closure, in the natural system, may be significantly affected by deposition of suspended rock and ice particles at the walls. Additional channel enlargement may occur by erosion at the wall and by capture of other conduits and cavities. Basal conduits and cavities may be advected against rock obstacles and pinched closed by ice deformation. Possibly at the base of an actively sliding normal glacier, conduits may be sheared closed or advected away from the glacier bed along shallow englacial thrust surfaces. The water discharge previously flowing through a newly closed conduit would be forced into nearby basal cavities and conduits. Local water pressure would temporarily rise until a more favorable outlet for the water was obtained. Water conduits in glacier ice that is highly charged with fine sediment are expected to be considerably different than conduits in a clean glacier at the interface with solid bedrock. Basal tunnels in a sediment-rich system, lined with a large amount of clay-sized sediment, could either suddenly collapse or rapidly enlarge in the presence of relatively minor fluctuations in basal shear stress and water pressure,

while a similar tunnel system in a clean glacier would have a much slower response to the same changes, as indicated by Röthlisberger (1972), and Behrens et al. (1975).

Temporary storage of large volumes of water at the glacier bed may be locally important on some normal glaciers (Iken et al., 1972; Krimmel et al., 1973). The storage of water appears to be particularly significant for those glaciers where the annual variation in glacier flow velocity is observed to reach a maximum in spring or early summer, such as at Unteraargletcher (Iken et al., 1982), Findelen Glacier (Moeri, 1983; Iken and Binschadler, 1986), South Cascade Glacier (Meier and Tangborn, 1965; Tangborn et al., 1975; Hodge, 1976, 1979) and Nisqually Glacier (Meier, 1966; Hodge, 1972, 1974). The increased flow velocity at a time of sharply decreasing ice thickness is considered to represent increased basal sliding due to increased lubrication, and/or cavitation at the glacier bed (Weertman, 1969, 1979; Kamb, 1970; Lliboutry, 1968; Paterson, 1981; Röthlisberger, 1972).

In summary, both theory and observation of normal glaciers indicate that the stable drainage system consists of a single main conduit extending for a long distance upglacier from the terminus. The main conduit is fed by a branching network of smaller conduits. The motion of water and material suspended in each conduit is describable in terms of theory for the flow of a fluid in a single conduit. The storage of water in basal cavites appears to occur to a measurable degree in certain glaciers. Where storage of water at the glacier bed is suggested, the effects vary with the melt season and location on the glacier. In situations where basal sliding, basal thrust development, cavitation and/or basal sediment content are known to be significant, the Röthlisberger-Nye conduit model does not necessarily apply. The Röthlisberger-Nye model predicts that large basal water conduits exist at the glacier bed if it is

primarily composed of relatively solid rock, overlain by nearly sediment-free ice. During the melt season, at most locations on a normal glacier, water discharge moves through a dendritic network of macroscopic channels.

6.4.3. Previous Dye Tracer Experiments

The movement of water through a glacier to the ice terminus has been traced from the surface snowpack (Colbeck and Davidson, 1972; Krimmel et al., 1973; Fujino, 1971; Lang et al., 1972), from ice crevasses (Krimmel et al., 1973; Burkimsher, 1982), and from streams entering from a lateral margin of the glacier (Burkimsher, 1982), or through natural vertical water conduits (glacier moulins) (Ambach et al., 1972; Ambach and Jochum, 1973; Krimmel et al., 1973; Behrens et al., 1975; Irle, 1978; Lang et al., 1979; Moeri, 1983; Burkimsher, 1982). Tracing experiments have also been sucessfully conducted by injecting dye at the base of boreholes drilled to the glacier bed (Irle, unpubl., 1978; Moeri, 1983). Average dye transit velocities through six non-surging temperate glaciers are summarized on Table 6.3, for a large range in travel distances (0.2 to 19 km).

The average dye transit velocities listed in Table 6.3 and discussed throughout this thesis are calculated simply as distance traveled (measured along the glacier centerline or hydraulic gradeline to the terminus) divided by the measured transit time. These velocities will be less than the actual water flow velocity in the conduits, depending upon the sinuosity of the path actually traveled by the tracer.

The average dye transit speed through wet snow is 10^{-6} m/s (Table 6.3). Through the main mass of glacier ice and the basal conduit system, between a moulin or lateral stream and the glacier terminus, it is 0.6 m/s (average of 70 experiments), and from the base of a borehole to the glacier terminus it is 0.27 m/s (average of 10 experiments). Assuming the glacier water drains through a rough conduit ($n^* = 0.1 \mathrm{m}^{-1/3}\mathrm{s}$) with a mean flow velocity equal to the average dye transit velocity of $\overline{U} = 0.6$ m/s, along an average hydraulic gradient of 0.1 m/m, then R_H is 8 cm as

calculated from Equation (6.3). The corresponding mean radius R of a circular conduit ($R = 2R_H$) is 16 cm. If the channel sinuosity (defined as the channel length divided by the valley length) is on the order of 1 to 3, then the mean flow velocity between moulins and the glacier terminus is between 0.7 and 2.1 m/s, and the corresponding channel size is on the order of 10 cm to 1 m. A channel hydraulic radius R_H of 1 m is necessary in order to allow the passage of water at a mean transport speed of 2 m/s and discharge on the order of 1 to 10 m^3/s.

The observed discharge of the terminus outflow streams, indicated on Table 6.3, ranges from 2 to 43 m^3/s. The greatest stream discharge values of 29 to 43 m^3/s were measured at the terminus outflow of the Great Aletsch Glacier during the dye-tracing studies of Lang et al. (1979). The smallest stream discharges were measured for a short 300 m open channel stream segment near the terminus of Hintereisferner Glacier, Austria, as indicated by Ambach and Jochum (1973).

Mean dye transit velocities U and tracer dispersion in terms of parameters D, α, and β are shown in Table (6.4) for forty dye-tracing experiments conducted from moulins on four different non-surging glaciers. Results for experiments where the dye transit velocities were less than 0.006 m/s were excluded from this analysis. Only the main Gaussian-shaped portion of the dye-return curves was analyzed to obtain D and U values. The mean dye transit velocity and the observed stream discharge are used to calculate the hydraulic radius R_H of the conduit of assumed circular cross-section by the relationship $R_H = \sqrt{Q/4\pi U}$; this calculated value of R_H (averaged over the individual values from individual experiments conducted) is listed in column 5 of Table 6.4. Instead of the mean radius R, the hydraulic radius R_H is calculated here for comparison to R_H values obtained from the following dispersion

analysis of dye-tracing data. To calculate R_H from Q and U, it is assumed that the entire perimeter of the conduit is wetted and that the channel is approximately circular in cross-section. The calculated R_H for a conduit that is semi-circular is cross-section is approximately half the R_H value obtained for a conduit that is circular in cross-section.

The average dispersivity parameterization for dye-tracing experiments conducted through glacier moulins is shown on Table 6.4a. Again, only studies conducted on temperate glaciers were considered. In this section the discussion is limited to the non-surging glaciers Findelen, South Cascade, Aletsch and Hintereisferner. The Variegated Glacier results are discussed in the following sections. The parameterization provided on Table (6.4a) includes the glacier name, number of experiments averaged, date experiments were carried out, the slope distance from injection point to outflow measurement location X, and the average values of dispersivity α, flow velocity U, β, and calculated f^* for each glacier data set.

The dispersivities are calculated from the dispersion coefficient D and mean flow velocity U by Equation (6.1); α values were also computed directly from the dye-return curves. The average value of the dispersion coefficient for moulin dye-tracing experiments is $\overline{D} = 5$ m^2/s. The D obtained for glacier dye tracing from glacier moulins varies over the range from 0.6 to 9 m^2/s. The average dispersivity α is 10 m, and the range is from 1 to 20 m (Table 6.4). Dye transit velocities (Table 6.4) averaged between 0.1 and 1.7 m/s, and the stream discharges vary over the much larger range of 3 to 43 m^3/s.

Results from published dye tracer experiments conducted using glacier boreholes at Findelen, South Cascade and Variegated Glaciers are shown on Table 6.4b. At

Findelen Glacier a total of four experiments showed that the dye was carried at an average speed of 0.3 m/s between the base of the boreholes and the glacier terminus. The mean velocity of tracers injected into boreholes at the glacier bed (Table 6.4b) is about 1/2 to 1/3 the mean velocity of tracers injected into moulins (Table 6.4a). The mean tracer velocity in South Cascade Glacier (Table 6.4b) is much slower than in Findelen Glacier and indicates the that the borehole was very poorly connnected to the conduit system fed by moulins. The basal water system of a glacier such as Findelen Glacier, which appears to slide at its bed and form water filled cavities (Iken and Binschadler, 1986), is expected to have a more uniform basal water transmissivity than an otherwise similar non-sliding glacier, such as South Cascade Glacier (Hodge, 1976).

In order to test if dispersion observations from glacier tracing experiments conform to the relationship $D = \alpha U$ (Equation 6.1), the data for each experiment summarized in Tables 6.4a and 6.4b are plotted as D versus U in Figure 6.4 . Experiments suggesting a linear relationship between D and U (Equation 6.1) were conducted using the same injection site, with a short period of elapsed time between subsequent experiments. Examples of this linear relationship are observed for the open channel site at Hintereisferer Glacier (Ambach and Jochum, 1973), and moulin sites at Hintereisferner (Behrens et al., 1973) and at Findelen Glacier (Moeri, 1983). The least steep line has a slope of $\alpha = 3$m and is obtained for experiments conducted from an open channel site called "Gerinne" located 380 m from the terminus outflow at Hintereisferner Glacier (Ambach and Jochum, 1973). Tracer experiments conducted in Findelen Glacier by borehole injection gave the highest α values, 20 to 45 m, (Tables 6.4a and 6.4b). There is a large variation in D and U values for

experiments where $\alpha \geq 5$ m. Tracing experiments conducted through a single conduit on a non-surging glaciers indicate that D and U values tend to fall on a line of nearly a constant slope if $\alpha \leq 5$ m. Results shown in Figure 6.4 indicate that the relationship $D = \alpha U$ holds to a fair approximation for each conduit separately, and the value of α varies between conduits.

A non-constant α value is consistent with the single-conduit dispersion theories of Taylor (1954) and Fischer (1968) if the hydraulic radius, conduit shape and roughness varies between different conduits, or for the same conduit at different testing periods. A variation in subglacial conduit sizes is certainly expected, because the outflow streams vary in the water discharge. To test the data further, the value of α for each dye-tracing experiment is plotted in Figure 6.5 versus the R_H value calculated from the mean discharge Q. This value of R_H, based on the discharge of the outflow stream, is probably an overestimate of the actual value of R_H averaged over the total length a of water conduit, but it is the only information on R_H available for the tracing experiments. Data from experiments using the same injection location on the same day are shown in solid symbols on Fig. 6.4, while open symbols represent data from experiments conducted at different times and locations. A roughly linear relationship between α and R_H (as expected from Equation (6.2) with $L = R_H$) is suggested by results from experiments conducted at middle moulin on Hintereisferner Glacier (Behrens et al., 1975), and from the base of boreholes #22 and #24 on Findelen Glacier (Moeri, 1983). There is a slight suggestion of a linear trend for the results obtained over the time period of one month at the open channel studied by Ambach and Jochum (1973). The coefficient β varies considerably within the range from 1 to 40. The scatter on the plot of α versus R_H is in part due to the combined

measurement error from the contributing variables D, U, Q, and R_H, and in part due to a real variability in α due, for example, to variations in the conduit size, roughness, and travel path.

If the theoretical relationship (Equation 6.12)

$$\beta = \Gamma \sqrt{(1/8) f^*}$$

(from Equation 6.15) applies to glacier conduits and if the value of Γ is known from the theory, then the roughness coefficient f^* may be calculated for each conduit for which β values can be taken from Figure 6.5 or from Table 6.4a and 6.4b. The value of f^* indicated in Tables 6.4a and 6.4b, column 9, are calculated from Equation (6.5) using a theoretically and empirically based value of Γ =20 for dispersion in pipes, discussed in Section 6.2.2. Corresponding values of the Manning roughness n^* are obtained from the f^* values by the relationship (6.7) and are listed in column 9 of Table 6.4, and column 7 of of Table 6.5. The n^* values obtained in this way from tracer experiments conducted through moulins have an average value of 0.12 $m^{-1/3}s$, and range from $n^* = 0.017$ to 0.24 $m^{-1/3}s$ (column 7 Table 6.5). Results for experiments conducted from the base of boreholes (Tables 6.4b and 6.5) are greater than 1 $m^{-1/3}c$ for $\Gamma \approx 20$ [man-made pipes discussed by Taylor (1954)] and less than 1 for $\Gamma \approx 100$ [natural surface rivers discussed by Fischer (1968)].

A constant friction coefficient f^* has been suggested for water conduits in glaciers by Spring and Hutter (1982) and implies that the dispersion coefficient for different conduits is linearly related to the conduit radius in accordance with Equation (6.15). If the friction coefficient for all glacier water tunnels can be taken as a constant $f^* = 0.25$ in the manner of Spring and Hutter (1982), then the β coefficient is $\beta = .0.18\,\Gamma$. Thus, with $\Gamma = 20$, for dispersion in pipes, we should have $\beta = 3.5$.

Since the mean value of β for glacier conduits is about 10, the Γ value implied is 50. The observed range of β for glacier water conduits is about 2 to 40, and this corresponds to a Γ range of 10 to 250. This falls mostly within the range 20 - 200 of β values obtained for natural rivers (Table 6.2).

The representative Manning roughness for glacier conduits is given by Clarke, Mathews and Pack (1984) to be 0.05 to 0.12 $m^{-1/3}s$. This compares favorably with the n^* values inferred by Equations (6.7) and (6.15) from tracer dispersion, just discussed. The high values of n^* inferred from some of the experiments are equivalent to the conclusion that englacial conduits are sometimes quite rough, vary in size and cross-sectional shape, have numerous obstructions, and are sinuous (Gardiner and Dackombe, 1983, pp. 140-42).

The Manning equation (Equation 6.3) is used to calculate the n^* value corresponding to the Q, U and dh/dx measured during tracing experiments at Hintereisferner, South Cascade, Findelen, and Aletsch Glaciers. The dh/dx, Q, U, and n^* for different injection sites and the corresponding number of observations at each site are summarized on Table 6.5. The average dh/dx is about 0.1, and the average n^* is 0.26 $m^{-1/3}s$. The value of R_H for each experiment is shown on Table 6.4a. For comparison the average value of n^* implied by f^* from dispersion analysis described above is 0.14 $m^{-1/3}s$. The dispersion theory n^* is given in column 7 of Table 6.5, and is calculated from α, R_H and a theoretical Γ of 20 for water flow in a pipe. For most of the dye-tracing experiments the value of n^* calculated using the Manning equation agrees within a factor of 2 with the n^* value implied by measured dispersivities.

In the relationship $\alpha = \beta L$ (Equation 6.2), the symbol L represents the scale length. As discussed earlier (Section 6.2.1) and shown schematically on Figure 6.2,

this scale length is taken to be the hydraulic radius of a single conduit (Fig. 6.2a), the grain size of a granular porous medium (Fig. 6.2b), the distance between conduit intersections of a multi-channel network without cavities (Fig. 6.2c), or the order of the distance between cavities in a linked cavity network (Fig. 6.2c). Observed pairs of values α and L for a variety of different drainage systems are plotted in Figure 6.6. A summary of dispersivity results is given in Table 6.6 and includes information on U, L, α, β, f^*, Γ. Lines on Figure 6.5 with a slope of 1 are drawn to represent the theoretical relationship $\alpha = \beta L$ (Equation 6.2). The lowest line in Figure 6.5 corresponds to $\beta = 1$. The dispersion results for smooth (cylindrical) pipes with n^* of about 0.006 $m^{-1/3}s$ and granular porous media composed of smooth glass beads plot approximately on this line for $\beta = 1$ as theoretically expected. Higher values, $\beta = 3$, correspond to semi-rough and/or curved pipes and are within the range of β values for normal glacier water conduits and wet snow as shown on Figure 6.6. The average β values are on the order of 10 for natural streams (on the surface and underground). The β for natural streams is normally higher than man-made pipes and approximately the same as streams connected to glacier moulins. Glacier conduits tested in experiments from moulins have average $\beta = 1$ to 20, and in borehole experiments $\beta =$ 27 to 45. The published data cited in this thesis provided no examples of β coefficients greater than 50 for a single conduit system.

If a system of multiple-interconnecting conduits and cavities of scale length $L \sim 1$ m carried the major water flow within the non-surging glaciers discussed in this thesis, then much higher values of $\beta > 100$ might have been attained.

The theoretically and empirically based β value for longitudinal dispersion in an isotropic matrix of glass beads is about 1/2 and cannot be distinguished from β values

for single conduit systems except by the facts that the L scale is on the order of the sediment grain size ($L = 10^{-3}$m) and, that the transit speed is slow ($U = 10^{-4}$ m/s).

Dispersivity values are about $\alpha = 10^{-3}$ to 10^{-2} m (Table 6.6) for granular media such as glass beads or snow of average grain size $L = 1$ mm. Natural porous media are found to have α values of order 10 to 1000 m (Table 6.6 and Figure 6.6). If the mean scale length of natural porous media is on the order of the grain size of about 1 to 10 mm, then the value of β is on the order of 10^4. For an aquifer rock or glacier ice with internal zones or paths of different hydraulic conductivity on a scale of many meters, the appropriate L is not the grain size but rather the longitudinal dimensions of these "seepage conduits." The large α observed for natural porous media (as summarized by Anderson, 1979) implies long interconnection lengths or equivalently large L.

All tracer experiments on glaciers (Table 6.2) where the tracer was initially spread out on the snow surface were excluded from Tables 6.4a and 6.4b. Mean flow velocities and dispersion coefficients for such experiments are controlled by the behavior of water flow through snow (Krimmel et al., 1973; Lang et al., 1979). Dispersion of a tracer through snow is basically the same as that in porous granular media. The dispersivity and mean flow velocity of water moving through the snow is calculated, as described in Section 6.2.4, from the dye-return curve measured at the terminus outflow, the known distance to the outflow X, and the depth of the snow and firn pack X'. Dispersivities and mean flow velocities calculated for the experimental results of Krimmel et al. (1973) and Lang et al. (1979) compare well with predicted values of α and U based on the theory of flow through granular porous media by Scheidegger (1954) or Saffman (1959).

A significant portion of the tracer-return curve for many normal glaciers (Moeri, 1983; Burkimsher, 1982) is the distinctive quasi-exponential tail of the curve $C(t)$. The quasi-exponential curve is attributed to the effect of "storage," the possible nature or mechanism of which is discussed in Section 6.3. "Storage" chambers along the water conduits of open glacier conduits have been suggested by Ambach and Jochum (1973), to explain the quasi-exponential tails of their observed tracer-return curves.

The tracer dispersion behavior observed for normal, non-surging glaciers can be explained in terms of water flow in single conduits, for reasonable values of f^* (or n^* and R) and Γ. The values of the friction coefficients f^* or n^* implied for the glacial conduits suggest that the wall surfaces are very rough, and contain numerous flow obstructions. The conduits are probably sinuous, and $\Gamma \approx 20$ (assuming a conduit of roughly circular or semi-circular cross section). Dispersion experiments conducted through glacier moulins and boreholes on non-surging glaciers do not indicate β values higher than are found for water flow in pipes or natural rivers. As indicated by the dispersion results, the main subsurface water drainage system of a normal, non-surging glacier appears to be composed of a network of large single conduits.

6.4.4. Interpretation of 1983 Variegated Glacier Tracing Experiment No. 3: The Non-Surging State

In the non-surging state, the behavior of a surge-type glacier resembles a normal non-surging glacier in almost every directly observable respect. The relative daily and seasonal variations in borehole water pressure, stream discharge, internal deformation and basal sliding behavior of a non-surging glacier are best exemplified by published studies on Nisqually, South Cascade, and Blue glaciers in Washington State (Hodge, 1972; Hodge, 1976,78; Meier et al., 1974; Kamb et al., 1979), and on Unteraargletscher (Iken et al., 1983) and Findelengletscher (Iken and Bindschadler, 1986). All of these observations are similar to the equivalent properties of Variegated Glacier before, and after its 1983 surge (Raymond and Harrison, 1979; Bindschadler et al., 1977; Bindschadler, 1982; Kamb et al., 1985; Kamb and Engelhardt, 1986). Also, the dispersivity and mean flow velocity of the Variegated Glacier during the non-surging state are similar to that observed on normal glaciers that do not surge.

The tracer return for the non-surging state of Variegated Glacier is dominated by storage-retardation and dispersion effects are slight and are only estimated as an upper limit. This is reasonable because of the strong similarities in the shape of dye-return curves of the Variegated in the non-surging state and curves from normal, non-surging glaciers [notably Findelen Glacier (Moeri, 1983); South Cascade Glacier (Irle, 1978); Aletsch Glacier (Lang et al., 1979)]. The first and primary concentration peak normally observed in glacier-tracing experiments is best represented by the diffusive-dispersion theory (Section 6.2), and the relatively minor trailing portion of the return curve is modeled by the storage-retardation theory (Section 6.3). The dye-return curve for the non-surging state of Variegated Glacier as sampled (Chapter

4) is best described by the storage-retardation theory as discussed in Chapter 5.

Comparison of the dye-return curve $C(t)$, and integrated dye-return curve for the post-surge Variegated Glacier to published experimental results from tracer experiments on non-surging glaciers strongly suggests the initial peak, due to normal diffusive-dispersion mechanisms, may have been missed between sampling intervals. The upper limit of diffusive-dispersion effects and the mean transport velocity of tracer for the Variegated Glacier in the non-surging state are estimated for this peak as shown on Fig 5.8.

The dye for the post-surge experiment was observed to exit the glacier at a single terminus stream (LTS). This stream had the highest sediment load and water discharge of any of the terminus outflow streams operating at the time of the experiment.

6.4.4.1. Retardation of Tracer Due to Adsorption Effects

As shown in Sections 3.5 and 6.3, the retardation of the dye relative to the water, due to instantaneous dye adsorption on rock-particle surfaces in the conduit walls, must be known to calculate the actual mean flow velocity of the water U from the mean velocity of dye transit U_{dye}. The maximum retardation coefficient R_a calculated for experiment 3 by the method (Section 6.3) is on the order of one. Therefore, the mean dye transit velocity measured in experiment 3 is essentially equal to the mean water transport velocity between the base of the injection borehole and the glacier terminus.

The mean velocity of water within the conduit after the surge ended was therefore about 0.7 m/sec if the basal conduit was straight for its entire length and if the

bottom of the borehole was directly connected to the conduit.

The impedance to water flow between the base of the borehole and the main conduit is unknown. It appears to have been minimal, as judged from the rapid arrival of the tracer at the terminus and from the relatively low value of dispersivity ($\alpha \leq 1$m) inferred from the tracing results.

6.4.4.2. Conduit Size

For Variegated Glacier in the post-surge experiment the minimum water velocity U is 0.7 m/s, and the conduit radius on the order of 1 m as will be shown presently. The Reynolds number calculated from these values is 10^6, much greater than value of 2,200 for transition from turbulent to laminar flow. Consequently, the water flow in such conduits should be modeled with turbulent flow theory.

The value of 0.1 m/m for the hydraulic gradient is obtained from the measured bed slope of Variegated Glacier – 1000 m vertical elevation change per 10,000 m horizontal distance. Over a distance of 10 km average bed slope, surface slope and hydraulic gradient at Variegated Glacier are approximately equal.

The conduit radius for turbulent flow at the hydraulic gradient 0.1 m/m is estimated using the Manning formula (Eqn. 6.3) with roughness $n^* = 0.05\text{m}^{-1/3}/\text{s}$. For a conduit of circular cross section this n^* gives a mean radius of 0.075 m, which corresponds to $R_H = 0.037$m. For a Manning roughness n^* of 0.1 $\text{m}^{-1/3}\text{s}$, the predicted hydraulic radius R_H is 0.1, and for $n^* = 0.01$ the hydraulic radius is 0.003 m.

The actual fluid velocity in the conduit is expected to be higher than the mean longitudinial velocity due to channel sinuosity. The length of a sinuous channel is

greater than the valley length, by the factor $\Omega > 1$, where Ω is called the sinuosity. For a valley of mean gradient dh/dx of 0.1 and stream discharge Q of 30 to 40 m^3/s, the corresponding average sinuosity, Ω, is 3 based on empirical results from a variety of open channels (Richards, 1982, Fig. 7.1d, p. 181). For a conduit length three times the valley length, or a sinuosity of three, the actual mean flow velocity is 2 m/sec . A speed as high as 2 m/sec has been measured in water tracing experiments in other glaciers (Table 6.2), and could have occurred in Variegated Glacier in the non-surging state. In a sinuous conduit, the average hydraulic gradient is reduced by the factor Ω^{-1}, and the average flow velocity is increased by the factor Ω. The calculated hydraulic radius is thus increased by a factor $\Omega^{9/4}$. Consequently, if the likelihood of conduit sinuosity $\Omega = 3$ is taken into account, the hydraulic radius of the conduit is calculated to be about 0.04 to 1.2 m in size, depending upon the conduit roughness ($n^* = 0.01, 0.1 m^{-1/3}$, respectively).

An independent estimate of conduit size may be obtained from the stream discharge and mean flow velocity information. The conduit radius R for a conduit of circular cross section is

$$R = tild \sqrt{\frac{Q}{4\,\pi\,U}}$$

$$= tild \sqrt{\frac{40\ m^3/s}{4\pi\ 0.7\ m/s}}$$

where Q is the discharge carried by the conduit with water flow at mean speed U. The corresponding hydraulic radius is $R_H = R/2$. The calculated radius is about 4.3 m for a mean flow velocity of 0.7 m/s and the estimated discharge Q of 40 m^3/s (Fig. 4.11b). If the actual stream flow is about 2 m/s, then the conduit radius is about 2.5

m. Therefore, a conduit radius in the range of about 2.5 m and conduit sinuosity of 3 results in agreement between the velocity given by Manning's formula for flow in a circular tunnel with rough walls (n^*=0.1m$^{-1/3}$s) and the velocity compatible with the observed terminus stream discharge during the post-surge dye-tracing experiment, this velocity being 2 m/s.

6.4.4.3. Diffusive-Dispersion Effects

The values of D and α can be explained by the same theories used to describe dispersion in natural surface and underground rivers (Fig. 6.1). If the conduit was within the ice mass it would have low wall friction and a low value of dispersivity similar to man-made pipes (Fig. 6.1). The somewhat higher dispersivity values obtained for non-surging glaciers in general, including the post-surge Variegated Glacier, indicate that main drainage conduits probably lie at the base of the glacier. From Equation (6.12) the friction coefficient implied by assuming $\beta = 5$ is

$$f^* = 8\left\{\frac{\beta}{\Gamma}\right\}^2 = \frac{200}{\Gamma^2} \quad .$$

According to (Taylor, 1954), the value of Γ for flow in a circular conduit with logarithmic transverse profile of flow velocity, as observed in turbulent flow, is 20. The corresponding value of f^* is about 0.5. The average Γ for natural streams is 100 (Fischer, 1968), and the corresponding calculated f^* is 0.02. Therefore, the minimal value for the friction coefficient of a water conduit within Variegated Glacier in the non-surging state is $f^* = 0.01$, and an upper limit for the Manning roughness (conduit radius on the order of 1 m) is $n^* = 0.01$ to 0.1 m$^{-1/3}$/s. These n^* values do not differ greatly from the range given by Clarke et al. (1984) ($n^* = 0.05$ to 0.12

$m^{-1/3}s$), and the range of f^* values includes the value of $f^* = 0.25$ recommended by Hutter and Spring (1984).

6.4.4.4. Storage-Retardation Effects

For glaciers in the non-surging state, the initial Gaussian peak of the dye-return curve is produced by diffusive-type dispersion mechanisms, and is followed by a quasi-exponential tail produced by storage-retardation-type mechanisms. The tail for the tracer return in the post-surge experiment in Variegated Glacier is quite pronounced. The rate coefficients a ($10^{-5}s^{-1}$) and b (10^{-4} s^{-1}) in Eqn. (5.17), calculated in Section 5.5, are similar to values obtained from similar tracer experiments conducted in normal, non-surging glaciers such as Findelen Glacier (Moeri, 1983) and South Cascade Glacier (Irle, unpubl., 1978). The slightly less accentuated tails observed in the dye return from these glaciers, as compared to the the tail in the return from the post-surge experiment in Variegated Glacier or from an experiment conducted from Koncordiaplatz on Aletsch Glacier by Lang et al. (1979), may be due to the shorter travel distances involved for Findelen and South Cascade glaciers.

On first glance it might seem that the simplest explanation for the quasi-exponential tail is a borehole storage mechanism, caused by slow release of dye at the base of the injection borehole. The dye transport may have been slightly impeded during its movement from the base of the glacier to a nearby major water channel; nevertheless, observations indicate that the dye travel time to the glacier terminus was very short, and the dispersion of the initial tracer peak was very small. The borehole storage mechanism is considered further in Section 6.3. That consideration leads to the conclusion that borehole storage is not likely to be the main cause of the

observed quasi-exponential tail, and that storage mechanisms along the flow path of the tracer at the base of the glacier are instead responsible.

As shown in Section 5.5, a quasi-exponential tail following an initial sharp dye-return pulse is predicted by the simple model of storage and release in which the rate of dye transfer from the flow system (conduit) to storage is proportional to dye concentration in the conduit and in which the rate of dye release from storage back into the conduit is proportional to dye concentration in the storage "reservoirs." According to the dye-return curve that results from this model, Eqn. (5.27), the height and length of the tail should increase as the travel distance through the conduit system increases. This may explain the fact that the exponential tail is more pronounced for the dye-return curve of Variegated Glacier experiment 3, with a travel distance of about 10 km, than for experiments conducted through moulins and boreholes located at distances closer to the termini of other non-surging glaciers.

Section 6.3 describes how the storage and release phenomenon can be explained mechanistically in terms of dye transfer between "mobile" and "immobile" zones in the water flow system. The immobile zones may consist of slow-moving or stagnant water associated with back-eddies, meander bends, or water-filled chambers partially connected to the main conduit. The existence of chambers that can temporarily isolate water from the main conduit is indicated by the fact that a secondary dye peak was observed on the day following the dye injection (Section 4.4). Directly observed dye transfer from immobile zones of water located at the inside of meander bends to the main flow of a natural surface stream, Green River (Washington) (Fischer, 1968), produces only a small accentuation of the dye-return tail, barely noticeable in the presence of the tail produced by the diffusive-dispersion mechanisms in the mobile

zone, for a travel distance similar to the third tracing experiment in Variegated Glacier. Since the exponential tail in the dye return curve appears to be of major importance for Variegated Glacier in its non-surging state, the results suggest that the main water conduit must be associated with a very large number of nearby water-filled cavities, be highly tortuous, or have numerous obstacles in the flow path, as compared to a natural surface stream.

If the conduit lies at the base of the glacier, as suggested by the dispersivity values, then adsorption of dye on sediment or rock surfaces at the bed might contribute to the storage-and-release phenomenon. This would be the case if the adsorptive equilibrium were not instantaneous (involving finite rate constants), or if the sites of adsorption were not in immediate contact with the water of the conduit, so that they could be reached only by some type of diffusion path, as in the "matrix diffusion" model noted in Section 6.3. (Instantaneous adsorption leads instead to the retardation phenomonon discussed in Section 6.3.)

The dye-return curve for Variegated Glacier in the non-surging state can be accounted for in a general way by the pulse and quasi-exponential tail predicted by the storage-and-release theory, combined with a small amount of diffusive spreading of the initial pulse. What is still needed, however, is to relate the a and b parameters of the theory to the detailed physical mechanisms of a model. For either the sediment-adsorption model or the stagnant-water model, the values of a, b, D and U that fit the dye-return curve cannot be related in detail to features of a model; the general exponential shape of the curve can be explained. In all likelihood, the exponential tail is produced by a variety of dispersion mechanisms that transfer dye between various types of immobile and mobile zones.

6.5. Water Transport Systems of a Surging Glacier

6.5.1. Theory of Basal Water Flow

The basal drainage system of an actively surging glacier has been hypothesized to consist of one of the following possiblities: 1. a thin sheet of water as described by Weertman (1969); 2. a series of linked conduits and cavities as described by Kamb et al. (1985); 3. an extensive layer of easily deformed subglacial sediment (Boulton, 1979, pp. 29-43). There are no other known possibilities that can account for the extremely rapid basal sliding velocities observed (10 to 100 m/day). The objective of the following interpretation of the results of the first tracer experiment on Variegated Glacier, under surge , is to distinguish among the above three possibilities.

6.5.2. Interpretation of 1983 Variegated Glacier Experiment No. 1: The Surging State

6.5.2.1. Linked-Cavity Model of the Basal Water System

The tracer-return data from experiment 1, together with other observations of Variegated Glacier in surge in 1982-3, have been interpreted in a preliminary way and on this basis a provisional model formulated of the basal water system in surge, as follows (Kamb and others, 1985, pp. 477-478): "Water transport through Variegated Glacier in surge cannot be in a normal tunnel system, because the observed average water-flow speed (0.02 m/s) is much too slow in relation to the outlet stream discharge at the time of observation (7 m^3/s). To permit a water-flow speed of only 0.02 m/s down the actual gradient (0.1), a tunnel would have to be only $\approx$1 mm in

diameter and would carry a discharge of only $\approx 10^{-8}$ m^3/s. Thus, there must be many water-conducting passageways, distributed across the width of the glacier bed. A limiting case of this would be a continuous gap, about 1 mm thick, between the ice and its bed, which is similar to the model proposed for surging glaciers by Weertman (1969). However, even in this limiting case the water flux carried by the system would be much too small, only ≈ 0.02 m^3/s. From this we are forced to conclude that the system consists not of conduits or gaps of uniform width or thickness but rather of relatively large cavities linked by narrow, gaplike orifices that conduct the water flow from one cavity to the next. The overall flow rate (water discharge) is controlled by high-speed flow through the narrow orifices, whereas most of the travel time for water transport through the system is taken in slow-speed flow through the large cavities. We believe that this system of linked cavities forms by the process of ice-bedrock separation or basal cavitation (Lliboutry, 1968; Weertman, 1964; Kamb, 1970, p. 720; Iken, 1981). The cavities, which form on the lee sides of bedrock protuberances when the basal sliding velocity and basal water pressure are high (as they are in surge), probably have horizontal dimensions of a few meters and heights of a meter or less. The connections between them, which are in places where cavitation occurs only marginally, must be only a few centimeters high to throttle the flow. The observed values of U (0.02 m/s) and Q (7 m^3/s) require that the cavities have an average area of 200 m^2 in lateral cross section, which means that their average height is 200 m^2 divided by 1000 m (the glacier width). Thus the cavity height is about 0.2 m. The opening or closing of such a cavity system would store or release water (as in the large floods observed in connection with major slowdowns in surge speed) and would cause the glacier surface to rise or fall by 0.2 m, which is of the order of magnitude of

the drop actually observed at surge termination. The widespread distribution of the passageways across the glacier bed accords with the greatly increased turbidity of the outflow water during surge: by comparison with a normal tunnel system, it allows a much more extensive access of the basal water to the source of comminuted rock debris that is generally present between the base of the ice and the underlying bedrock."

In this thesis the preceding linked-cavity model will be further examined and tested in detail on the basis of the results of the tracer experiments reported here upon which the theory was based. Where possible, the ability of the linked-cavity model to explain the tracer results will be compared with the abilities of the basal sheet-flow model and of the subglacial sediment model (nos. 1 and 3 in Section 6.5.1).

6.5.2.2. Dimensions in the Conduit System

The conduit radius (or gap width) during the surge, predicted on the basis of Manning's equation and also laminar flow theory, is of the order of 1 mm. If these conduits lie at the glacier bed, as strongly suggested by independent lines of evidence (Chapter 4), then the calculated conduit size is much too small to carry the total amount of stream discharge observed. To account for the observed discharge at the glacier terminus and the measured dye transit velocity, many water channels must exist at the glacier bed, and the channels must have a radius on the order of 1 cm. Conduits of greater size, on the order of 10 cm, may exist if the water is temporarily stored in cavities between short conduit segments.

6.5.2.3. Volume of Stored Water

The total volume of stored water is estimated by integrating the volume discharged at the terminus, in excess of volume melted daily at the surface. Approximately 10 million m^3 of stored water were discharged from the glacier within the month after surge termination on July 4, 1983. This large amount of water storage, together with the observed drop of the glacier surface by 10 cm immediately upon surge termination, supports the concept that numerous cavities existed at the base of the glacier during surge. The amount of stored water discharged at the terminus within a few days of surge termination corresponds to a volume of 0.7 cubic meters per square meter of glacier bed.

At the height of the surge, the water level in boreholes was on average about 70 m below the ice surface at Km 9.5, where the ice was about 400 m thick; since the ice doubtless had an appreciable porosity due to crevasses, cracks, and other internal openings, a significant amount of water was stored within the ice mass during surge, and some of this stored water was released on surge termination, when the mean borehole water level dropped to about 120 m below the surface (Kamb and others, 1985, p. 476). Water was also stored in marginal lakes, two of which formed at the height of the surge and drained away on surge termination.

6.5.2.4. Retardation of Tracer Due to Adsorption Effects

The estimated K_a value for sediment remaining within the glacier during the surge is on the order of 10^{-4}(Section 3.5). For a conduit on the order of 1 mm radius, or larger, that is completely lined with adsorbing sediment, the value of $R_a \sim 1$, and no retardation is expected due to instantaneous adsorption effects at the conduit wall.

For significant retardation to occur the tracer must be adsorbed on very fine sediment, but such miron-sized sediment is readily carried by the transporting fluid. Thus, it is unlikely that retardation of the tracer will occur due to instantaneous adsorption effects, unless the dye is adsorbed at depth within immobile sediment. If adsorption of the tracer deeply within conduit walls is necessary to cause a significant retardation of the tracer, then other storage-retardation effects will come into play, as described by models of matrix-diffusion (Section 6.3.3) and mobile-immobile zones (Section 6.3.4), and is discussed below.

6.5.2.5. Storage-Retardation Models and Dispersion

The storage-retardation models such as matrix diffusion and immobile-mobile zones as discussed previously cannot explain the results observed for the Variegated Glacier in the surging state. These models predict that the dye-return curve would have a sharp onset and a gradual exponential tailing of the dye concentration with time. The observed tracer-return curve was quite different (Section 4.5).

6.5.2.6. Diffusion Models and Tracer Dispersion

The shape of the total dye-return curve in experiment 1 is described by the diffusive dispersion equation, as shown and discussed in Section 5.4. Mechanisms that can be considered to explain the diffusive dispersion include the concept of multiple conduits. This is because dye with nearly the same $C(t)$ distribution. This distribution has previously been was discharged from all of the many water outlet sites at the glacier terminus during the surge. Thus, the single conduit model can be discarded at the outset. The observed value for dispersivity within the surging glacier is

within the upper end of the observed α range for natural porous media (Anderson, 1979), but the mean flow velocity of water through the surging glacier is several orders of magnitude faster. The observed dispersivity for the glacier surge is a factor of 10 to 100 times greater than the average value of dispersivity in alluvial sediments and other assorted natural porous media (Table 6.6). If the characteristic scale length L for dispersion of a tracer through Variegated Glacier in the surging state is several orders of magnitude greater than the average L of porous media, then β values for porous media and the surging glacier are similar, and a single dispersion model may apply to both the surging glacier and porous media.

The multiple-interconnecting cavity-conduit model leads to the calculated variance of travel time through a multi-dimensional network of linked cavities as discussed in Section 6.2. The conduit width, roughness, tortuosity, segment length, and cavity dimensions are assumed to be described by a log-normal frequency distribution shown to correctly describe the observed variance in rock fracture width (Snow, 1970), grain-size distribution of crushed rock, and many other natural variates (Aitchison and Brown, 1957).

The observed high value of longitudinal dispersivity and the slow mean flow velocity can be explained by a model of many cavities connected by channels. The scale length L of the system is equal to the distance l between internal connection points in the multiple-conduit system. This value is much greater than the mean grain size of sediment (as required for the granular porous media model of Scheidegger, 1954) but much smaller than the total distance traveled, X (as required for the "channeling" model of Neretnieks, 1983). The multiple-interconnecting channel-cavity model predicts a scale length L or the mean cavity spacing l that is

on the order of 0.1 m to 1 m . Length scales of this order are observed on deglaciated terrain and are indicated by theoretical expectations based on the linked-cavity sliding theory of Kamb (1985, unpublished). The important quantity is the variance of the log-normal size distribution of each variable contributing to the mean transit time, including cavity size and the radius, length, roughness and tortuosity of the connecting channels.

The granular-porous-medium model of the water transport system predicts dispersivities on the order of the grain size of sediment. It is assumed that the mean grain size of sediment remaining in contact with moving water within the glacier is about sand size or larger (i.e., $>=$ 1 mm), because sediment finer than this size is unlikely to remain immobile while in contact with water flowing at a mean speed on the order of 0.01 m/s or greater. If the subglacial debris is composed of coarse gravely till, and the mean sediment size length L is on the order of 10 cm, then the predicted dispersivity for water flow through the subglacial debris is on the order of 0.1 m (Scheidegger, 1957). The observed dispersivity (see Section 5.4) was larger than this by at least a factor of 1000. Therefore the drainage of the surging glacier was not controled by the flow of water through subglacial debris.

The mixing region for the linked-cavity model may consist of a cavity or a length scale of the glacier necessary for total mixing of glacier runoff to occur. The linked-cavity model of mixing volumes, referred to as "perfect-mixers" by Bear (1979), is used to calculate that the mean distance between mixing volumes is $L = 2\alpha$. For the surging glacier, the calculated L is on the order 1 kilometer. For a system of actual linked basal water cavities, this result is clearly unrealistic, but for a linked system of arbitrary mixing volumes, a spacing distance on the order of the glacier

width is plausible. In this sense, the glacier must be heterogeneous on the scale of one kilometer, but may be homogeneous at a scale equal to the total travel distance X, if X is much greater than L.

If superimposed on the transit time model for linked cavities described above, the dye is temporarily stored for a time proportional to the size of each cavity according to the log-normal probability density distribution, then the total variance in transit time is further increased.

6.5.2.7. Conclusion of Dispersion Analysis for Surging Glacier

The multiple-interconnecting cavity conduit model best predicts the high values of dispersivity observed for the glacier during the surging state. Most of the main drainage tunnels and cavities must have been situated at the base of the glacier, because of the large amount of suspended sediment carried by the water. The effect of retardation of the tracer due to adsorption on immobile sediment is considered negligible, because most of the tracer was adsorbed on highly mobile, fine-grained sediment carried by the water flow. In addition, the retardation must be negligible in order to explain the rapid appearance of dye at the terminus, both on sediment and dissolved in water. The variables determining the transit time variation of the multiple interconnecting channel-cavity model included the log-normal variances of conduit size, cavity length and width, and channel segment length. The predicted spacing between cavities in the multiple-interconnecting conduit system ranges from 0.1 to 1 m, as suggested by independent lines of evidence (Kamb et al., 1985). The size of cavities is of the same order as the distance between cavities. Mass balance of the total amount of stored water released at surge termination and the total amount that

can possibly be stored at the glacier bed in cavities strongly suggests that at least 10 to 20 percent of the extra water within the glacier during the surge could have been stored in basal cavities. The remaining extra water was stored within the surging glacier and in lakes situated along the glacier margin.

Table 6.1
Dispersion Parameters from Tracer Experiments in Pipes[1]

	n^* ($m^{-1/3}s$)	f^* -	X (m)	U (m/s)	α (m)	R_H (m)	Γ -
Straight Pipes							
Set A	0.007	0.026	3	2.2	0.003	0.0025	23
	0.007	0.026	16	2.2	0.003	0.0025	20
	0.007	0.031	16	1.4	0.004	0.0025	25
	0.010	0.012	-	1.1	0.208	0.25	21
Set B	0.018	0.13	3	1.5	0.008	0.0025	21
Curved Pipes							
Set C	0.031	0.145	1,250	1.4	0.14	0.127	23
	0.024	0.118	38,324	1.1	0.041	0.051	19
Set D	0.008	0.036	2.5	1.1	0.007	0.0025	44
	0.007	0.031	2.5	2.0	0.005	0.0025	30

1. Data from Taylor (1953, p. 463). Data sets A, B, and D are from small-scale laboratory experiments; set C from large-scale experiments in pipelines, the first example a water pipeline between El Segundo and Montebello, California; the second a water pipeline from San Pablo to Richmond, California. Experiments in set D were carried out in a curved laboratory pipe, the radius of curvature of which was 570 times the radius of the pipe cross-section. The wall-friction coefficient f^* for each experiment is based on the measured fluid flow, via Equation (6.5). The corresponding value of the Manning roughness n^* is obtained from the relation (6.3) or (6.7). The experimentally observed dispersion coefficient D is expressed in terms of α via Equation (6.1), and the parameter Γ is calculated from α via Equation (6.15), using the stated value of f^*.

Table 6.2
Dispersion Parameters in Natural Rivers

River Name	X (km)	R_H (m)	U (m/s)	α (m)	β	Γ
Surface Streams						
Green River (1)	2	1.1	0.29	17	15	86
	-	1.1	0.32	10	9	50
	3	1.1	0.29	20	18	101
"	4	1.1	0.29	16	15	84
	-	1.1	0.32	22	20	112
"	7	1.1	0.32	30	30	168
Average	4	1	0.3	3	20	100
One Eye River (2)	1	1	0.25	9	45	200
"	6	1	0.25	10	50	200
Underground Streams						
One Eye River	5		0.043	10	4	25

1. Manning roughness $n^* = 0.058 m^{-1/3} s$, mean discharge Q = 8.5 m^3/s, $f^* = 0.26$ (Fischer, 1968). In calculating β from α, Equation (6.2) is used with $L = R_H$.

2. Q = 2.6-7.5 m^3/s, width 12-24 m (Smart, 1976).

Table 6.3
Water Velocities in Temperate Glaciers

Injection Site	No. of Obs.	Glacier	Year	X (km)	U_{mean} (m/s)	U_{range} (m/s)	Reference
Snow	4	(various)	(various)	0.01	10^{-6}	10^{-5}–10^{-7}	Krimmel et al. (1973) Colbeck (1972) Fujino (1971) Lang (1972)
Lateral Stream	4	Pasterze	1979-80	4.0	1.2	0.8-1.8	Burkimsher (1983)
"	8	-	1972	0.4	0.96	0.49-1.4	Ambach et al. (1973)
Moulin	8	Pasterze	1979	0.2-2	0.43	0.2-0.8	Burkimsher (1983)
"	8	"	1980	"	0.51	0.1-1.8	"
"	5	"	1980	"	0.38	0.03-1.07	"
"	13	Hintereisferner	1971	1-5	0.53	0.19-0.76	Ambach et al. (1972)
"	7	"	1972	1-5	0.7	0.5-1.1	Behrens et al. (1975)
"	2	Aletsch	1977-78	6-19	1.3	0.8-1.7	Lang et al. (1979)
"	9	South Cascade	1959-71	0.7	0.6	0.1-1.0	Krimmel et al. (1973)
"	2	"	1977	0.7-1.0	0.3	-	Irle (1978)
"	4	Findelen	1982	0.8	0.4	-	Moeri (1983)
	AVERAGE			0.2-19	0.6	0.03-1.8	
Borehole	8	Findelen	1982	1.7-2.7	0.36	0.21-0.58	Moeri (1983)
"	2	South Cascade	1977	0.9	0.16	0.12-0.19	Irle (1978)
	AVERAGE			0.9-2.7	0.27	0.12-0.58	

Table 6.4a
Moulin Dye Tracing Results

Glacier Site	No. of Obs.[b]	Year -	X (km)	R_H[a] (m)	U (m/s)	α (m)	β -	f^* $m^{-1/3}s$	References
Hintereisferner	5	1971	0.8	1.0	0.4	18	15	4.5	Ambach et al.(1972)
"	1	1972	0.8	1.1	0.1	1	1	0.02	Behrens et al. (1975)
Hintereisferner	2	1971	1.7	1.1	0.34	15	14	3.92	Behrens et al.(1975)
"	8	1972a	1.7	0.8	0.81	6	7	0.98	"
"	1	1972b	1.7	1.0	0.52	2	2	0.08	"
Hintereisferner	9	1971	2.	0.8	0.6	15	17	4.5	Ambach et al.(1972)
South Cascade	1	1970	0.6	1.2	0.17	4	3	0.18	Krimmel et al.(1973)
South Cascade	2	1978	0.9	1.5	0.16	10	7	0.98	Irle(1978)
Findelen	2	1982a	1.7	0.8	0.3	8	9	2	Moeri(1983)
Findelen	2	1982b	2.7	0.9	0.5	12	13	3.4	"
Aletsch	1	1978	6.3	1.4	1.65	2	2	0.05	Lang et al.(1979)
Aletsch	1	1977	19.3	1.9	0.84	11	12	2.9	"
AVERAGE	35	-	-	0.9	0.5	10	10	2.4	-
(open channel)	6	1970	.4	0.4	0.96	2	6	0.82	Ambach et al.(1973)

Table 6.4b
Borehole Dye Tracing Experiments

Glacier Site	No. of Obs.[a]	Year	X (km)	R_H[b] (m)	U (m/s)	α (m)	β	f^* $m^{-1/3}s$	References
Findelen	2	1982	2.2	0.8	0.3	21	27	–	Moeri (1983)
"	2	1982	2.4	1.0	0.2	45	45	–	"
Variegated (Surge)	1	1983	8	<1[c]	0.0024	1,250	>1000	–	-
" (Post-Surge)	1	1983	10	2.1	0.7	<9	<4	0.07	-

(a) R_H values calculated directly from the Manning equation from observed stream discharge, mean velocity, and gradient.

(b) The data values are averages from the numbers of individual observations listed.

(c) Size deduced from mean flow velocity by assuming laminar flow in conduits of circular cross section.

Table 6.5
Roughness of Glacier Water Conduits[a]

Glacier	Glacier Surface Slope m/m	$-dh/dx$ Hydraulic Gradient m/m	Q $m^3/2$	U m/s	n^* (based on discharge)[b] $m^{-1/3}s$	n^* (based on dispersivity)[c] $m^{-1/3}s$
Open Channel		(0.1)[d]	2	0.96	0.114	0.017
Hintereisferner	0.19	(0.08)	4	0.41	0.28	0.16
			6	0.4	0.25	0.017
"	0.15	(0.08)	4	0.34	0.36	0.21
			6.8	0.81	0.095	0.11
			6.2	0.52	0.177	0.033
"	0.10	(0.08)	4	0.6	0.17	0.24
Average	0.098	(0.08)	5.2	0.6	0.14	
South Cascade	0.33	0.08	3	0.17	0.9	0.13
	0.23	0.08	3	0.16	0.9	0.11
	0.18	0.08				
Findelen		(0.08)	6	0.3	0.37	0.14
		(0.08)	6	0.5	0.19	0.21
Average	0.08	(0.08)	6	0.4	0.23	
Aletsch						
Katzlocher	0.108	(0.06)	43	1.65	0.02	0.024
Koncordiaplatz	0.064	0.06	29	0.84	0.056	0.203
AVERAGE	~ 0.1	~ 0.1	~ 10	~ 1	0.26	0.14
Variegated (Post-surge)	0.1	0.1	40	0.7	0.064	0.07
				Average =	0.26	

[a] Except for the case of Variegated Glacier, data cited in this table is based on results of dye-tracing experiments conducted through glacier moulins.

[b] This estimate of n^* based on discharge, is obtained from the Manning equation (6.3), The shape of the channel is assumed to be circular in cross section.

[c] This estimate of n^* based on dispersivity, is obtained from Equations (6.7) and (6.15) with $\Gamma = 20$.

[d] Parentheses indicate best estimate of average hydraulic gradient from available data on surface, bed and borehole water levels.

Table 6.6
Summary of Dispersivity Data – Typical Values

System	U (m/s)	L (m)	α (m)	β	f^*	Γ
Porous Media						
Glass Beads	10^{-5}	10^{-3}	10^{-3}	1	-	-
Snow	10^{-5}	10^{-3}	10^{-2}	10	-	-
Alluvium[a]	10^{-4}	-	10	10^4	-	-
Assorted Natural[a]	10^{-8}	-	10^2	10^5	-	-
Single Pipe Conduits		(R_H)				
smooth (n^*=0.01), narrow	1	0.001	0.001	1	0.03	23
smooth (n^*=0.01), wide	1	0.1	0.1	1	0.01	21
rough (n^*=0.02), narrow	1	0.001	0.01	3	0.18	21
curved (n^*=0.01), narrow	1	0.001	0.01	2	0.04	37
curved (n^*=0.01), wide	1	0.1	0.1	1	0.03	21
Rivers, surface	0.3	1	10	10	0.26	100
Rivers, underground	0.04	2	10	10	0.26	50
Non-Surging Glaciers						
Moulin injection	0.5	1	10	10	0.25[b]	50
Borehole injection	0.2	1	40	40	0.25	230
Variegated Glacier						
Surge						
Total Tracer	0.024	-	1,100	-	0.25	-
Dissolved Tracer	0.042	-	240	-	0.25	-
Post Surge						
Total Tracer	0.7	2	<10	<4	0.25	<23
2nd Peak	0.1	2	40	30	0.25	170

[a] Estimated grain size 1 mm.
[b] Estimated coefficient (Spring and Hutter, 1982)

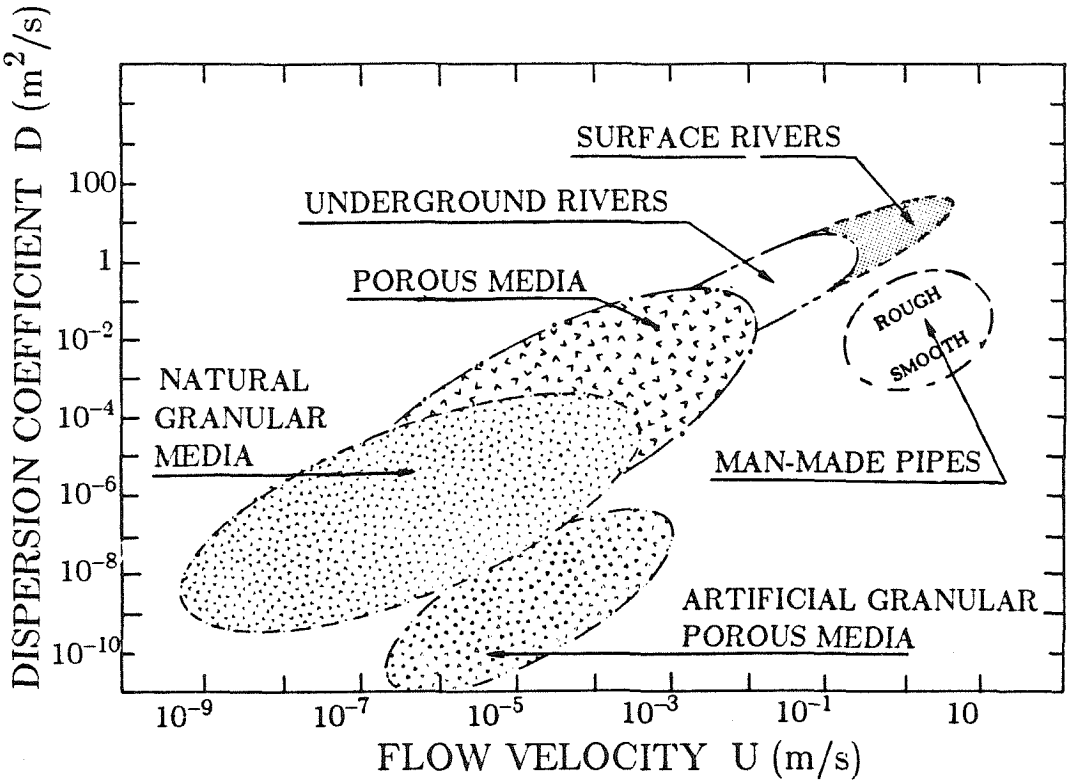

Figure 6.1 Plot of dispersion coefficient versus flow velocity for various conduit systems including porous media and single channels. The range of D and U values for each natural and artificial system considered is shown by shaded patterns as indicated.

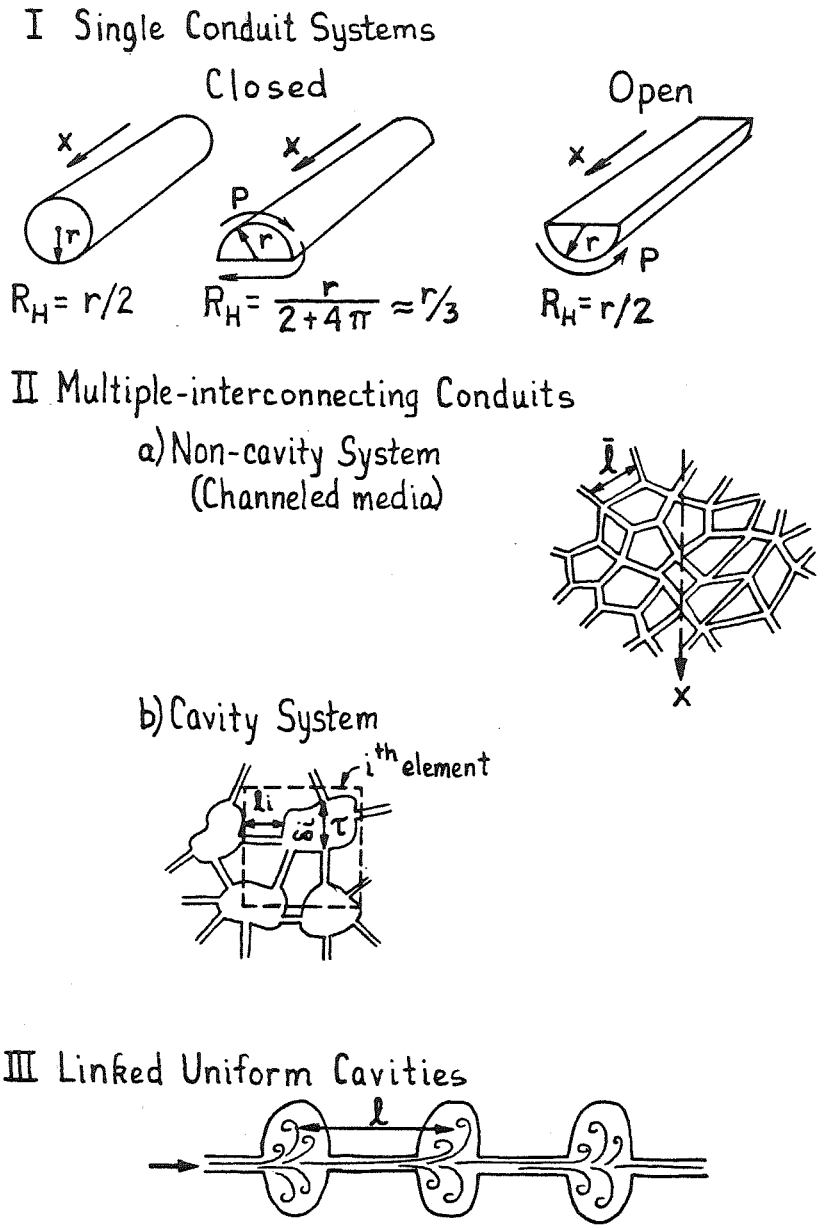

Figure 6.2 Model drainage systems that can produce a Gaussian dye-return curve as required by diffusive dispersion. Single conduit and multiple- interconnecting conduits (with and without cavities) and linked uniform cavities are represented.

SCHEMATIC OF GLACIER AQUIFER ZONATION:

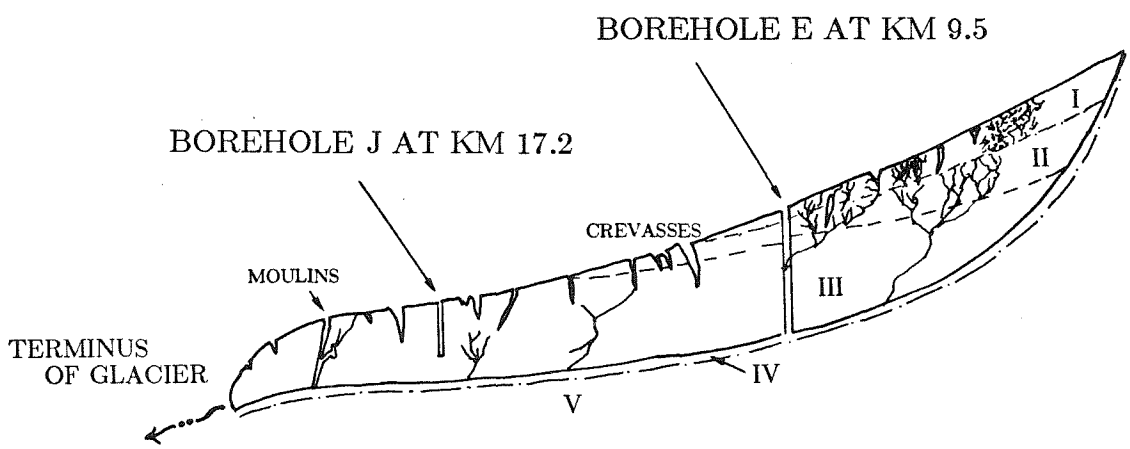

Figure 6.3 Schematic of glacier aquifer zonation showing: I. snow; II. firn; III. glacier ice; IV. basal conduits; V. subsole rock and sediment. The approximate location of 1983 Variegated tracer injections made at Km 9.5 (Rhodamine dye) and Km 17.2 (Tinopal dye) are shown. Previous dye-tracer studies at other temperate glaciers, compared in Tables 6.4 - 6.5, were conducted through moulins, crevasses, marginal streams, boreholes (drilled to different depths and aquifer zones I - III) and snow on firn surface, and these glacier features are included in this idealized sketch.

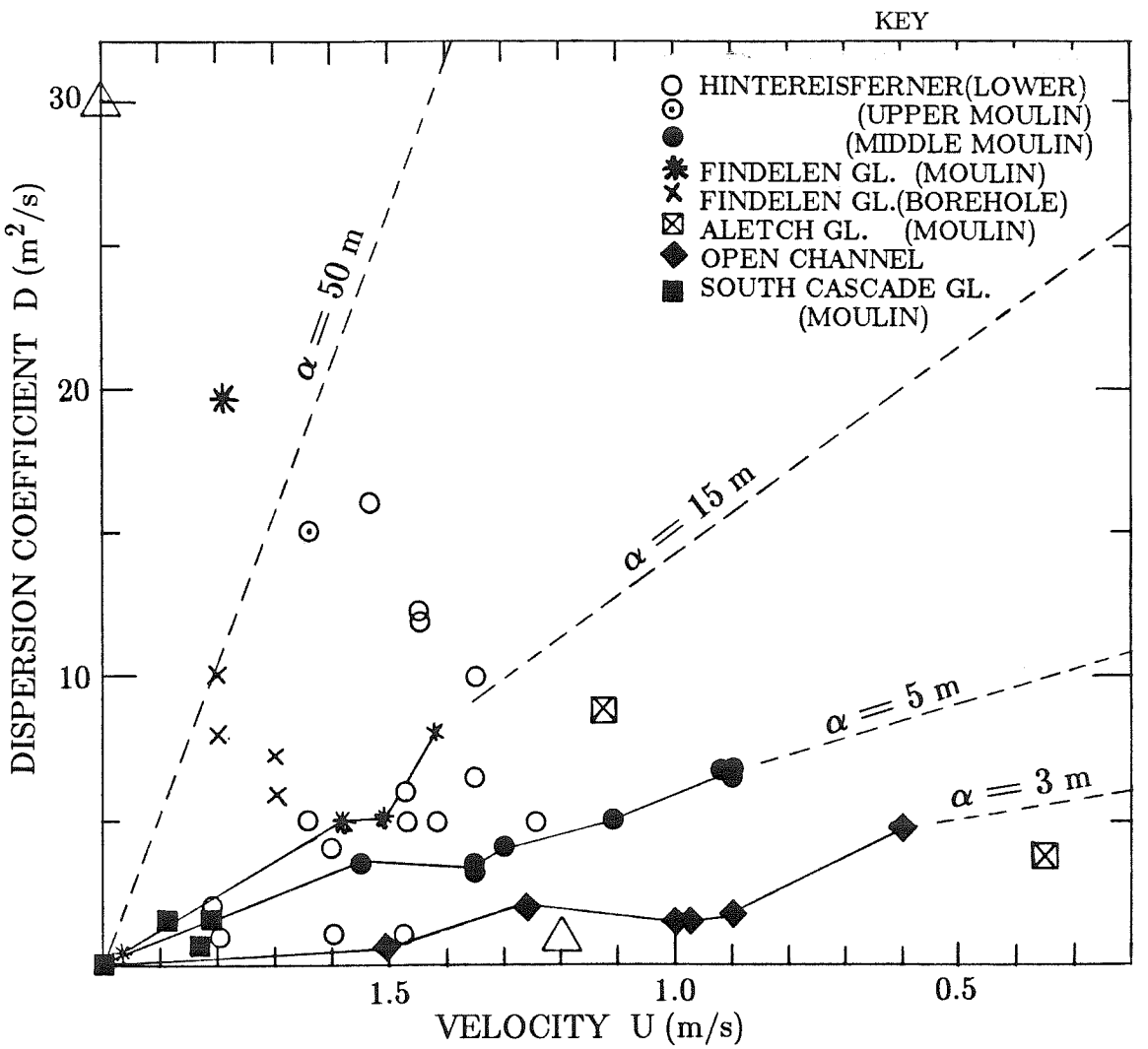

Figure 6.4 Plot of dispersion coefficient versus mean flow velocity for dye tracing results from experiments conducted through moulins on Hintereisferner, Findelen, Aletsch, and South Cascade glaciers, and through boreholes reaching glacier bed in Findelen and Variegated glaciers. Only data for experiments indicating a mean transport flow velocity greater than 0.01 m/s are considered. Also, only cases where main dye peak could be modeled by diffusive dispersion theory are included. Data obtained at close time intervals, through the same water conduit, are interconnected by a solid line. Dashed lines of slope $\alpha =$ 3, 5, 15, 50 m are shown for comparison to model predictions (Section 6.2).

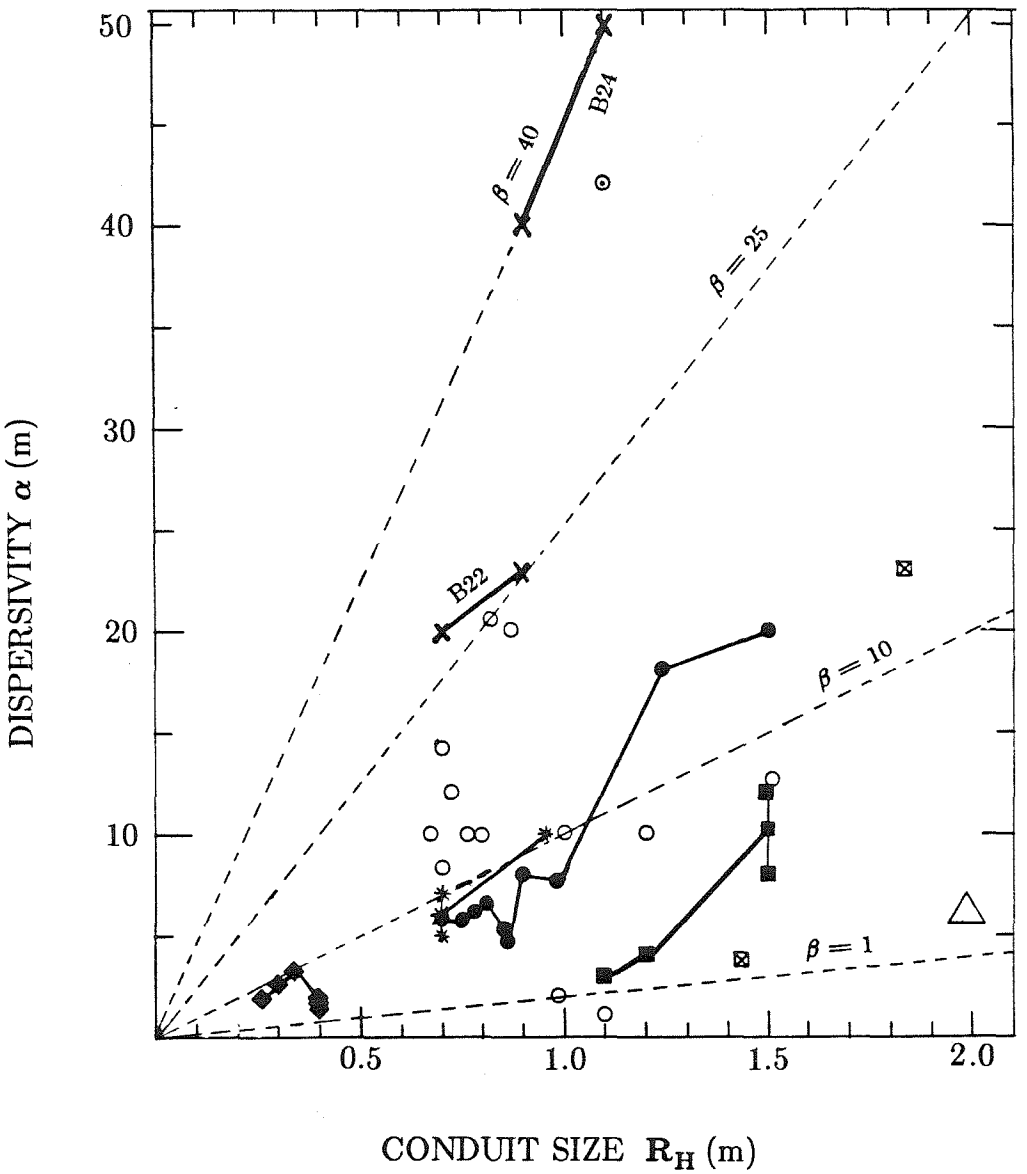

Figure 6.5 Dispersivity versus conduit size for moulin dye tracing experiments from various temperate glaciers, based on data in Fig. 6.4. Solid lines/symbols are used to indicate experiments conducted in same moulin or borehole within a few hours to weeks. Dashed lines indicate constant values of $\beta =$ 1, 10, 25 and 40.

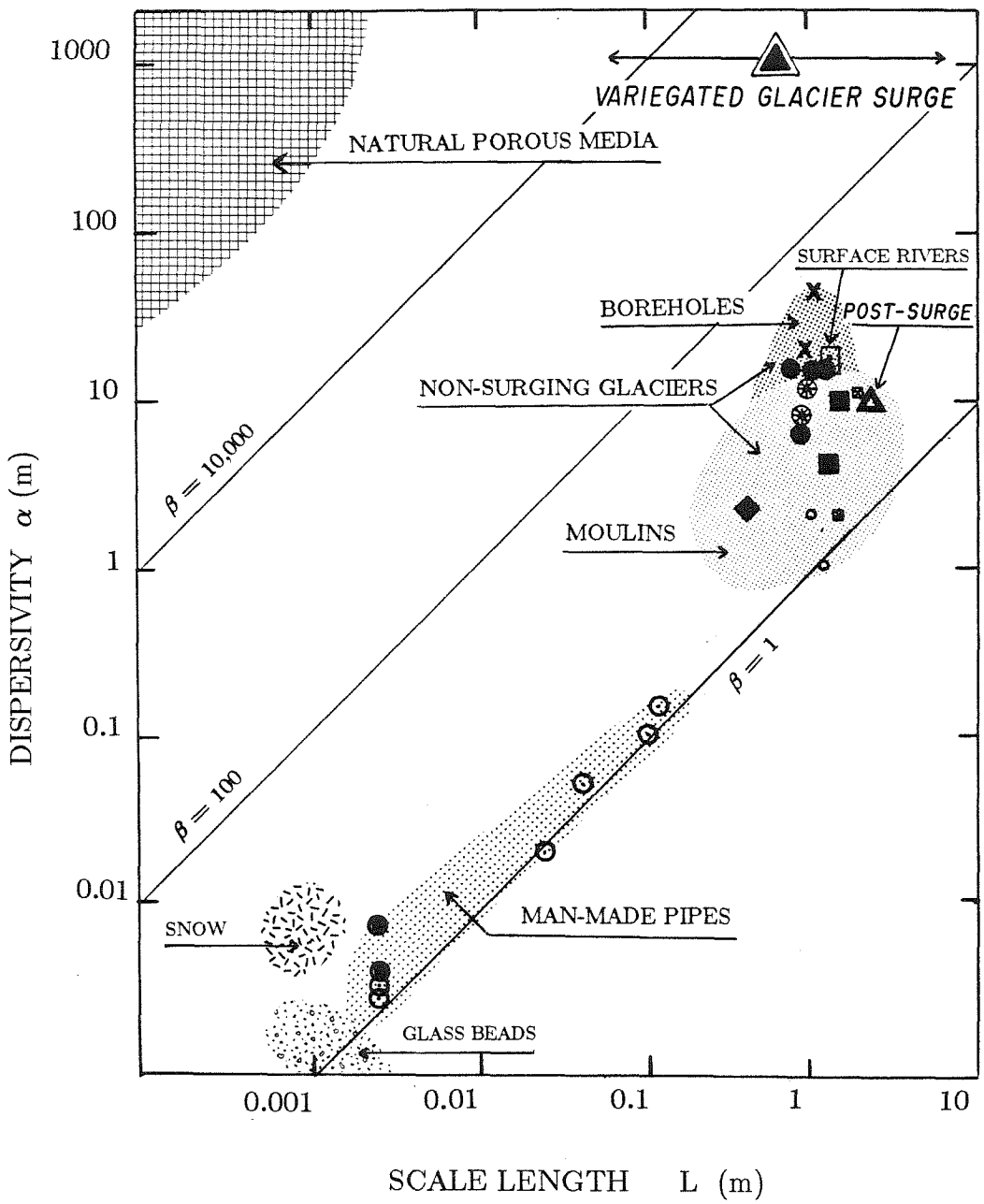

Figure 6.6 Log-log plot of dispersivity versus scale length L for different drainage systems including natural and artificial porous rock materials, snow, man made pipes, natural rivers, basal and englacial conduits in non-surging glaciers (studied through moulin and borehole injections) and basal conduits in Variegated glacier in surging and non-surging states.

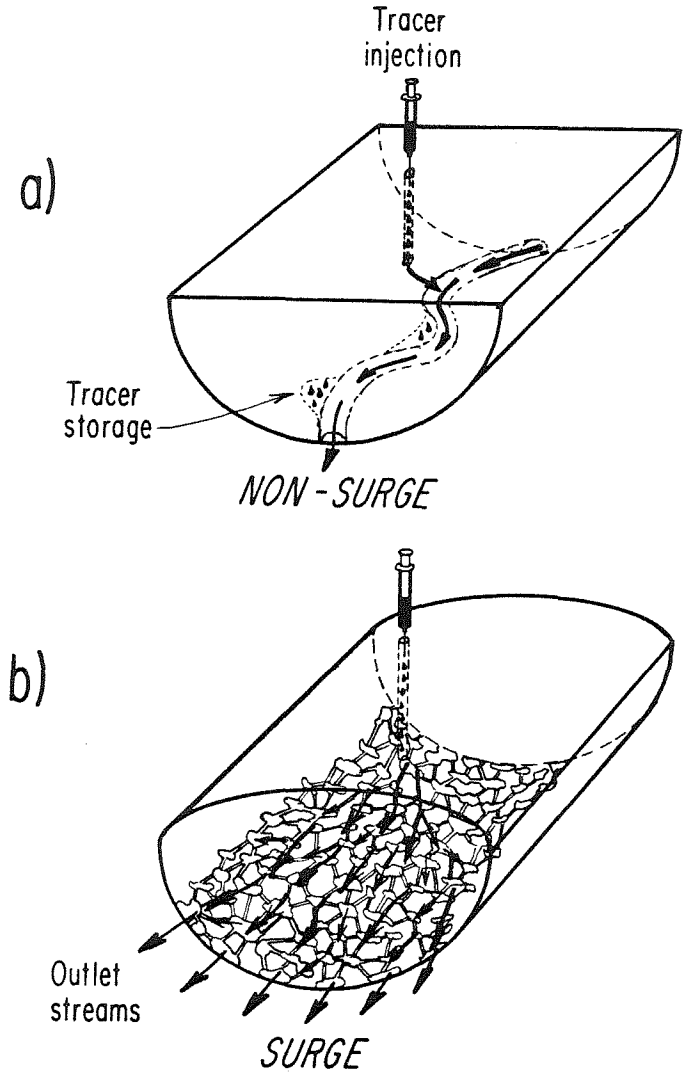

Figure 6.7 (a) Sketch of single-conduit basal water system of a temperate glacier in the non-surging state as suggested by modeling of tracer experiments where dye was injected at base of glacier through moulins and boreholes.
(b) Basal conduit system of a surging glacier, as indicated by dye tracer results from Variegated glacier. This drainage pattern is composed of multiple-interconnecting conduits and cavities, and is the type of linked cavity system discussed by Kamb et al. (1985).

Chapter VII:
CONCLUSIONS

7.1. Comparison of Basal Water Systems in the Surging and Non-Surging States

The drainage system of Variegated Glacier in the surging state is found to be composed of an interconnecting network of conduits and cavities, and is strikingly different from the tunnel system indicated by tracing experiments for the non-surging state. At surge termination the multiple-conduit-cavity system collapsed, and at the same time a dendritic drainage system rapidly developed. The collapse of the conduit-cavity system occurred during and after one of the most dramatic peaks in water discharge at the glacier terminus. After termination, discharge remained relatively high as compared to both surge and pre-surge average values and most of the glacier water emanated from a single outlet stream. The switch from a multiple-interconnecting conduit-cavity system active in the surging state to the trunk tunnel system active in the non-surging state is correlated to the large changes observed in stream discharge, ice velocity, and sediment discharge. Both theory and observation strongly suggest that most of the glacier runoff travels at the glacier bed for surging and non-surging glacier states. Theoretical models of possible drainage system configurations were compared with dye-tracing observations to infer the details of water flow at the bed of the glacier.

7.2. Tracer Dispersion and Storage

Spreading of the dye-return peak by diffusive dispersion, which is described by the diffusion equation, can be parameterized in terms of a longitudinal dispersion coefficient D. Models of tracer dispersion in single conduits, in systems of multiple interconnecting conduits (such as porous media), and in linked-cavity systems indicate that for all of these systems D depends on water flow velocity U via the simple relation $D = \alpha U$; the factor α, called the longitudinal dispersivity, is used in interpreting experimental results (as in Section 6.2 and 6.5). The models further show that $\alpha = \beta L$, where L is a fundamental length scale for each system and β is a dimensionless proportionality constant, whose value can in some cases be calculated theoretically.

The shape of the dye-return peak is also affected by a second type of process, here called a "storage-retardation" process, which generates (from a slug injection) a dye-return curve consisting of a sharp initial peak followed by a quasi-exponentially decreasing tail.

The dye-return points for the tracer experiment during the surge have a large scatter around a theoretical Gaussian curve (Section 5.4); this contrasts with the lack of scatter in the post-surge experiment, in which the data points follow rather well a dye-return curve of storage-retardation type (Section 5.5). The scatter in dye return pattern for the surge experiments is probably due to the continually changing nature of the glacier drainage system in the surge.

Transverse distribution of tracer at the terminus differed greatly from surge to non-surge states. During the surge the dye tracer was observed to emanate simultaneously from all terminus streams. The transverse dispersion was large for the

surging glacier and on the order of the longitudinal dispersion. After the surge, only one stream carried the tracer at detectible concentrations. This evidence contributes to the conclusion that a major change in water drainage sytem occurred at surge termination.

7.3. Specific Features of the Conduit System at the Glacier Bed During the Surge

The size of a rough conduit calculated from the dye transit velocity for the surging state of the glacier is about 1 mm, as compared to about 1 m the non-surging state. These channel sizes are calculated assuming a Manning's roughness, n^*, of 0.1 $m^{-1/3}s$, a hydraulic gradient of 1/10, and a sinuosity of 1 to 3. Although the total water flux measured at the terminus for the non-surging state is readily carried by a conduit of radius 1 m, the water flux for the surging-state is too large to be transported solely through basal conduits with radius as small as 1 mm. In order to transport the observed total flux of water to the glacier terminus during the surge at the slow transit velocity observed, basal conduits must be of radius 1 cm or larger. If basal conduits during the surge are larger than radius 1 cm, each conduit must interconnect chambers where the forward movement of the dye is temporarily arrested.

The tracer return pattern for the surging glacier is approximately Gaussian in shape. Storage-retardation models such as slow release of tracer from the base of a borehole, interaction of immobile-mobile zones, and matrix diffusion would predict a different shape for the dye return curve than that actually observed during the glacier surge.

The diffusive-dispersion model corresponds to the case of the surging glacier. The dispersion parameterization of the tracer for the surging glacier is $D = 30$ m^2/s, and $U = 0.024$m/s. The implied dispersivity is $\alpha = 1{,}100$ m. This value of dispersivity is higher than observed in most tracing studies. The dispersivity for the surging glacier resembles values for natural fractured and microscopically channeled porous media. The α values are similar, even though the mean flow velocity of the dye through the surging glacier is many orders of magnitude higher than normal groundwater flow velocities.

Dispersion through a network of randomly oriented channel segments, such as that in isotropic granular porous media, involves a dispersivity that is on the order of the grain size of the granular medium. The granular porous media have dispersivities much smaller than that actually observed in the glacier tracing experiment. The drainage system of the surging glacier can not be described by flow through a granular basal substrate.

The theories for dispersion of a solute in single conduits and non-interconnecting linked cavities both give lower dispersivity values than that measured for the surging glacier. The single-conduit flow theory is not consistent with the high dispersivity and slow tracer velocities observed during the glacier surge. The velocity and dispersivity of a water tracer traveling at the bed of the surging glacier cannot be estimated with reasonable input constraints, unless the water drainage system is composed of many conduit segments linking various water-filled cavities.

The fact that dispersivities measured for natural groundwater flow over large distances have high values approaching that observed for the surging glacier suggests that the highly dispersive drainage system controlling water transport in Variegated

Glacier during the surging state may be described by the same general diffusive-dispersion model used to describe groundwater flow systems. The dye-return pattern for the glacier in the surging state can be explained best by a drainage system composed of many cavities, having a log-normal size distribution, and with log-normal variance of order unity, tha cavities being interconnected by short channel segments that also have a log-normal size distribution with similar variance. This model is consistent with the high value of dispersivity ($\alpha = 1{,}100$ m) evaluated from the dye-tracing experiment conducted during glacier surge. The statistical calculation of dispersion within this type of the drainage system uses a log-normal size distribution for channel radius, channel segment length, cavity size, tortuosity, and conduit roughness. The scale length L of the system is equivalent to the distance between interconnection points. The dispersivity is the aggregate effect of all variances of variables controlling the transit time of tracer from one interconnection point to the next. The β coefficient can be as large as $\sim 10^4$ as estimated stochastically for this type of drainage sytem. The flow in each conduit can be either laminar or turbulent. For reasonable values of L $\sim$ 10 cm to 10 m, and for a value of β that is possible theoretically, the observed $\alpha \sim 1{,}000$ m can be accounted for.

In addition to the pattern of dye dispersion, the observed mean velocity and the stream discharge are compatible with this unusual basal water system, characteristic of the glacier in the surging state. For an average conduit height of 0.1 to 1 m, and a mean flow velocity of 0.02 m/s over the glacier width of 1 km, the terminus stream discharge would be 2 to 20 m^3/s. The average discharge monitored during the dye-tracing experiment conducted during the glacier surge, about 15 m^3/s, was within this range. The observed 0.1 m drop in height of the glacier surface at surge termination

is compatible with the closure of cavities of average height 0.1 m. Because of the large volume of sediment carried by the surge water, it is concluded that these cavities and the main interconnecting channels were probably located at the glacier bed.

Strong evidence in support of the existence of water-filled cavities within the glacier also comes from the observation of the large volume of water discharged concurrently with each major deceleration in glacier velocity, including the termination of the surge. The water discharged at these times far exceeds the daily water input that can be accounted for by surface melt, rainwater input, and frictional melting at the bed.

The model of multiply interconnecting cavities discussed in this thesis is consistent with a theoretical model of the basal water system in surge recently developed by Kamb (unpublished) on the basis of the surge observations.

The integrated dye return curve indicates that about 50% of the injected Rhodamine WT tracer was detected reaching the terminus in the first tracer experiment. The missing tracer may have been adsorbed on immobile basal sediment or stored in isolated cavities while the water and dye were enroute to the the glacier terminus, and may have been continuously discharged at undetectable concentrations for weeks to months after injection.

7.4. Specific Features of Basal Water Conduits After Surge Termination

The longitudinal dispersivity ($\alpha \leq 1$m) and mean velocity ($U_{dye} = 0.7$ m/s) values for dye transport through Variegated Glacier after the end of the 1983 surge are consistent with those of normal, non-surging glaciers. The parameters inferred for the single main basal conduit after the glacier surge ended are: hydraulic radius 1.5

m, sinuosity Ω about 3, water flow velocity in the conduit about 2 m/s, Manning roughness 0.1 $m^{-1/3}s$, and Γ parameter 20 . The observed discharge of the terminus stream can be explained by these values using Manning's Equation (6.3). The dispersivity can be accounted for by eddy-diffusion theory (Taylor, 1954) applied to a very rough and meandering conduit. These results are in general agreement with theoretical predictions concerning the water drainage system for normal, non-surging glaciers as described by Röthlisberger (1972), Shreve (1972), and Nye (1976). A value $n^* = 0.1\ m^{-1/3}$ is in agreement with independent estimates of Manning roughness for glacier conduits by Clarke et al. (1984), and indicates that the basal conduits are very rough and tortuous.

If a high initial tracer peak appeared at the glacier terminus, as suggested by the fact that 60 % of the tracer was unaccounted for, then it must be concluded that the peak arrived between two sampling times, 40 minutes apart. The probable arrival time is prior to the first terminus stream sample containing a high concentration of tracer, and after the last clean sample. To estimate dispersion parameters for the non-surging glacier, the total tracer volume returned was assumed to be approximately equal to the amount of dye initially injected at the glacier bed.

If water conduits existed within the ice mass they would be expected to have very low wall friction. Such englacial channels would probably have friction factors and cross-sectional velocity profiles similar to man-made pipes. Clean-ice-walled englacial water channels would produce dispersivities approximately 1/10 to 1/1000 smaller than dispersivities of a natural shallow stream flowing over a moderately rough bed. The dispersivity values derived for non-surging glaciers in general, including the post-surge Variegated Glacier, indicate that main drainage conduits probably

lie at the base of the glacier.

The tracer-return curves obtained in the non-surging state of Variegated and other normal glaciers indicate that one or more storage-retardation mechanisms are active. The measured portion of the dye-return curve for the non-surging Variegated Glacier is described by a decreasing exponential curve of tracer concentration. The exponential tailing of the dye-return curve is caused by storage and release processes described by a model of stationary and moving zones with transfer of tracer between the mobile and immobile zones. The immobile zones probably do not consist of sediment but rather are probably water chambers poorly connected to the main flow (Ambach and Jochum, 1973), back-eddies behind flow obstructions, or slack water at sharp meander bends. Such a string of immobile zones connected to the main drainage conduit can explain the observed exponential tailing commonly observed for non-surging glaciers and natural surface streams.

7.5. Adsorption of Dye on Suspended Sediment

The adsorption of Rhodamine WT on suspended sediment proves to be important in the tracing experiments conducted during and after the glacier surge. The return curves for dissolved, adsorbed and total Rhodamine WT tracer had to be measured separately, in order to analyze reliably the dye return from the basal water tracing experiments.

A new technique was devised for extraction of tracer from suspended sediment. It involves methanol extraction and fluorometry of the extracted Rhodamine WT in methanol solution. The limit of detection for dissolved and adsorbed Rhodamine WT was 0.01 ppb.

Eighty percent of the tracer detected at the terminus of the glacier in surge was adsorbed on suspended sediment, the remaining twenty percent being in solution. After the surge only a minor amount, less than ten percent, was found adsorbed on suspended sediment.

The terminus streams are highly charged with easily suspended, fine sediment. The suspended sediment content of the outflow streams during the surge was very high and variable, ranging from 20 to 110 g/l. After the surge termination, the content of suspended sediment dropped off sharply to a level between 0.1 to 20 g/l. The high sediment contents in the terminus streams for both the surging and non-surging states strongly suggest that main water conduits lie at the glacier bed.

Data on sediment load in relation to dissolved and adsorbed tracer concentrations, for samples and standards prepared from Variegated Glacier stream water, were analyzed for their conformity to adsorption theory. Results indicated that the dissolved tracer concentration was linearly related to the adsorbed concentration. The observed sediment adsorption behavior for Rhodamine WT can be explained in terms of the Langmuir adsorption isotherm theory for dilute solutions, or Henry's linear law for adsorption. The adsorption behavior of sediment and consequently the value of the volume distribution coefficient K_d is strongly dependent upon the grain size of sediment.

Although most of the dye transported to the glacier terminus during the glacier surge was found adsorbed on fine sediment, dye adsorption behavior cannot account for either the slow mean transport velocity nor the unusually high dispersivity measured. The finest sediment is carried by the flow of water, and it is just this type of sediment that causes the large K_d values. The coarser sediment that is not in

suspension is expected to have a lower value of adsorptivity inversely in proportion to the sediment grain size. Most of the dye tracer is carried to the terminus on fine sediment that remained in continuous adsorptive equilibrium with the water the sediment remained in association with. Due to the predominance of micron-sized particles in the discharge waters, it is probable that the sediment was carried along with the fluid without the occurrence of any significant additional retardation or dispersion due to settling and saltation processes enroute. There was a much greater abundance of very fine sediment suspended in the terminus stream discharge during the surge. The abundance of micron-sized sediment accounts for the large distribution coefficients K_d, measured for suspended sediment during the first experiment. The highest values for the distribution coefficient, observed during the glacier surge, were approximately coincident with the highest ice flow velocities and major outburst floods at the terminus.

Perhaps, the very fine, highly adsorbing sediment is produced by increased grinding of basal rock fragments during major motion events of the surging glacier. Another possible explanation for the high K_d values is that a larger area of the glacier bed, and, consequently, basal sediment, is exposed to flowing water during the motion events. Increased cavitation and separation at the basal ice-rock interface during major motion events can explain not only the correlation between increased K_d and increased ice motion during the surge, but also the increased value of K_d observed for the glacier in the surging as compared to the non-surging states.

7.6. Recommendations for Future Work

The information in this thesis provides a theoretical and observational basis for the design, execution and interpretation of glacier water tracing studies. The dispersion information potentially provided by glacier dye tracing experiments has been under-utilized in the past. Results of this study indicate that storage-retardation mechanisms strongly affect the transport of a solute transported at the base of a non-surging glacier, and a better understanding of the basic processes involved is necessary. In particular, I suggest that a realistic assessment be carried out of the effects of eddy-diffusion and solute transport between the mobile zone of a stream and proposed immobile (or slack water) zones associated with stream meanders, ice and rock obstacles, pockets of adsorbing sediment, and nearby water storage chambers. Finally, this study has shown for the first time that tracer dispersion within a glacier, either in the surging or non-surging state, is partially akin to tracer dispersion in natural groundwater aquifers, and this relationship should be explored further.

REFERENCES

Aitchison, J. and Brown, J. A. C. (1957). *The Lognormal Distribution.* University Press, Cambridge, England.

Aley, T. and Fletcher, M. W. (1976). Water Tracers Cookbook. *Journal of the Missouri Speleological Survey,* Vol. 16, No. 3, pp. 1-32.

Ambach, W. and Jochum, O. (1973). Zur Dispersion im offenen Gerinne: Einfluss von Randzonen bei Gletscherbächen. *Z. Gletscherkd. Glazialgeol.*, Bd. 9, Ht. 1-2, pp. 181-88.

Ambach, von W., H. Behrens, H. Bergmann und H. Moser (1972). Markierungsversuche im inneren Abfluss-System des Hintereisferners (Ötztaler Alpen), *Z. Gletscherkd. Glazialgeol.*, Bd. 8, Ht. 1-2, pp. 137-145.

Anderson, M. P. (1979). Using models to simulate the movement of contaminants through groundwater flow systems. *CRC Critical Reviews in Environmental Control,* ed. by C. P. Staub, CRC Press Inc., Vol. 9, p. 97-152.

Aris, R. (1953). On the dispersion of a solute in a fluid flowing through a tube. *Proc. R. Soc. London, Ser* A. 235, pp. 67-78.

Bagnold, R. A. (1960). Some aspects of the shape of river meanders, *U. S. Geological Survey Professional Paper* 282-E.

Baetsle, L. H. (1967). Computational methods for the prediction of underground movement of radionuclides, *Nuclear Safety: Consequences of Activity Release,* Vol. 8, No. 6, pp. 576-588.

Bear, J. (1972). *Dynamics of fluids in porous media.* American Elsevier, New York.

Bear, J. (1979). *Hydraulics of Groundwater.* McGraw-Hill Interscience, New York.

Behrens, H., H. Bergmann, H. Moser, W. Rauert, W. Stichler, W. Ambach, H. Eisner, K. Pessl (1971). Study of the discharge of alpine glaciers by means of environmental isotopes and dye tracers. *Z. Gletscherkd. Glazialgeol.*, Bd. 7, Ht. 1-2, pp. 79-102.

Behrens. H. (1973). Eine verbesserte Nachweismethode fur Fluoreszenzindikatoren und ihre Anwendung zur Feststellung von Fliesswegen im Grundwasser. *Zeitschrift der Deutschen Geologischen Gesellschaft,* Bd. 124, Teil 2, p. 535-544.

Behrens, H., H. Behrens, H.Bergmann, H. Moser, W. Ambach, and O. Jochum. 1975. On the water channels of the internal drainage system of the Hintereisferner,

Ötztal Alps, Austria. *J. Glaciol.*, Vol. 14, No. 72., pp. 375-382.

Benedict, B. A (1980). Analytical models for mixing of toxic spills in rivers, *Proceedings of the Hydrologic Transport Modeling Symposium, Dec. 10-11, 1979,* Am. Soc. of Agri. Eng., St. Joseph, Michigan, pp. 108-117.

Bencala, K.E., R. E. Tathburn, A. P. Jackman, V. C. Kennedy, G. W. Zellwege and R. J. Avanzino (1984). Rhodamine WT dye losses is a mountain stream environment. *Water Res. Bull.* , Vol. 19, No. 6, pp. 943-50.

Bindschadler, R., W. D. Harrison, C. F. Raymond and R. Crosson (1977). Geometry and dynamics of a surge-type glacier. *J. Glaciol.*, Vol. 16, pp. 181-194.

Bindschadler, R. (1982). A numerical model of temperate glacier flow applied to the quiescent phase of a surge type glacier. *J. Glaciol.*, Vol. 28, No. 991, pp. 239-266.

Boulton, G. S. and A. S. Jones (1979). Stability of temperate ice caps and ice sheets resting on beds of deformable sediment. *J. Glaciol.*, Vol. 24, pp. 29-43.

Bredehoeft, J. D. and G. F. Pinder (1973). Mass transport in flowing groundwater. *Water Resour. Res.*, Vol. 9, p. 194.

Budd, W. F. (1975). A first simple model for periodically self-surging glaciers. *J. Glaciol.*, Vol. 14, pp. 3-21.

Burington, R. S. and D. C. May (1970). *Handbook of Probability and Statistics With Tables. 2nd edition.* McGraw-Hill, New York.

Burkimsher, M. (1983). Investigations of glacier hydrological systems using dye tracer techniques: observations at Pasterzengletscher, Austria. *J. Glaciol.*, Vol. 29, pp. 403-416.

CIBA-GEIGY (1977). A Guide to Tinopal Fluorescent Whitening Agents. *Technical Bulletin.* Greensboro, North Carolina, Ciba-Geigy Corporation.

CIBA-GEIGY (1981). A Guide to Tinopal Fluorescent Whitening Agents for the Soap and Detergent Industry. *Technical Bulletin.* Ciba-Geigy Corporation, Greensboro, North Carolina.

Clarke, G. K. C. (1976). Thermal regulation of glacier surging. *J. Glaciol.*, Vol. 16, pp. 231-250.

Clarke, G. K. C., Mathews, W. H., and Pack, R. T. (1984). Outburst floods from Glacial Lake Missoula. *Quaternary Res.*, Vol. 22, pp. 289-299.

Colbeck, S. C. and F. A. Anderson (1984). The permeability of a melting snow cover, *Water Resources Research*, Vol. 18, No. 4, pp. 904-908.

Colbeck, S. C. and E. Davidson (1973). Water percolation through homogeneous snow, in *The Role of Snow and Ice in Hydrology, Vol. 1.* UNESCO-WMO-IAHS, Geneva.

Crank, J. (1956). *Mathematics of Diffusion.* Clarendon Press, Oxford.

Dagan, G. (1971). Perturbation solutions of the dispersion equation in porous mediums, *Water Resour. Res.*, No. 1, pp. 135-142.

Danckwerts, P. V. (1953). Continuous flow systems. *Chemical Engineering Science*, Vol. 2, No. 1, pp. 1-13.

De Jong, Josselin (1958). Longitudinal and traverse diffusion in granular deposits. *Trans. Am. Geophys, Union*, Vol. 39, pp. 67-75.

De Smedt, F. and P.J. Wierenga (1984). Solute transfer through columns of glass beads. *Water Resour. Res.*, Vol. 20, pp. 225-232.

Dolgoushin, L. D., and G. B. Osipova (1973). The regime of a surging glacier. *Int. Assoc. Hydrol. Sci. Publ.*, Vol. 107, pp. 1150-1159.

Dolgoushin, L. D., and G. B. Osipova (1973). Glacier surges and the problem of their forcasting. *Int. Assoc. Hydrol. Sci. Publ.*, Vol. 107, pp. 292-304.

Elder, J. W. (1959). The dispersion of marked fluid in turbulent shear flow. *Journal Fluid Mechanics*, Vol. 5, pp. 544-560.

Engelhardt, H. F., W. B. Kamb, C. F. Raymond, and W. D. Harrison (1979). Observation of basal sliding of Variegated Glacier, Alaska. *J. Glaciol.*, Vol. 20, pp. 469-508.

Engelhardt, H. F., W. D. Harrison, and B. Kamb (1978). Basal sliding and conditions at the glacier bay as revealed by borehole photography. *J. Glaciol.*, Vol. 20, pp. 409-508.

Ferguson, R. I. (1973). Sinuosity of supraglacial streams. *Geological Society of America Bulletin*, Vol. 84, pp. 251-256.

Fischer, H. B. (1968). Methods for predicting dispersion coefficients in natural streams, with applications to lower reaches of the Green and Duwamish Rivers, Washington. *U. S. Geological Survey, Professional Paper* 582-A.

Fleagle, R. G. and J. A. Businger. (1963). *Atmospheric Physics.* New York, Academic Press.

Freeze, R. A., and J. A. Cherry (1979). *Groundwater.* Englewood Cliffs, New Jersey, Prentice-Hall, Inc.

Frind, E. O. and G. F. Pinder (1973). Galerkin solution of the inverse problem for aquifer transmissivity, *Water Resour. Res.*, Vol. 9, p. 1397.

Fried, V., H. F. Hameka, and U. Blukis (1977). *Physical Chemistry.* New York, Macmillan.

Garder, A. O., Jr., D. W. Peaceman, and A. L. Jr. Pozzi (1964). Numerical calculation of multidimensioal miscible displacement by the method of characteristics, *Soc. Petrol, Eng. J.,* Vol. 4, No. 1, pp. 26-36.

Gardiner, V., and R. Dackombe (1983). *Geomorphological Field Manual.* Allen and Undwin Inc., Winchester, Massachusetts.

Gelhar, L. W. and M. A. Collins (1971). General analysis of longitudinal dispersion in nonuniform flow. *Water Resour. Res.*, Vol. 7, p. 1511.

Gillham, R. W., E. A. Sudicky, J. A. Cherry, and E. O. Frind (1984). An advective-diffusion concept for solute transport in heterogeneous unconsolidated geological deposits. *Water Resour. Res.*, Vol. 20, No. 3, pp. 369-78.

Gupta, V. K. and R. N. Battacharrya (1986). Solute dispersion in multidimensional periodic saturated porous media. *Water Resourc. Res.*, Vol. 22, No. 2, pp. 156-164.

Güven, O.,F. J. Molz, and J. G. Melville (1984). An analysis of dispersion in a stratified aquifer. *Water Resourc. Res.*, Vol. 20, No. 10, pp. 1337-54.

Harrison, A. E. (1964). Ice surges of Muldrow Glacier. *J. Glaciol.*, Vol. 5, pp. 365-368.

Harrison, W. D. (1972). Temperature of a temperate glacier. *J. Glaciol.*, Vol. 11, pp. 15-29.

Hinze, J. O. (1959). *Turbulence: An Introduction to Its Mechanism and Theory.* McGraw-Hill, Inc., New York.

Hodge, S. M. (1972). The movement and basal sliding of the Nisqually Glacier, Mt. Rainier. *University of Washington, Department of Atmospheric Sciences, Scientific Report 13,* Seattle, Washington, U.S.A.

Hodge, S. M. (1974). Variations in the sliding of a temperate glacier. *J. Glaciol.*, Vol. 13, pp. 349-369.

Hodge, S. M. (1976). Direct measurement of basal water pressures: a pilot study. *J. Glaciol.*, Vol. 16, pp. 205-218.

Hodge, S. M. (1979). Direct measurement of basal water pressures: progress and problems. *J. Glaciol.*, Vol. 23, pp. 309-319.

Hooke, R. (1984). On the role of mechanical energy in maintaining subglacial water conduits at atmospheric pressure. *J. Glaciol.*, Vol. 3, No. 105, pp. 180-187.

Hughes, T. J. (1973). Is the West Antarctic ice sheet disintegrating? *J. Geophys. Res.*, Vol. 78, pp. 7884-7910.

Hughes, T. J. (1977). West Antarctic ice streams. *Rev. Geophys. and Space Phys.*, Vol. 15, pp. 1-46.

Iken, A. (1981). The effect of the subglacial water pressure on the sliding velocity of a glacier in an idealized numerical model. *J. Glaciol.*, Vol. 27, pp. 407-21.

Iken, A. and R. A. Bindschadler (1986). Combined measurements of subglacial water pressure and surface velocity of Findelengletscher, Switzerland: Conclusions about drainage system and sliding mechanisms. *J. Glaciol.*, Vol. 32, pp. 101-119.

Iken, H. Röthlisberger, A., H. Flotron, and W. Haeberli (1983). The uplift of the Unterargletscher at the beginning of the melt season - a consequence of water storage at bed? *J. Glaciol.*, Vol. 29, pp. 28-47.

Irle, P. (1978). *unpublished* Results of 1977 dye-tracing experiments conducted at South Cascade Glacier, U.S.A., 12 pp.

Jackson, R. G., II. (1977). Mechanisms and hydrodynamic factors of sediment transport in alluvial Streams. *In* Davidson-Arnott, R. and Nickling, W., *eds. Research in Fluvial Geomorphology.* Geo Abstracts Ltd., Norwich, England.

Jury, W. A. (1982). Simulation of solute transport using a transfer function model. *Water Resour. Res.*, Vol. 18, pp. 363-8.

Jury, W. A. and L. H. Stolzy (1982). A field test of the transfer function model for predicting solute transport. *Water Resour. Res.*, Vol. 18, pp. 369-75.

Jury, W. A., G. Sposito, and R. E. White (1986). A transfer function model of solute transport through soil, 1. Fundamental concepts. *Water Resour. Res.*, Vol. 22, pp. 243-7.

Kamb, B. (1970). Sliding motion of glaciers: theory and observation. *Rev. Geophys. Space Phys.*, Vol. 8, pp. 673-728.

Kamb, B., H. F. Engelhardt, and W. D. Harrison (1979). The ice-rock interface and basal sliding process as revealed by direct observation in bore holes and tunnels. *J. Glaciol.*, Vol. 23, pp. 416-19.

Kamb, B., C. F. Raymond, W. D. Harrison, H. Engelhardt, K. A. Echelmeyer, N. Humphrey, M. M. Brugman, and T. Pfeffer. (1985). Glacier surge mechanism: 1982-1983 surge of Variegated Glacier, Alaska. *Science*, Vol. 227, No. 4686, pp. 469-479.

Kamb, B. and H. Engelhardt (1986). Waves of accelerated motion in a glacier approaching a surge: the mini-surges of Variegated Glacier, Alaska. *J. Glaciol.*, in press.

Konikow, L. F., and J. D. Bredehoeft (1974). Modeling flow and chemical quality changes in an irrigated stream-aquifer system. *Water Resour. Res.*, Vol. 10, No. 3, pp. 546-562.

Konikow, L. F. and J. D. Bredehoeft (1978). Computer model of two-dimensional solute transport and dispersion in ground water, *U. S. Geological Survey Techniques of Water Resources Investigations*, Book 7, C2.

Koutitas, C. G. (1983). *Elements of Computational Hydraulics.* Pentech Press, London.

Krimmel, R. M., R. M. Krimmel, W. V. Tangborn and M. F. Meier. (1973). Water flow through a temperate glacier. *The role of snow and ice in hydrology. Proceedings of the Banff symposia, September 1972.* Paris, UNESCO; Geneva, WMO; IAHS, Budapest, pp. 401-416.

Krumbein, W. C. and L. L. Slass (1963). *Stratigraphy and Sedimentation. 2nd edition.* W. H. Freeman and Company, San Fransisco.

Kunze, R. J., and D. R. Nielsen (1982). Finite-difference solutions of the infiltration equation. *Soil Science*, Vol. 134, No. 2, pp. 81-88.

Krupp, H. K. and D. E. Elrich (1968). Miscible displacement in an unstaturated glass bead medium. *Water Resourc. Res.* , Vol. 4, pp. 809-815.

Lang, H. (1966). Hydrometeorologische Ergebnisse aus Abflussmessungen im Bereich des Hintereisferners (Ötztaler Alpen) in den Jahren 1957 bis 1959. *Archivrür Meteorologie, Geophysik und Bioklimatologic*, Ser. B, Bd. 14, Ht. 3-4, pp. 280-302.

Lang, H., C. Leibundgut, and E. Festel (1979). Results from tracer experiments on the water flow through the Aletschgletscher. *Z. Gletsherkd. Glazialgeol.*, Bd. 15, Ht. 2, pp. 209-218.

Leliavsky, S. (1966). *An Introduction to Fluvial Hydraulics.* Dover Publications, Inc., New York.

Leopold, L. B. and W. B. Langbein (1966). River Meanders. *Scientific American* , Vol. 214, p. 60.

Leopold, L. B. and M. G. Wolman (1960). River Meanders. *Geol. Soc. Am. Bull.* , Vol. 71, No. 6, p. 769.

Lerman, A. (1979). *Geochemical Processes Water and Sediment Environments.* John Wiley & Sons, New York.

Lliboutry, L. (1964). *Traite de Glaciologie.* Tome 1, Masson, Paris, France.

Lliboutry, L. (1968). General theory of subglacial cavitation and sliding of temperate glaciers. *J. Glaciol.*, Vol. 7, pp. 21-58.

Meier, M. F. (1965). Glaciers and climate. *In* H. E. Wright and D. G. Frey, *eds. The Quaternary of the United States.* Princeton University Press, Princeton, New Jersey.

Meier, M. F. (1966). Some glaciological interpretations of remapping programs on South Cascade, Nisqually, and Klawatti Glaciers, Washington. *Can. J. Earth Sci.*, Vol. 3, pp. 811-818.

Meier, M. F. and W. V. Tangborn (1965). Distinctive characteristics of glacier runoff. *U.S. Geol. Surv. Prof. Pap. 424B*, pp. 14-16.

Meier, M. F., and A. S. Post (1969). What are glacier surges? *Can. J. of Earth Sci.*, Vol. 3, pp. 811-817.

Meier, M. F. and B. Kamb, C. R. Allen and R. P. Sharp (1974). Flow of Blue Glacier, Olympic Mountains, Washington, U.S.A. *J. Glaciol.*, Vol. 13, pp. 187-212.

Mercado, A., and E. Halevy (1966). Determining the average porosity and permeability of a stratified aquifer with the aid of radioactive tracers. *Water Resour. Res.*, Vol. 12, No. 3, pp. 525-531.

Moeri, T. (1983). *Beitrag zum Abflussgeschehen des Findelengletschers.* Bern, Geographisches Institut der Universitäaet Bern.

Morisawa, M. (1968). *Streams: their dynamics and morphology.* McGraw-Hill Book Company, New York.

Neretnieks, I. (1983). A note on fracture flow dispersion mechanisms in the ground. *Water Resour. Res.*, Vol. 19, No. 2, pp. 364-370.

Neretnieks, I., T. Eriksen, and P. Tahtinen (1982). Tracer movement in a single fissure in granitic rock: some experimental results and their interpretation. *Water Resour. Res.*, Vol. 18, pp. 849-862.

Nye, J. F. (1953). The flow law of ice from measurements in glaciers, laboratory experiments and the Jungfraufirn borehole experiment. *Proc. R. Soc. London. Ser. A.*, Vol. 219, pp. 477-489.

Nye, J. F. (1976). Water Flow in Glaciers: Jökulhlaups, Tunnels and Veins. *Journal of Glaciology,* Vol. 17, No. 76, pp. 181-207.

Nye, J. F., and F. C. Frank (1973). Hydrology of the intergranular veins in a temperate glacier. *IASH,* Vol. 95, pp. 157-161.

Ogata, A. and R. B. Banks (1961). A solution of the differential equation of longitudinal dispersion in porous media, *U.S. Geological Survey, Professional Paper,* 411-A.

Ogata, A. (1961). Transverse diffision in saturated isotropic granular media, *U. S. Geological Survey Professional Paper,* 411-B.

Ogata, A. (1964). The spread of a dye stream in an isotropic granular medium, *U. S. Geological Survey, Professional Paper,* 411-G.

Ogata, A. (1964). Mathematics of dispersion with linear adsorption isotherm, *U. S. Geological Survey, Professional Paper,* 411-H.

Paterson, W. S. B. (1981). *The Physics of Glaciers.* Pergamon Press, New York.

Pickens, J. F. and W. C. Lennox (1976). Numerical simulation of waste movement in steady ground water flow systems. *Water Resour. Res.*, Vol. 12, No. 2, pp. 171-180.

Pinder, G. F. (1973). A Galerkin-finite element simulation of ground water contamination of Long Island. *Water Resour. Res.*, Vol. 9, pp. 1657.

Pinder, G. F. (1974). Progress in simulation of contaminant transport in porous media. *In* S. C. Csallany, Z. A. Saleem, and W. J. Roberts, *eds. A Decade of Progress in Water Resources.* American Water Research Assn., Urbana, Ill., p. 223.

Pinder, G. F., and W. G. Gray (1977). *Finite Element Simulation in Surface and Subsurface Hydrology.* Academic Press, New York.

Raymond, C. F. and W. D. Harrison (1975). Some observations on the behavior of liquid and gas phases in temperate glacier ice, *J. Glaciol.*, Vol. 14, pp. 213-33.

Richards, K. (1982). *Rivers, Form and Process in Alluvial Channels.* Methuen, New York.

Robin, G. de Q. and J. Weertman (1973). Cyclic surging of glaciers. *J. Glaciol.*, Vol. 12, pp. 3-18.

Röthlisberger, H. (1972). Water pressure in intra- and subglacial channels. *Journal of Glaciology,* Vol. 11, No. 62, pp. 177-203.

Saffman, P. G. (1959). A theory of dispersion in a porous medium. *J. Fluid Mech.*, Part 3, Vol. 6, p. 321.

Saffman, P. G. (1960). Dispersion due to molecular diffusion and macroscopic mixing in flow through a network of capillaries. *J. Fluid Mech.*, Part 2, Vol. 7, p. 194.

Scheidegger, A. E. (1954). Statistical hydrodynamics in porous media. *J. Appl. Phys.*, Vol. 25, p. 994.

Scheidegger, A. E. (1957). *The Physics of Flow Through Porous Media.* MacMillan Co., New York.

Scheidegger, A. E. (1961). General theory of dispersion in porous media. *J. Geophys. Res.*, Vol. 66, p. 3273.

Shamir, U. Y., and D. R. F. Harleman (1967). Numerical solutions for dispersion in porous mediums. *Water Resources Research,* Vol. 6, No. 2, p. 557-581.

Shreve, R. L. (1972). Movement of water in glaciers. *Journal of Glaciology,,* Vol. 11, No. 62, pp. 206-214.

Simons, D. B., and F. Senturk (1977). *Sediment Transport Technology.* Colorado, Water Resources Publications, Ft. Collins, Colorado.

Smart, P. L. (1976). The use of optical brighteners for water tracing. *Trans. British Cave Research Assoc.*, Vol. 3, No. 2, pp. 62-76.

Smart, P. L., B. L. Finlayson, W. D. Rylands, and C. M. Ball (1976). The relation of fluorescence to dissolved organic carbon in surface waters. *Water Research,* Vol. 10, pp. 805-811.

Smart, P. L., and D. I. Smith (1976). Water tracing in tropical regions, the use of fluorometric techniques in Jamaica. *Journal of Hydrology*, Vol. 30, pp. 79-195.

Smart, P. L., and I. M. S. Laidlaw (1976). An evaluation of some fluorescent dyes for water tracing. *Water Resources Research*, Vol. 13 No. 1, pp. 15-33.

Snow, D.T. (1970). Frequency of apertures in fractured rock. *Int. J. Rock Mech. Min. Sci.*, Vol. 7, pp. 23-37.

Sposito, G., R. E. White, P. R. Darrah, and W. Jury (1986). A transfer function model of solute transport through soil 3. The convective-dispersion equation. *Water Resources Research*, Vol. 22, No. 2, pp. 225-62.

Sposito, G., W. Jury, and V. K. Gupta (1986). Fundamental problems in the stochastic convection-dispersion model of solute transport in aquifers and field soils. *Water Resources Research*, Vol. 22, No. 1, p. 77-62.

Spring, U., and K. Hutter (1982). Conduit flow of a fluid through its solid phase and its application to intraglacial channel flow. *International Journal of Engineering Science*, Vol. 20, pp. 327-63.

Sudicky, E. A., J. A. Cherry, and E. O. Frind (1983). Migration of contaminants in groundwater at a landfill: A case study, 3, A natural gradient dispersion test. *J. Hydrol.*, Vol. 63, pp. 473-477.

Tang, D. H., E. O. Frind, and E. Sudicky (1980). Contaminant transport in fractured porous media: An analytical solution for a single fracture. *Rep.T*-132, Univ. Waterloo, Waterloo, Ont.

Tang, D. H., F. W. Schwartz, and L. Smith (1984). Stochastic modeling of mass transport in a random velocity field. *Water Resour. Res.*, Vol. 20, No. 2, pp. 150-9.

Tangborn, W. V., R. M. Krimmel and M. F. Meier (1975). A comparison of glacier mass balance by glaciological, hydrological and mapping methods, South Cascade Glacier, Washington. *IAHS*, Vol. 104, pp. 185-196.

Taylor, G. (1953). Dispersion of soluble matter in solvent flowing slowly through a tube. *Proc. R. Soc. London.* Ser. A, Vol. 219, p. 186.

Taylor, G. I. (1954). The dispersion of matter in turbulent flow through a pipe. *Proc. R. Soc. London.* Ser. A, Vol. 223, No. 1155, pp. 446-68.

Turcotte, D. L. and G. Schubert (1982). *Geodynamics.* Wiley and Sons, New York.

Turner Designs (1977). *Operating & Service Manual,* Model 10 Series Fluorometers. Turner Designs, Mountain View, California.

Turner Designs (1981). *Fluoremetric Facts: Fluorescent Tracer Dyes.* Bulletin 102. Turner Designs, Mountain View, California.

Vivian, R. and G. Bocquet (1973). Subglacial cavitation phenomena under the Glacier D'Argentiere, Mont Blanc, France. *J. Glaciol.*, Vol. 12, pp. 439-451.

Walder , J. and B. Hallet (1979). Geometry of former subglacial water channels and cavities. *J. Glaciol.*, Vol. 23, pp. 335-346.

Ward, P. R. B. (1974). Transverse dispersion in oscillatory channel flow. *Journal of the Hydraulics Division,* Proceedings of American Society of Civil Engineers, Vol. 100, No. HY6, p. 755.

Weertman, J. (1964). The theory of glacier sliding. *J. Glaciol.*, Vol. 5, pp. 287-303.

Weertman, J. (1969). Water lubrication mechanism for glacier surges. *Can. J. Earth Sci..*, Vol. 6, pp. 929-942.

Weertman, J. (1972). General theory of water flow at the base of a glacier or ice sheet. *Rev. Geophys. Space Phys.*, Vol. 10, pp. 287-333.

Weertman, J. (1979). The unsolved general glacier sliding problem. *J. Glaciol.*, Vol 23, pp. 97-115.

Wilson, P. (1968). Water tracing technique using fluorescent dyes. *U.S. Geol. Surv. Report.*

Yotsukura, N., and E. D. Cobb (1972). Transverse diffusion of solutes in natural streams. *U. S. Geological Survey, Professional Paper* 582-C.

Zachmann, D. W., P. C. Du Chateau and A. Klute (1982). Simultaneous identification. *Soil Science,* Vol. 134, No. 3, pp. 157-163.